Modulation of papain-like cysteine proteases in microbial interactions

Inaugural-Dissertation

zur Erlangung des Doktorgrades

Dr. rer. nat.

der Mathematisch-Naturwissenschaftlichen Fakultät

der Universität zu Köln

vorgelegt von

M. Sc. Daniel Moser

aus Düsseldorf

Angenommen im Jahr 2025

Modulation of papain-like cysteine proteases in microbial interactions

Inaugural-Dissertation

zur Erlangung des Doktorgrades

Dr. rer. nat.

der Mathematisch-Naturwissenschaftlichen Fakultät

der Universität zu Köln

vorgelegt von

M. Sc. Daniel Moser

aus Düsseldorf

Angenommen im Jahr 2025

Die Untersuchungen der vorliegenden Arbeit wurden im Zeitraum von Oktober 2020 bis Dezember 2024 am Lehrstuhl für Terrestrische Mikrobiologie der Universität zu Köln unter der Leitung von Herrn Prof. Dr. Gunther Döhlemann durchgeführt.

Erstgutachter:	Prof. Dr. Gunther Döhlemann
Zweitgutachter:	Prof. Dr. Bart Thomma
Prüfungsvorsitzender:	Prof. Dr. Kay Hofmann

Tag der mündlichen Prüfung: 17.03.2025

Diese Dissertation entstand im Rahmen des

„Science, for me, gives a partial explanation for life. In so far as it goes, it is based on fact, experience and experiment."

Rosalind Elsie Franklin,
The first lady of DNA
(1920-1958)

Erklärung zur Dissertation

gemäß der Promotionsordnung vom 12. März 2020

Hiermit versichere ich an Eides statt, dass ich die vorliegende Dissertation selbstständig und ohne die Benutzung anderer als der angegebenen Hilfsmittel und Literatur angefertigt habe. Alle Stellen, die wörtlich oder sinngemäß aus veröffentlichten und nicht veröffentlichten Werken dem Wortlaut oder dem Sinn nach entnommen wurden, sind als solche kenntlich gemacht. Ich versichere an Eides statt, dass diese Dissertation noch keiner anderen Fakultät oder Universität zur Prüfung vorgelegen hat; dass sie - abgesehen von unten angegebenen Teilpublikationen und eingebundenen Artikeln und Manuskripten - noch nicht veröffentlicht worden ist sowie, dass ich eine Veröffentlichung der Dissertation vor Abschluss der Promotion nicht ohne Genehmigung des Promotionsausschusses vornehmen werde. Die Bestimmungen dieser Ordnung sind mir bekannt. Darüber hinaus erkläre ich hiermit, dass ich die Ordnung zur Sicherung guter wissenschaftlicher Praxis und zum Umgang mit wissenschaftlichem Fehlverhalten der Universität zu Köln gelesen und sie bei der Durchführung der Dissertation zugrundeliegenden Arbeiten und der schriftlich verfassten Dissertation beachtet habe und verpflichte mich hiermit, die dort genannten Vorgaben bei allen wissenschaftlichen Tätigkeiten zu beachten und umzusetzen. Ich versichere, dass die eingereichte elektronische Fassung der eingereichten Druckfassung vollständig entspricht.

Teilpublikationen:

/

Köln, 11.01.2025

Daniel Moser

Summary

Plants engage in interactions with a highly diverse range of microorganisms, which must circumvent the plant's immune system in order to establish an interaction. Plants defend against microbes using a two-branched immune system. Proteases, particularly papain-like cysteine proteases (PLCPs), play a crucial role in this process, as they are essential for pathogen recognition and the regulation of immune responses. In maize, specific PLCPs are activated in leaves and roots by the phytohormone salicylic acid (SA). Consequently, microbes frequently target PLCPs using effectors with the aim of suppressing immunity. However, the role of microbial PLCP inhibitors in non-pathogenic interactions as well as research on root-associated microbes in the rhizosphere remains relatively limited. The interactions between plants and microbes in crops such as maize remain understudied. This study explores how SA-activated root PLCPs and their microbial inhibitors shape microbial interactions on maize roots. This thesis hypothesizes that non-pathogenic bacteria secrete PLCP inhibitors to modulate protease activity promoting root colonization.

Bacterial culture supernatants of maize root-colonizing bacteria were screened for PLCP inhibition, resulting in the suppression of PLCP activity by the *Pseudomonas putida* supernatant. The PLCP inhibitor *P. putida* PpCip1, which is conserved in all Pseudomonas species and has a chagasin motif required for PLCP inhibition, was identified via a computational search. Furthermore, signal peptide predictions as well as cell fractionation experiments, fluorescence microscopy, and surface protein labeling using Flag- or mCherry-tagged PpCip1 showed that PpCip1 is a surface-localized PLCP inhibitor. Moreover, preliminary results suggest that surface-localized PpCip1 may protect bacterial surface proteins from cleavage by plant PLCPs. Root colonization experiments on *A. thaliana* demonstrated that PpCip1 facilitates the early colonization of the meristematic, elongation, and transition zones. Supernatants of *P. putida* mutants lacking PpCip1 were still capable of inhibiting the activity of PLCPs, indicating that *P. putida* secrets unknown inhibitors different than PpCip1. A diverse range of computational and biochemical approaches were used to identify 15 putative inhibitor candidates, of which two proteins were identified as potential substrate-like inhibitors.

This study shows that also non-pathogenic bacteria use PLCP inhibitors to modulate protease activity thereby promoting root colonization and influencing the bacterial root community structure. Moreover, newly secreted substrate-like PLCP inhibitors have been discovered although their role in plant-microbe interactions still needs to be elucidated.

Abbreviations

Abbreviation	Full name
ABPP	Activity-based protein profiling
AMC	7-amino-4-methyl coumarin
BLAST	Basic Local Alignment Search Tool
CC1	Corn cystatin 1
CERK1	Chitin elicitor receptor kinase 1
Cip1	C14-inhibiting protein 1
CP1A	Cysteine protease 1A
CV	Column volume
DAMPs	Damage-associated molecular patterns
dYT	Double yeast extract tryptone medium
ETI	Effector-triggered immunity
EVC	Empty vector control
FLS2	Flagellin-sensitive 2 protein
GOI	Gene of interest
GPI	Glycolylphosphatidylinositol
HMWF	High-molecular weight fraction
HR	Hypersensitive response
IC50	Half maximal inhibitory concentration
IPTG	Isopropyl-B-D-thiogalactopyranoside
LAF	Leaf apoplastic fluid
LB	Lysogeny broth
LC-MS	Liquid chromatography-mass spectrometry
LFQ	Label-free quantitation
LMWF	Low-molecular weight fraction
MAMP	Microbe-associated molecular patterns
MAPK	Mitogen-activated protein kinase
MoClo	Modular cloning
MS	Mass spectrometry
MSA	Multiple sequence alignment
MW	Molecular weight
MWCO	Molecular weight cut-off
NLR	Nucleotide-binding leucine-rich repeat-containing receptor
OD_{600}	Optical density at 600 nm
OMV	Outer membrane vesicle

Pa	*P. aeruginosa*
PAA	Polyacrylamide
PAMP	Pathogen-associated molecular patterns
PCR	Polymerase chain reaction
Pep1	Plant elicitor peptide 1
PFA	Paraformaldehyde
PICS	Proteomic Identification of protease Cleavage Sites
PLCP	Papain-like cysteine protease
Pp	*P. putida*
Ps	*P. syringae*
PTI	PRR-triggered immunity
R gene	Resistance gene
RAF	Root apoplastic fluid
Rcr3	Required for *C. fulvum* resistance 3
RD19	Responsive to desiccation-19
RD21	Responsive to desiccation-21
RMDS	Root mean square deviation
ROS	Reactive oxygen species
RT	Room temperature
SA	Salicylic acid
SDS-PAGE	Sodium dodecyl sulfate polyacrylamide gel electrophoresis
SEC	Size-exclusion chromatography
SEM	Standard error of the mean
SP	Signal peptide
SynCom	Synthetic community
Tc	*T. cruzi*
TRIS	Tris(hydroxymethyl)aminomethane
TSE	Tris-sucrose-EDTA
TTSS	Type III secretion system
WCF	Whole cell fraction
XCP	Xylem cysteine protease
YT	Yeast extract tryptone medium
Zip1	*Zea mays* immune signaling peptide 1
Z-LR-AMC	N-carbobenzyloxy-Leu-Arg-7-amino-4-methylcoumarin

Table of Contents

1. Introduction

1.1. Plant-microbe interactions on the root

1.1.1. Root-colonizing microbes

A high diversity of microorganisms coexist and interact with plants (Bulgarelli *et al.*, 2013). Plants, as sessile organisms, have a complex immune system to cope with pathogens and other intruders, while non-pathogenic microorganism need to bypass this plant defense to achieve symbiosis (Harris *et al.*, 2020b). Substantial information can be found about plant interactions with leaf associated microorganisms (Nishad *et al.*, 2020), but in contrast less is known about the interaction with microbes below ground (Harris *et al.*, 2020b). The space around living roots is called rhizosphere (Hiltner, 1904) and it is densely populated with other soil-borne organism, ranging from bacteria, fungi and nematodes to insects (Haichar *et al.*, 2014).

Roots can be divided into four distinct developmental zones: The meristematic zones, where active cell division occurs. The transition zone, which is characterized by slow cell growth in width and length. The elongation zone, showing faster cell growth with only elongation in length (Verbelen *et al.*, 2006). The differentiation zone is where cell elongation slows down, cells mature and acquire specialized properties and functions (Petricka *et al.*, 2012). Plants modify their soil environment, the rhizosphere, through the release of metabolites, depositing up to 50% of their photosynthetically fixed carbon in the soil, thereby attracting microbes and shaping the rhizosphere community (Haichar *et al.*, 2014; Rizaludin *et al.*, 2021). Primary metabolites (sugars, amino acids, and organic acids) but also more complex metabolites are primarily exuded from the undifferentiated root apex, from the meristematic to the elongation zone, where apoplastic diffusion of metabolites is not hindered as in the differentiation zone which has the Casparian strip as an apoplastic barrier (Canarini *et al.*, 2019; Jones *et al.*, 2009). Additionally, also secondary metabolites acting as chemoattractants are exudated from these zones (Haichar *et al.*, 2014; Hale & Moore, 1980). Bacteria tend to colonize in the grooves between epidermal cells or where lateral root emerge (Schmidt *et al.*, 2018; Tsai *et al.*, 2023). Moreover, some microbes have also been observed to increase root exudation by plants (Canarini *et al.*, 2019). Overall, soil and roots are colonized by a larger and more diverse microbiota than the above-ground parts of the plant (Bai *et al.*, 2015;

Bulgarelli *et al.*, 2013). These microbiota can have plant-growth promoting effects or act as biocontrol agents, e.g. by fixation of nitrogen, solubilization of other nutrients, or by controlling pathogens with antibacterial or antifungal compounds (Bulgarelli *et al.*, 2013).

While a lot of research is performed on model plants like *Arabidopsis thaliana* (Bai *et al.*, 2015; Bulgarelli *et al.*, 2013), the understanding of plant-microbe interactions and plant immunity in non-model plants is still limited. In this work, we focus on the non-model monocot plant maize, which is one of the most important crops in the world (Goldschein, 2011) and which is estimated to lose up to 10% of its annual maize yield to diseases in the US (D. Mueller *et al.*, 2020), highlighting the importance of gaining a better understanding of plant-microbe interactions and plant immunity in this non-model plant. Similar to the community structure found on *A. thaliana* roots (Bai *et al.*, 2015), maize roots were shown to be colonized by a diverse community of bacteria constituted mostly of Proteobacteria, Firmicutes, Bacteroidetes, and Actinobacteria (Niu *et al.*, 2017). From this community isolated from maize roots, a simplified but representative synthetic community (SynCom) comprised of *Stenotrophomonas maltophilia*, *Ochrobactrum pituitosum*, *Curtobacterium pusillum*, *Enterobacter cloacae*, *Chryseobacterium indologenes*, *Herbaspirillum frisingense*, and *Pseudomonas putida*, was established (Niu *et al.*, 2017). Interestingly, two members of the maize SynCom, *P. putida* and *E. cloacae*, were essential for the stability of the community structure on maize roots (Niu *et al.*, 2017). Notably, the maize root SynCom did not show a growth promotive effect to maize seedlings grown on agar (Niu *et al.*, 2017). However, the SynCom delayed the growth of the fungal pathogen *Fusarium verticillioides* on maize seedlings (Niu *et al.*, 2017), stressing the positive role of microbial communities in disease suppression. Members of the genera *Enterobacter, Stenotrophomonas* and *Pseudomonas* were often shown to be overrepresented in disease-suppressive and plant-growth-promoting soils (Gómez Expósito *et al.*, 2017; Rascovan *et al.*, 2016; Trivedi *et al.*, 2017). Many non-pathogenic Pseudomonads, such as *Pseudomonas fluorescens*, *Pseudomonas protegens* and *P. putida*, are commonly found in the rhizosphere of a wide range of plants. These bacteria are often beneficial to the plant, e.g. through plant growth promotion or biocontrol activities (Costa-Gutierrez *et al.*, 2022; Rivilla & Malone, 2023; Schroth *et al.*, 2006). Pathogenic plant-colonizing

Pseudomonads, such as *Pseudomonas syringae* or *Pseudomonas solanacearum,* have typically acquired multiple virulence traits: for example proteins associated with apoplast water soaking, manipulation of host immune signaling and defense suppression are often encoded in pathogenicity islands (Xin *et al.*, 2018). In contrast, non-pathogenic Pseudomonads require traits that allow them to successfully colonize the rhizosphere (Espinosa-Urgel & Ramos-González, 2023; Zboralski & Filion, 2020). For example, bacteria need to detect the presence of metabolites through chemoreceptors and to move to these sites by swimming, swarming and twitching (chemotaxis) (Matilla *et al.*, 2007; Muriel *et al.*, 2015; Parales *et al.*, 2013; Redondo-Nieto *et al.*, 2013; Sampedro *et al.*, 2014). Moreover, these plant-beneficial Pseudomonads often form biofilms on roots, protecting them from various stresses and improving nutrient assimilation (Collins *et al.*, 2020; Danhorn & Fuqua, 2007; Flemming & Wingender, 2010; Hinsa *et al.*, 2003; Martínez-Gil *et al.*, 2010; Yousef-Coronado *et al.*, 2008). In addition, root-colonizing bacteria also need to cope and compete with their neighbors, for example by producing antimicrobial compounds or by competing for nutrients (Bernal *et al.*, 2018; Biessy & Filion, 2018; Geudens & Martins, 2018; Ghequire & De Mot, 2014; Gross & Loper, 2009; Meyer, 2000). Finally, they also need to evade the plant's immune response, e.g., by avoiding their detection or by suppressing the immune response with proteins secreted by the type III secretion system (Berendsen *et al.*, 2015; Liu *et al.*, 2018b; Loper *et al.*, 2012; Mavrodi *et al.*, 2011; Yu *et al.*, 2019; Zamioudis & Pieterse, 2012).

1.1.2. The plant immune system in a nutshell

To be able to recognize and respond to the colonization or infection by microbes, plants rely on a complex two-branched innate immune system that potentiates each other (Figure 1) (Chai *et al.*, 2023; Feehan *et al.*, 2023; Jones & Dangl, 2006; Yuan *et al.*, 2021):

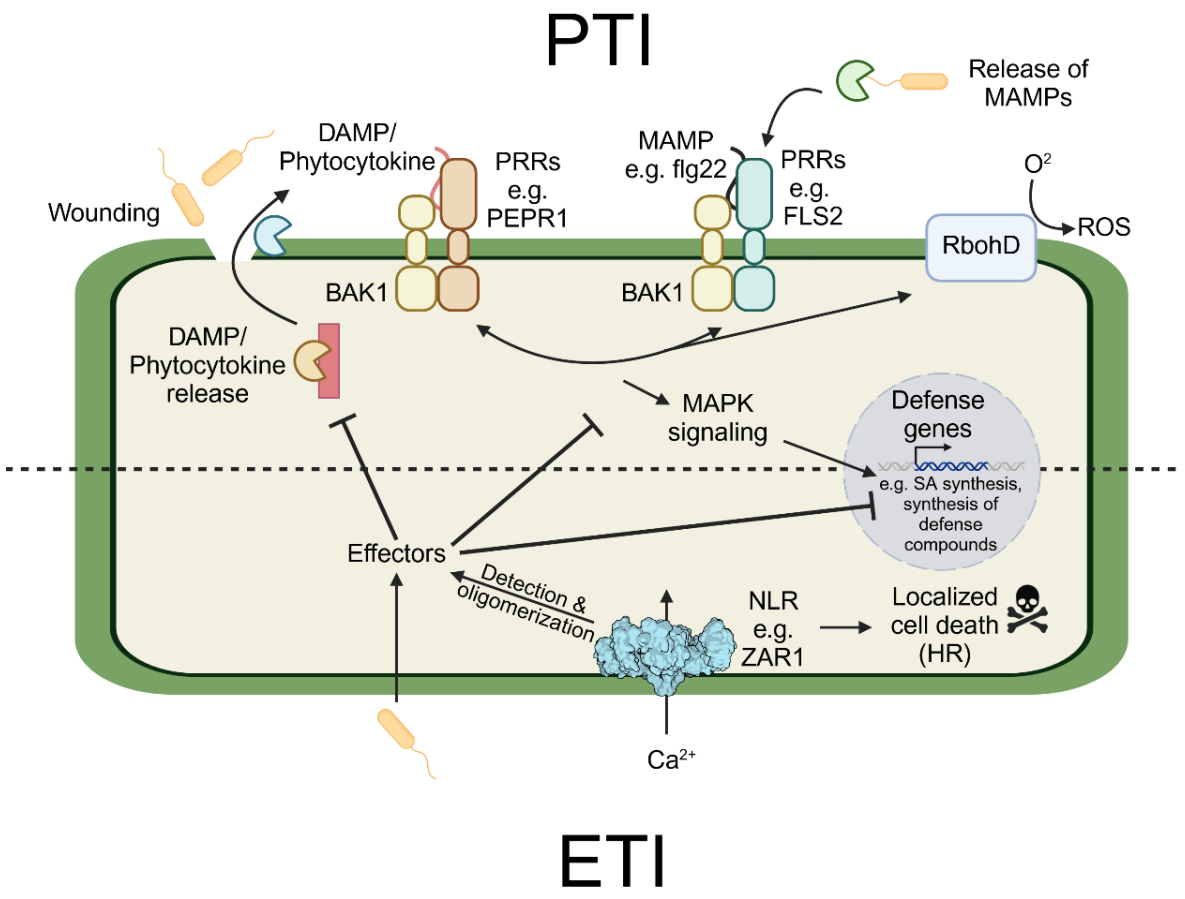

Figure 1: Plants rely on a two-branched immune system to recognize microbes.

In the first branch of plant immunity, **pattern-triggered immunity (PTI)**, microbe- or host-derived patterns trigger immune responses (Li *et al.*, 2024b). Microbe-associated molecular patterns (MAMPs), such as flg22 which is proteolytically released from flagellin, can be recognized by the BAK1-dependent pattern-recognition receptor (PRR) FLS2 (FLAGELLIN-SENSITIVE 2) (Buscaill *et al.*, 2019; Chinchilla *et al.*, 2006; Felix *et al.*, 1999; Gómez-Gómez & Boller, 2000; Gómez-Gómez *et al.*, 1999). Similarly, damage-associated molecular patterns (DAMPs) like cell wall fragments or ATP can be released from leaking cells upon cell damage (Vega-Muñoz *et al.*, 2020; Zhou & Zhang, 2020). Moreover, phytocytokines are actively released from their precursors by plant proteases upon wounding (Rzemieniewski & Stegmann, 2022). For example, the phytocytokines plant elicitor peptide 1 (pep1) is released from its precursor ProPep1 by a metacaspase. DAMPs and phytocytokines are also recognized by PRRs, as observed for Pep1 recognition by the BAK1-dependent receptor PEPR1 (Hander *et al.*, 2019; Huffaker *et al.*, 2006; Shen *et al.*, 2019; Yamaguchi *et al.*, 2010). Their detection triggers multiple defense responses such as Ca^{2+} influx, mitogen-activated protein kinase (MAPK) signaling and synthesis of apoplastic reactive oxygen species (ROS burst) by RbohD (Conrath *et al.*, 2015). Moreover, MAPK signaling cause the upregulation of SA synthesis and the production of defense compounds (Conrath *et al.*, 2015). In the second branch of plants immunity, **effector-triggered immunity (ETI)**, effectors, employed by microbes to modulate host immunity, are detected by nucleotide-binding leucine-rich repeat-containing receptors (NLRs) (Jones *et al.*, 2016; Remick *et al.*, 2023). Some NLRs, like ZAR1 (PDB: 6J5T), have been shown to form nonselective Ca^{2+}-permeable ion channel, called the resistosome, triggering localized cell death (hypersensitive response, HR) (Bi *et al.*, 2021; Lewis *et al.*, 2010; Ma *et al.*, 2006). Nevertheless, ETI and PTI signaling have been shown to converge in similar downstream responses and to be also interconnected (Chai *et al.*, 2023; Feehan *et al.*, 2023; Wang *et al.*, 2019a; Yuan *et al.*, 2021).

In the first branch, the pattern-triggered immunity (sometimes also termed PRR-triggered or PAMP-triggered immunity) (PTI), microbe- or host-derived patterns

can be recognized. These molecular patterns are recognized by pattern recognition receptors (PRRs), which often rely on the coreceptor Brassinosteroid activated kinase 1 (BAK1), resulting in PTI (Heese *et al.*, 2007; Li *et al.*, 2024b). Their detection triggers multiple defense responses such as Ca^{2+} influx, mitogen-activated protein kinase (MAPK) signaling and synthesis of apoplastic reactive oxygen species (ROS burst) (Conrath *et al.*, 2015). These signals can also be amplified by phytohormones like salicylic acid (SA), jasmonic acid (JA) and ethylene (ET), which play a major role in immune signaling (Couto & Zipfel, 2016; Pieterse *et al.*, 2012). For example the major immune signaling hormone salicylic acid (SA) plays an essential role in the plant's complex immune system as it is an important signal amplifier upon detection of biotrophic pathogens, which require living tissue for their infection (Conrath *et al.*, 2015). The SA signaling can lead to the release of defense compounds (e.g. secondary metabolites and pathogenesis related (PR) proteins like chitinases and glucanases), stomatal closure, callose and lignin deposition aiming to restrict the biotrophic pathogen infection by localized cell death (Conrath *et al.*, 2015; Saijo *et al.*, 2018; Van Loon *et al.*, 2006). SA can also induce systemic acquired resistance (SAR) in tissues distant from the infection site protecting the plant from the spread of a pathogen into other parts of the plant (de Wit, 2007; Klessig *et al.*, 2018). In contrast, JA antagonizes SA signaling and is synthesized upon infection by herbivores and necrotrophic pathogens, which require dead plant material as a nutrient source (Gfeller *et al.*, 2010; Glazebrook, 2005).

These molecular-patterns triggering PTI are usually released from their precursors by lytic enzymes, for example proteases or cell-wall degrading enzymes, however the responsible enzymes are many cases not known yet (Zhou & Zhang, 2020). These molecular patterns can be divided into three categories:

First, exogenous molecules such as microbial- or pathogen-associated molecular patterns (MAMPs or PAMPs) are derived from proteins, cell wall components, polysaccharides or other molecules of the colonizing microbe (Saijo *et al.*, 2018). A well-known example is the flg22 peptide which is released from bacterial flagellin and detected by BAK1-dependent FLS2 (FLAGELLIN-SENSITIVE 2) (Buscaill *et al.*, 2019; Chinchilla *et al.*, 2006; Felix *et al.*, 1999; Gómez-Gómez & Boller, 2000; Gómez-Gómez *et al.*, 1999). Recently, the subtilisin-like proteases (subtilases) SBT5.2 and SBT1.7 have been reported to release flg22 (Matsui *et al.*, 2024), but

other reports indicate that they rather inactivate flg22 to control immunity (Buscaill *et al.*, 2024), similar to the inactivation of the MAMP csp22 of *P. syringae* by SBT5.2 (Chen *et al.*, 2024a). Another example are chitin oligosaccharides which are released from the fungal cell wall and are detected by the chitin elicitor receptor kinase 1 (CERK1) (Kaku *et al.*, 2006; Miya *et al.*, 2007).

Second, endogenous damage-associated molecular patterns (DAMPs) are immunogenic cell debris components (e.g. cell wall fragments, ATP, peptides, sugars, DNA and more) released from leaking damaged cells and/or by enzymatic cleavage (Vega-Muñoz *et al.*, 2020; Zhou & Zhang, 2020). For example, ATP is released from the cell upon damage within minutes and detected by a P2-type immune purinoceptors (Chen *et al.*, 2017; Demidchik *et al.*, 2009; Song *et al.*, 2006). Another example are oligogalacturonides which are released from the pectin component homogalacturonan by host or microbial polygalacturonases during pathogen infection (Brutus *et al.*, 2010; Cervone *et al.*, 1989; Orozco-Cardenas & Ryan, 1999).

Recently, a third origin was defined: Phytocytokines, also termed inducible DAMPs, are endogenous peptides actively released by the plant during the immune response (Rzemieniewski & Stegmann, 2022). For example, upon damage the plant elicitor peptide 1 (Pep1) is released from its precursor protein by a Ca^{2+}-dependent metacaspase MC4 and detected by receptor-like kinases PEP receptor 1 and 2 (PEPR1 & 2) (Hander *et al.*, 2019; Huffaker *et al.*, 2006; Shen *et al.*, 2019; Yamaguchi *et al.*, 2010). Another example of a phytocytokine is the *Zea mays* immune signaling peptide 1 (Zip1) (Koenig *et al.*, 2023; Ziemann *et al.*, 2018), which was recently shown to be released by the Ca^{2+}-dependent metacaspase ZmMC9 and is detected by a yet unknown receptor (König, 2024). These phytocytokines often are signals which have also functions in development and have been hypothesized to play a role in cell to cell communication (Rzemieniewski & Stegmann, 2022).

Importantly, the simultaneous presence of signals from different origins is crucial. It has been shown that both MAMPs perception and tissue damage are required by the plant to trigger a localized immune response, which is favorable for the plant as it would spare commensals in contrast to pathogens, which cause cell damage (Zhou *et al.*, 2020). In contrast to MAMPs, phytocytokines do not induce cell death as

an immune response upon wounding, indicating that the activated immune responses of MAMPs are similar but also in parts antagonistic (Koenig *et al.*, 2023).

In the second branch of immunity, effector-triggered immunity (ETI), effectors are recognized by the plant and trigger a strong immune response. Effectors are proteins secreted by microbes to modulate the host cell, e.g. the immune system but also developmental and other processes (Remick *et al.*, 2023). These effectors can be recognized by nucleotide-binding leucine-rich repeat-containing receptor (NLR) proteins, which are encoded by resistance genes (R-genes) (Jones *et al.*, 2016). Many of these NLRs have been shown to form effector-activated oligomers (resistosomes) and to act as nonselective Ca^{2+}-permeable ion channel (Chai *et al.*, 2023). However, besides effectors also the effector targets (guardees) or alternative targets (decoys) can be monitored by these receptors (Ngou *et al.*, 2022). The detection of effectors often initiates a localized cell death (hypersensitive) response at the site of infection limiting the spread of pathogens (Shepherd *et al.*, 2023). For example, the NLR ZAR1 (HOPZ-ACTIVATED RESISTANCE1) recognizes *P. syringae* acetyltransferase effector HopZ1a (Lewis *et al.*, 2010; Ma *et al.*, 2006). HopZ1a was shown to acetylate the pseudokinase ZED1 (hopZ-ETI-deficient1) thereby acting as decoy mimicking kinases targeted by HopZ1a such as MAPK Kinase7 (MKK7) (Bastedo *et al.*, 2019; Lewis *et al.*, 2013; Rufián *et al.*, 2021). More effectors targeting ZED1-like kinases were afterwards identified and shown to trigger ZAR1-mediated ETI (Laflamme *et al.*, 2020; Seto *et al.*, 2017; Wang *et al.*, 2015). Upon detection of effectors, ZAR1 forms pentameric resistosomes in the plasma membrane causing Ca^{2+} influx followed by perturbation of subcellular structures, ROS production, and HR (Bi *et al.*, 2021).

Even though both immunity branches, PTI and ETI, are activated differently and require different components, there is strong evidence that both immune signals converge into similar downstream responses and their interplay often potentiates defenses (Chai *et al.*, 2023; Feehan *et al.*, 2023; Yuan *et al.*, 2021).

1.2. Proteases as the first line of defense in plant immunity

1.2.1. The role of proteases in plant immunity

All organisms including viruses have proteases stressing their importance for life (Liu *et al.*, 2024c). For instance, plants have a high number of proteases encoded in their genomes (Rawlings *et al.*, 2014; Van Der Hoorn, 2008). The enzymatic function of proteases is the hydrolysis of peptide bonds, either cleaving substrates internally (endopeptidases), N-terminally (aminopeptidases) or C-terminally (carboxypeptidases). Since this enzymatically catalyzed reaction is irreversible, their activity is usually highly substrate specific and regulated (Van Der Hoorn, 2008). All proteases can be grouped in clans, depending on their catalytic residue which acts as nucleophile in the hydrolysis reaction: cysteine peptidase (e.g. papain-like cysteine proteases or metacaspases), serine peptidases (e.g. subtilases), aspartic peptidase, metallopeptidase, glutamic peptidase, threonine peptidase, asparagine lyase and peptidases of mixed catalytic type (Rawlings *et al.*, 2014).

Plant proteases have been shown to have essential functions in immunity but also in development and other processes (Liu *et al.*, 2024c). Moreover, many proteases are secreted into the apoplast and are thereby at the frontline of the plant defense (Van Der Hoorn, 2008). In plant immunity their function can be categorized in four major groups (Figure 2) (Liu *et al.*, 2024c):

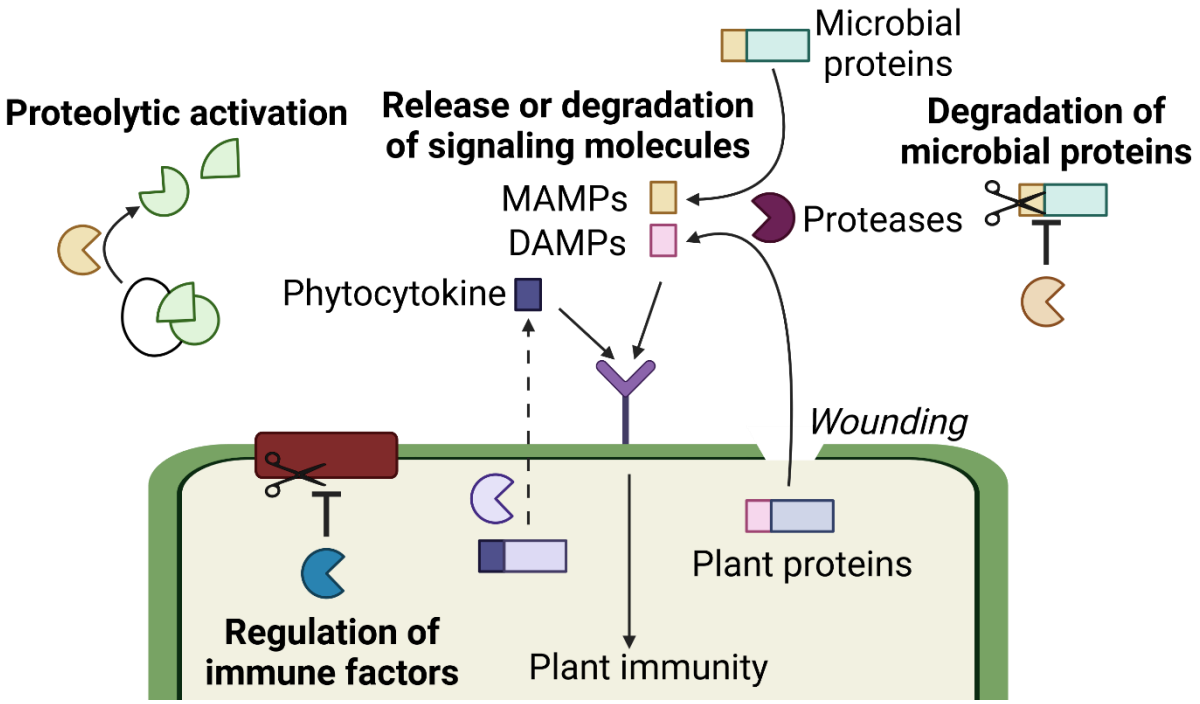

Figure 2: Functions of proteases in plant immunity.

The functions of proteases in plant immunity can be divided into four groups: First, proteases can degrade pathogen proteins thereby inactivating them. Secondly, proteases can activate other host immune proteins, e.g. by removal of the inhibitory domain of proteases. Third, proteases can regulate the stability of immune factors thereby regulating their activity. Fourth, proteases can release signaling molecules from plant and microbial precursor proteins. Phytocytokines are actively released and transported to the apoplast, whereas DAMPs are released into the apoplast from leaking cells during wounding. MAMPs are released from microbial proteins. These signaling molecules can be detected by immune receptors and trigger plant immunity. Furthermore, proteases can also degrade signaling molecules.

The first function is the degradation of pathogen proteins. For example, the bacterial periplasmic serine endoprotease MucD is cleaved by *Arabidopsis thaliana* SECRETED ASPARTIC PROTEASE 1 and 2 (SAP1 and SAP2) during *P. syringae* infection reducing bacterial growth (Wang *et al.*, 2019b). Another example are phytaspases (Asp-specific subtilases) inactivating *Agrobacterium tumefaciens* (*A. tumefaciens*) effector VirD2, which is required for the transport of T-DNA to the nucleus (Reavy *et al.*, 2007).

The second function is the activation of host immune proteins by proteolytic activation. Many proteases are activated by self-cleavage or by another protease. An example is the activation of the tomato cysteine protease Rcr3 which is activated by the subtilase P69B (Paulus *et al.*, 2020). Another example is the regulation of the activity of receptor-like kinase BAK1 by calcium-dependent cleavage (Zhou *et al.*, 2019).

A third function is the regulation of the stability and thereby the activity of other immune factors. For example, XYLEM CYSTEINE PROTEASE 1 (XCP1) is responsible in *A. thaliana* vacuoles for the degradation of RESPIRATORY BURST OXIDASE HOMOLOG D (RBOHD) (Liu *et al.*, 2024b), which is required for the generation of ROS during PTI (Miller *et al.*, 2009). Therefore, XCP1 is an important factor avoiding harmful production of ROS when it is not needed. Upon infection with *P. syringae*, the protease inhibitor CYSTATIN 6 (CYS6) is upregulated and inhibits XCP1 activity thereby stabilizing RBOHD resulting in ROS production (Liu *et al.*, 2024b).

The fourth function of proteases in plant immunity is the release or degradation of signaling peptides. Two examples mentioned before are the release of the phytocytokines Pep1 and Zip1 by metacaspases (Hander *et al.*, 2019; König, 2024) or the release of the MAMP flg22 by proteases, although which protease is responsible for the release not clear yet (Buscaill *et al.*, 2019, 2024; Matsui *et al.*, 2024). Notably, bacteria protect the flg22 epitope region in flagellin by O-glycans to avoid cleavage by proteases, therefore plants employ glycosidase β-galactosidase 1 (BGAL1) removing these O-glycans prior to proteolytic cleavage (Buscaill *et al.*, 2019). Besides, there are many more protease-released signaling peptides reported (Rzemieniewski & Stegmann, 2022), as for example the release of CAP-derived peptide 9 (CAPE9) from PATHOGENESIS-RELATED 1 (PR1) by XCP1 activating antimicrobial and anti-herbivory responses (Chen *et al.*, 2023, 2014). In addition to the release of immune signaling peptides, also the degradation of immune peptides has been hypothesized, for example the inactivation of Zip1 by cysteine proteases of maize (König, 2024) or of csp22 by subtilases of *Nicotiana benthamiana* (Chen *et al.*, 2024a). Also pathogen use proteases to avoid recognition by their host: The flg22 peptide of *Pseudomonas* can be degraded by the bacterial metalloprotease AprA preventing PTI activation (Bardoel *et al.*, 2011).

1.2.2. Papain-like cysteine proteases as key players in plant immunity

A key player in plant immunity are papain-like cysteine proteases (PLCPs) (Misas-Villamil *et al.*, 2016; Shindo & Van der Hoorn, 2008). PLCPs belong to the family C1 clan CA (CA: peptidases with structures similar to papain) (Rawlings *et al.*, 2014) and are named after the namesake member papain from the

plant *Carica papaya* (Turk *et al.*, 1997; Wurtz & Bouchut, 1879). Besides being found in plants, PLCP are also found in all other phylogenetic groups except fungi (Rawlings *et al.*, 2014). Plant PLCPs are endo- and exo-peptidases and are further classified into nine subfamilies based on their phylogeny (Richau *et al.*, 2012). They are usually 25-35 kDa in size (Misas-Villamil *et al.*, 2016), localized inside the cell (family C1B) or in the apoplast (family C1A), and contain a catalytic Cys-His-Asn triad in their protease domain (Liu *et al.*, 2018a; Richau *et al.*, 2012).

Furthermore, they have an auto-inhibitory prodomain and can be activated auto-catalytically or by other proteases as mechanism to prevent unwanted degradation of targets (Richau *et al.*, 2012). Further regulation of their activity can be achieved by transcriptional and post-translational regulation, their localization, pH and by inhibitors (Fernández-Fernández *et al.*, 2023; Lampl *et al.*, 2013; Martínez *et al.*, 2012; Martinez & Diaz, 2008; Richau *et al.*, 2012; van der Linde *et al.*, 2012a, 2012b; Verma *et al.*, 2016). Some precursors contain different motifs that allow them to be transported to distinct locations in the cell such as a signal peptide for secretion into the apoplast, a C-terminal KDEL motif for transport to the endoplasmic reticulum or a N-terminal NPIR motif for vacuolar localization (Richau *et al.*, 2012). Some PLCPs of the subfamilies RD21-like and XBCP3-like additionally have a proline-rich region followed by a granulin domain, which was shown in animals to be a growth hormone and to be released after wounding. However, this domain is autocatalytically removed in plants and its function is yet unknown (Bateman & Bennett, 1998; Gu *et al.*, 2012; Richau *et al.*, 2012; Yamada *et al.*, 2001).

Apoplastic PLCPs are known to be hubs in plant immunity and were hypothesized to release DAMPs and/or MAMPs from endogenous and microbial proteins, respectively (Misas-Villamil *et al.*, 2016; Shindo & Van der Hoorn, 2008). They have been shown to be up-regulated and accumulate at infection sites during plant-pathogen interactions and wounding (Avrova *et al.*, 1999; Azarkan *et al.*, 2006; El Moussaoui *et al.*, 2001; Krüger *et al.*, 2002; Pechan *et al.*, 2000; Rooney *et al.*, 2005; Tian *et al.*, 2007). Protease depletion often makes plants more susceptible to pathogens, e.g. *A. thaliana* lacking the PLCP RD21A (Responsive to Dehydration 21A) infected with the necrotrophic fungus *Botrytis cinerea,* the root-knot nematode *Meloidogyne incognita,* and the bacterial pathogen *Pseudomonas syringae* pv. *tomato* (*Pst*) DC300 becomes more susceptible to infection (Shindo *et al.*, 2012; Yu *et al.*, 2024). Furthermore, C14

protease silencing in *Nicotiana benthamiana* showed increased susceptibility after infection with the oomycete *Phytophthora infestans* (Bozkurt *et al.*, 2011; Kaschani *et al.*, 2010). Moreover, *Solanum lycopersicum* lacking the PLCP Rcr3 (required for *Cladosporium fulvum* resistance 3) and infected with *P. infestans* also showed higher susceptibility to the pathogen (Ilyas *et al.*, 2015; Song *et al.*, 2009). Likewise, the overexpression of PLCPs has been shown to increase resistance of different plants to different pathogens (Bozkurt *et al.*, 2011; Li *et al.*, 2024a; Liu *et al.* 2024a; Niño *et al.*, 2020; Zeng *et al.*, 2023). However, it also has been observed that the lack of a PLCP might contribute to the susceptibility to one pathogen but not to others (Shindo *et al.*, 2012), indicating either redundancy of PLCP function or differential effects depending on the pathogen's lifestyle. Many more examples have been reported for other plants infected with a variety of pathogens, confirming the role of PLCPs as central components in plant immunity (Misas-Villamil *et al.*, 2016).

1.2.3. Modulation of PLCPs by microbial effectors

Since proteases are hubs in plant immunity, a variety of microbes employ effectors which modulate the activity of PLCPs to overcome the activation of immune responses (Misas-Villamil *et al.*, 2016). There are over 20 families of proteinaceous inhibitors of cysteine proteases categorized by their amino acid sequence similarities, but only few of those have been shown yet to inhibit plant PLCPs (Rawlings *et al.*, 2014):

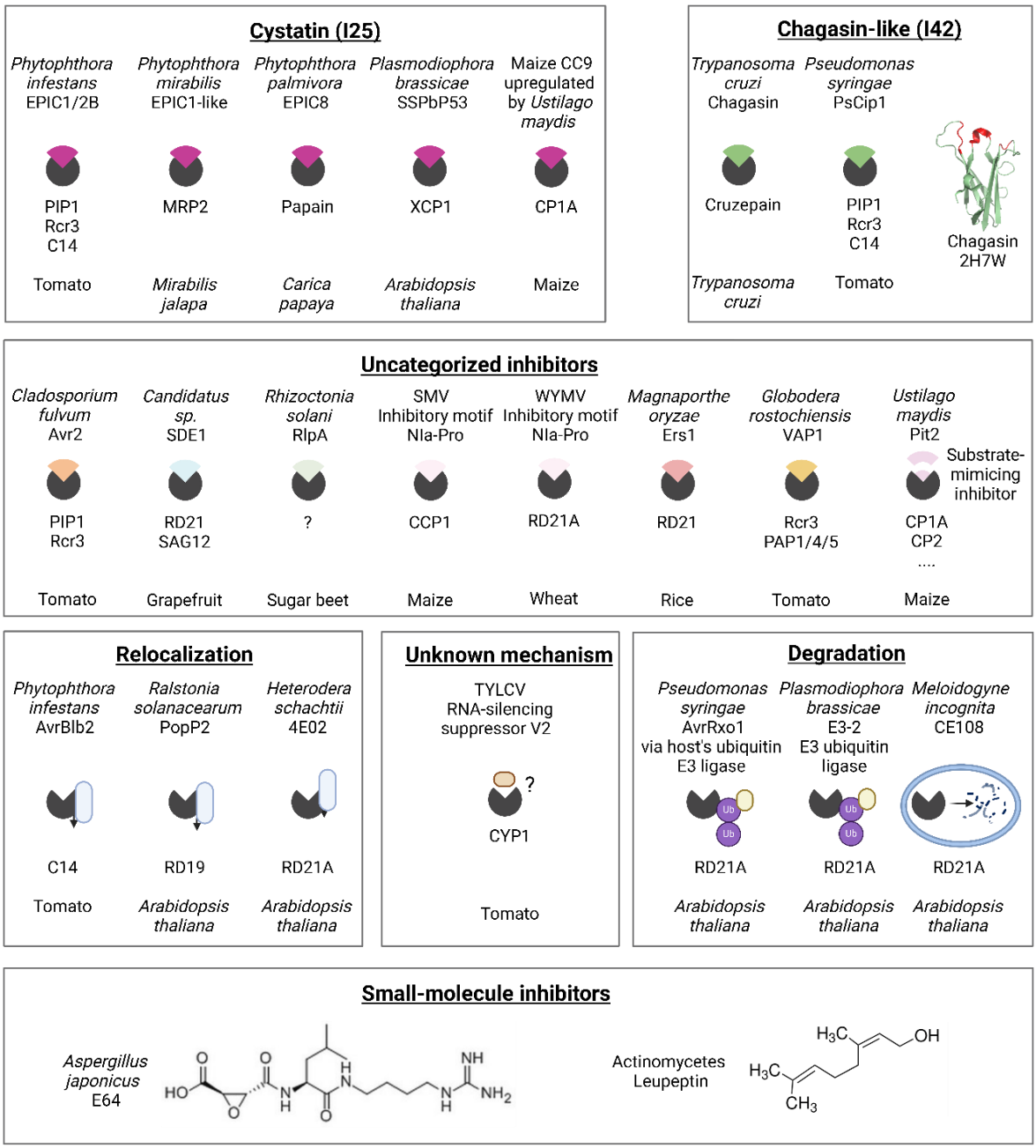

Figure 3: Suppression of papain-like cysteine proteases (PLCPs).

Examples of molecules that suppress the activity of PLCPs via different mechanisms: Cystatins (I25) and chagasin-like inhibitors (I42) are competitive reversible inhibitors tightly binding to their target PLCPs (Balbinott & Margis, 2022; Costa & Lima, 2016). Other inhibitors directly inhibiting PLCPs are not yet categorized, e.g. Avr2 or Pit2 (Misas Villamil *et al.*, 2019; Mueller *et al.*, 2013; Shabab *et al.*, 2008; Van Esse *et al.*, 2008). For other suppressors the mechanism of inhibition is not known, e.g. the RNA-silencing suppressor V2 of tomato yellow leaf curl geminivirus (TYLCG) (Bar-Ziv *et al.*, 2012). Also, small molecule inhibitors can strongly inhibit PLCPs, e.g. E64 or Leupeptin (Hanada *et al.*, 1978; Kondo *et al.*, 1969). In contrast to a direct inhibition, PLCP activity can also be suppressed by relocalization or degradation (Bernoux *et al.*, 2008; Bozkurt *et al.*, 2011; Li *et al.*, 2023; Liu *et al.*, 2020; Pogorelko *et al.*, 2019; Yu *et al.*, 2024). Abbreviations: sugarcane mosaic virus (SMV), tomato yellow leaf curl geminivirus (TYLCV), wheat yellow mosaic virus (WYMV).

Cystatins (family I25) are competitive reversible inhibitors which tightly bind to PLCPs (Figure 3). They have five antiparallel beta sheets and a central alpha-helix, with the resulting loops blocking the active site of the protease (Balbinott & Margis, 2022; Benchabane *et al.*, 2010). This family is further divided into stefins, cystatins, and kininogens (Tušar *et al.*, 2021). There are many examples of cystatins playing a role in plant-microbe interactions: The oomycete and potato late blight pathogen *P. infestans* secrets the cystatin-like extracellular proteinase inhibitor C1 (EPIC1) and C2B (EPIC2B), which inhibit the PLCP *Phytophthora* Inhibited Protease 1 (PIP1), Rcr3 and C14 of tomato (Kaschani *et al.*, 2010; Kaschani & van der Hoorn, 2011; Song *et al.*, 2009; Tian *et al.*, 2007). Closely related *Phytophthora mirabilis* was also shown to use a secreted EPIC1-like protease inhibitor during infection of *Mirabilis jalapa* to inhibit *Mirabilis* RCR3-like protease 2 (MRP2) (Dong *et al.*, 2014). Similar inhibition of papain in *Carica papaya* by EPIC8, a cystatin-like inhibitor of another *Phytophthora* relative, was reported to contribute to virulence (Gumtow *et al.*, 2018). Also other species use cystatin-like inhibitors: The parasitic protist *Plasmodiophora brassicae* inhibits *A. thaliana* XYLEM CYSTEINE PEPTIDASE 1 (XCP1) with its cystatin-like SSPbP53 thereby contributing to club root disease (Pérez-López *et al.*, 2021). Pathogens not only employ their own inhibitors of PLCPs, but they can also utilize endogenous inhibitors of their host plants for modulation of PLCPs: For example, the Corn Cystatin-9 (CC9) is a compatibility factor induced upon penetration of maize by the biotrophic pathogen *Ustilago maydis* and inhibits maize PLCPs (van der Linde *et al.*, 2012a, 2012b).

Chagasin-like inhibitors (family I42) are competitive reversible inhibitors with an inhibitory constant in the nanomolar range and showed a broad-spectrum inhibition of different PLCPs (Figure 3) (Costa & Lima, 2016). They have an immunoglobulin fold (Costa & Lima, 2016; Redzynia *et al.*, 2009) which also contains conserved chagasin motifs in their three exposed loops (NPTTG, GxGG and (Q/R)PW) (dos Reis *et al.*, 2008; Shindo *et al.*, 2016), which are essential to block the PLCP active site (Redzynia *et al.*, 2008, 2009). Chagasin is a highly potent PLCP inhibitor found in the protozoan intracellular parasite *Trypanosoma cruzi* causing the chagas disease, but orthologs were also identified in other protozoan (Besteiro *et al.*, 2004; Costa *et al.*, 2022; dos Reis *et al.*, 2008; Monteiro *et al.*, 2001; Santos *et al.*, 2005; Uehara *et al.*, 2012; Wang *et al.*, 2007). Chagasin regulates the activity of the

endogenous PLCP cruzipain of *T. cruzi*, which is important for the parasitic infection (Monteiro *et al.*, 2001; Santos *et al.*, 2005; Uehara *et al.*, 2012; Wang *et al.*, 2007). This inhibitor class has so far shown to suppress only the activity of proteases of the C1 family (PLCPs) (Costa & Lima, 2016; Kantyka *et al.*, 2010). Chagasin-like inhibitors were also identified in other protozoa, but also in some bacteria and archaea (Costa & Lima, 2016). Another example of a chagasin-like inhibitor is the *P. syringae* C14-inhibiting protein 1, PsCip1, which inhibits the secreted immune protease C14 of tomato and was found to be conserved in most Pseudomonads (Shindo *et al.*, 2016).

There are also some inhibitors not assigned to any families yet (Figure 3): The Avr2 effector of the fungal pathogen *Cladosporium fulvum* inhibits Rcr3 and PIP1 of tomato, however does not show similarity to any other inhibitors (Krüger *et al.*, 2002; Shabab *et al.*, 2008). Another example for a yet unassigned inhibitor is the PLCP inhibitor UmPit2 (Proteins important for tumors 2) of the smut fungus *U. maydis*, which is an essential core effector for maintaining fungal biotrophy (Doehlemann *et al.*, 2011; Mueller *et al.*, 2013) and contains an inter-kingdom conserved 14 amino acid motif (PID14) acting as a substrate mimicking molecule inhibiting apoplastic maize PLCPs (Misas Villamil *et al.*, 2019; Mueller *et al.*, 2013). Based on the PID14 sequence, an inhibitory inter-kingdom motif, termed conserved microbial inhibitor of proteases (cMIP), could be found in several plant associated fungi and bacteria (Misas Villamil *et al.*, 2019). Furthermore, the Sec-delivered effector 1 (SDE1) of the bacterium *Candidatus* Liberibacter asiaticus was shown to inhibit citrus PLCPs during citrus greening disease and thereby promoting bacterial infection (Clark *et al.*, 2018, 2020). Additionally, the soil-borne bacterial pathogen *Rhizoctonia solani* (Rs) employs the secreted rare lipoprotein A (RsRlpA) with a double-psi beta-barrel fold to inhibit sugar beet PLCPs suppressing ROS burst and HR (Charova *et al.*, 2020). Similarly, an inhibitory motif identified in the cysteine proteases (family C4) NIa-Pro of sugarcane mosaic virus (SMV) and wheat yellow mosaic virus (WYMV) were found to target maize and wheat PLCPs, respectively, and to contribute to the virulence of the viruses (Liu *et al.*, 2023; Yuan *et al.*, 2024). Another recent example is the secreted effector MoErs1 of the rice blast fungus *Magnaporthe oryzae* inhibiting the activity of rice papain-like cysteine protease OsRD21 leading to reduced ROS accumulation and increased virulence (Liu *et al.*, 2024a). All mentioned inhibitors have no similarity to

the well characterized inhibitor families involved in plant-microbe interactions highlighting the widespread evolution of novel mechanisms of PLCP inhibition.

Additionally, small-molecule inhibitors such as the irreversible PLCP inhibitor E64 produced by the Ascomycete *Aspergillus japonicus* (Barrett *et al.*, 1982; Hanada *et al.*, 1978; Matsumoto *et al.*, 1989; Varughese *et al.*, 1989) or the reversible cysteine and serine protease inhibitor leupeptin produced by Actinomycetes (Aoyagi *et al.*, 1969; Kondo *et al.*, 1969; McConnell *et al.*, 1993) have been mechanistically well characterized and are widely used in experimental biology (Figure 3), but they have not been investigated in in planta interactions yet.

There are also other ways to modulate PLCP activity than by direct inhibition, for example by the relocalization of PLCPs preventing access to their substrate(s) or by degradation of the PLCPs (Figure 3): An example is the prevented secretion of tomato C14 by an effector of *P. infestans*, AvrBlb2 (Bozkurt *et al.*, 2011). Another example is the relocalization of *A. thaliana* RD19 (Responsive to Dehydration 19) to the nucleus by the bacterial *Ralstonia solanacearum* PopP2 (*Pseudomonas* outer protein P2) effector during bacterial wilt (Bernoux *et al.*, 2008). Similarly, the effector 4E02 of the sugar beet cyst nematode *Heterodera schachtii* relocalized *A. thaliana* RD21A from the vacuole to the nucleus and the cytoplasm (Pogorelko *et al.*, 2019). Another strategy was shown for *P. syringae* infecting *A. thaliana* under draught conditions, here the degradation of a PLCP was induced: The bacterial type III effector AvrRxo1 enhanced the activity of the host's ubiquitin E3 ligase SINAT4 (SEVEN IN ABSENTIA 4), thereby inducing the degradation of RD21A (Liu *et al.*, 2020). The protist *Plasmodiophora brassicae* employs the Really Interesting New Gene (RING)-type E3 ubiquitin ligase 2 (PbE3-2) and two other secreted RING-type E3 ubiquitin ligases, which also ubiquitinate RD21A leading to degradation of the PLCP, reducing the ROS burst and SA signaling thereby increasing susceptibility (Li *et al.*, 2023). Likewise, the root-knot nematode *Meloidogyne incognita* also employs a venom allergen-like protein (VAP1)-like PLCP inhibitor suppressing PTI by promoting the degradation via the endosomal-dependent pathway (Yu *et al.*, 2024), while a perturbation of the active site of tomato Rcr3 by PLCP inhibitor GrVAP1 of the root rot nematode *Globodera rostochiensis* was hypothesized as inhibition mechanism (Lozano-Torres *et al.*, 2012, 2014). Moreover, the RNA-silencing suppressor V2 from

the tomato yellow leaf curl geminivirus was shown to suppress PLCP activity, however its mechanism of modulation is yet not fully understood (Bar-Ziv *et al.*, 2012, 2015).

All these examples show how important it is for microbes to suppress plant PLCPs to modulate immunity. Notably, most described examples of PLCP modulation are from interactions of plants with foliar pathogen, but not much is known about whether the modulation of PLCP activity is also a strategy employed by non-pathogenic plant colonizers. The only example indicating that this strategy also applies to beneficial microbes can be found in the close symbiotic interaction of the grass *Lolium perenne* with its endophytic fungus *Epichloë festucae*, where PLCP activity was shown to be suppressed during the mutualistic association with the fungus *Epichloë festucae* (Passarge *et al.*, 2021). Apart from this example, it is yet unknown whether beneficial or commensal microbes modulate PLCPs to achieve symbiotic interactions, and especially how this is facilitated in more complex interactions on the roots. Besides this, the current knowledge about bacterial PLCP suppression is so far limited to three known inhibitors: PsCip1, SDE1 and AvrRxo1 (Figure 3) (Clark *et al.*, 2018, 2020; Liu *et al.*, 2020; Shindo *et al.*, 2016).

To respond to the inhibitor-mediated PTI-suppression by pathogens, plants also evolved another strategy: PLCPs can be used by plants as a co-receptor for recognition of some effectors by NLRs (Misas-Villamil *et al.*, 2016), as was shown for the recognition of tomato Rcr3 in complex with the PLCP inhibitors Avr2 of *C. fulvum* or GrVAP1 of root parasitic nematode *G. rostochiensis*. These complexes were recognized by the NLR Cf-2, resulting in resistance to the pathogens (Lozano-Torres *et al.*, 2012, 2014; Paulus *et al.*, 2020; Rooney *et al.*, 2005).

1.2.4. Apoplastic maize PLCPs as part of the salicylic acid triggered immune response

In maize leaves, five apoplastic PLCPs are activated by the phytohormone SA (Schulze Hüynck *et al.*, 2019; van der Linde *et al.*, 2012a; Ziemann *et al.*, 2018): the RD21A-like CP1A and CP1B, the Cathepsin B-like CathB, the XCP1-like Xylem Cysteine Protease 2 (XCP2), and the AALP-like Cysteine Protease 2 (CP2) (van der Linde, Hemetsberger, *et al.*, 2012). Especially the RD21A-like PLCP family was previously shown to be targeted by pathogens, e.g. in maize by the smut fungus *U. maydis* (Mueller *et al.*, 2013) or in tomato by *P. syringae* (Shindo *et al.*, 2016). In

contrast, in the maize root apoplast the activity of the three PLCPs THI1-like (B4FS65), RD19A-like (Q10716), and XBCP3-like (B4FYA3) was significantly increased upon treatment with SA (Schulze Hüynck *et al.*, 2019). However, also many other PLCPs have been shown to be highly abundant and active independent of SA treatment, as for example RD21A-like (Schulze Hüynck *et al.*, 2019). So far, the function of SA-activated root PLCPs in plant immunity of *Z. mays* is unknown (Schulze Hüynck *et al.*, 2019). Little is known from their role in other plants, but also maize: Maize RD19A-like was recently proposed to be specifically activated 24 hours after the treatment of maize leaves with the mycotoxin Fumonisin B1 or the detection of the avirulent effector AvrRxoI by the NLR RxoI (reaction to *Xanthomonas oryzae* pv. *oryzicola*) which trigger cell death in maize (Barghahn *et al.*, 2023). Besides being activated by SA in roots, RD19A-like expression has been shown to be upregulated in maize leaves upon treatment with SA and the phytocytokines Zip1 and SIGGI (Katzy, 2025, in prep.). Homologs of RD19A-like are involved in *A. thaliana* immunity and targeted by the *Ralstonia* effector PopP2 (Bernoux *et al.*, 2008). Recently, RD19A in *A. thaliana* was reported to be associated with PHYTOALEXIN DEFICIENT 4 (PAD4), which has a crucial function in pathogen resistance in complex with ENHANCED DISEASE SUSCEPTIBILITY 1 (EDS1) and promoted EDS1- and PAD4-mediated ETI (Dongus & Parker, 2021; Zeng *et al.*, 2023). Overexpression of RD19A led to EDS1- and PAD4-dependent autoimmunity and increased resistance against pathogens. Furthermore, PAD4 promoted nuclear accumulation of processed forms of RD19A (Zeng *et al.*, 2023). Additionally, RD19A-mediated immune activation was shown to depend on BRASSINOSTEROID-SIGNALING KINASE1 (BSK1), an interactor of FLS2 and which positively regulates plant innate immunity (Li *et al.*, 2024a). Unlike RD19A-like, less is known for THI1-like and XBCP3-like PLCPs and their role in immunity. The THI1-like cysteine protease 51, CP51, of *A. thaliana* is highly expressed in flowers (Richau *et al.*, 2012) and is essential for pollen exine formation and anther development (Yang *et al.*, 2014). The XBCP3-like CP14 was proposed to be involved in programmed cell death in *Nicotiana benthamiana* during development (Paireder *et al.*, 2016).

1.3. Aims of this study

PLCPs are central modulators of plant immunity. Therefore, they are targeted by a variety of pathogens thereby suppressing protease activity and also immunity. So far there has been more focus on plant-pathogen interactions and mostly on infections in aerial parts. However, there is a lack of research on the role of proteases and their inhibitors in complex microbial interactions below ground, especially on bacterial inhibitors. Furthermore, research on protease inhibitors has primarily focused on model plants such as *A. thaliana* or tomato.

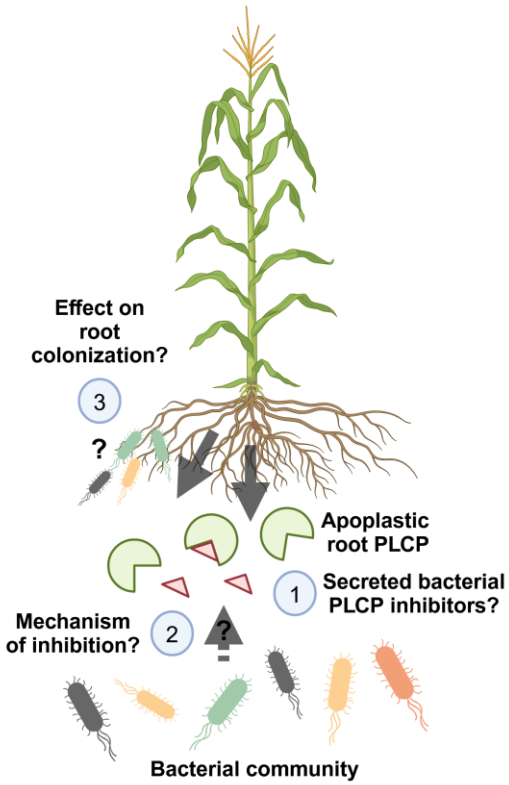

Figure 4: Working hypothesis: Non-pathogenic bacteria also secrete inhibitors to modulate PLCP activity.

Apoplastic root PLCPs, such as the SA-activated RD19A-like, THI1-like, and XBCP3-like but also the immunity-related CP1A have been shown to be active in the maize root apoplast (Schulze Hüynck *et al.*, 2019). Different pathogens target PLCPs to modulate plant immunity (Misas-Villamil *et al.*, 2016). However, there is still much to learn about, whether non-pathogenic bacteria use similar strategies, such as the secretion of PLCP inhibitors. In this thesis we hypothesize that also non-pathogenic bacteria colonizing the maize root secret inhibitors to modulate PLCP activity and thereby allowing their successful colonization of the root. Therefore, this thesis aims to answer the following questions: (1) Do non-pathogenic bacteria also produce protease inhibitors to suppress PLCP activity? (2) How can the bacterial PLCP inhibitor perform its function? (3) Which role do the identified inhibitor(s) have in the colonization of the individual root colonizing bacteria and in complex interactions between the plant and a bacterial community?

I hypothesize that also non-pathogenic microorganisms use similar strategies as pathogens to modulate PLCP activity and promote host colonization (Figure 4). My first question was therefore whether non-pathogenic bacteria also produce protease inhibitors to suppress PLCP activity (Figure 4, Question 1). To answer this question, I screened maize root colonizing bacteria for the inhibition of SA-activated root PLCPs of maize and tried to identify the putative inhibitor(s) with various methods ranging from computational analysis (Sequence-homology searches and AlphaFold Multimer modeling) to biochemical studies (Pulldown and affinity chromatography with papain, as well as size-based separation of secreted proteins, followed by proteomics).

My second question was how the bacterial PLCP inhibitor can perform its function (Figure 4, Question 2). Therefore, we characterized the identified (putative) inhibitor(s) for their inhibition spectrum and mode of action. A major focus was on how the bacterial inhibitor comes into contact with its target. Therefore, we used biochemical cell fractionation methods, fluorescence microscopy with the fluorophore-tagged inhibitor and attempted to perform immunogold-labeling with transmission electron microcopy to determine its localization.

My last question was which role the identified inhibitor(s) have in the colonization of the individual root colonizing bacteria and in complex interactions between the plant and a bacterial community (Figure 4, Question 3). Therefore, knock-out mutants lacking the inhibitor were generated and their performance in root colonization was evaluated in *A. thaliana* and maize, in the case of maize also as part of a bacterial community.

2. Results

2.1. Modulation of PLCPs by commensal bacteria

2.1.1. Screening of bacterial supernatants for PLCP inhibition

I hypothesized that similar to pathogens also non-pathogenic microorganisms use secreted PLCP inhibitors to modulate PLCP activity and promote host colonization (Figure 4). To assess whether bacterial commensals secrete PLCP inhibitors, supernatants of the seven-member maize synthetic community (SynCom) were tested in an activity assay for their ability to inhibit apoplastic root PLCPs using the synthetic substrate Z-LR-AMC. The substrate Z-LR-AMC, which contains the amino acids Leu-Arg has previously been demonstrated to be a suitable substrate for maize root PLCPs (Schulze Hüynck, 2019). Upon cleavage of the substrate, the fluorescence of the released 7-amino-4-methylcoumarin (AMC) increases and can thereby be used as a readout for protease activity (Kanaoka *et al.*, 1982). First, root apoplastic fluid (RAF) was extracted from SA-treated maize roots and PLCP activity was monitored with the PLCP-specific probe MV201 (Richau *et al.*, 2012) using activity-based protein profiling (ABPP) (van der Hoorn *et al.*, 2004). This experiment revealed at least three prominent bands at approximately 25, 30 and 35 kDa, confirming the activation of root PLCPs in these samples (Suppl. Fig. 1). Subsequently, culture supernatants from each individual SynCom member were incubated in minimal medium and collected after 24 hours of incubation. To enhance the protein concentration of the bacterial culture supernatants, the supernatants were concentrated using centrifugal concentrator columns with a molecular weight cut-off (MWCO) of 5 kDa. Additionally, the separation of the supernatant according to molecular weights allowed to distinguish the effects caused by the high-molecular weight fraction (HMWF), which mainly contained proteinaceous inhibitors, from the effects caused by the low-molecular weight fraction (LMWF), as the concentration of molecules smaller than 5 kDa should be the same in LMWF and HMWF. Therefore, an inhibition caused by putative small molecule inhibitors, peptides, pH changes or changes in the redox status of the tested proteases should be visible in LMWF and HMWF, which is not the case, indicating that the effects observed by HMWF are due to molecules larger than 5 kDa. These two fractionated supernatants (HMWF, >5 kDa) and the flow-through (LMWF, < 5 kDa) were then tested for the inhibition of PLCPs in root apoplastic fluid (Figure 5A).

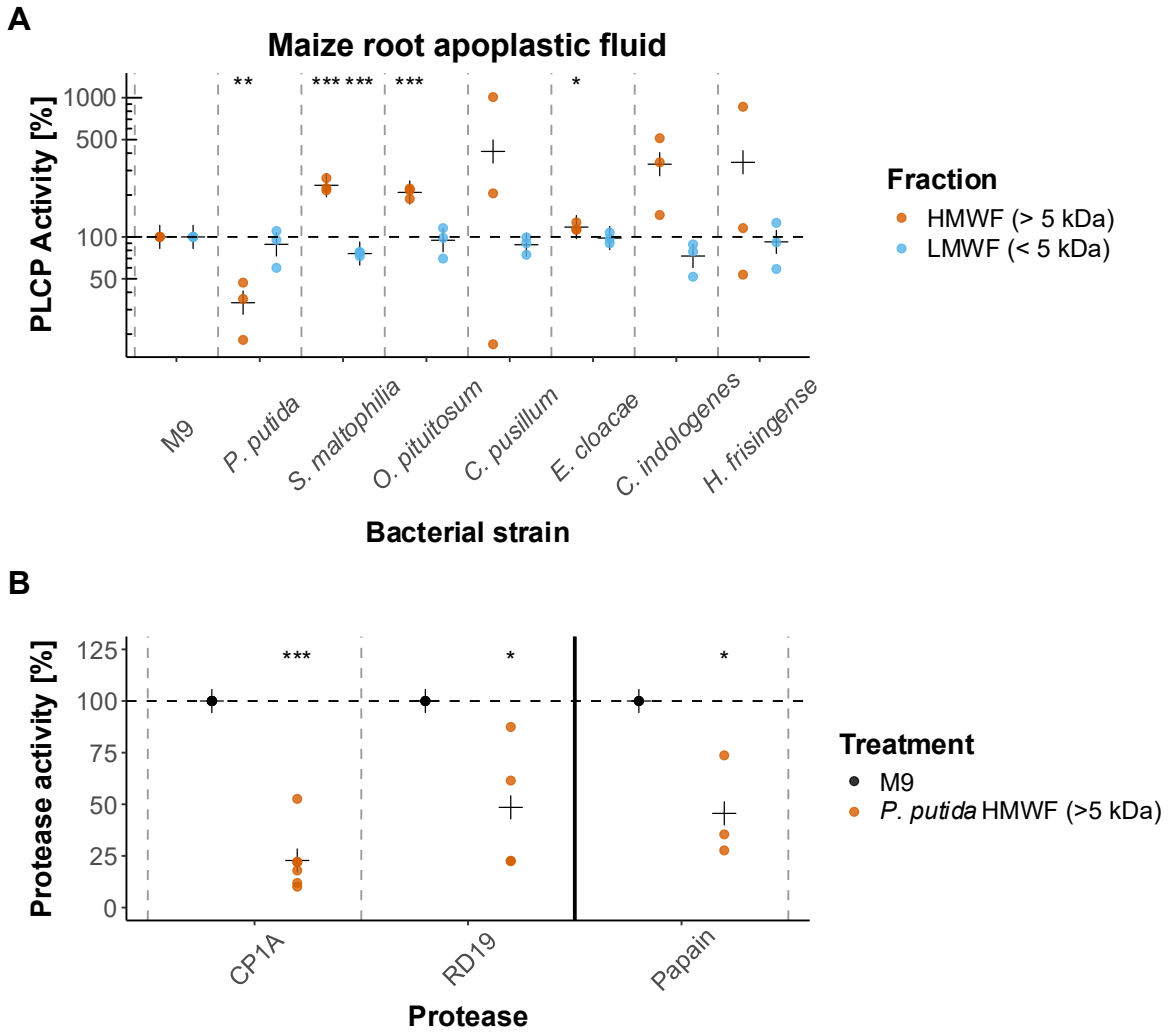

Figure 5: Modulation of PLCP activity of maize root apoplastic fluids by fractions of bacterial culture supernatants.

High-molecular weight fractions (HMWF) and low-molecular weight fractions (LMWF) were collected by concentrating the bacterial culture supernatants 10-folds using a concentrator column (MWCO: 5 kDa). **(A)** SA-treated maize root apoplastic fluid (RAF), **(B)** apoplastic fluids with heterologous expressed CP1A or RD19A-like, or 10 µg/ml Papain were pre-incubated with either M9 media, E64, HMWF or LMWF for 15 minutes. Afterward, the cleavage of the Z-LR-AMC substrate was measured as the increase of AMC fluorescence. After subtracting non-PLCP activity (E64 control), the Z-LR-AMC cleavage activity of each treated sample was normalized to the M9 media control set to 100%. **(B)** The activity of CP1A and RD19A-like was additionally normalized to the *N. benthamiana* background activity ($CP1A_{mut}$-mCherry). These experiments were performed with at least three independent biological replicates (dots) with each having four technical replicates. Means are represented as black crosses. A two-sided t-test was performed ($p<0.05$: *; $p<0.01$: **; $p<0.001$: ***). These results obtained during my Master thesis are published in (Moser, 2021).

A significant PLCP inhibition of 66 % by the HMWF of *P. putida* supernatant was observed (Figure 5A), indicating that the putative inhibitor might be larger than 5 kDa. No significant inhibition by the corresponding LMWF was observed, confirming that neither metabolites, other small molecules nor the pH or redox status can be

responsible for the observed effect. Notably, a 24 % PLCP inhibition by the *S. maltophilia* LMWF was observed (Figure 5A), suggesting an effect by a molecule smaller than 5 kDa which could be a small molecule PLCP inhibitor or could be caused by the alteration of the pH or redox status altering PLCP activity. Furthermore, a significantly increased substrate cleavage activity was observed for supernatants of *S. maltophilia*, *O. pituitosum* and *C. pusillum* (Figure 5A). This increased activity is likely due to substrate cleavage by bacterial proteases present in the supernatants as incubation of the supernatants without the addition of apoplastic fluid showed enzymatic activity (Suppl. Fig. 2).

To test whether the specific SA-activated root PLCPs (RD19A-like, THI1-like, and XBCP3-like) (Schulze Hüynck *et al.*, 2019) can be inhibited by the *P. putida* supernatant, these PLCPs as well as a positive control (the immunity-related RD21-like PLCP, CP1A (van der Linde *et al.*, 2012a)) and a background control (inactive $CP1A_{mut}$-mCherry (Schulze Hüynck, 2019)) were heterologously expressed via *Agrobacterium*-mediated transformation in *Nicotiana benthamiana* leaves using the *Nicotiana tabacum* PR1 signal peptide for apoplastic localization. While some proteases can be easily heterologously produced and purified (Ling *et al.*, 2015; Mueller *et al.*, 2013; Schuster *et al.*, 2022; van Midden *et al.*, 2024), for the root PLCPs and CP1A, this is so far not the case, as purification tags are commonly removed during *in planta* overexpression (Schulze Hüynck, 2019) or proteases recombinantly produced in *E. coli* are not properly folded thus not active after purification (not shown, approach of purification via protocol of (van Midden *et al.*, 2024)). Therefore, heterologously expressed PLCPs isolated from apoplastic fluid of *N. benthamiana* leaves are for now the best option to obtain active PLCPs although not pure, making the enzyme concentration challenging to be quantified.

To confirm the expression and isolation of active PLCPs, apoplastic fluid from these leaves was isolated and the activity of the heterologously expressed PLCPs was tested using the MV201 probe (Richau *et al.*, 2012). Labeling showed prominent bands at approx. 30 and 40 kDa corresponding to the active CP1A and two bands at approx. 30 kDa corresponding to RD19A-like (Suppl. Fig. 3A&C). These bands were not visible in the samples treated with E64 (irreversible and covalent PLCP-specific inhibitor (Hanada *et al.*, 1978)) nor in the background control confirming its specificity (Suppl. Fig. 3A). In contrast, the heterologous expression of active THI1-like and XBCP3-like

was not successful as no prominent bands differing from the controls were observed in the labeling (Suppl. Fig. 3A). To rule out that the activity of TH1-like and XBCP3-like cannot be observed due to less specificity to the MV201 probe, the DCG-04 probe (Greenbaum *et al.*, 2000) containing the same warhead as MV201 probe but bearing a biotin moiety instead of a fluorophore was used for labeling. Labeling of TH1-like and XBCP3-like with DCG-04 did not show specific bands confirming the previous results (Suppl. Fig. 3B) and suggesting that these proteins were either not expressed or not active. To confirm the activity of RD19A-like and CP1A, the substrate Z-LR-AMC was used in a substrate cleavage assay. Both proteases cleave Z-LR-AMC although, RD19A-like cleaved the substrate approx. 18-times less than CP1A, suggesting that RD19A-like cleaves either slower or has a different substrate specificity (Suppl. Fig. 3D). Since RD19A-like might have another substrate specificity than CP1A, Proteomic Identification of Protease Cleavage Sites (PICS) analysis was attempted. Peptide libraries in which primary amines have been protected, are incubated with the active or inactive protease of interest. After proteolytic cleavage primary amines at newly formed and free N-termini will be biotinylated, isolated and identified by mass spectrometry (MS) allowing the identification of cleavage sites (Schilling *et al.*, 2011). This PICS analysis was performed multiple times with active RD19A-like, according to ABPP analysis. However, PICS analysis did not reveal a clear substrate specificity in multiple replicates (not shown, in collaboration with Melissa Mantz and Prof. Dr. Pitter Huesgen from University of Freiburg).

To test whether the SA-activated root PLCP RD19A-like and the immunity-associated CP1A can be inhibited by the *P. putida* supernatant, the inhibition of both heterologously expressed proteases in apoplastic fluid was tested in a substrate cleavage assay with *P. putida* HMWF and LMWF. Inactive $CP1A_{mut}$-mCherry was used as a background control (Schulze Hüynck, 2019). Incubation of *P. putida* HMWF with overexpressed CP1A or RD19A-like in apoplastic fluids resulted in inhibition of both proteases (Figure 5B), confirming the previous results in experiments with root apoplastic fluid and indicating that the putative inhibitor can also inhibit CP1A and RD19A-like. Notably, the HMWF of *P. putida* showed a lower inhibitory effect on RD19A-like, 54 % inhibition, than on CP1A, 77 % inhibition, which could indicate a lower specificity of the putative inhibitor to RD19A-like compared to CP1A. However, since the concentration of active PLCPs in the apoplastic fluid can only be estimated,

this difference in specificity is only speculative. A similar inhibition of papain by *P. putida* HMWF but not by the LMWF was observed (Figure 5B), showing a broad inhibitory effect of *P. putida* supernatants for a spectrum of different PLCPs.

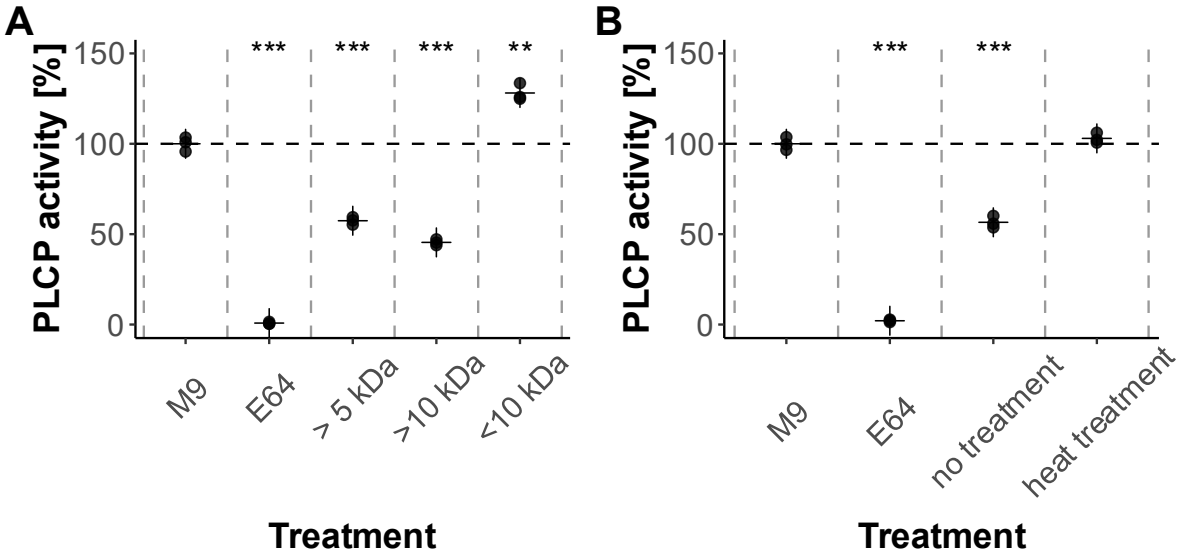

Figure 6: Putative PLCP inhibitor(s) of *P. putida* is proteinaceous.

High molecular weight fractions (HMWF) and low molecular weight fractions (LMWF) were collected by concentrating the bacterial culture supernatant of *P. putida* by 10-fold using a protein concentrator column with a MWCO of 5 kDa or 10 kDa. Furthermore, 5 kDa HMWF was either heat treated for 15 min at 95°C or not. SA-treated maize root apoplastic fluid (RAF) was preincubated with either M9 media, E64, **(A)** HMWF (> 5 kDa), HMWF (> 10 kDa) or LMWF (< 10 kDa), or **(B)** HMWF "no treatment" (not treated with heat) or HMWF "heat treatment" (treated with heat) for 15 minutes. Afterward, the cleavage of the Z-LR-AMC substrate was measured as the increase of AMC fluorescence. The Z-LR-AMC cleavage activity of each treated sample was normalized to the M9 media control set to 100%. The experiment was performed with three technical replicates (dots). Means are represented as black crosses. A two-sided t-test was performed and asterisks indicate significance ($p<0.05$: *; $p<0.01$: **; $p<0.001$: ***).

Substrate cleavage assays with root apoplastic fluid (RAF) using supernatants of *P. putida* filtered using a concentrator column with a MWCO of 10 kDa showed PLCP inhibition with this fraction indicating that the putative secreted inhibitor is larger than 10 kDa (Figure 6A). Besides, upon heat denaturation the supernatant lost its inhibitory capacity (Figure 6B), suggesting that the putative inhibitor is proteinaceous or heat unstable. In conclusion, the *P. putida* HMWF fraction was shown to contain a proteinaceous PLCP inhibitor larger than 10 kDa, which can inhibit apoplastic maize root PLCPs, as well as the immunity-associated CP1A and SA-activated root PLCP RD19A-like *in vitro.*

2.1.2. Identification of PLCP inhibitors in *P. putida* based on sequence homology

To identify the putative inhibitor in the HMWF of *P. putida* that caused the suppression of PLCPs, all predicted *P. putida* proteins were screened for sequence homology to already reported PLCP inhibitors. *P. putida* proteins were predicted *in silico* using the dFAST software (Tanizawa *et al.*, 2016, 2018). Sequences of 2650 proteins classified as cysteine protease inhibitors in the MEROPS database (Rawlings *et al.*, 2014) (Suppl. Table 1) and eight sequences of PLCP inhibitors reported in plant-microbe interactions obtained from a literature search (Suppl. Table 2) were used as queries. These sequences were searched in a protein-protein Basic Local Alignment Search Tool (BLASTp) search via BLAST+ (Altschul *et al.*, 1990; Camacho *et al.*, 2009) against a database containing all predicted *P. putida* proteins. Next, the presence of a signal peptide for secretion was predicted using SignalP5 (Almagro Armenteros *et al.*, 2019). The hits of these searches were filtered based on their similarity to the query and the presence of a signal peptide for secretion (criteria: identity > 20%, query coverage > 20%, presence of signal peptide of the Sec or Tat pathway), and this filtering resulted in 9 remaining hits (Table 1).

Table 1: Inhibitor candidates identified by sequence homology search.

Sequences of PLCP inhibitors derived from MEROPS database or literature search were used as queries in a BLASTp search against all predicted proteins of *P. putida*. BLASTp results were filtered by identity (>20%), query coverage (>20%), and for presence of signal peptide (+). These results were obtained during my Master thesis and published in (Moser, 2021).

Subject	Query	Family	E-value	Identity [%]	Query coverage [%]
Ppu_4597	MER0034541	I39	$0.00x10^{+00}$	53	99
Ppu_0767 (PpCip1)	**PsCip1** [Q87XG7] (*P. syringae*)	I42	$3.75x10^{-55}$	61	97
Ppu_0260	MER0174564	I39	$2.00x10^{-12}$	35	82
Ppu_0767 (PpCip1)	MER0090314	I42	$4.00x10^{-10}$	29	92
Ppu_1612	MER0174564	I39	$2.00x10^{-05}$	36	71
Ppu_2850	MER0174433	I39	$4.00x10^{-05}$	43	40
Ppu_5433	MER0174564	I39	$8.00x10^{-05}$	28	86
Ppu_4222	MER0174571	I39	$2.00x10^{-04}$	30	68
Ppu_1767	MER0174564	I39	$3.00x10^{-04}$	28	92
Ppu_3894	MER0174616	I39	$5.00x10^{-04}$	29	87

Eight of these hits belonged to the I39 family of protease inhibitors, termed α-macroglobulin-inhibitors (α-MG) and had 28-53% sequence identity to *P. putida* proteins (Table 1). α-Macroglobulins are large glycoproteins and were shown to be located in the bacterial inner membrane facing towards the periplasm (Robert-Genthon *et al.*, 2013). They are broad-spectrum protease inhibitors, targeting serine, cysteine, metallo- and carboxy proteases (Rehman *et al.*, 2013). They have a unique mechanism of action: rather than inactivating the proteases, they block the substrate access by irreversibly trapping the protease upon cleavage of a bait region and conformational changes in the protein structure (Goulas *et al.*, 2017). They were hypothesized to protect the bacterial peptidoglycan from cleavage by host proteases when the outer membrane is breached and the peptidoglycan is accessible (Goulas *et al.*, 2017).

The remaining hit belonged to the I42 family of protease inhibitors. This class of inhibitors is often annotated as chagasin-like inhibitors, but also annotated as inhibitors of cysteine peptidases (ICP) (Sanderson *et al.*, 2003). The BLAST search revealed a strong similarity between *Pseudomonas syringae* C14-inhibiting protein 1 (PsCip1) (Shindo *et al.*, 2016) and *P. putida* Ppu_0767 (hereafter referred to as PpCip1) with 61% sequence similarity. PpCip1 shares 29% similarity with MER0090314, which is a chagasin-like inhibitor of *Clostridium botulinum* (Table 1). PpCip1, but also PsCip1 and MER0090314, also contain motifs (NPTTG, GxGG and (Q/R)PW) (Figure 7), known to be conserved in chagasin-like inhibitors and required for the inhibition of PLCPs (dos Reis *et al.*, 2008; Shindo *et al.*, 2016), indicating that PpCip1 is indeed a chagasin-like inhibitor of PLCPs.

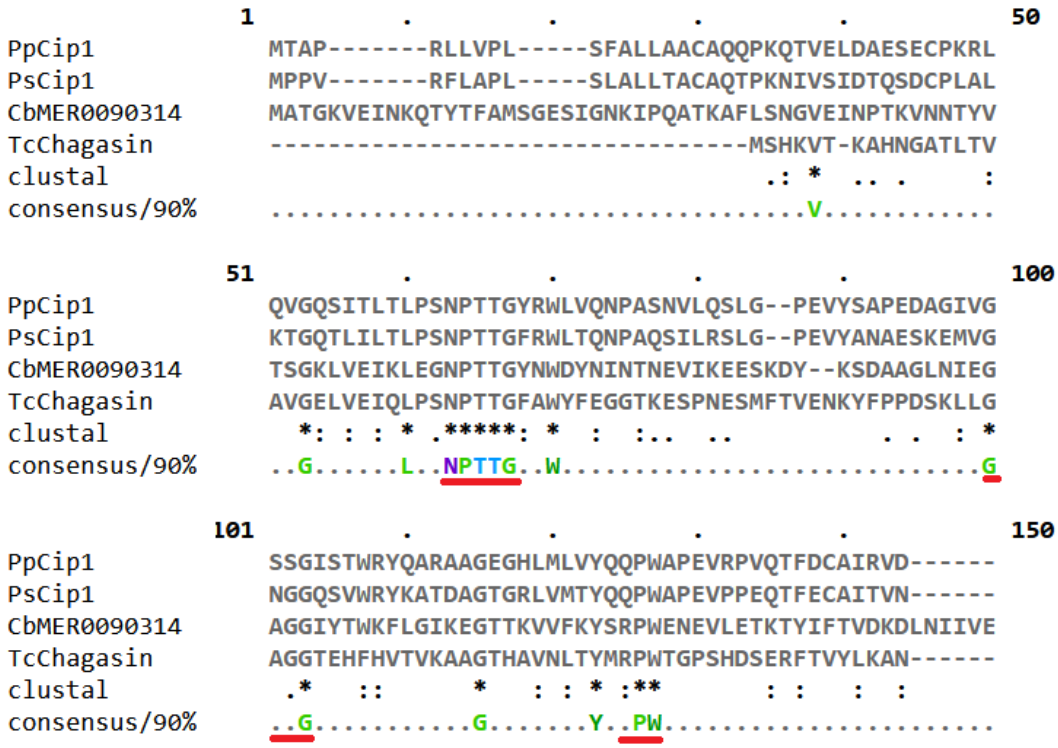

Figure 7: Alignment PpCip1 to other chagasin-like inhibitors.

CLUSTAL alignment (Sievers *et al.*, 2011) of *P. putida* Ppu_0767 (PpCip1) to other chagasin-like inhibitors: *Pseudomonas syringae* PsCip1, *Clostridium botulinum* ClMER0090314 (only inhibitory domain M103-E252) and the original *Trypanosoma cruzi* chagasin. The chagasin motifs (red line), which are required for inhibition of PLCPs, are present in all sequences (NPTTG, GxGG and (Q/R)PW). Stars indicate identical amino acids in all sequences. Double points indicate conserved substitutions. Points indicate semiconserved amino acids, i.e. amino acids having similar shapes. Colors of identical amino acids indicate their categorization into amino acids with similar chemical properties.

Chagasin-like inhibitors are highly potent PLCP inhibitor found in the protozoans, like *Trypanosoma cruzi* (dos Reis *et al.*, 2008; Monteiro *et al.*, 2001). While these inhibitors

target endogenous proteases in protozoans (Besteiro *et al.*, 2004; Costa *et al.*, 2022; Santos *et al.*, 2005; Uehara *et al.*, 2012), many Pseudomonads such as *P. putida* do not have a C1 protease, indicating that their target might not be an endogenous PLCP but rather a host PLCP (Kantyka *et al.*, 2010; Sanderson *et al.*, 2003). Moreover, PsCip1 was shown to inhibit the tomato PLCPs C14, Pip1, and Rcr3 as well as papain and the virulence of the *P. syringae* Δ*cip1* mutant strain on tomato leaves was reduced in the absence of *cip1* (Shindo *et al.*, 2016).

Since α-macroglobulin-inhibitors were shown to be acting in the periplasm rather than being fully secreted (Robert-Genthon *et al.*, 2013), further research was conducted on PpCip1, whose ortholog in *P. syringae*, PsCip1, has already been shown to be important for virulence *in planta* as it targets plant PLCPs (Shindo *et al.*, 2016).

2.1.3. Characterization of chagasin-like inhibitors

PpCip1 has a predicted immunoglobin-like fold similar to chagasin (Costa & Lima, 2016; Redzynia *et al.*, 2009) (Figure 8A). It also contains the motifs known to be conserved in the three exposed loops of chagasin-like inhibitors (NPTTG, GxGG and (Q/R)PW) (dos Reis *et al.*, 2008; Shindo *et al.*, 2016) (Figure 8A-C), which are required to block the PLCP active site (Redzynia *et al.*, 2008, 2009). The AlphaFold model of the complex of PpCip1 and papain suggests that PpCip1 also blocks the active site of papain similar to chagasin (Figure 8A).

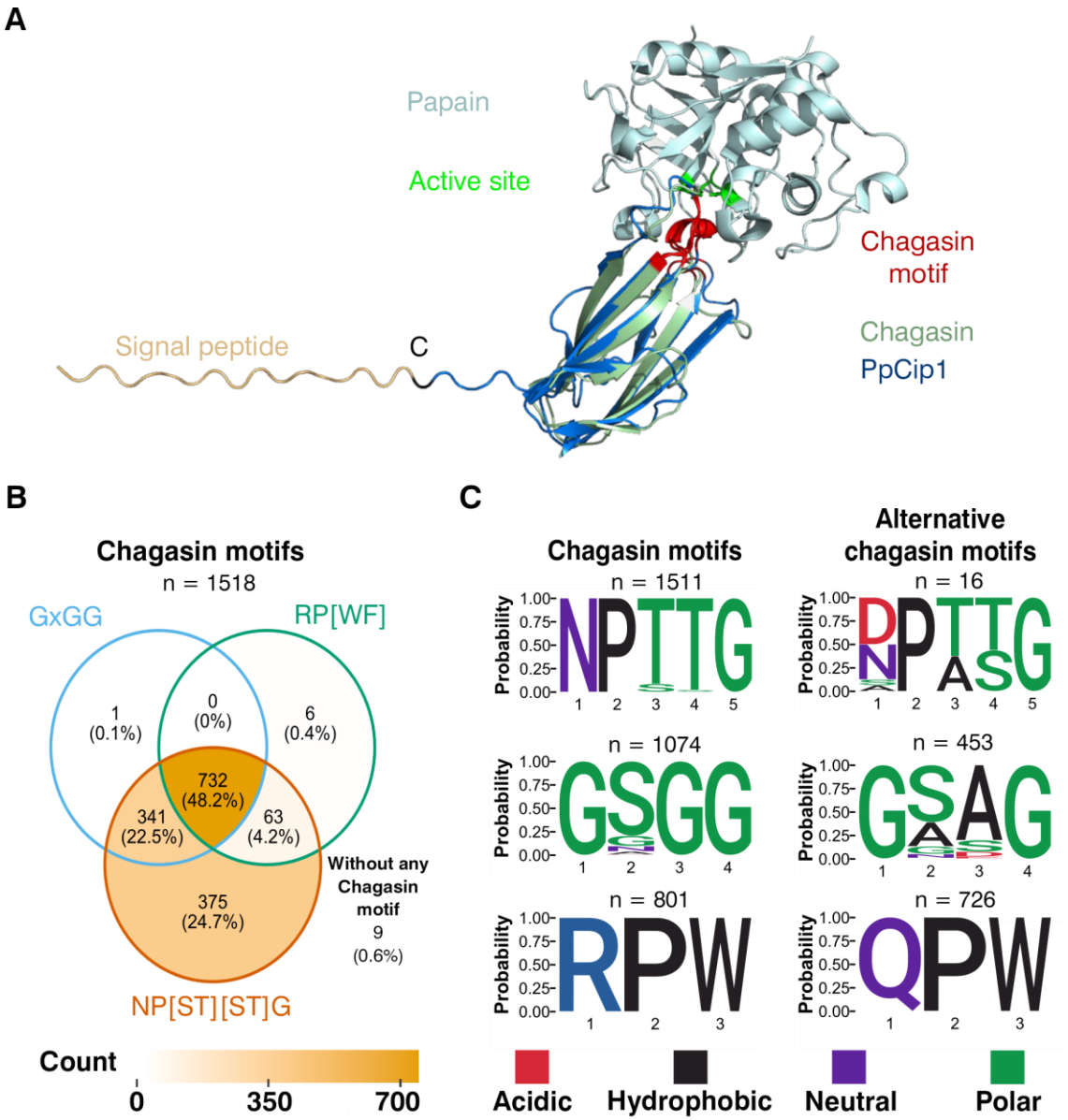

Figure 8: PpCip1 is a chagasin-like inhibitor.

(A) Chagasin (light green) and PpCip1 (dark blue) are predicted to inhibit PLCPs (papain, light blue) by blocking the protease active site (green) with its chagasin motifs (red). PpCip1 was modelled with AlphaFold (pTM = 0.76) (Jumper *et al.*, 2021). The model of PpCip1 was aligned to the structure of TcChagasin (root mean square deviation (RMSD): 1.04 Å) in a complex with papain (PDB: 3E1Z) (Redzynia *et al.*, 2009). Most parts of PpCip1 aligned well to TcChagasin, with the exception of the signal peptide (orange). C represents the cysteine residue following the lipobox. **(B)** 1527 complete *Pseudomonas* proteomes deposited in the Pseudomonas Genome Database (Winsor *et al.*, 2016) were screened with a DIAMOND BLASTp search (Buchfink *et al.*, 2015) for orthologs of PpCip1 (E < 0.0001). PpCip1-orthologs were aligned via CLUSTAL (Sievers *et al.*, 2011) and tested for presence or absence of the original chagasin motifs (NP[ST][ST]G, GxGG, and RP[WF]) (dos Reis *et al.*, 2008; Shindo *et al.*, 2016). Presence and absence are displayed in a venn diagram (Gao *et al.*, 2021, 2024) showing the overlap of the presence of the different chagasin motifs. **(C)** Motif logos of the original chagasin motifs (upper panel) and the alternative chagasin motifs (lower panel) were created using ggseqlogo (Wagih, 2017). Amino acids are colored based on their chemical properties.

To identify orthologs of PpCip1 in other Pseudomonads, a DIAMOND BLASTp search (Buchfink *et al.*, 2015) with PpCip1 was performed on all 1527 complete *Pseudomonas* proteomes deposited in the Pseudomonas Genome Database (Winsor *et al.*, 2016) (E < 0.0001). All proteomes contained a chagasin-like inhibitor ortholog with at least 40% sequence identity (Figure 8B-C, Suppl. Fig. 4). Furthermore, it was tested whether these proteins contain the original chagasin motifs (NPTTG, GxGG and (Q/R)PW) required for an inhibitory function (dos Reis *et al.*, 2008; Shindo *et al.*, 2016). While only 48.2% of the sequences had all three of the original chagasin motifs, 26.7% had two of the motifs and 25.2% had one of the motifs (Figure 8B, Figure 8C left panel, Suppl. Fig. 4). Only 0.6% had none of the three original chagasin motifs (Figure 8B). An analysis of the orthologs missing an original motif revealed that most of these sequences however contained similar motifs ([DN]P[TA][TS]G], [G[SA][AG]G, QPW, Figure 8C right panel, Suppl. Fig. 4) to the original chagasin motifs. These alternative chagasin motifs might still allow the inhibitory function of the proteins, since only a few amino acids were substituted to amino acids with similar properties (e.g. Thr to Ser). However, the alternative motifs need to be considered with caution, since the Pseudomonas Genome Database is highly enriched with *P. aeruginosa* strains (Suppl. Fig. 4) (Winsor *et al.*, 2016), biasing the result of such an analysis.

In conclusion, chagasin-like proteins like PpCip1 are conserved in Pseudomonads and contain chagasin motifs or similar motifs, which are required for inhibition of PLCPs, suggesting that PpCip1 and its orthologs are PLCP inhibitors.

2.1.4. Evaluation of PLCP inhibition by PpCip1

To test whether PpCip1 is indeed an inhibitor of plant PLCPs, PpCip1 was heterologously expressed in *E. coli* without signal peptide (SP) (Figure 9A) and its effect on PLCP activity was tested in a substrate cleavage assay. PpCip1ΔSP could strongly inhibit overexpressed CP1A in apoplastic fluids in a concentration-dependent manner with an IC_{50} of approx. 13 nM (Figure 9B) (Neubig *et al.*, 2003), which is in good agreement with the nanomolar K_i reported for other chagasins (dos Reis *et al.*, 2008; Monteiro *et al.*, 2001). Overexpressed RD19A-like in apoplastic fluids could also be inhibited by PpCip1 in a similar concentration range (Figure 9C).

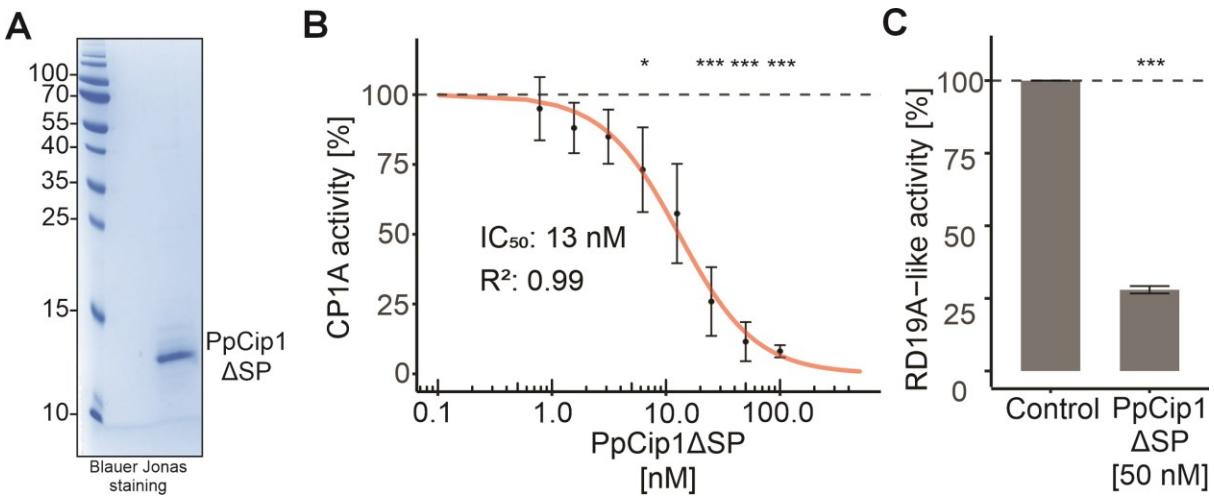

Figure 9: Heterologous expressed PpCip1 inhibits root PLCPs.

(A) His-SUMO-PpCip1ΔSP was heterologous expressed in *E. coli* and purified by affinity chromatography. Afterward, the His-SUMO tag was removed by precision protease cleavage and tag-free PpCip1 was purified by size-exclusion chromatography. Purity of heterologous expressed PpCip1 (12.6 kDa) after purification was confirmed by SDS-PAGE followed by Blauer Jonas staining. **(B)** 50 nM PpCip1 inhibits RD19A-like activity. Overexpressed RD19A-like in apoplastic fluids was preincubated with either water or 50 nM PpCip1. Afterward, the cleavage of the Z-LR-AMC substrate was measured as the increase of AMC fluorescence. The Z-LR-AMC cleavage activity of each treated sample was normalized to the water control set to 100%. This experiment was performed with three independent biological replicates with each having at least two technical replicates. Means are represented as grey bars. Error bars represent the standard error of the mean. A two-sided t-test was performed ($p<0.05$: *; $p<0.01$: **; $p<0.001$: ***). **(C)** PpCip1-like inhibits CP1A activity in nanomolar range. Overexpressed CP1A in apoplastic fluids was preincubated with either water or different concentrations of heterologous expressed PpCip1 diluted in water. Afterward, the cleavage of the Z-LR-AMC substrate was measured as the increase of AMC fluorescence. The Z-LR-AMC cleavage activity of each treated sample was normalized to water control set to 100%. IC_{50} was estimated by fitting the data with the sigmoid Hill function (Neubig *et al.*, 2003). This experiment was performed with at least three independent biological replicates with each having at least two technical replicates. Means are represented as black dots. Error bars represent the standard error of the mean. A two-sided t-test was performed ($p<0.05$: *; $p<0.01$: **; $p<0.001$: ***).

Interestingly, some Pseudomonads have been reported to have a protease with structural and functional similarity to papain (clan CA), but not belonging to the C1 family (PLCPs) (Shindo & Van der Hoorn, 2008). Therefore, it was investigated via BLASTp search using sequences deposited in the MEROPS database, whether *P. putida* has endogenous clan CA proteases. Three putative clan CA proteases from different families (C19, C39 and C93) were identified, two of which have a predicted signal peptide for the Sec translocon (Table 2), suggesting that these could be possible endogenous targets of PpCip1.

Table 2: Putative clan CA proteases identified in *P. putida*.

Putative clan CA proteases were identified by BLASTp search of using sequences deposited in the MEROPs database (Rawlings *et al.*, 2014). Hits were filtered according to E-value (<0.001), query coverage (>70%) and identity (>30%). Signal peptides were predicted by SignalP6 (Teufel *et al.*, 2022).

Family	Query	Subject	Annotation	E value	Query coverage [%]	Identity [%]	SignalP prediction
C93	MER0002914	Ppu_5046	Transglutaminase -like cysteine peptidase	$6.1x10^{-147}$	100	91	Sec/SP
C39	MER0088057	Ppu_2615	C39 family peptidase	$6.1x10^{-107}$	100	93	Sec/SP
C19	MER0535982	Ppu_4014	HK97 family Phage prohead protease	$1.2x10^{-04}$	74	35	No SP

In conclusion, PpCip1 was shown to inhibit overexpressed CP1A and RD19A-like in apoplastic fluids. Furthermore, other clan A proteases of *P. putida* have been identified that could be endogenous targets of PpCip1.

2.2. The surface-exposed PLCP inhibitor PpCip1 promotes root colonization

2.2.1. Lipoprotein prediction of PpCip1

PsCip1 was previously reported to be secreted (Shindo *et al.*, 2016). To determine, whether PpCip1 is also secreted, the signal peptide of PpCip1 was predicted via SignalP6 (Teufel *et al.*, 2022).

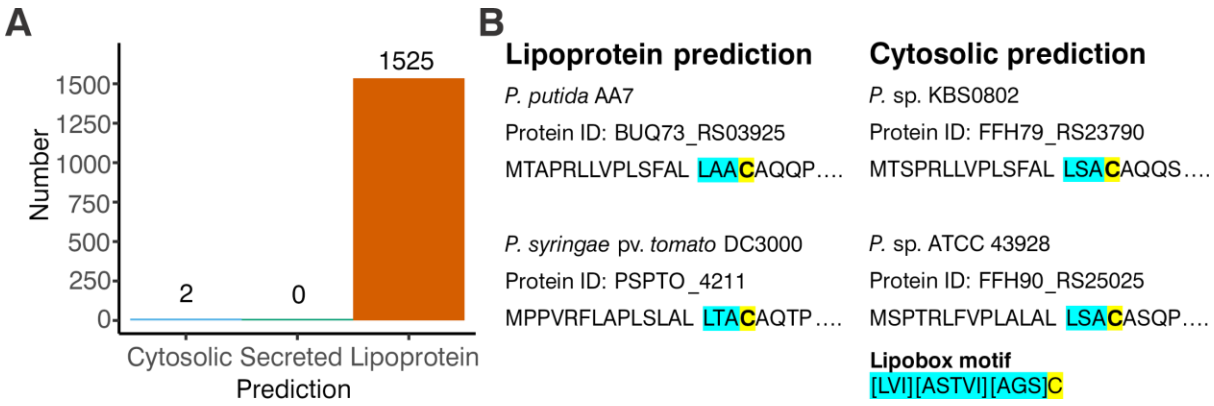

Figure 10: Chagasin-like inhibitor proteins containing a lipobox motif are conserved in Pseudomonads.

1527 complete *Pseudomonas* proteomes deposited in the Pseudomonas Genome Database (Winsor *et al.*, 2016) were screened with a DIAMOND BLASTp search (Buchfink *et al.*, 2015) for orthologs of PpCip1 (E < 0.0001). **(A)** Signal peptides of the 1527 Cip1 orthologs were predicted with SignalPv6 (Teufel *et al.*, 2022). (B) Comparison of N-terminal regions of selected Cip1 orthologs with lipoprotein and cytosolic prediction. Strain and protein IDs according to Pseudomonas Genome Database (Winsor *et al.*, 2016). Two Cip1 orthologs with prediction to be cytosolic proteins have a lipobox motif (blue and yellow: lipobox motif [LVI][ASTVI][AGS]C (LoVullo *et al.*, 2015).

Interestingly, while PpCip1 was predicted to have a signal peptide, this signal peptide was also predicted to contain a lipobox motif ([LVI][ASTVI][AGS] (LoVullo *et al.*, 2015)) (Figure 10), suggesting that PpCip1 might rather be a lipoprotein. Similarly, also all *Pseudomonas* chagasin-like inhibitors except two proteins were predicted to be lipoproteins (Figure 10). These two proteins were predicted to be cytosolic (*Pseudomonas* sp. KBS0802 FFH79_RS23790 and *Pseudomonas* sp. ATCC 43928 FFH90_RS25025) (Figure 10). However, both proteins have a lipobox motif (Figure 10, blue and yellow). Therefore, it can be speculated, that SignalP6 might not have been able to detect their putative signal peptide. In conclusion, the prediction of a lipobox in all Pseudomonads, suggests that all chagasin-like inhibitors in Pseudomonads might be lipoproteins. This would be in contrast to the report that PsCip1 is secreted and could be found in culture supernatants (Shindo *et al.*, 2016). However, in that study PsCip1 was detected with a very weak signal, leaving open the possibility that the PsCip1 found in the supernatant might have been released by cell damage or in some other way.

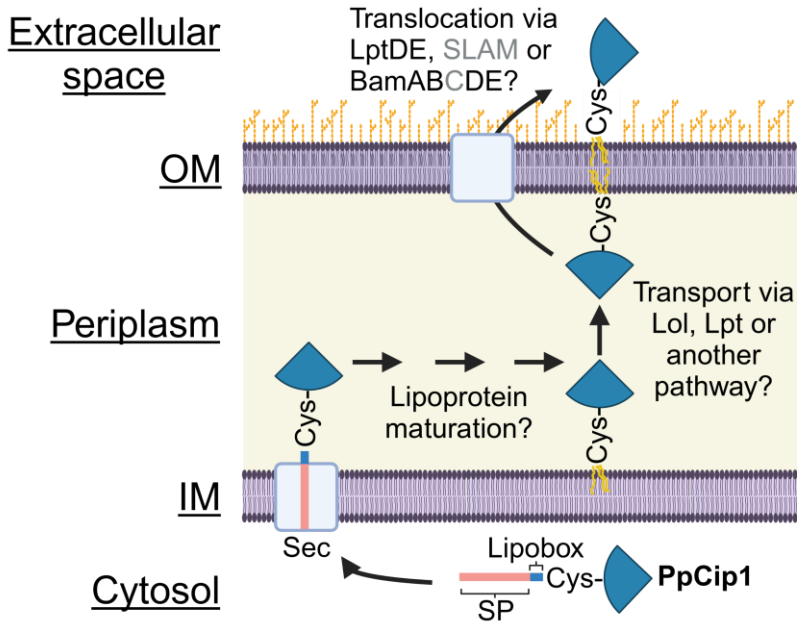

Figure 11: Model of the putative transport of membrane-anchored PpCip1 to the cell surface.

Proteins with a Sec signal peptide and a lipobox ([LVI][ASTVI][AGS]) will be secreted by the Sec translocon into the periplasm, where their signal peptide will be removed. This prolipoprotein will be lipidated at the N-terminal cysteine following the lipobox, thereby anchoring the lipoproteins to the inner membrane (Gupta *et al.*, 1993; LoVullo *et al.*, 2015; Natale *et al.*, 2008; Sankaran & Wu, 1994; Tokunaga *et al.*, 1982, 1984). Finally, the mature lipoprotein can either stay in the inner membrane, if it contains a retention signal, or can be relocalized to the outer membrane via the Lol (localization of lipoproteins) or the LptDE (lipopolysaccharide transport) pathway (He *et al.*, 2023; LoVullo *et al.*, 2015; Luo *et al.*, 2022; Narita & Tokuda, 2007; Remans *et al.*, 2010). Lipoproteins can either stay on the periplasmic side of the outer membrane or can be translocated across the outer membrane. Several translocator complexes have been shown to be involved in this process in different organisms, as for example the β-barrel assembly machinery (Bam) complex exporting mainly β-barrel proteins (Leyton *et al.*, 2012), the surface lipoprotein assembly modulator (SLAM) (Hooda *et al.*, 2016, 2017; Huynh *et al.*, 2022) or the outer membrane LPS translocase LptDE (lipopolysaccharide transport D and E), which also transports glycolipids (He *et al.*, 2023; Luo *et al.*, 2022). Proteins not identified in *P. putida* via BLASTp search have been marked in grey.

Lipoproteins will be secreted into the periplasm via the Sec translocon and their signal peptide will be removed. Next, these prolipoprotein will be lipidated at the N-terminal cysteine following the lipobox anchoring the lipoproteins to the inner membrane (Figure 11, Suppl. Fig. 5) (LoVullo *et al.*, 2015; Natale *et al.*, 2008). If the chagasin-like inhibitors in Pseudomonads are indeed lipoproteins, they can be localized at the inner membrane, could be transported to the periplasmic side of the outer membrane (inner leaflet) or could be translocated across the outer membrane to the cell surface (Figure 11, Suppl. Fig. 5). Lipoproteins were shown to remain at the inner membrane, if they have a retention signal (Gennity & Inouye, 1991; Grabowicz, 2019; Lewenza *et al.*, 2006, 2008; Lorenz *et al.*, 2019; Narita & Tokuda, 2007; Seydel *et al.*, 1999; Tanaka *et al.*, 2007; Terada *et al.*, 2001; Yamaguchi *et al.*, 1988). The transport of lipoproteins from the inner to the outer membrane was proposed to

occur via the Lol (localization of lipoproteins) pathway (LoVullo *et al.*, 2015; Narita & Tokuda, 2007; Remans *et al.*, 2010) or the Lpt pathway (lipopolysaccharide transport) (He *et al.*, 2023; Luo *et al.*, 2022). Several transporters have been proposed to be responsible for the transport across the outer membrane (e.g. β-barrel assembly machinery (Bam) complex, the surface lipoprotein assembly modulator (SLAM), or the LptDE complex) (He *et al.*, 2023; Hooda *et al.*, 2016, 2017; Huynh *et al.*, 2022; Leyton *et al.*, 2012; Luo *et al.*, 2022). However, many required signals and mechanisms are not well understood yet (Cole *et al.*, 2021; Huynh *et al.*, 2022).

The sequence of PpCip1 nor other Pseudomonas chagasin-like proteins do not have any of the reported retention signals (Figure 10, Suppl. Fig. 4, Suppl. Table 3), suggesting that these chagasin-like proteins are not retained in the inner membrane. Additionally, all components required for the maturation of lipoproteins, the transport via the Lpt and the Lol pathway, and translocation across the outer membrane (except SLAM and a part of the Bam complex (BamC)) could be identified in the predicted *P. putida* proteome via a BLASTp search (Suppl. Table 4), suggesting that PpCip1 can become a mature lipoprotein, which might be transported to outer membrane and the cell surface.

In contrast to chagasin-like inhibitors in Pseudomonads, chagasin does not have a predicted / known SP (Figure 7) (Costa & Lima, 2016), which is in line with its function as a regulator of an endogenous PLCP (Santos *et al.*, 2006). In the procyclic life cycle stage the C-terminally mNeonGreen-tagged chagasin was found in the cytoplasm, flagellar cytoplasm and nuclear lumen (Billington *et al.*, 2023). However, in some parasite developmental states, it was found to be linked to the membrane via a glycolylphosphatidylinositol (GPI) anchor and was identified also on the parasites surface via immunocytochemistry (Monteiro *et al.*, 2001), suggesting that it might also be a surface-localized lipoprotein in *T. cruzi*.

In conclusion, all chagasin-like inhibitors in Pseudomonads have been shown to have a lipobox which might result in the maturation to lipoproteins, anchoring these proteins to the inner membrane. PpCip1 has no retention signal, therefore a transport to the outer membrane via the Lol or an Lol-independent pathway (e.g. Lpt pathway) is likely. Lastly, *P. putida* encodes the Bam and Lpt complex, which could allow the translocation of PpCip1 to the cell surface.

2.2.2. Membrane localization of PpCip1

Based on the bioinformatics analysis predicting PpCip1 to be a lipoprotein, we hypothesized that PpCip1 could be membrane-localized and potentially extracellularly exposed via a lipid anchor (Figure 11), since only in this location it could encounter and inhibit plant C1 proteases. To test this hypothesis, we used two methods to determine the localization of PpCip1 in the bacterial cell: A biochemical approach using the separation of cell compartments followed by identification via Western blots and fluorescence microscopy monitoring PpCip1-mCherry localization in the cell.

First, we used a biochemical approach where we separated cell compartments via cell disruption, different ultra-centrifugation steps and specific buffers for the different compartments (Paredes-Osses & Hardie, 2013) (Figure 12). Two marker-less *P. putida* knock-out (KO) mutants Δ*cip1* #2 and #3 were generated via integration of the 1000 bp genomic region lacking the gene encoding PpCip1 in a two-step allelic exchange. The deletions were confirmed by colony PCR and sequencing (Suppl. Fig. 6). The mutants did not show any growth defect when grown in full growth medium (Suppl. Fig. 7). *P. putida* Δ*cip1* mutant #*2* was complemented with *cip1* using an episomal vector for constitutive expression driven by the Neomycin promotor (pNm) and adding a C-terminally 3xFlag-tag resulting in *P. putida* Δ*cip1*_PpCip1-Flag.

P. putida WT, *P. putida* Δ*cip1* mutant #2 and *P. putida* Δ*cip1*_PpCip1-Flag growing in full medium were tested for PpCip1 expression after one and five hours growth via qPCR using PpCip1-specific primers. The absence of *cip1* transcripts was confirmed in the knockout mutant, while normal expression levels were observed for *P. putida* WT (Suppl. Fig. 8, threshold Ct<35). In the complemented *P. putida* Δ*cip1*_PpCip1-Flag strain *cip1* was strongly expressed, approx. 100-fold more than in WT, as confirmed by qPCR using *cip1*-specific primers (Suppl. Fig. 8) and by Western Blot with an anti-Flag antibody (Figure 12). These data indicate that *cip1* is expressed in axenic cultures. Notably, expression of *cip1* was similar in all strains when incubated in M9 medium (Suppl. Fig. 8).

P. putida Δ*cip1*_PpCip1-Flag was used to monitor the localization of PpCip1. As controls antibodies against proteins with known localization in other bacterial strains were used to confirm the successful compartmentalization.

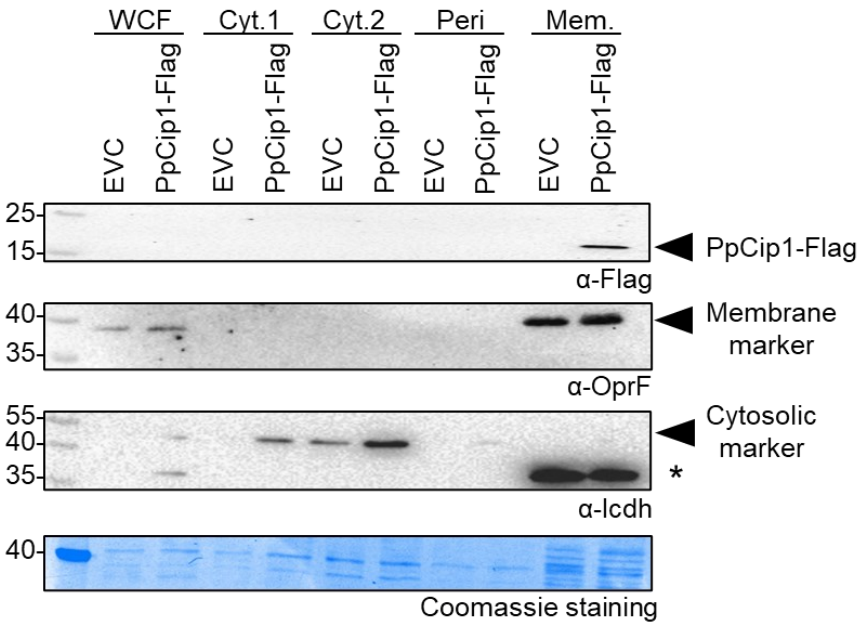

Figure 12: PpCip1-Flag localizes in membrane fraction.

Cells of *P. putida* Δ*cip1*_PpCip1-Flag were fractionated to different cell compartments (WCF: whole cell fraction, Peri.: Periplasm, Cyt.: Cytosol, Mem.: Membrane) using cell disruption, specific buffers (e.g. Tris-EDTA-sucrose (TSE) buffer), and various centrifugation steps. Western blot analysis was performed to monitor the localization of PpCip1-Flag (approx. 17 kDa) as well as the known outer membrane protein porin F (OprF) (approx. 36 kDa) and the cytosolic marker isocitrate dehydrogenase (IcdH) (approx. 45 kDa) used as controls for the successful separation of cell compartments (indicated by arrowhead). Asterisk indicates background signal. These experiments were performed by Nina Solia during her Master thesis project (Solia, 2023) under my supervision. This experiment was performed twice with similar results.

We observed that PpCip1-Flag (approx. 17 kDa) could be found only in the membrane fraction, similar to the known membrane marker protein outer membrane protein porin F (OprF) (approx. 36 kDa) (Figure 12). In contrast, the cytosolic marker protein isocitrate dehydrogenase (IcdH) (approx. 45 kDa) was only found in the cytosolic fractions. Although, also bands corresponding to smaller proteins could be observed for IcdH in the membrane fraction, likely showing unspecific binding of the antibody, as it is not specific for *P. putida* IcdH, or degradation products of IcdH. Unfortunately, contamination with periplasmic proteins during cell fractionation cannot be ruled out due to the missing periplasmic control. All tested antibodies for periplasmic control proteins did not function (not shown). Nevertheless, no leakage of the highly abundant cytosolic Icdh was observed (Figure 12), indicating intact cell membranes, at least an intact inner membrane. In summary, PpCip1 could be identified in the membrane fraction after separation of cell compartments, indicating that PpCip1 is membrane-anchored.

As a second approach to confirm the biochemical analysis, fluorescence microscopy was performed with PpCip1 tagged with mCherry (PpCip1-mCherry) to monitor the localization of PpCip1 in the cell. As a control, the gene for cytosolic superfolder GFP (sfGFP) with a constitutive pNm promoter was integrated into the attTn7 site downstream of the *glmS* gene (Matsumoto *et al.*, 2022) in the genome of *P. putida* WT and *P. putida* Δ*cip1* via two-step allelic exchange (Huang & Wilks, 2017) using 500 bp sequences upstream and downstream from the integration site. The genomic integration of *sfgfp* was confirmed for fluorescent clones by colony PCR and sequencing (Suppl. Fig. 9). An episomal vector for constitutive expression of mCherry or PpCip1-mCherry under the pNm promotor was cloned and transformed into the *P. putida* WT_sfGFP strain, resulting in *P. putida* WT_sfGFP_mCherry and *P. putida* WT_sfGFP_PpCip1-mCherry.

Using fluorescence microscopy, we observed that PpCip1-mCherry was significantly enriched at the cell periphery and reduced in the middle of the cells compared to the signals of sfGFP and mCherry, which were expressed in the cytosol (Solia, 2023) (Figure 13), suggesting that PpCip1 is localized at the membrane.

In conclusion, the results of the fluorescence microscopy observing PpCip1-mCherry at the cell periphery confirm our biochemical results detecting PpCip1 in the membrane fraction of the *P. putida* cells. These results strongly suggest that PpCip1 is indeed a lipoprotein and is anchored to a membrane of *P. putida*.

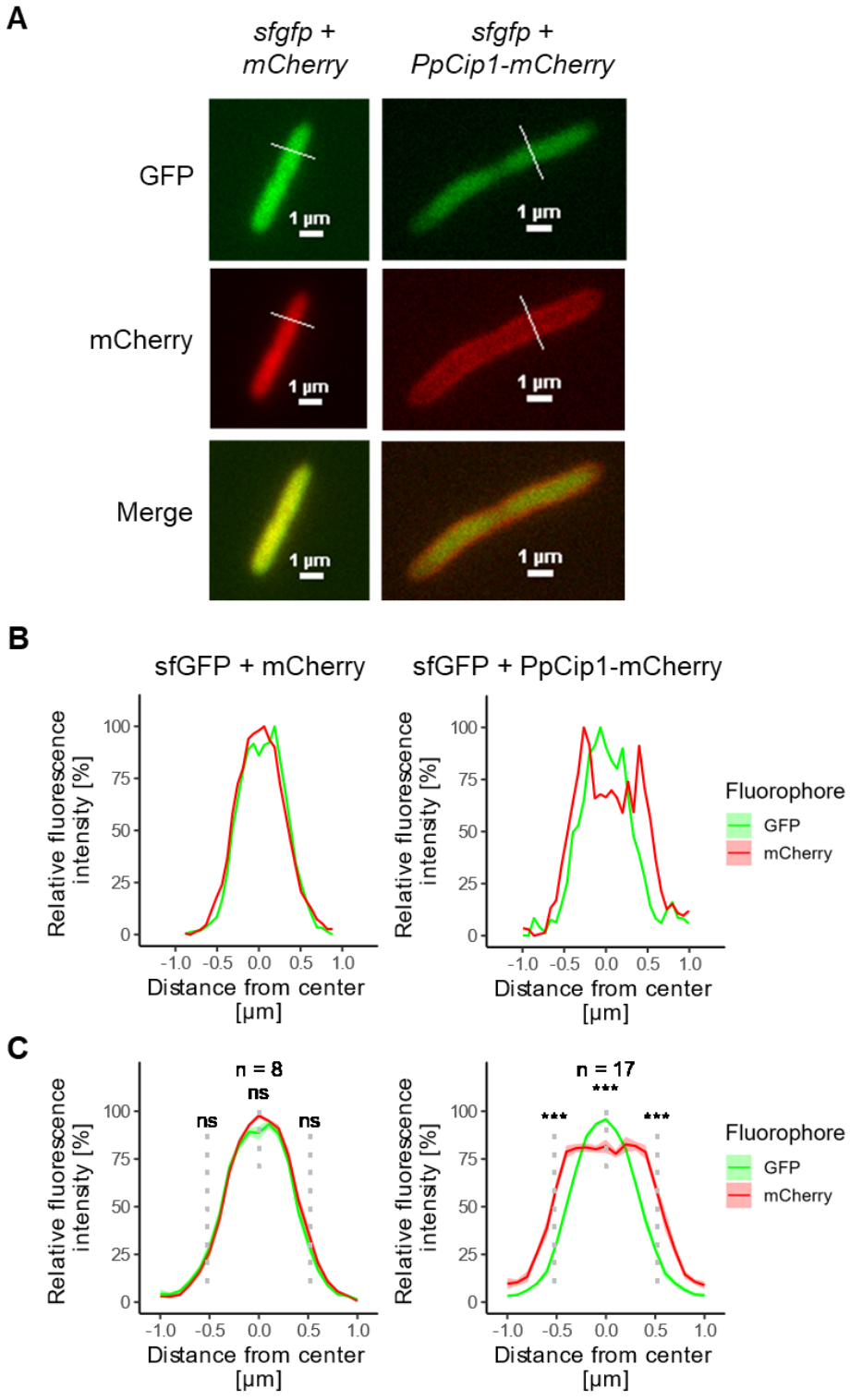

Figure 13: The PpCip1-mCherry fusion protein localizes to the cell envelope of *P. putida*.

(A) Representative microscopy pictures and fluorescence histograms of *P. putida* WT_sfGFP_ mCherry (left) or *P. putida* WT_sfGFP_PpCip1-mCherry (right). The signal in PpCip1-mCherry expressing cells is stronger in the cell periphery (cell envelope) when compared to cells expressing only mCherry. **(B)** Fluorescence histograms depicting the relative fluorescence intensity of the *P. putida* WT_sfGFP_ mCherry cell shown in (A, left) expressing cytosolic sfGFP (genomically integrated) (green) as well as mCherry (vector) (red, left) or of the *P. putida* WT_sfGFP_PpCip1-mCherry cell shown in (A, right)

expressing cytosolic sfGFP (genomically integrated) (green) as well as PpCip1-mCherry (vector) (red, right). **(C)** Average of the relative fluorescence intensity of different cells (n) expressing cytosolic sfGFP (green) as well as cytosolic mCherry (red, upper panel) or PpCip1-mCherry (red, lower panel). The mean of the measured fluorescence (darker line) is displayed with the standard error of the mean (SEM, light color). The difference between the sfGFP and mCherry signals at approx. -0.52 µm, 0 µm, and 0.52 µm distance from the center was tested using a paired 2-sided t-test using the t-test function implemented in R. Significance was displayed with asterisks according to the calculated p-value ($p<0.001$: ***, $p<0.01$: **, $p<0.05$: *, $p>0.05$: ns). Some of the strains used in this experiment were kindly provided by Nina Solia and figure panels A and B were generated during her Master thesis project (Solia, 2023) under my supervision.

2.2.3. Surface localization of PpCip1

Since PpCip1 was shown to be membrane anchored and *P. putida* does not have an endogenous C1 protease, I hypothesized that PpCip1 is surface localized to be able to target PLCPs secreted by the plant.

To investigate whether PpCip1 is surface localized, biotin labeling of surface localized proteins of *P. putida* was performed. *P. putida* Δ*cip1*_sfGFP was transformed with the vector for pNm-driven expression of PpCip1-Flag, resulting in *P. putida* Δ*cip1*_sfGFP_PpCip1-Flag. Cells of *P. putida* Δ*cip1*_sfGFP_PpCip1-Flag were washed to remove secreted proteins and medium. Next, the cell surface proteins were covalently labeled for 30 min at room temperature using the membrane-impermeable Sulfo-NHS-Biotin reagent (Daniels & Amara, 1998; Huh & Wenthold, 1999). Afterwards, the reagent was quenched with glycine and cells were washed again. In the next step, cells were lysed and biotinylated proteins were pulled down in a membrane lysis buffer using streptavidin beads. After washing the beads, proteins were eluted from the beads with SDS-loading dye at 98°C and were analyzed via SDS-PAGE and Western blot.

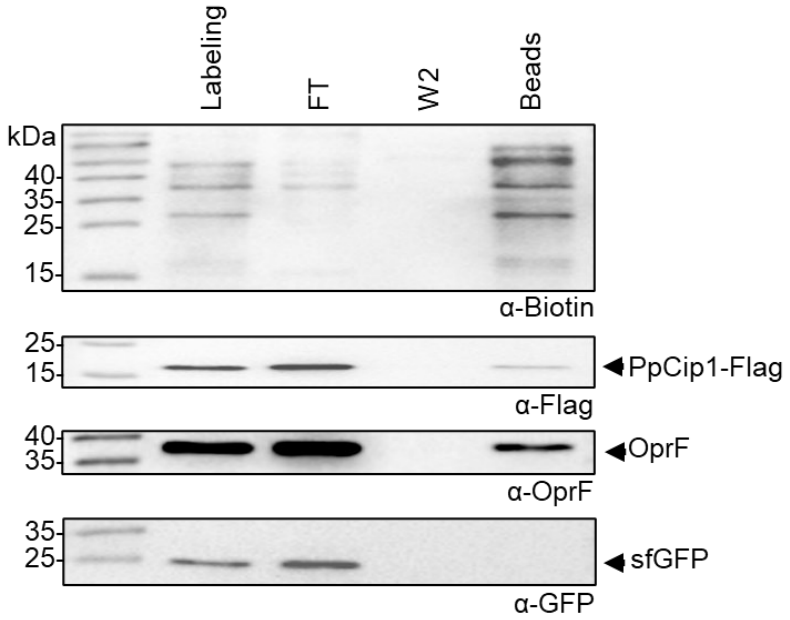

Figure 14: PpCip1 is localized at the surface of the bacterial outer membrane.

Biotin labeling using the membrane-impermeable Sulfo-NHS-Biotin agent was used to covalently label all surface-localized proteins of *P. putida* Δ*cip1*_sfGFP_PpCip1-Flag. After surface-localized proteins were labeled, the Sulfo-HNS-Biotin reagent was inactivated, and biotinylated proteins were pulled down using streptavidin beads. Proteins were detected via Western Blot using specific antibodies: anti-biotin to observe pulled down biotinylated proteins, anti-Flag for PpCip1-Flag, anti-OprF for the outer membrane protein F (OprF) as a positive control and anti-GFP for the cytosolic (cyt.) sfGFP as a negative control (arrowhead points at expected protein molecular weight). Coomassie staining did not show any bands, since the protein concentration in the sample was apparently too low for detection, therefore it is not displayed.

The Western blot using antibodies against biotin revealed that many proteins were biotinylated and successfully pulled down (Figure 14). Antibodies against the Flag-tag of PpCip1-Flag showed that PpCip1-Flag was also pulled down with the streptavidin beads (Figure 14), indicating that PpCip1-Flag was biotinylated and surface localized. As a control for the specific labeling of surface proteins, antibodies against OprF and sfGFP were used confirming that while the outer membrane protein OprF was labeled and detected, the cytosolic sfGFP was not (Figure 14), indicating that the method is reliable in labeling only surface proteins and that the cells remained intact during labeling. These results indicate that PpCip1-Flag is a membrane bound and surface-localized protein.

To further support that PpCip1 is surface localized, transmission electron microscopy (TEM) of immunogold-labeled PpCip1-mCherry with a polyclonal antibody against mCherry was performed. Therefore, *P. putida* Δ*cip1* was transformed with the vector for constitutive expression of PpCip1-mCherry, resulting in *P. putida*

Δ*cip1*_PpCip1-mCherry. When immunogold labeling of *P. putida* Δ*cip1*_PpCip1-mCherry is monitored, the observation of gold particles would be predicted in the cytosol, at the inner- and outer membrane as well as on the surface (Suppl. Fig. 10A). Gold particles labeling PpCip1-mCherry were also expected in the cytosol, as PpCip1-mCherry is produced in the cytosol and was also still observed in the cytosol using the fluorescence microscope (Suppl. Fig. 10A). As controls, *P. putida* Δ*cip1* transformed with an empty-vector control (EVC), resulting in *P. putida* Δ*cip1*_EVC, and *P. putida* Δ*cip1* transformed with the vector for constitutive expression of cytosolic mCherry, resulting in *P. putida* Δ*cip1*_mCherry, were used. While no labeling would be expected for *P. putida* Δ*cip1*_EVC, only cytosolic labeling would be expected for *P. putida* Δ*cip1*_mCherry (Suppl. Fig. 10A).

While the detection of immunogold labeled cytosolic mCherry with the mCherry antibody was successful (Suppl. Fig. 10C), only a few gold particles could be observed *P. putida* Δ*cip1*_PpCip1-mCherry (Suppl. Fig. 10D). Unfortunately, the amount of gold particles was similar or less than observed with the control (P. *putida* Δ*cip1*_EVC) (Suppl. Fig. 10B), indicating an unspecific binding of the antibody and likely very low PpCip1-mCherry availability. A quantification of the immunogold particles in the different compartments showed minor differences in their localization (Suppl. Table 5). For example, mCherry is more likely to be found in the cytosol, while PpCip1-mCherry is more likely to be found in the periplasm and on the surface (Suppl. Table 5). These differences correspond to the surface localization observed with the biotin reagent (Figure 14). Even though a minor relationship between the different proteins and their localization was seen, the unspecific binding of the mCherry antibody in the P. *putida* Δ*cip1*_EVC strongly reduces the confidence in this method, suggesting that this experiment can neither confirm nor contradict our hypothesis that PpCip1 is surface localized.

Immunogold-labeling is a method with spatially high resolution, however low sensitivity (Guo & Huang, 2015). Fluorescence microscopy with cytosolic mCherry and PpCip1-mCherry showed less mCherry fluorescence detectable in WT_sfGFP_PpCip1-mCherry in comparison to WT_sfGFP_mCherry (Figure 13). This aligns to lower PpCip1-Flag levels compared to the OprF levels observed in the biotin labeling of surface proteins (Figure 14). These observations might indicate low levels of PpCip1-mCherry and therefore less particles were observed in the immunogold

labeling. A smaller tag like the Flag-tag might allow better detection by the antibodies due to less steric hinderance and better secretion/translocation. Immunogold-labeling of PpCip1-Flag using antibodies against the Flag-tag are ongoing experiments, however so far trials with different antibodies resulted in no labeling of PpCip1-Flag, indicating that they did not detect the Flag epitope.

In conclusion, the labeling of surface proteins indicates that PpCip1 is surface localized. Immunogold-labeling of tagged PpCip1 did neither confirm nor contradict the biochemical results.

2.2.4. Protection of surface proteins from proteolytic cleavage by PpCip1

The biochemical analysis indicated that PpCip1 is localized at the cell surface. Furthermore, the most likely target of PpCip1 are apoplastic plant PLCPs. Therefore, I hypothesized that PpCip1 may protect surface proteins from being cleaved by plant PLCPs. To test this hypothesis, *P. putida* WT and *P. putida* Δ*cip1* #2 cells were incubated with 100 nM papain for 30 min at room temperature. Afterwards, papain was inactivated with E64 and released peptides were removed by washing. The surface-localized proteins were again biotinylated with the Sulfo-NHS-Biotin agent, the reagent was quenched and labeled proteins were pulled down with Streptavidin beads. Pulled down biotinylated proteins were detected by Western Blot using an anti-Biotin antibody. If surface-localized proteins are protected by PpCip1, a shift in the band pattern would be observed, when comparing *P. putida* WT vs. Δ*cip1* in the presence of papain. Different labeling patterns would indicate that surface proteins are cleaved resulting in different molecular weight sizes.

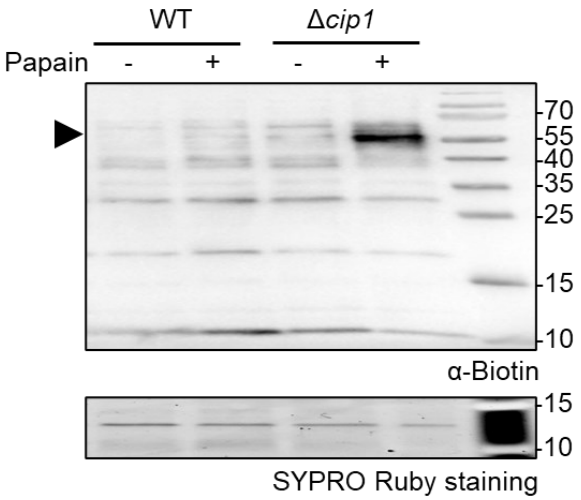

Figure 15: Biotin labeling of surface proteins after incubation with papain.

P. putida WT and *P. putida* Δ*cip1* #2 cells were incubated with 100 nM papain for 30 min at room temperature. Afterwards, papain was inactivated with E64. Remaining inactive papain and released peptides were removed by washing. Next, surface proteins were biotinylated using the membrane-impermeable Sulfo-NHS-Biotin agent. Finally, the biotinylation reagent was quenched with glycine and biotinylated proteins were pulled down in a membrane protein buffer using Streptavidin beads. The biotinylated proteins were detected using an anti-Biotin antibody. Protein band of interest marked with an arrowhead. The biotinylated proteins will be identified via MS. This experiment has been performed four times with similar results. Coomassie staining did not show any bands, since the protein concentration in the sample was apparently too low for detection, therefore it is not displayed.

In the absence of papain, no significant differences of the biotinylated proteins pulled down from *P. putida* WT and Δ*cip1* cells was observed (Figure 15). In contrast, the addition of papain to *P. putida* WT cells resulted in a slight increase in signals between 40-55 kDa compared to other bands identified in the same sample and to the bands identified for *P. putida* WT cells incubated without papain. However, the same treatment on *P. putida* Δ*cip1* cells caused the accumulation of a strong band at approx. 55 kDa and some less intense bands with a similar size. It also appears that bands at 40 kDa became weaker. These samples with biotinylated proteins were sent to MS analysis; however, the analysis in collaboration with Farnusch Kaschani (University Duisburg-Essen) has not been completed at the time of submission of this thesis. The MS analysis is expected to reveal, which surface proteins still remained at/in the outer membrane upon the papain treatment and it might indicate which proteins have been processed by papain activity.

The altered labeling of surface-localized proteins upon incubation with papain suggests that PpCip1 might protect surface proteins from papain cleavage, as a papain- and PpCip1-dependent differential pattern in the labeling of surface localized proteins was observed.

2.2.5. Promotion of root colonization by PpCip1

Experiments shown in this thesis suggest that PpCip1 might protect surface proteins from cleavage by host PLCPs. These surface proteins might be important for bacterial fitness and survival but their cleavage and thereby the release of putative MAMPs might also trigger immune responses of the plant. This might influence the ability of *P. putida* to colonize a host.

To understand the role of PpCip1 in root colonization, the root colonization of maize roots by *P. putida* was tested. Maize plants were grown in sterile soil and the soil was inoculated with *P. putida* WT or *P. putida* Δ*cip1*. Whole roots were isolated from the soil after 3 hpi (0 dpi) and 6 dpi, washed twice with water and the root material was ground to isolate bacteria from the roots (endophytes and epiphytes). Bacterial counts (Colony forming units, cfu) were determined by dilution series on agar plates. An increase of cfu within six days was observed for both strains, however there was no significant difference in colonization (Suppl. Fig. 11) (Solia, 2023). Additionally, many different timepoints were tested but no significant difference in the abundance of the two strains in the whole root samples could be observed (Solia, 2023). The lack of a differential phenotype could be due to local differences in the root colonization. Alternatively, the tested time point could be too early or too late to observe differences. Unfortunately, the sites of the colonization could not be determined using GFP-labeled strains, since the autofluorescence of the thick maize roots was too high generating a high background difficult to distinguish from the sfGFP fluorescence of the *P. putida* strains (Goodwin & Kavanagh, 1948; Harris & Hartley, 1980; Somssich *et al.*, 2016).

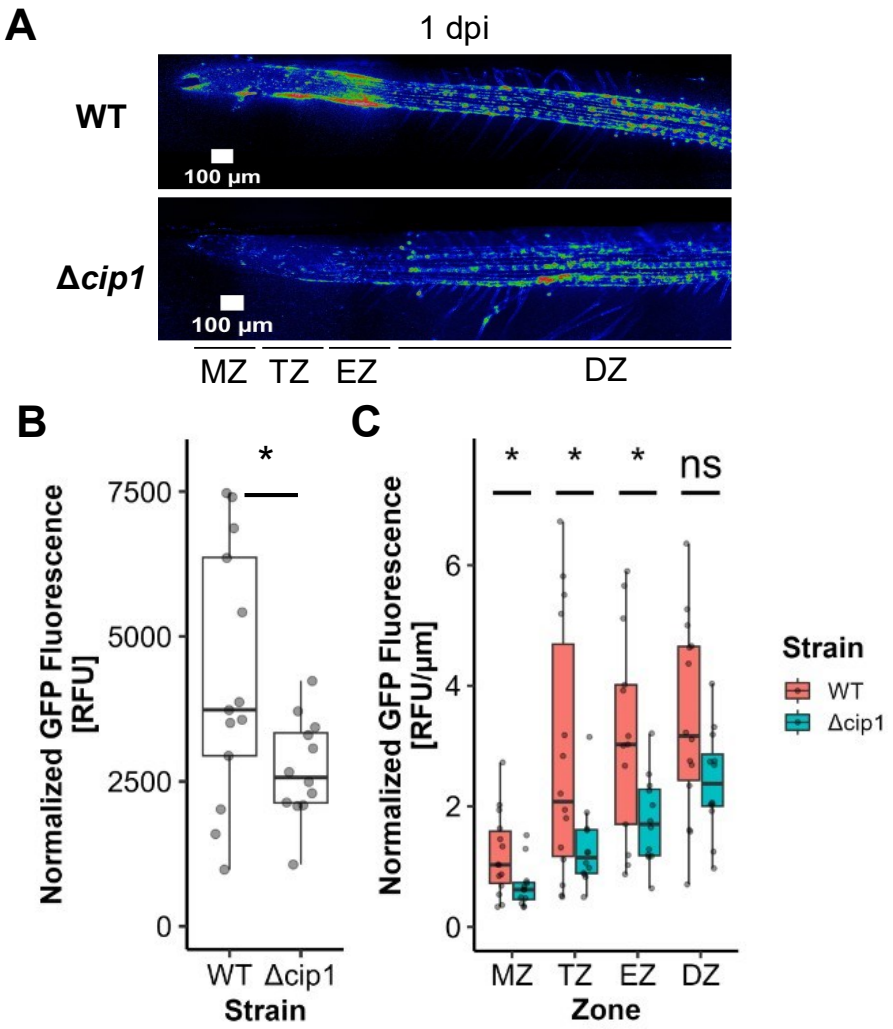

Figure 16: PpCip1 promotes early root colonization in the meristematic and elongation zone of *A. thaliana* Col-0.

(A) *P. putida* WT_sfGFP or *P. putida* Δ*cip1*_sfGFP were inoculated onto 10 days old *A. thaliana* Col-0 roots growing in a root-on-a-chip (modified version of chip reported by (Guichard *et al.*, 2020)). 1 dpi GFP fluorescence on the root was imaged. GFP fluorescence is visualized by rainbow coloring (low: blue, high: red). Meristematic zone (MZ): 0-200 µm from root tip, transition zone (TZ): 200-520 µm from root tip, elongation zone (EZ): 520-850 µm from root tip, and differentiation zone (DZ): 850-1500 µm from root tip, estimated according to Verbelen *et al.* (2006). White rectangle corresponds to a 100 µm scale bar. This experiment was performed in cooperation with Christian-Frederic Kaiser, Sabrina Egli and Prof. Dr. Guido Grossmann at the Heinrich-Heine University Düsseldorf. **(B)** Total GFP fluorescence was quantified and normalized to the background. Normalized GFP fluorescence was summed up on the first 1500 µm from the root tip. Within three biological replicates, a total of 14 roots inoculated with *P. putida* WT_sfGFP and 12 roots inoculated with *P. putida* Δ*cip1*_sfGFP were measured. A two-sided t-test was performed (p> 0.05: ns., p<0.05: *; p<0.01: **; p<0.001: ***). **(C)** GFP fluorescence of different root zones was quantified and normalized to the background. Normalized GFP fluorescence was summed up for each developmental zone (Meristematic zone: 0-200 µm from root tip, transition zone: 200-520 µm from root tip, elongation zone: 520-850 µm from root tip, and differentiation zone: 850-1500 µm from root tip, estimated according to Verbelen *et al.*, 2006). Within three biological replicates, a total of 14 roots inoculated with *P. putida* WT_sfGFP and 12 roots inoculated with *P. putida* Δ*cip1*_sfGFP were measured. A two-sided t-test was performed (p> 0.05: ns., p<0.05: *; p<0.01: **; p<0.001: ***).

As another approach to investigate the colonization of roots by *P. putida* with better spatial resolution, the colonization of *P. putida* was monitored on *Arabidopsis thaliana* Col-0 roots, for which more methods are established to follow bacterial root colonization. To test the colonization of *A. thaliana* Col-0 roots by *P. putida* WT_sfGFP or *P. putida* Δ*cip1* WT_sfGFP, a root-on-a-chip approach was performed (Guichard *et al.*, 2020). In this approach the roots grow into chambers of a sterile chip, while the foliar parts grow outside the chip. The plants were grown for 10 days into the chips and then the sfGFP-labeled bacteria were inoculated into the chambers. On the next day, the GFP fluorescence of the bacteria on the roots was imaged. The GFP fluorescence on the root was quantified, normalized to the background and analyzed. GFP signals were mostly observed within the first 3000 µm from the root tip (Figure 16A, Suppl. Fig. 12). The signal increased within the first 1000-1500 µm from the root tip and slowly decreased from 2000 µm to 3000 µm away from the root tip, indicating that the bacteria mostly colonize the younger parts of the root. Higher normalized GFP fluorescence was observed on roots colonized with *P. putida* WT_sfGFP compared to *P. putida* Δ*cip1*_sfGFP within the first 1000 µm from the root tip (Figure 16B, Suppl. Fig. 12) as well as in spots also within the range 1000 µm to 3000 µm away from the root tip (Suppl. Fig. 12), indicating that *P. putida* requires PpCip1 to colonize this region.

Since the major differences were observed within the first 1000 µm of the root, this region of the root was further analyzed to possibly link the developmental states of the root zones to the colonization. The developmental zones were estimated based on Verbelen *et al.* (2006) (Figure 16A) and GFP fluorescence per µm per zone was determined. Higher normalized GFP fluorescence per µm was observed for *P. putida* WT_sfGFP compared to *P. putida* Δ*cip1* sfGFP in the meristematic, transition and elongation zone, but not in the differentiation zone (Figure 16C), indicating that PpCip1 only has an effect in the colonization of these developmental zones.

In conclusion, these results suggest that PpCip1 promotes the early colonization of *P. putida* in the meristematic, transition and elongation zone of the root.

2.2.6. Effect of PpCip1 on the bacterial community colonizing maize roots

The previous experiments showed that PpCip1 promotes the early colonization of *A. thaliana* roots but not the late colonization of maize roots by *P. putida*. However, it was still unclear how PpCip1 would affect the colonization of *P. putida* in the presence of other bacteria, as well as their colonization. To determine whether PpCip1 might also have an effect on the microbial community, the dynamics of the whole maize synthetic community (SynCom) on the maize root was studied using an initial 16S DNA amplicon sequencing experiment.

The seven strains corresponding to the maize SynCom from Niu *et al.* (2017) were co-inoculated at an OD_{600} of 0.0001 with either *P. putida* WT or *P. putida* Δ*cip1* into sterile soil and maize seedlings were grown for up to 14 days (Figure 17A). For each time point (3 hpi, 7 dpi and 14 dpi), seedlings were removed from the soil, the roots were washed several times by vortexing with water and the whole roots were frozen. DNA was isolated from the root samples and 16S DNA was amplified and barcoded with specific primers. The amplified bacterial 16S DNA was sent for amplicon sequencing.

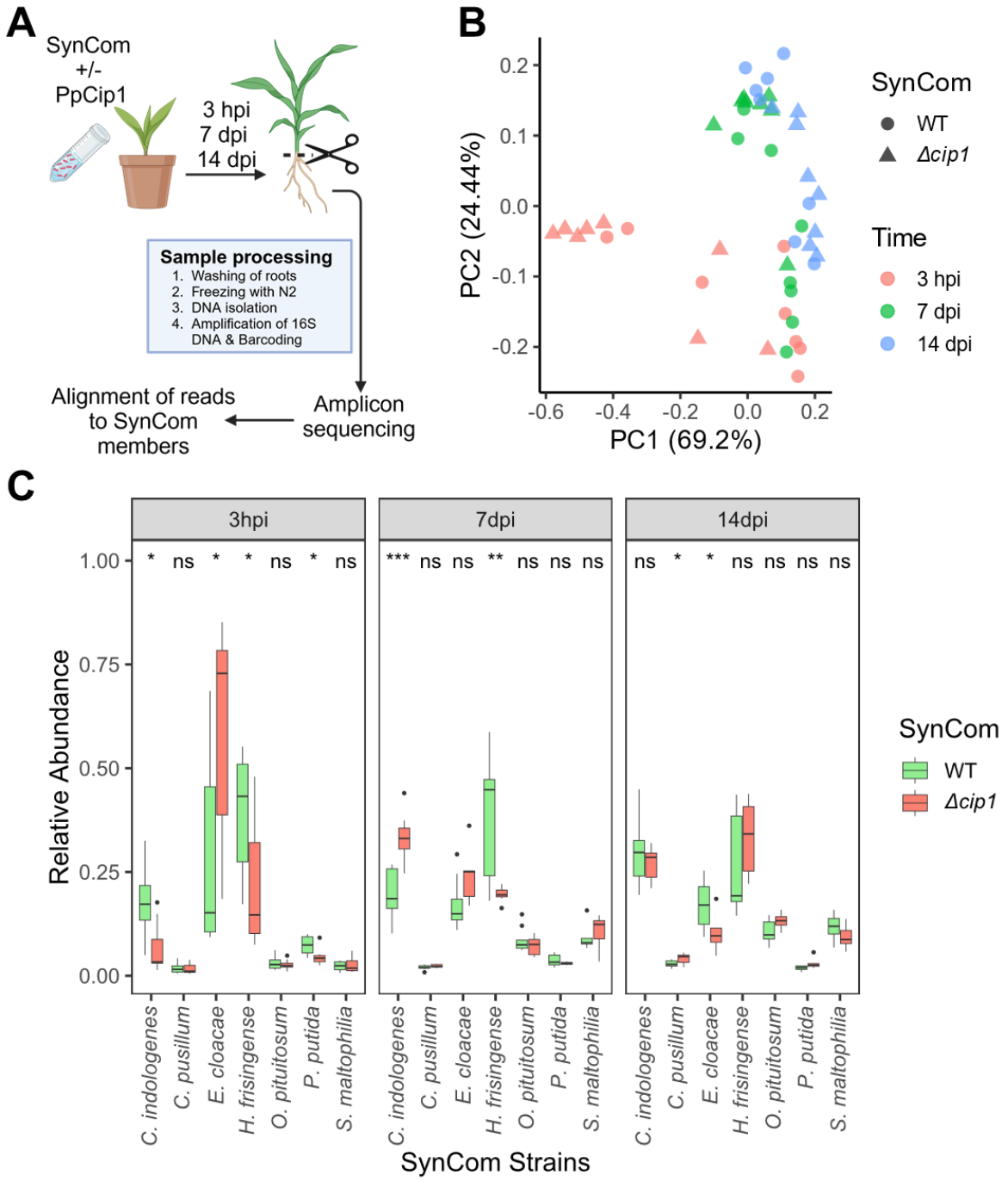

Figure 17: Presence of PpCip1 modulates the structure of the synthetic community (SynCom).

(A) Maize plants were grown in soil containing the six SynCom members and with either *P. putida* WT or *P. putida* Δ*cip1* (inoculated to OD_{600} of 0.0001). Maize roots were collected at 3 hpi, 7 dpi and 14 dpi from maize roots, washed several times by vortexing in water, and samples were frozen with liquid nitrogen. DNA was isolated and 16S sequence was amplified via PCR, barcoded and sent for amplicon sequencing. Reads were aligned to the SynCom members 16S RNA sequences and quantified. This experiment was performed once with eight biological replicates per timepoint and SynCom. This experiment was performed in cooperation with Lioba Rüger, Dr. Noah Kürtös, Dr. Ryohei Thomas Nakano and Dr. Tonni Grube Andersen at Max Planck Institute for Plant Breeding Research in Cologne. **(B)** Principal Coordinate Analysis (PCoA) of quantified reads was performed using a Bray distance matrix to graphically represent all samples. The principal components (PC1 and PC2) represent the

variance in the data. **(C)** The abundance of all SynCom members was quantified based on the aligned reads and normalized to the total amount of reads in a sample. A two-sided t-test was performed ($p<0.05$: *; $p<0.01$: **; $p<0.001$: ***).

We observed that already after 3 hpi the community structure has significantly changed (Figure 17B). At 3 hpi we observed significantly more *E. cloacae* in the community lacking PpCip1 and less *C. indologenes*, *H. frisingense* and *P. putida* itself (Figure 17C). Unfortunately, no sample was collected from the SynCom prior to the inoculation of the plants. Therefore, it cannot be distinguished whether this effect might be due to a difference in the input communities, e.g. caused by pipetting errors, or whether these were already early effects caused by the lack of PpCip1. At 7 dpi *C. indologenes* was significantly more abundant in the community lacking PpCip1, whereas *H. frisingense* is less abundant (Figure 17C). After 14 dpi *C. pusillum* was more abundant in the community lacking PpCip1, whereas *E. cloacae* was less abundant (Figure 17C).

In conclusion, PpCip1-dependent changes in the root community structure could be observed already at 3 hpi but also at later timepoints, suggesting that PpCip1 might have an effect on the ability of *P. putida* to colonize the maize root, thereby indirectly altering the community structure. Alternatively, PpCip1 could also have a direct effect on other microbes or on their ability to colonize the root. Notably, also an effect of PpCip1 on the early colonization (3 hpi) of *P. putida* on maize roots could be observed. However, further experiments including an input control are needed to substantiate these results.

It might be possible that PpCip1 can not only inhibit maize PLCPs but could also inhibit putative PLCPs of other SynCom members. To determine, whether the SynCom members encode genes for PLCPs, a BLASTp search (Altschul *et al.*, 1990; Camacho *et al.*, 2009) was performed using sequences of family C1 proteases (PLCPs) deposited in the MEROPS database (Rawlings *et al.*, 2014) as queries to search for PLCPs in the predicted proteome of all SynCom members. Only one putative C1 family peptidase (Cin_2970) ($E<10^{-3}$) could be identified in *C. indologenes* (Suppl. Table 6). The putative protease of *C. indologenes* is also predicted by SignalP6 analysis (Teufel *et al.*, 2022) to be secreted (Suppl. Table 6). However, it cannot be ruled out that PpCip1 can also inhibit proteases which are not in the C1

family, even though this was never reported for chagasin-like inhibitors (Costa & Lima, 2016; Fu, 2009; Kantyka *et al.*, 2010).

In conclusion, an effect of PpCip1 on the early colonization (<24 hpi) of *A. thaliana* roots (Figure 16) as well as on maize roots (Figure 17) was observed. In contrast, there was no significant effect on late colonization of maize roots (Figure 17, Suppl. Fig. 11). Altogether these results suggest that PpCip1 plays an important role in the early colonization of roots by *P. putida*.

In this chapter, it was shown that bacterial supernatants of *P. putida* can suppress PLCP activity (Figure 5). Moreover, PpCip1 was characterized as a chagasin-like PLCP inhibitor, which might be surface-localized (Figures 7-14). Finally, PpCip1 was observed to promote the early colonization of *A. thaliana* roots, particularly from the meristematic to the elongation zone (Figure 16, Suppl. Fig. 12), but also influences the dynamics of a small bacterial SynCom colonizing maize (Figure 17).

2.3. Screening for additional PLCP inhibitors

2.3.1. Another inhibitor than PpCip1 is responsible for PLCP inhibition by *P. putida* supernatant

PpCip1 was shown to inhibit maize PLCPs CP1A and RD19A-like (Figure 9B-C). However, in contrast to a secreted PLCP inhibitor, PpCip1 as a membrane-anchored inhibitor (Figure 12) should not be present in bacterial culture supernatant. Therefore, it is unlikely that PpCip1 is responsible for the inhibition of maize PLCPs observed for *P. putida* culture supernatant.

To test whether the observed inhibition of PLCPs by the *P. putida* culture supernatant is due to PpCip1, the HMWF of the supernatants of the two marker-less *P. putida* knock-out mutants Δ*cip1* #2 and #3 were used in a substrate cleavage assay with CP1A and RD19A-like and their inhibitory capacities were compared to the supernatant of *P. putida* WT.

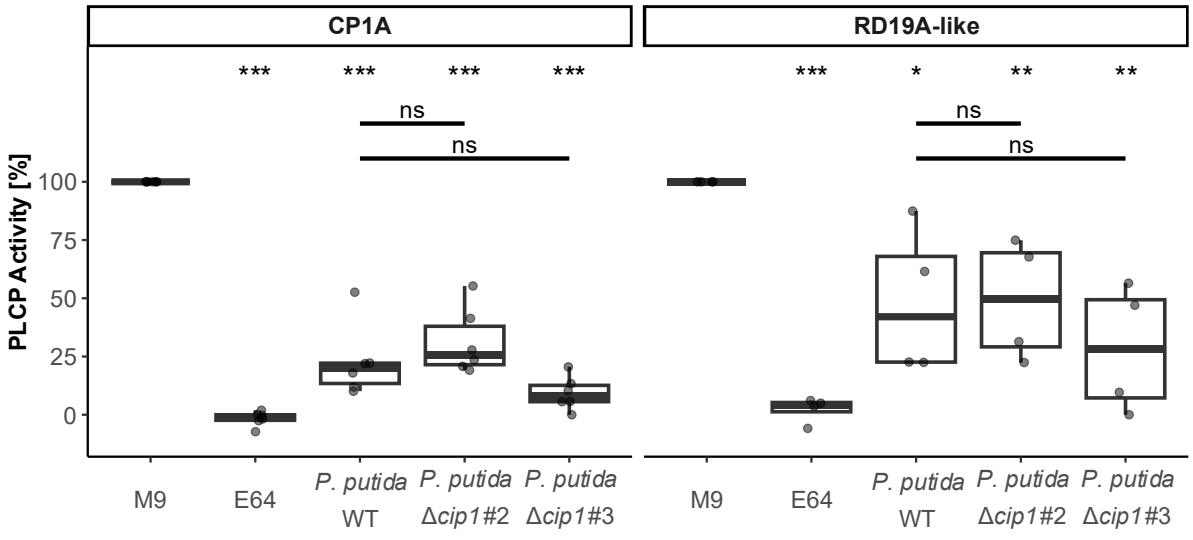

Figure 18: The supernatant of *P. putida* Δ*cip1* is still able to inhibit root PLCPs similar to the wild type.

High molecular weight fractions (HMWF) were collected from bacterial culture supernatants of *P. putida* WT and Δ*cip1* #2/#3. These supernatants were 10X concentrated using a protein concentrator column (MWCO: 5 kDa). CP1A and RD19A-like were preincubated each with either M9 media, E64, or *P. putida* HMWFs. Afterward, the cleavage of the Z-LR-AMC substrate was measured as the increase of AMC fluorescence. The Z-LR-AMC cleavage activity of each sample was normalized twice to the M9 media control set to 100% and to the *N. benthamiana* background activity ($CP1A_{mut}$-mCherry). This experiment was performed with six (CP1A) / four (RD19A-like) biological replicates. Significance was determined by t-test (***: p<0.001, **: p<0.01, *: p<0.05, ns: p>0.05). Some replicates were performed by the student Dorrie Wamser.

CP1A and RD19A-like activity was significantly reduced when incubated with the HMWF of *P. putida* WT or of both *P. putida* Δ*cip1* mutants (Figure 18). However, the inhibition of CP1A and RD19A-like by HMWF of *P. putida* WT was as strong as by the HMWFs of the *P. putida* Δ*cip1* mutants #2 and #3 (Figure 18), indicating that PpCip1 is not responsible for the observed inhibition seen by *P. putida* supernatants. This lack of inhibition fits to the previous results showing that PpCip1 is a membrane localized protein (Figures 12-14), supporting the idea that PpCip1 cannot be responsible for the inhibition observed in bacterial supernatant. Therefore, another putative PLCP inhibitor must be responsible for the PLCP inhibition observed for *P. putida* supernatant, as no loss of inhibition could be observed when the *cip1* gene was deleted.

To identify the putative inhibitor, different screening approaches were established and tested. These screenings were based on four main approaches:

- prediction of interaction via AlphaFold Multimer (Chapter 2.3.2.)
- size-exclusion chromatography (Chapter 2.3.3.)
- interactor pulldown with papain (Chapter 2.3.4.)
- affinity chromatography with papain beads (Chapter 2.3.5.)

2.3.2. Inhibitor screening based on AlphaFold multimer predictions

Recently, a publication reported the successful identification of novel protease inhibitors via AlphaFold Multimer (AF-Multimer) (Homma *et al.*, 2023, 2024). The authors screened small, secreted proteins of seven pathogens (including *P. syringae* pv. *syringae*) with AF-Multimer for interactors of six defense-related hydrolases of tomato, including the tomato PLCP Pip1. Structures of complex models with interface scores (iptm+ptm) above a threshold of 0.75 were manually evaluated. Complexes where candidates blocked the active site of the hydrolases were tested for inhibition of hydrolases. Using this method, the authors could identify novel subtilase inhibitors, indicating that this computational artificial intelligence-based approach can help to identify yet unknown protein-protein interactions. However, they did not identify a novel inhibitor for PLCPs, indicating that either *P. syringae* has no other PLCP inhibitor except PsCip1 or their approach was just not able to identify a putative PLCP inhibitor.

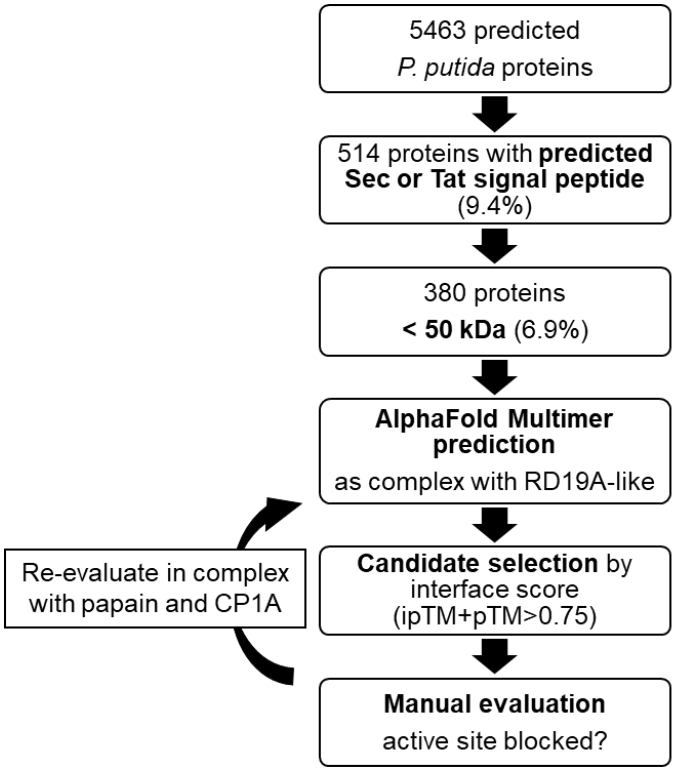

Figure 19: AlphaFold Multimer analysis pipeline used for PLCP inhibitor search.

Of the 5463 predicted *P. putida* proteins only 514 proteins were predicted to have a Sec or a Tat signal peptide via SignalP6 (Teufel *et al.*, 2022). 380 of these proteins are smaller than 50 kDa. These 380 proteins were used for AlphaFold Multimer predictions (Evans *et al.*, 2022; Jumper *et al.*, 2021) in complex with RD19A-like. Candidates were selected based on an ipTM+pTM score of above 0.75. These candidates were reevaluated in AlphaFold Multimer predictions with papain and CP1A. Finally, the protein structure predictions of these proteins were manually evaluated to ensure the active site of the proteases was indeed blocked.

Since the proteome of *P. syringae* differs from *P. putida*, we chose to perform this approach with secreted proteins from *P. putida*. 380 proteins were selected based on their prediction to be secreted (predicted Tat or Sec signal peptide in SignalP6 analysis (Teufel *et al.*, 2022)) and on their size (<50 kDa) as many reported effectors have a size in that range (Figure 19). AF-Multimer predictions (Evans *et al.*, 2022; Jumper *et al.*, 2021) of complexes between RD19A-like and the candidates were performed, and interface scores (iptm+ptm) were determined (Figure 19). 31 complexes had interface scores above 0.75 (Figure 19, Figure 20A) and were selected for further analysis and the complexes were manually evaluated to determine whether the active site is blocked. 15 of these 31 candidates were predicted to bind close to the active site (Figure 19) and were included in further analysis. These 15 candidates were also modeled and scored with papain and CP1A (Figure 19).

A

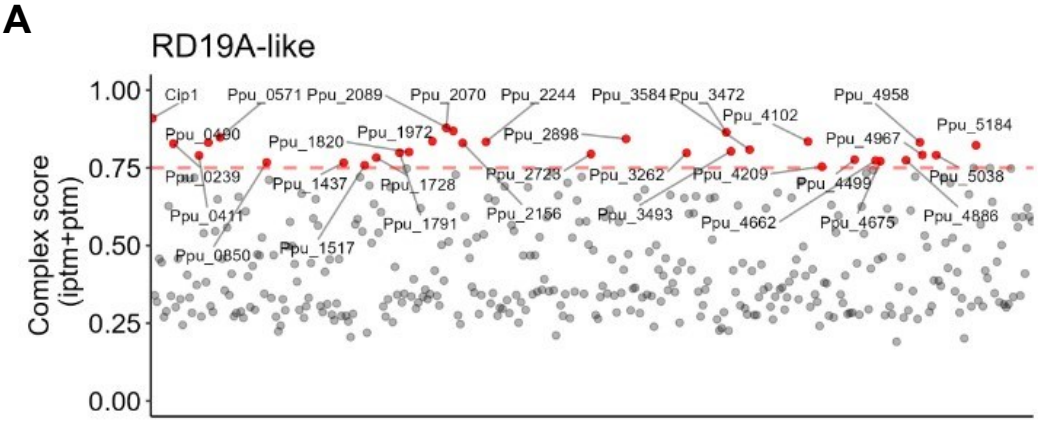

B

ID	Description	SP	Papain	CP1A	RD19A	Mean	Mw
Ppu_1972	DUF2950 domain-containing protein	Sec	0.88	0.85	0.84	0.85	30
Ppu_0571	Polysaccharide deacetylase family protein	Sec	0.82	0.87	0.85	0.85	41
Ppu_2089	Hypothetical protein	Sec	0.81	0.83	0.87	0.84	15
Ppu_5184	Substrate-binding domain-containing protein	Sec	0.83	0.81	0.82	0.82	25
Ppu_1728	Copper chaperone PCu(A)C	Sec	0.78	0.59	0.78	0.72	14
Ppu_2070	Class C beta-lactamase	Sec	0.82	0.38	0.88	0.69	39
Ppu_4209	Carbohydrate porin OprB	Sec	0.85	0.38	0.75	0.66	47
Ppu_2723	Cupin domain-containing protein	Sec	0.28	0.86	0.79	0.64	15
Ppu_1517	TRAP transporter substrate-binding protein	TAT	0.53	0.57	0.76	0.62	34

31 / 380 predictions (8.2%) with score > 0.75
15 / 380 candidates (3.9%) close to active site
5 / 380 candidates (1.3%) similar results with papain &/or CP1A

Figure 20: AlphaFold Multimer screening of PLCPs in complex with secreted *P. putida* proteins to identify suitable PLCP inhibitor candidates.

(A) Interface scores from complexes of RD19A-like and secreted *P. putida* proteins (grey and red points). Complexes with interface scores (iptm+ptm) above 0.75 were considered good candidates for additional rounds of screening (red points). **(B)** Scores of complexes with papain, CP1A, and RD19A-like of candidates with mean above 0.60 and their descriptions. Candidates included for further testing are marked in bold. SP: Signal peptide. Mw: Molecular weight.

Only five complexes with an average score for all three proteases above 0.7 were considered as suitable candidates and were used for further analysis: Ppu_0571, Ppu_1728, Ppu_1972, Ppu_2089, Ppu_5184 (Figure 19+20). Notably, none of these candidates was predicted to be a PLCP inhibitor (Figure 20B). All candidates were predicted to bind close to the active site of RD19A-like (Figure 21), suggesting that they may be able to block substrate access to the active site. However, unlike PpCip1, the candidates did not form loops that directly block the active site residues (Figure 21). In conclusion, AlphaFold Multimer predictions with different maize PLCPs led to the discovery of five inhibitor candidates, which will be tested for their potential to inhibit PLCPs (Chapter 2.3.6).

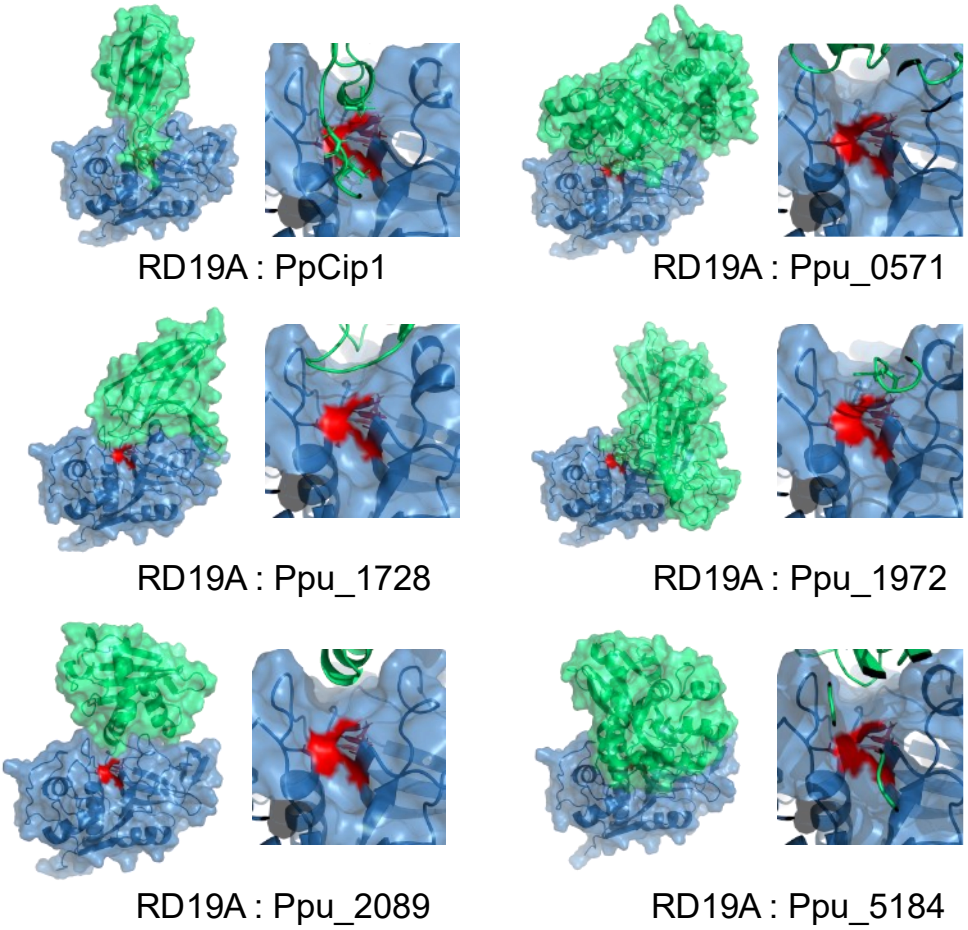

Figure 21: Predicted protein structure of the final candidates in complex with RD19A-like.

Complexes of RD19A-like (blue) and candidates (green) were predicted using AlphaFold Multimer (Evans *et al.*, 2022; Jumper *et al.*, 2021). The active site of RD19A-like is labeled in red. Full representation of each complex (left) and zoom on the active site (right) are shown.

2.3.3. Inhibitor screening based on size-exclusion chromatography

The previous experiments indicated the presence of another proteinaceous PLCP inhibitor of *P. putida* except PpCip1. While the AF-Multimer modeling led to the discovery of some inhibitor candidates, a biochemical approach was used to identify the putative inhibitor from another angle. To obtain more insights about the size of the putative inhibitor, the secreted *P. putida* proteins were separated by molecular size. Therefore, size-exclusion chromatography was performed with the *P. putida* Δ*cip1* culture supernatant. Even though the peaks of protein UV absorbance were not well separated (Figure 22A, black line), some size-dependent separation of proteins was observed upon SDS-PAGE and SYPRO Ruby staining (Figure 22B). Notably, the

combined fraction E4-9 contained proteins of all sizes probably due to aggregation or denaturation of proteins causing a shorter retention time of smaller proteins from the beads. When the combined fractions were tested for inhibition of CP1A in a substrate cleavage assay, fractions E4-9, E35-39 and E44-55 showed PLCP inhibition ranging from 20 to 60 % (Figure 22A, orange), suggesting different inhibitors present in the sample. Interestingly, while most fractions that showed inhibition contained multiple proteins according to the sensitive SYPRO Ruby staining, the PLCP-inhibiting fraction E44-55 contained a dominant band corresponding to proteins with approx. 15 kDa and showed approx. 20% inhibition. Similar results were obtained from another size-exclusion chromatography, where a band of the same size was identified in the fraction showing PLCP inhibition (Suppl. Fig. 13). These results indicate that E44-55 might contain the protein(s) causing PLCP inhibition, therefore the band was excised and sent for analysis via mass spectrometry (MS, in collaboration with Farnusch Kaschani).

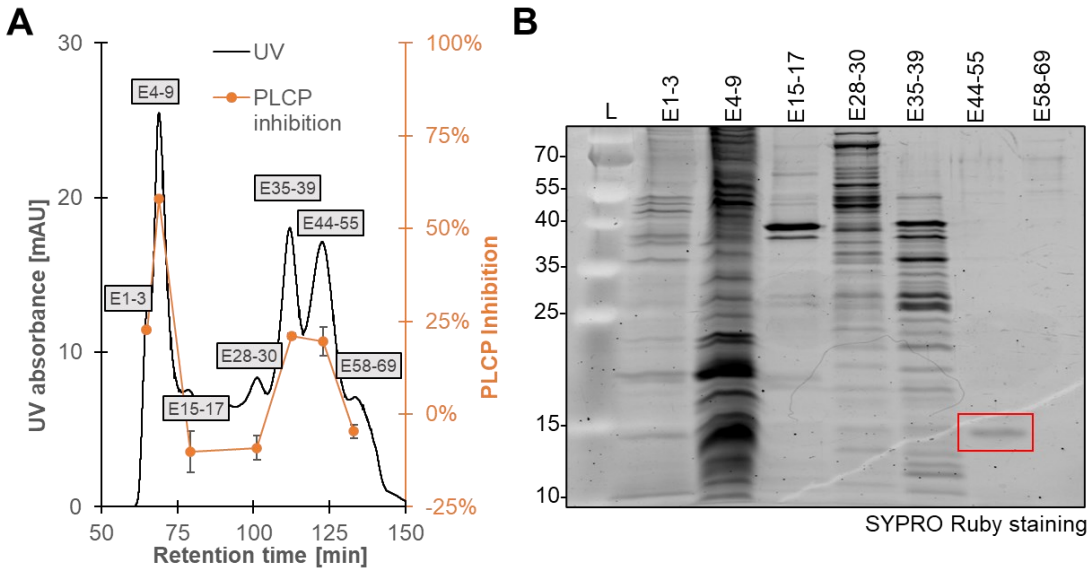

Figure 22: Identification of PLCP inhibitors via size-exclusion chromatography (SEC) of *P. putida* culture supernatant.

(A) SEC of 10X concentrated HMWF of *P. putida* Δ*cip1* culture supernatant was performed with Tris-HCl buffer pH7, 500 mM NaCl. Fractions of UV absorbance peaks (black) were pooled and tested for CP1A inhibition (orange) via the substrate cleavage assay with Z-LR-AMC. This experiment was performed once. **(B)** Pooled fractions were loaded onto polyacrylamide gels and SDS-PAGE was performed to separate proteins in the samples by size. SYPRO Ruby staining of the proteins was performed. Red box indicates an excised band for mass spectrometry (MS) analysis.

42 proteins were detected via MS in the excised band of fraction E44-55. Most hits matched the expected size of approx. 15 kDa. Next, the proteins were classified based

on their localization prediction via SignalP6 (Teufel *et al.*, 2022), resulting in 24 cytosolic , 13 secreted (Sec/SPI, TAT) and five lipoprotein (Sec/SPII) proteins (Suppl. Table 7). Since the putative inhibitor was predicted to be secreted and should not be annotated with another function yet, only five secreted and not (well) annotated proteins were selected as candidates for further analysis (Suppl. Table 7): Ppu_1728, Ppu_2677, Ppu_3965, Ppu_4449, Ppu_4944. Notably, Ppu_1728 was also identified as putative PLCP inhibitor candidate via AF-Multimer modeling. The remaining cytosolic proteins and lipoproteins were most likely released from broken cells and were not taken into consideration for further analysis.

In conclusion, the size-separation of proteins in the bacterial supernatant led to the discovery of five possible inhibitor candidates, which will be tested for their potential to inhibit PLCPs (Chapter 2.3.6).

2.3.4. Inhibitor screening based on pulldown with papain

Since *P. putida* supernatant was shown to also inhibit papain (Figure 5), it might be possible to pull-down the PLCP inhibitor with papain-coupled to agarose beads, as was shown also in previous publications (Barrett, 1985; Cotabarren *et al.*, 2021; Guo & Ruckenstein, 2002; Kędzior *et al.*, 2018; Pernas *et al.*, 1998; Ryan *et al.*, 1998; Yadav *et al.*, 2013). As a proof of concept, the already characterized maize cystatin and PLCP inhibitor CC1 (Schulze Hüynck, 2019) was heterologously produced with an C-terminal His-Tag, purified by affinity chromatography (Suppl. Fig. 14) and tested as a positive control to show the feasibility of using papain beads for enrichment of PLCP inhibitors.

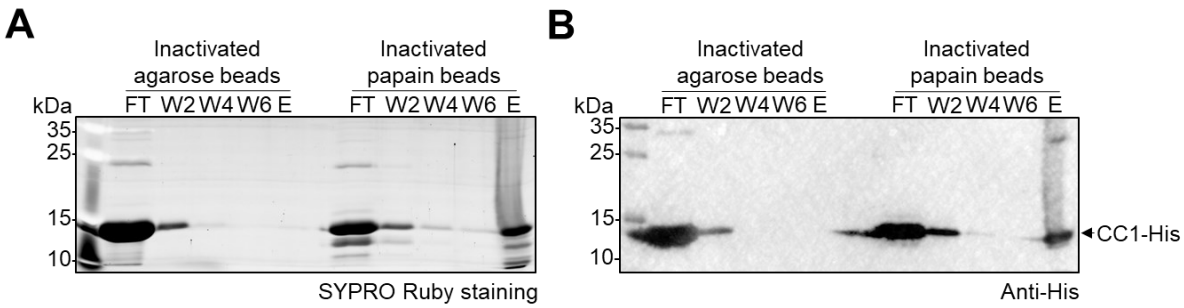

Figure 23: Proof-of-concept of PLCP inhibitor pulldown using papain beads and maize cystatin CC1.

Heterologously expressed and purified CC1-His was used for pulldown with papain beads as a proof-of-concept. Agarose and papain beads were inactivated using S-carboxymethylation and these beads were incubated with CC1-His. Supernatant was collected (FT). Finally, beads were washed (W1-6) and the presence of CC1-His on agarose and papain beads (elution, E) was evaluated using SDS-PAGE, followed by **(A)** SYPRO Ruby staining and **(B)** Western Blot with primary antibody against the His-tag.

Agarose beads were used as a negative control to determine which proteins bind specifically to papain and not to the agarose matrix used to immobilize papain. The agarose and papain beads were inactivated with sodium chloroacetate, since this was previously reported to be important for the enrichment of protease interacting proteins (Kędzior *et al.*, 2018). Afterwards, the sample with CC1-His was incubated with the agarose and papain beads for 12 hours at 4°C, and beads were washed six times with a buffer (W1-6). Proteins were eluted from the beads (E) by heating with 6X SDS-loading buffer at 98°C. Samples from every step were taken and analyzed by SYPRO Ruby staining (Figure 23A) or western blot with α-His antibodies to monitor CC1-His presence (Figure 23B). While small amounts of CC1-His were washed off from both bead types, almost no CC1-His was visible in the last wash fraction indicating good binding to the papain beads. CC1-His was bound to the papain beads but not to the agarose beads (Figure 23), indicating that CC1-His specifically binds to papain and not to the agarose matrix used for papain immobilization proving the usability of the papain beads for inhibitor enrichment. This result indicates that the pulldown using papain-beads can enrich PLCP inhibitors.

After the successful enrichment of CC1-His with papain, the same protocol was used for the pull-down of the putative inhibitor. Agarose and (active and inactive) papain beads were incubated with 10X concentrated HMWF of *P. putida* supernatant for 24 hours at 4°C. Additionally, inactive papain beads not incubated with the supernatant were included as a control. The washed beads were split after the

washing step into two samples used for the visualization on SDS-PAGE and for the MS analysis.

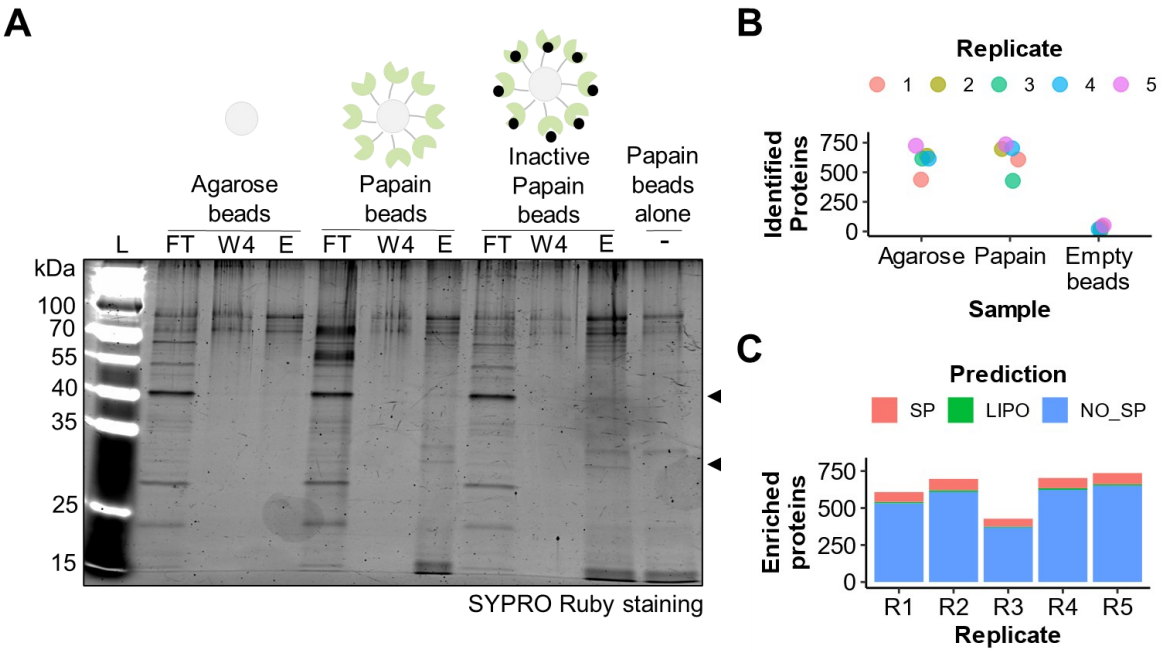

Figure 24: PLCP inhibitor pull-down with papain beads.

(A) 10X HMWF of *P. putida* Δ*cip1* supernatant was incubated with either agarose beads, active or inactivated papain beads for 24 hours at 4°C. Papain beads without supernatant incubation were used as a control (-). Afterwards, the remaining supernatant (FT) was collected and the beads were washed six times (W1-4). The remaining beads (E) were analyzed via SDS-PAGE followed by SYPRO Ruby staining. Black arrows indicate protein bands of interest present on papain beads but not on agarose beads or papain beads without supernatant. This experiment was performed once with five replicates. **(B)** Number of proteins found on the agarose, papain, or papain-alone beads after MS analyses. **(C)** Number of absolutely enriched proteins (LFQ intensity difference between papain and agarose beads) of each replicate and their predicted localization via SignalP6 (Teufel *et al.*, 2022) SP: Sec and Tat signal peptide, LIPO: Lipoprotein, NO_SP: no predicted signal peptide.

The SDS-PAGE of the proteins in all flow-through (FT), wash (W) and elution (E) samples showed that these samples contained many proteins larger than 55 kDa which are present on agarose and papain beads (Figure 24A), indicating that these proteins bind to the agarose matrix. Furthermore, the elution of papain beads but not agarose beads showed a band corresponding to an approx. 23 kDa protein, which is likely papain (Vernet *et al.*, 1991), as it could also be found on papain beads alone (Figure 24A). Interestingly, in the elution from active and inactive papain beads incubated with the supernatant, two prominent bands corresponding to proteins with a molecular weight of approx. 20 kDa and 35 kDa are visible (Figure 24A). These bands were not present in the elution from agarose beads or papain beads not

incubated with the supernatant. Therefore, it is likely that these proteins specifically interact with papain. This experiment was repeated five times showing comparable results however the quantity of the two papain specific bands as well as the background signals varied strongly. Unfortunately, also the amount of beads was extremely variable. Approximately 400 to 700 proteins identified by MS were present on agarose and inactive papain beads incubated with the supernatant, while only less than 100 proteins were found on the papain beads without sample (Figure 24B), likely being contaminations or carrier-over during the LC-MS. The untargeted label-free quantitation (LFQ) intensities corresponding to the proteins found on the agarose beads were subtracted from the intensities corresponding to proteins on the papain beads (absolute enrichment, difference > 0). Beads from replicates 1, 2, 4 and 5 had at least 400 enriched proteins but replicate 3 had only less than 100 enriched proteins (Figure 24C), indicating a specific binding of proteins to the papain beads but not to the agarose beads. Replicate 3 was considered as outlier and excluded in the following analysis.

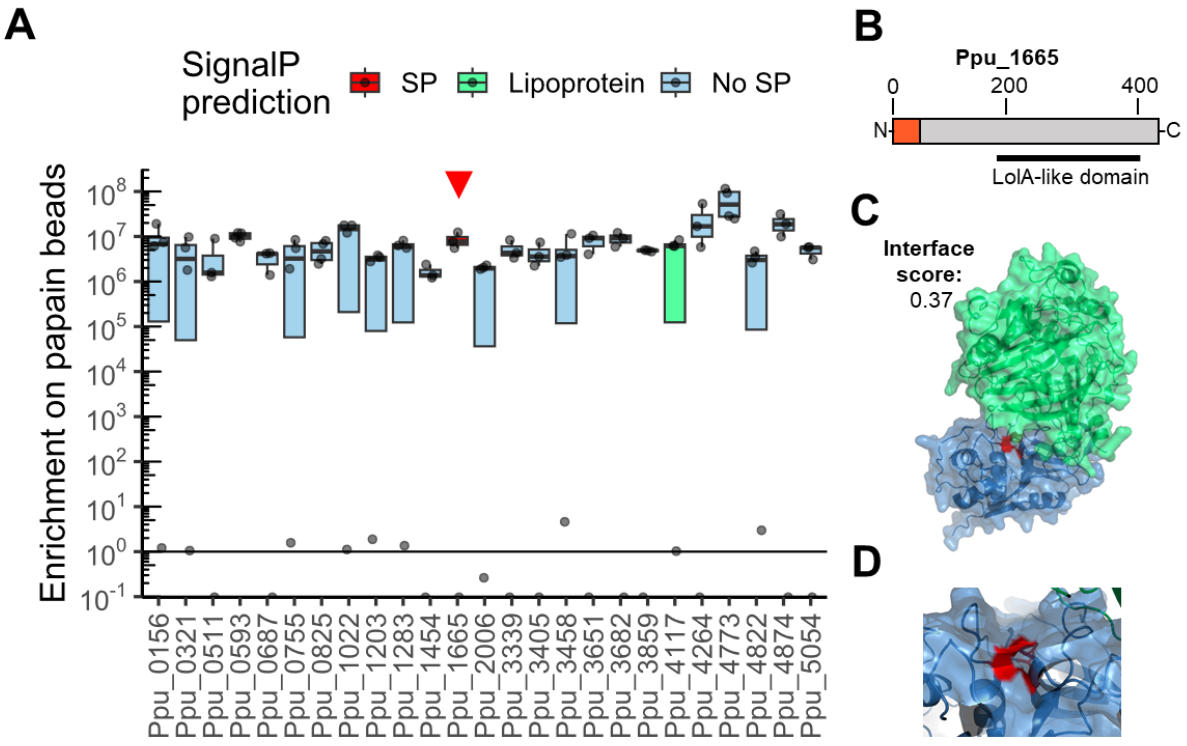

Figure 25: One secreted protein enriched on papain beads after pulldown.

(A) The relative enrichment on papain beads compared to agarose beads was determined by dividing the LFQ intensities of proteins found on papain beads by the LFQ intensities of proteins found on agarose beads plus 1 (no division by zero). Only proteins enriched on papain beads by at least factor 100 compared to agarose beads in at least three of four replicates were selected. Signal peptide

prediction was performed using SignalP6 (Teufel *et al.*, 2022). SP: Signal peptide. Red triangle: Ppu_1665. **(B)** InterPro database search with Ppu_1665 sequence reveals LolA like domain. Orange: Signal peptide **(C, D)** Complex of RD19A-like (blue) and Ppu_1665 (green) was predicted using AlphaFold Multimer (Evans *et al.*, 2022; Jumper *et al.*, 2021). The active site of RD19A-like is labeled in red. Full representation of each complex (C) and zoom on the active site (D) are shown.

To determine which proteins were enriched on papain beads, the relative enrichment on papain beads compared to agarose beads was calculated by dividing the LFQ intensities of candidates found on papain beads by the LFQ intensities of candidates found on agarose beads plus 1 (no division by zero). Proteins enriched on the papain beads were categorized by their localization predicted via SignalP6 (Teufel *et al.*, 2022). Notably, most of the proteins found on the beads were not predicted to be secreted, while the rest (approx. 20) were predicted to be secreted (Figure 24C), indicating cell death or leakage during the long incubation to obtain bacterial supernatants.

As many proteins were found to be enriched on papain beads, only proteins enriched on papain beads by factor 100 compared to agarose beads in at least three of four replicates were selected for further analysis, resulting in 25 proteins, which were specifically enriched on papain beads (Figure 24A). Of these 25 protein, only one protein, Ppu_1665, was predicted by SignalP6 (Teufel *et al.*, 2022) to be secreted (Figure 24A). Ppu_1665 is yet uncharacterized and belongs to the DUF1329 family which is mostly found in *Pseudomonads* according to the InterPro database (Hunter *et al.*, 2009). The protein also contains a LolA-like domain (Figure 24B), which has a low similarity to periplasmic molecular chaperone LolA, the outer membrane lipoprotein receptor LolB and the periplasmic protein RseB, which all have a similar structure, according to the database entry in the InterPro database (Hunter *et al.*, 2009). Additionally, LolA-like proteins were predicted to play a role in the outer membrane biogenesis (Price *et al.*, 2018) by interfering with the Lol system (Wang *et al.*, 2021a). Recently, DUF1329 family proteins were also hypothesized to function as esterases (Thompson *et al.*, 2020). Notably, AlphaFold Multimer predictions (Evans *et al.*, 2022; Jumper *et al.*, 2021) of the complex between RD19A-like and Ppu_1665 indicate an interaction between the proteins (Figure 24C), however with a low interface score and without a blocked active site (Figure 24D). In conclusion, from the papain beads pull down analysis we have identified one putative secreted protein, Ppu_1665, suggesting that it might specifically interact with

papain and will be tested for its potential to inhibit PLCPs (Chapter 2.3.6). Notably, Ppu_1665 was not identified in any of the other screening approaches.

2.3.5. Inhibitor screening using affinity chromatography with papain beads

The previous approach with papain beads pull-down suggested a problem with unspecific binding likely due to long incubation times of the beads. Moreover, to avoid cell leakage during incubation of *P. putida* in M9 medium, shorter incubation times (four hours) were used to obtain bacterial supernatant in this approach. In order to address these issues, an affinity chromatography system was established allowing shorter incubation times on the beads.

To identify further putative inhibitors, papain coupled to agarose beads (papain beads) was again utilized to pull down possible inhibitors from solution using affinity chromatography and a salt gradient for elution. As a control, only agarose beads (without coupled of papain) were used. The beads were filled into 1 ml columns and were connected to an ÄKTA system. *P. putida* was incubated for four hours in M9 medium. Afterwards, the supernatant was collected and concentrated with a 5 kDa MWCO filter column. Finally, the HMWF was loaded onto the column and the beads were washed. Bound proteins were eluted by increasing salt concentrations (Figure 26A), as it was planned to test the elution fractions for inhibition and to reuse the columns, if possible. While a strong elution peak was observed with papain beads, no such peak was observed with agarose beads (Figure 26A). The elution fractions were collected, concentrated with a 3 kDa MWCO concentrator filter and sent for MS analysis. Multiple proteins were visible when the concentrated elution sample was analyzed by SDS-PAGE: Major bands were present at molecular weights between approximately 10 and 60 kDa (Figure 26B).

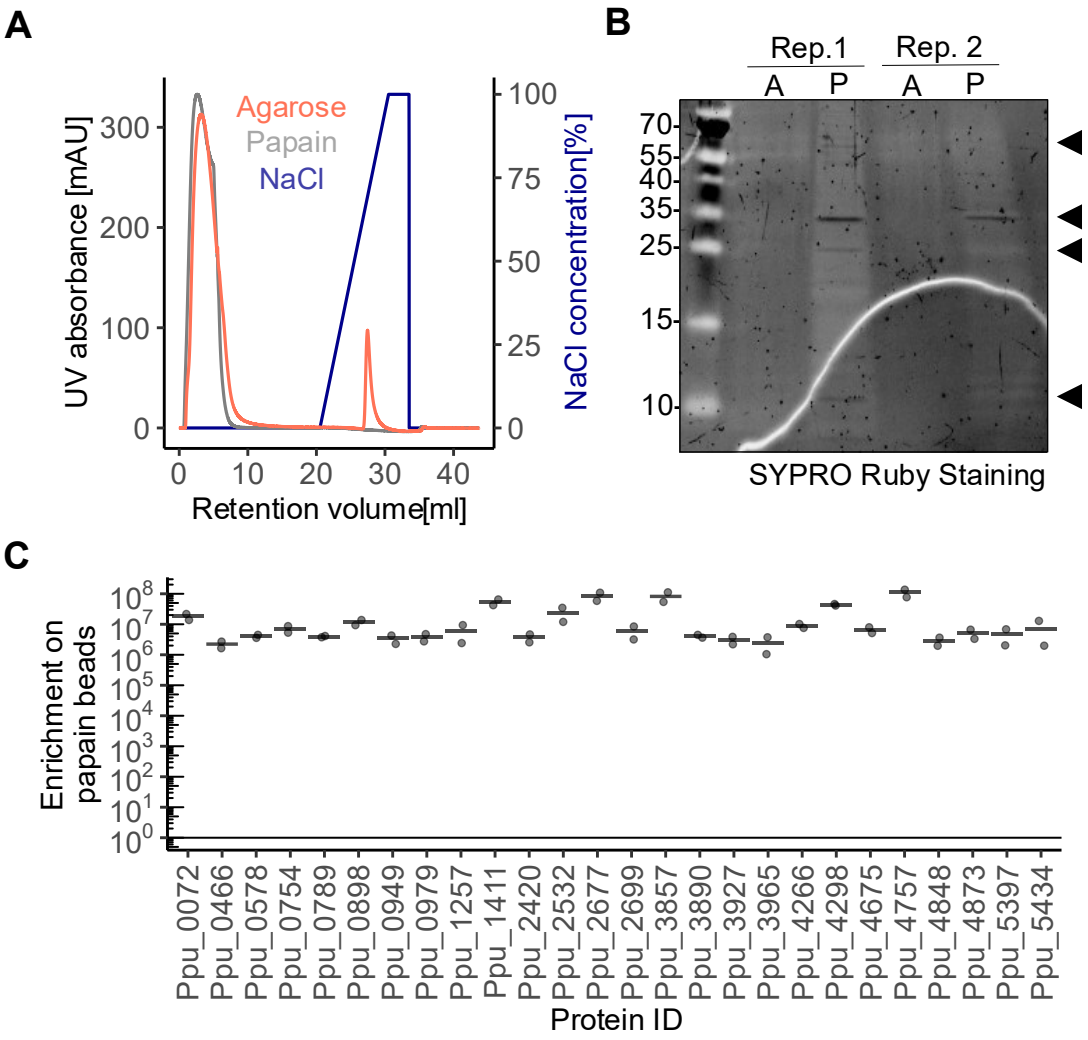

Figure 26: Affinity chromatography of *P. putida* supernatants with papain beads identified potential inhibitor candidates.

As matrix, either agarose beads coupled with papain or agarose beads alone were used and filled into 1 ml columns. *P. putida* was incubated for four hours in M9 medium and afterwards the supernatant was concentrated with a protein concentrator column (MWCO 5 kDa). The elution was performed with a linear gradient from 0 to 3 M NaCl. The experiment was performed once with two replicates. **(A)** Chromatogram of affinity chromatography on agarose (black) or papain (red) beads. The salt content (green) was increased after 20 ml retention volume. An elution peak was visible only on papain beads after approx. 60% 3 M NaCl., but not on agarose beads. **(B)** The elution fractions were combined, concentrated and an SDS-PAGE was performed. Several protein bands (red arrows) were visualized by SYPRO Ruby staining (e.g. with approx. 10 kDa, 25 kDa, 35 kDa and 70 kDa). **(C)** The relative enrichment proteins eluted from papain beads compared to agarose beads was determined by dividing the LFQ intensities of proteins eluted from papain beads by the LFQ intensities of proteins eluted from agarose beads plus 1 (no division by zero). Only secreted proteins relatively enriched by at least a factor of 100 in both replicates were selected.

318 proteins were identified via MS to be eluted at least 100-times more from the papain beads compared to agarose beads. Only 26 of these proteins were predicted to be secreted (Figure 26C, Suppl. Table 8). Only 14 of these proteins did not have a

specific annotation whereas proteins with annotations unlikely to be inhibitors such as a predicted membrane localization or peptidases were not considered further in the analysis. Of the promising 14 candidates, only six proteins have no (clear) functional annotation (Ppu_2677, Ppu_2699, Ppu_3857, Ppu_4298, Ppu_4757) (Suppl. Table 8). One candidate, Ppu_2532 draw our attention, since it is the serpin-like serine protease inhibitor ecotin, which is so far not known to be also an inhibitor of cysteine proteases (De Meyer & Carlier, 2023), however other inhibitors have been shown to have dual functionality targeting proteases with different catalytic residues (Bode & Huber, 2000; Cohen *et al.*, 2019; Grosse-Holz & van der Hoorn, 2016).

In conclusion, the established approach showed less unspecific binding of proteins to agarose beads compared to what was observed in the pull-down with papain beads. Moreover, this approach yielded six inhibitor candidates which were eluted from papain beads, which will be tested for their potential to inhibit PLCPs (Chapter 2.3.6). Interestingly, Ppu_2532 and Ppu_2677 were also identified with the screening using size-exclusion chromatography, indicating that they might be responsible for the inhibition of PLCP activity by the inhibitory fraction of *P. putida* supernatant collected during size-exclusion chromatography. Moreover, Ppu_4298 was also identified on the papain-beads after the pull down, however it was not enriched on the papain beads, suggesting that it was not binding specifically to papain.

The four screening approaches yielded a total of 15 inhibitor candidates (Table 3), four of which were identified by two different approaches. In conclusion, the computational approach utilizing AF-Multimer facilitated the rapid screening of a comprehensive range of proteins for potential protein-protein interactions. Nevertheless, the generation of a more comprehensive structure and sequence database of MSAs encompassing sequences analogous to the tested candidate is necessary to achieve reliable complex predictions, which is currently not feasible. Moreover, the screening based on size-exclusion chromatography is rather unspecific, yet it led to the discovery of an inhibitory fraction. It is noteworthy that the majority of proteins identified in the fraction of the bacterial culture supernatant have been predicted to be intracellular, which suggests that cell death or leakage may have occurred during the incubation of the bacterial cells in M9 medium. It is therefore recommended that shorter incubation times to be employed in subsequent tests. Furthermore, the pulldown and affinity chromatography using papain beads led to the identification of proteins that

specifically bind to papain. It is notable that many proteins bound to the agarose matrix; thus, it may be beneficial to test other matrixes to immobilize papain. Similar to the results obtained from size-exclusion chromatography, many proteins enriched on papain beads were also predicted to be intracellular.

2.3.6. Testing of candidates for PLCP inhibition

The four approaches yielded 15 inhibitor candidates (Table 3). 14 sequences of these candidates were cloned into the pOPIN-K expression vectors (Bentham *et al.*, 2021), with an N-terminal His-tag and were heterologously expressed in *E. coli* BL21 cells.

Table 3: Inhibitor candidates from screenings.

Candidates from all four screenings (AlphaFold (AF) Multimer, size-exclusion chromatography (SEC), pulldown with papain beads, and affinity chromatography (AC) with papain beads) are listed and ordered by their number of identifications. Cells filled with black color indicate that the candidate was found in the respective screening. Their molecular weight (MW) and signal peptide prediction are displayed. Proteins were screened for inhibition: dark-grey: tested after full purification, light-grey: only whole cell fraction was tested, white: not tested. Proteins which showed inhibition in a substrate cleavage assay with CP1A are filled with red. Red star: Protein was identified on papain beads upon pulldown but was not enriched. The tests were performed by Eva Slavic, Melina Laporta and myself.

ID	Ppu_1728	Ppu_2532	Ppu_2677	Ppu_4298*	Ppu_0571	Ppu_1665	Ppu_1972	Ppu_2089	Ppu_2699	Ppu_3857	Ppu_3965	Ppu_4449	Ppu_4757	Ppu_4944	Ppu_5184
Description	Copper chaperone PCu(A)C	Serine protease inhibitor ecotin	Hypothetical protein	SIMPL domain-containing protein	Polysaccharide deacetylase protein	DUF1329 domain-containing protein	DUF2950 domain-containing protein	Hypothetical protein	YMGG-like glycine zipper-containing protein	Hypothetical protein	Quorum-sensing-regulated virulence factor protein	Hypothetical protein	DUF1090 domain-containing protein	DUF4399 domain-containing protein	Substrate-binding domain-containing protein
AF Multimer	■				■		■	■							■
SEC	■	■	■								■	■		■	
Pulldown				■		■									
AC		■	■	■					■	■			■		
MW [kDa]	17	17	21	26	44	50	33	17	16	45	15	17	14	17	26
Screened	■	■	■	■	■	■	■	■	■		■	■	■	■	■
Confirmed inhibition						■						■	■		

Unfortunately, one candidate could not be tested due to unsuccessful cloning (Table 3, screened for inhibition: white). Twelve heterologously expressed proteins were purified via affinity chromatography and size-exclusion chromatography (Table 3, screened for inhibition: orange). Two of the candidates could not be purified due to time limitations, and therefore soluble fractions of sonicated bacteria heterologously expressing candidate proteins were used for the testing (Table 3, screened for inhibition: grey). These His-tagged proteins or supernatants were tested in a substrate cleavage assays with Z-LR-AMC for the inhibition of heterologously expressed CP1A.

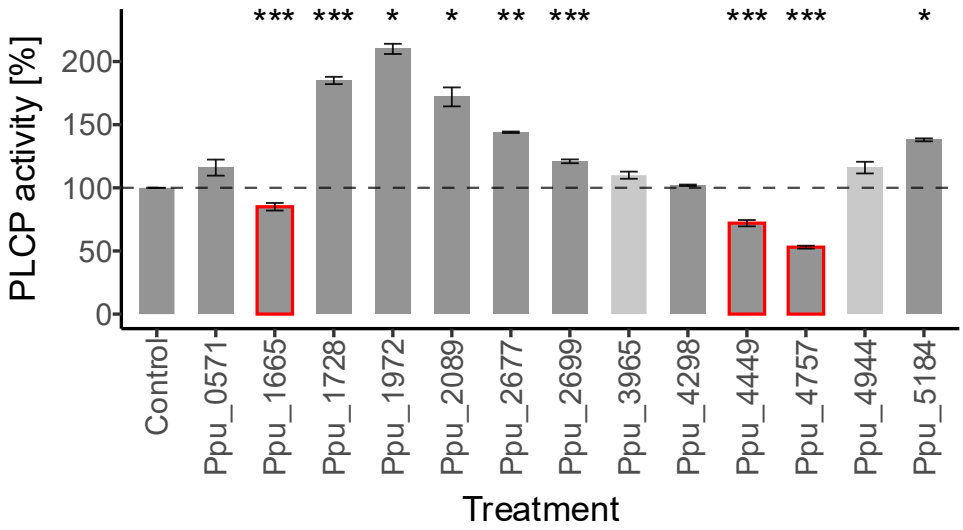

Figure 27: Testing of PLCP inhibitor candidates for inhibition of CP1A.

Heterologously expressed CP1A was preincubated with either a control (buffer used for purification), E64, or the candidate (dark-grey fill: purified candidate, light-grey fill: supernatant containing candidate, red outline: significant inhibition) for 15 minutes. Afterward, the cleavage of the Z-LR-AMC substrate was measured as the increase of AMC fluorescence. After subtracting non-PLCP activity (E64 control), the Z-LR-AMC cleavage activity of each treated sample was normalized to the control set to 100%. The experiment was performed once with at least three technical replicates. Different concentrations of purified candidates were used: 1 µM: Ppu_1665, Ppu_1972, Ppu_2089; 5 µM: Ppu_0571, Ppu_1728, Ppu_2677, Ppu_2699, Ppu_4298, Ppu_4757, Ppu_5184; 10 µM: Ppu_4449.Error bars represent the SEM. Two-sided t-tests were performed against the control ($p<0.05$: *; $p<0.01$: **; $p<0.001$: ***). The tests were performed by Eva Slavic, Melina Laporta and myself.

Of the tested candidates only three candidates showed significant reduction of PLCP activity, Ppu_1665, Ppu_4449 and Ppu_4757 (Figure 27, Table 3, confirmed inhibition: red), suggesting that they might be PLCP inhibitors. In contrast, other candidates did increase the PLCP activity, suggesting that they might stabilize CP1A activity, or did not show any effect (Figure 27). For example, the increase in PLCP activity could be due to the stabilization of CP1A by the candidates, as was observed for *A. thaliana* PIRIN2 (PRN2) stabilizing XCP2 by suppression of its autolysis (Zhang *et al.*, 2014).

It is important to mention that for the candidates Ppu_3965, and Ppu_4944, which were not tested as purified proteins, still a purification step is required.

The concentration of Ppu_4449 and Ppu_4757 required to obtain 50% inhibition (IC_{50}) (Neubig *et al.*, 2003) was in the micromolar range, with IC_{50} of 33 µM for Ppu_4449 and approx. 5 µM for Ppu_4757 (Figure 28A, Figure 29A), indicating these proteins to be rather good substrates competing with the 10 µM Z-LR-AMC substrate for cleavage. While 1 µM His_Ppu_1665 showed 15 % inhibition of CP1A (Figure 27), an IC_{50} of Ppu_1665 could not be determined, as the concentration of purified His-Ppu_1665 was too low to obtain 50% PLCP inhibition.

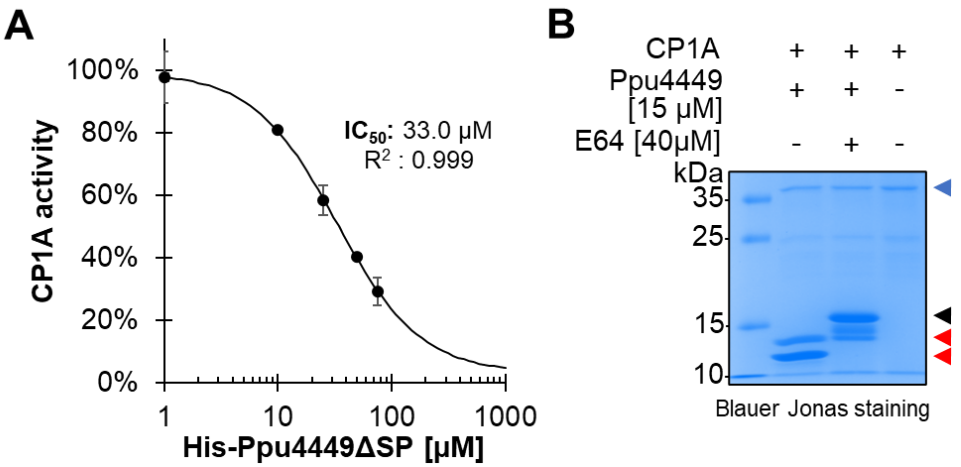

Figure 28: Ppu_4449 is likely a PLCP substrate.

(A) His-Ppu_4449 was heterologous expressed and purified. Different concentrations of His-Ppu_4449 were tested for CP1A inhibition in substrate cleavage assay with 10 µM Z-LR-AMC. IC_{50} was estimated by fitting the data with sigmoid function Hill-function (Neubig *et al.*, 2003) (Hill1) in Origin. The experiment was performed once with at least three technical replicates. **(B)** The stability of His-Ppu_4449 in presence of CP1A was tested by incubating leaf apoplastic fluid with heterologously expressed CP1A (blue triangle) with His-Ppu_4449 (black triangle), and with or without the PLCP inhibitor E64 (Hanada *et al.*, 1978) for 30 min at room temperature. Afterwards the samples were visualized by SDS-PAGE followed by Blauer Jonas staining. Processed His-Ppu_4449 is indicated by red triangles. The experiment was performed once.

To test whether His-Ppu_4449 is cleaved by CP1A, 15 µM of His-Ppu_4449 was incubated for 30 min at room temperature with *N. benthamiana* apoplastic fluids containing overexpressed CP1A as well as with or without E64. Visualization of the samples by SDS-PAGE followed by staining showed that His-Ppu_4449 was cleaved only by active CP1A resulting in multiple smaller fragments (Figure 28B). These findings indicate that His-Ppu_4449 is rather a substrate for CP1A than a classical PLCP inhibitor.

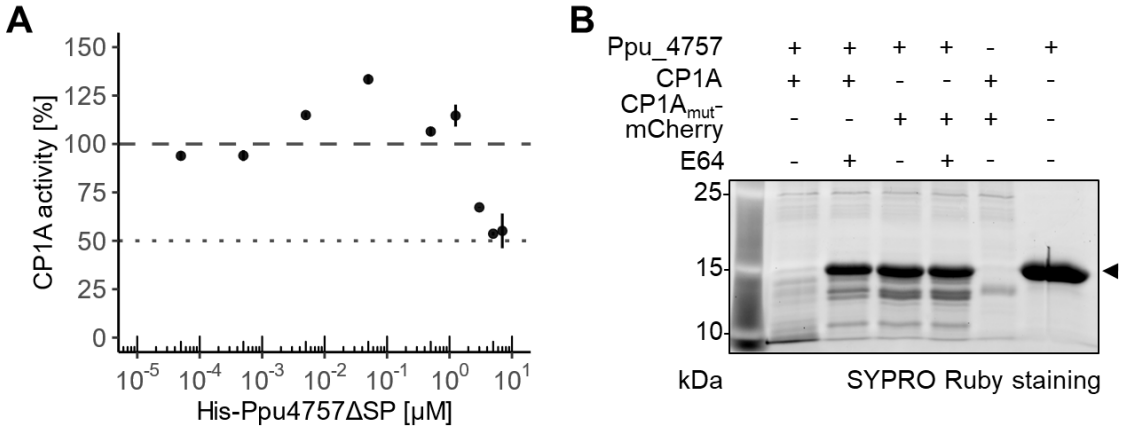

Figure 29: Ppu_4757 is likely a PLCP substrate.

(A) His-Ppu_4757 was heterologous expressed and purified. Different concentrations of His-Ppu_4757 were tested for CP1A inhibition in substrate cleavage assay with 10 µM Z-LR-AMC. No fitting using Hill-function was possible. IC_{50} was estimated based on 50% inhibition of CP1A. Dashed line: 100% CP1A activity, dotted line: 50% CP1A activity. The experiment was performed once with at least three technical replicates. **(B)** The stability of 500 ng His-Ppu_4757 in presence of CP1A was tested by incubating CP1A or inactive $CP1A_{mut}$-mCherry with His-Ppu_4757, and with or without the PLCP inhibitor E64 (Hanada *et al.*, 1978) for 30 min at room temperature. Afterwards the samples were visualized by SDS-PAGE followed by SYPRO Ruby staining. Arrowhead indicates His-Ppu_4757. The experiment was performed twice. The experiments displayed in this figure were performed under my supervision by Eva Slavic during her Master thesis.

To test whether His-Ppu_4757 is cleaved by CP1A, 500 ng of His-Ppu_4757 was incubated for 30 min at room temperature with *N. benthamiana* apoplastic fluids containing overexpressed CP1A or inactive $CP1A_{mut}$-mCherry as well as with or without E64. Visualization of the samples by SDS-PAGE followed by staining showed that His-Ppu_4757 was absent when incubated with active CP1A (Figure 29B), but not when CP1A was inactivated with E64 (Figure 29B), indicating cleavage by CP1A. Moreover, two smaller fragments of approx. 10 and 13 kDa were observed when more His-Ppu_4757 was incubated with overexpressed CP1A, but was not observed in the controls (Suppl. Fig. 16), suggesting that the His-Ppu_4757 contains at least two cleavage sites for CP1A. These findings indicate that His-Ppu_4757 is rather a substrate for CP1A than a classical PLCP inhibitor. Moreover, fragments with approx. 10 to 13 kDa were observed in the background control containing inactive $CP1A_{mut}$-mCherry incubated with E64 (Figure 29B), indicating that also other proteases in the apoplastic fluid except PLCPs cleave this protein. Unfortunately, it could not be tested whether His-Ppu_1665 can also be cleaved by CP1A due to time limitations. In conclusion, in our screening two inhibitor candidates, Ppu_4449 and Ppu_4757, could be identified, which might be substrate-like inhibitors. Furthermore, some candidates still need to be tested further.

3. Discussion and future perspectives

In this study, the aim was to understand whether also non-pathogenic bacteria suppress PLCP activity, since PLCPs are central hubs in plant immunity and have been shown to be targeted by many pathogens (Misas-Villamil *et al.*, 2016). The screening of bacterial supernatants from bacteria colonizing maize roots indicated that one bacterium, *P. putida*, can suppress PLCP activity (Figure 5). Our results suggest that PpCip1 is a surface-localized chagasin-like PLCP inhibitor (Figure 12-14). Moreover, PpCip1 was shown to promote the early colonization of *A. thaliana* roots, particularly from the meristematic to the elongation zone (Figure 16). Interestingly, PpCip1 was shown to not be responsible for the PLCP inhibition observed with *P. putida* supernatant (Figure 18), indicating that (an)other PLCP inhibitor(s) might be present in the supernatant. The biochemical and computational screenings identified 15 inhibitor candidates, of which three candidates, Ppu_1665, Ppu_4449 and Ppu_4757, suppressed PLCP activity (Figure 27, Table 3).

3.1. The surface-localized chagasin-like inhibitor PpCip1 promotes colonization of the root commensal bacterium *P. putida*

3.1.1. Conserved bacterial chagasin-like inhibitors and their potential targets

P. putida PpCip1, similar to its ortholog PsCip1 (Shindo *et al.*, 2016), was shown to be a chagasin-like inhibitor, as it has a sequence and predicted structure similar to chagasin and contains the conserved chagasin motif NPTTG (Figure 7), which is necessary for the inhibition of PLCPs (dos Reis *et al.*, 2008). The functional characterization of PpCip1 confirmed that it is indeed a strong PLCP inhibitor (Figure 9), as reported for other chagasin-like inhibitors from protozoan parasites, *P. syringae* and *P. aeruginosa* (dos Reis *et al.*, 2008; Fu, 2009; Monteiro *et al.*, 2001; Shindo *et al.*, 2016). Cip1-like inhibitors have been shown to be conserved in all Pseudomonas (Shindo *et al.*, 2016), which was also confirmed in this thesis (Figure 8). Additionally, it could be shown that most Pseudomonas orthologs have some or all original chagasin like-motifs (Figure 8). Interestingly, when alternative chagasin motifs, with high similarity to the originally reported (Figure 8), are included in the analysis and assumed to be functional, then all Pseudomonads can be considered to have functional chagasin-like inhibitors. The original motifs were mostly based on protozoan

chagasin-like inhibitors (dos Reis *et al.*, 2008; Salmon *et al.*, 2006), which could explain the variation, when screened in Pseudomonads. Evolutionary diversification of the chagasin-like inhibitors in Pseudomonads can be due to the diverse host range and habitats colonized by these bacteria, e.g. humans, soil, different plant species, marine sediment and different animals (Peix *et al.*, 2018), as well as a continuous arms race between hosts and colonizing bacteria (Anderson *et al.*, 2010; Canarini *et al.*, 2019; Stavrinides *et al.*, 2008). The newly discovered amino acid variations could be tested for their inhibitory potential by replacing the original motifs in PpCip1 and assessing maize PLCP inhibition. The presence of this class of inhibitors in Pseudomonads colonizing different hosts indicates that they might be essential proteins for host interactions. Indeed, chagasin-like inhibitors were yet only shown to suppress the activity of PLCPs (family C1) (Costa & Lima, 2016; Fu, 2009; Kantyka *et al.*, 2010). In protozoan parasites chagasin-like inhibitors regulate the activity of their endogenous PLCP, which is important for the parasitic infection (Besteiro *et al.*, 2004; Costa *et al.*, 2022; Monteiro *et al.*, 2001; Santos *et al.*, 2005; Uehara *et al.*, 2012; Wang *et al.*, 2007). In addition to the inhibition of their endogenous PLCP, it has been speculated that protozoan chagasin-like inhibitors could also target their host's PLCPs, which could not be confirmed yet (Besteiro *et al.*, 2004; Costa *et al.*, 2022). In contrast to protozoan chagasin, no members of the C1 protease family (PLCPs) as endogenous target of PpCip1 were identified in *P. putida* (Table 2), correlating to what has been reported for PsCip1 or PaCip1 (Fu, 2009; Shindo *et al.*, 2016). This opens the question, what is the target of chagasin-like inhibitors of Pseudomonads? The most likely explanation is that the targets are host proteases. *In vitro* assays demonstrated that PpCip1 strongly inhibits RD21-like CP1A and RD19A-like (Figure 9), supporting the hypothesis that maize PLCPs are the target of PpCip1. Similarly, PsCip1 was shown to inhibit tomato PLCPs *in vitro* (Shindo *et al.*, 2016).

Interestingly, the gene encoding the chagasin-like inhibitor in *P. putida*, but also at least in two other Pseudomonads, *P. aeruginosa* and *P. syringae* pv. *tomato* DC3000, is located next to the gene encoding a cytoplasmic Lon-type protease (Suppl. Fig. 17), possibly in the same operon (Rigden *et al.*, 2002), indicating a putative interaction or similar regulation as it was generally observed for genes in bacterial operons. Lon-type serine proteases have been shown to be involved in the degradation of misfolded

proteins (Gottesman, 1996; Van Melderen & Aertsen, 2009). In *P. syringae* pv. *tomato* DC3000 a Lon-type protease was shown to degrade hrp (hypersensitive response and *pathogenicity)* type III secretion system (TTSS) as well as TTSS-dependent effector prior to secretion, thereby regulating their stability and the secretion of these effectors, leading to reduced pathogenicity and higher ETI responses in lon null mutants due to hypersecretion of effector proteins (Bretz *et al.*, 2002; Lan *et al.*, 2007; Losada & Hutcheson, 2005). As the proximity of the *cip1* gene to the gene encoding a lon-type protease (Suppl. Fig. 17) might indicate a possible interaction, it has been hypothesized, that chagasin-like inhibitors might also inhibit the Lon-type protease (Rigden *et al.*, 2002), as a dual functionality towards different catalytic types of proteases was also shown for other inhibitors (Bode & Huber, 2000; Cohen *et al.*, 2019; Grosse-Holz & van der Hoorn, 2016). Contradictory to this proposed dual-function, chagasin-like inhibitors of two protozoan pathogen *Leishmania mexicana* and *Trypanosoma brucei* as well as *P. aeruginosa* could inhibit protozoan and mammalian PLCPs but were not able to inhibit the clan CD cysteine peptidase caspase 3, the serine proteases trypsin and thrombin as well as the aspartic protease pepsin A (Fu, 2009; Sanderson *et al.*, 2003). Additionally, the lon-type protease is predicted to be localized in the cytosol (Suppl. Fig. 17), suggesting that contact to a surface-localized PpCip1 is unlikely. Moreover, it was reported that Pseudomonads have proteases with structural similarities to papain (clan CA) (Shindo & Van der Hoorn, 2008) and three of these clan CA protease have been identified in *P. putida* (Table 2). While chagasin-like inhibitors have so far been described to inhibit only family C1 protease (PLCPs), it is possible that they also can target other proteases than family C1 proteases. Therefore, it would be important to test for an additional inhibitory function of chagasin-like inhibitors against proteases of other protease clans and families present in Pseudomonads for example the identified Lon-type protease and the three clan CA proteases.

3.1.2. Promotion of *P. putida* root colonization by PpCip1

If the function of PpCip1 is the inhibition of maize PLCPs, we hypothesize that it might support the colonization of maize roots by *P. putida*, given that PsCip1 promotes the virulence of *P. syringae* in tomato (Shindo *et al.*, 2016). We tried to determine whether PpCip1 is necessary for the colonization of *P. putida* on maize roots by growing maize seedlings in soil inoculated with *P. putida* WT or *P. putid*a Δ*cip1* (Solia, 2023). After

six, seven and 13 dpi we could not observe significant differences in the abundance of the two strains after grinding the whole root samples (Solia, 2023). Microscopic approaches on the localization of the chromosomally marked bacteria with constitutively expressed GFP on the maize root did not show any conclusive results likely due to the high autofluorescence of phenolic compounds on the thick maize roots (Goodwin & Kavanagh, 1948; Harris & Hartley, 1980; Somssich *et al.*, 2016). Hence, I decided to investigate the localization of *P. putida* on *A. thaliana* roots instead, since root imaging in systems like the root-on-a-chip are already well established (Guichard *et al.*, 2020) and other *P. putida* species as well as other related Pseudomonads were already reported to colonize the *A. thaliana* root (Bai *et al.*, 2015; Esparza-Reynoso *et al.*, 2024). *P. putida* in *Arabidopsis* often showed growth-promoting effects for example due to alleviation of abiotic stresses when nutrients were solubilized or due to ethylene signaling (Arslan & Akkaya, 2020; Esparza-Reynoso *et al.*, 2024; Ghosh *et al.*, 2017; Harbort *et al.*, 2020; Ryu *et al.*, 2005; Srivastava *et al.*, 2012; Srivastava & Srivastava, 2020). Since the chagasin-like inhibitors and the chagasin motifs required for their function are highly conserved in Pseudomonads (Figure 8) (Shindo *et al.*, 2016), it is likely that findings observed in the *A. thaliana* system can be transferable to another host like maize, even though their root architecture and immune signaling might be partially different (De Vleesschauwer *et al.*, 2014; Hochholdinger & Zimmermann, 2008). When the root colonization of *P. putida* or *P. putid*a Δ*cip1* chromosomally marked with constitutively expressed sfGFP (*P. putida* WT_sfGFP and *P. putida* Δ*cip1*_sfGFP) on *A. thaliana* roots in a root-on-a-chip system was tested, we could observe a significantly stronger colonization at 1 dpi of *P. putida* WT_sfGFP in the first 3000 µm from the root tip compared to the mutant lacking PpCip1 (Figure 16), showing that PpCip1 is promoting early root colonization on *A. thaliana* roots. Especially higher colonization of *P. putida* WT_sfGFP was observed in the meristematic and elongation zone, but not in the differentiation zone (Figure 16, Suppl. Fig. 12). While the tested colonization time span was rather short, this would be in the same timeline with the rapid onset of immune signaling upon microbe detection (Ngou *et al.*, 2022) and in accordance to our hypothesis of MAMP release and recognition. How can the spatiotemporally PpCip1-dependent early colonization be explained?

Plants modify their soil environment, the rhizosphere, through the release of metabolites, thereby attracting microbes and shaping the rhizosphere community (Haichar *et al.*, 2014; Rizaludin *et al.*, 2021). Primary metabolites (sugars, amino acids, and organic acids) but also more complex metabolites are primarily exuded from the undifferentiated root apex and from the meristematic to the elongation zone (Canarini *et al.*, 2019; Jones *et al.*, 2009). Additionally, also secondary metabolites acting as chemoattractants are exuded from these zones (Haichar *et al.*, 2014; Hale & Moore, 1980). Furthermore, the elongation zone might be more susceptible to bacterial infections due to the ongoing remodeling of the thin cell wall and the absence of endodermal barriers (Lü *et al.*, 2022; Somssich *et al.*, 2016; Tsai *et al.*, 2023). Additionally, bacteria tend to colonize in the grooves between epidermal cells or where lateral root emerges (Schmidt *et al.*, 2018; Tsai *et al.*, 2023). The exudation of root exudates from the meristematic to the elongation zone and favorable properties of the root elongation zone might pose an ideal location for microbial colonization, as seen for *P. putida* in this study. To protect these vulnerable zones, microbe perception, immune signaling and defense responses have been shown to concentrate from the meristematic to the elongation zone (Calabria *et al.*, 2023; Chen *et al.*, 2024b; Emonet *et al.*, 2021; Millet *et al.*, 2010; Poncini *et al.*, 2017; Tsai *et al.*, 2023; Zhou *et al.*, 2020), indicating that plants evolved a spatiotemporal defense system to restrict colonization of vulnerable and for microbes attractive regions (Tsai *et al.*, 2023). One study reported the strong BAK1-dependent induction of MAMP-marker genes, exudation of antimicrobial camalexin and callose deposition in the elongation zone after flg22 or peptidoglycan treatment of *A. thaliana* roots (Millet *et al.*, 2010), even though FLS2 was shown to be present in the entire root (Robatzek *et al.*, 2006). Interestingly, the authors could show that some Pseudomonads (e.g. *Pseudomonas fluorescens* WCS417r) secret the phytotoxin coronatine, an Ile-jasmonic acid mimic, which could suppress this flg22-dependent immune responses (Millet *et al.*, 2010). Another study could confirm the observed induction of MAMP markers in the epidermal cell layer exclusively in the elongation zone upon treatment with flg22. However, also the beneficial *Pseudomonas protegens* CHA0 and the commensal *Pseudomonas* isolate R569 did strongly induce flg22- and FLS2-dependent MAMP responses in the epidermis of meristematic and elongation zone, while other tested Pseudomonads did not (Emonet *et al.*, 2021), indicating that the flg22-dependent MAMP response

suppression observed by Millet *et al.* (2010) cannot be generalized to all Pseudomonads. This is in line with the finding that Pseudomonads use different mechanisms to avoid the release of flg22, e.g. by suppressing the deglycosylation of flagellin, which makes flagellin inaccessible to proteolytic cleavage (Buscaill *et al.*, 2019). Moreover, it was shown that *P. syringae* and *P. fluorescens* CHA0 induced the release of phytocytokines Rapid Alkalization Factor 23 (RALF23), triggered cleavage and relocalization of its receptor FERONIA (FER) to the nucleus leading to PTI responses in the transition and elongation zone (Chen *et al.*, 2024b). In addition to MAMPs like flg22, wounding or phytocytokines/DAMPs are necessary for a strong PTI response in the meristematic and elongation zone (Poncini *et al.*, 2017; Zhou *et al.*, 2020). Furthermore, under non-infected conditions intracellular Botrytis–induced kinase 1 (BIK1), responsible for the activation of NADPH oxidase RBOHD triggering ROS-burst upon Pep1 recognition, is expressed in the epidermal layer of elongation and differentiation zone (Calabria *et al.*, 2023).

The previous examples support the idea that *P. putida* likely gets attracted to the meristematic and elongation zone where it encounters many factors of the plant immune system. Apoplastic PLCPs have been shown to be a major part of plant immunity as they are an early barrier for colonizing microbes (Misas-Villamil *et al.*, 2016). Apoplastic PLCPs like RD19A, RD19C, RD21A and RD21B have been shown to be highly expressed in *A. thaliana* root cap and root epidermis cells (Wendrich *et al.*, 2020), however their activity has not yet been investigated in the root apoplast. In contrast, highly active PLCPs were identified in maize root apoplastic fluid, where some PLCPs, e.g. RD19A-like, also were activated upon treatment with SA (Schulze Hüynck, 2019; Schulze Hüynck *et al.*, 2019). It is not yet clear how far these apoplastic PLCPs can disperse, for example, whether they can be exuded. Since bacteria colonizing the root rhizoplane could come into close proximity to the apoplast, it is likely that these bacteria also reach apoplastic PLCPs.

Many pathogens target PLCPs to suppress plant immunity as they are an early counterpart microbes need to overcome (Figure 3) (Misas-Villamil *et al.*, 2016). Therefore, I hypothesize that the chagasin-like PpCip1 similarly suppresses the activity of host PLCPs to protect bacterial proteins from cleavage. The released fragments of these cleaved bacterial proteins could be recognized by the plant as

MAMPs and trigger PTI defense responses. A similar mechanism was reported for the flg22 release from flagellin and recognition by FLS2 leading to PTI (Buscaill *et al.*, 2019; Chinchilla *et al.*, 2006; Felix *et al.*, 1999; Gómez-Gómez & Boller, 2000; Gómez-Gómez *et al.*, 1999), even though the responsible protease releasing flg22 was not conclusively identified yet (Buscaill *et al.*, 2024; Matsui *et al.*, 2024). Remarkably, bacteria use various mechanisms to avoid the release and recognition of MAMPs, e.g. prevention of release by post-translational modification (Buscaill *et al.*, 2019), sequence variation (Cheng *et al.*, 2021) or suppression of recognition (Millet *et al.*, 2010; Shan *et al.*, 2008). Therefore, the use of an inhibitor to suppress MAMP release would be an obvious alternative. Similarly, *P. infestans* employs the serine protease inhibitor EPI1 to protect its effector PC2 from cleavage by tomato subtilase P69B, thereby suppressing PTI triggered by PC2 fragments (Wang *et al.*, 2021b).

While PLCPs have not been shown to be involved in flg22 release (Buscaill *et al.*, 2024; Matsui *et al.*, 2024), they were shown to be involved in the release of phytocytokines (Chen *et al.*, 2023; Liu *et al.*, 2023). It might be still possible that MAMP precursors different than flagellin are cleaved by PLCPs. Besides, if wounding or cell damage occurs during colonization, a DAMP/phytocytokines could also be released by PLCPs. In such instances, their precursors could be protected by chagasin-like PpCip1. If my hypothesis is true, *P. putida* lacking PpCip1 would trigger PTI responses in contrast to the wild type explaining the observed colonization phenotype. Alternatively, it might also be possible that a surface-localized PpCip1 could protect proteins involved in motility. For example, damage of flagellum components, pili, or adhesins, which are required for swimming or sliding on surfaces, could slow or stop the root colonization (Wadhwa & Berg, 2022). Consequently, a mutant lacking PpCip1 impaired in its motility would then colonize the root to a lesser extent, particularly the fast-growing elongation zone. Moreover, also the protection of surface-localized proteins involved in the secretion of effectors, as for example the TTSS, might be possible, as they are central pathogenicity factors and required for virulence (Alfano *et al.*, 2000). If a secretion system is affected by PLCP activity, less secretion of effectors would be expected, resulting in the loss of virulence. In conclusion, it seems plausible to suggest that the observed phenotype of *P. putida* WT_sfGFP may be explained by the protection of surface proteins, including

components of MAMP precursors, and proteins involved in motility or effector secretion, from PLCP-mediated cleavage by PpCip1. This cleavage of a surface-protein might trigger immune responses due to MAMPs release, loss of effector secretion or hinder the bacteria in their motility.

Preliminary results of the experiment testing the ability of PpCip1 to protect surface proteins from cleavage from papain suggest that PpCip1 modulated the activity of papain. The observed size shifts of some surface proteins indicate that a part of the proteins was removed by cleavage, but only when PpCip1 was absent. While papain is not the natural target of PpCip1, it had to be used as no pure CP1A or RD19A-like were available and as it has a similar cleavage specificity like maize root PLCPs (Choe *et al.*, 2006; Misas Villamil *et al.*, 2019). The preliminary results indicate that its role is the protection of surface proteins from cleavage by PLCPs.

Our findings indicate the presence of a novel model of action of a protease inhibitor in plant-microbe interactions, since PpCip1 would be the first inhibitor to be reported as surface-localized rather than secreted in interaction with a plant (Suppl. Fig. 18). There are only two reports about other protease inhibitors, Omp19 and RlpA, which are (predicted) lipoproteins (Suppl. Fig. 18). The bacterial Omp19 lipoprotein of *Brucella abortus* was found to be a protease inhibitor protecting the bacterium from gastrointestinal and lysosomal cysteine, aspartyl and serine proteases (Coria *et al.*, 2016; Ibañez *et al.*, 2015; Laura Darriba *et al.*, 2022; Pasquevich *et al.*, 2019; Tibor *et al.*, 1999). Interestingly, membrane-anchored Omp19 was shown to protect the outer membrane protein Omp25 from pancreatic elastase digestion (Pasquevich *et al.*, 2019), similarly to what we hypothesize for PpCip1. Overall, strains lacking Omp19 showed higher susceptibility to host proteases, cell division defects, and increased macrophage killing (Pasquevich *et al.*, 2019). In contrast, the fungal effector RsRlpA of *Rhizoctonia solani* has not been shown to be a lipoprotein yet, but it has a similar sequence to a bacterial lipoprotein, named rare lipoprotein A (RlpA) (Charova *et al.*, 2020). Besides this, RsRlpA has been shown to inhibit sugar beet PLCPs suppressing ROS burst and HR (Charova *et al.*, 2020).

Since a PpCip1-dependent root colonization was observed in mono-association with *A. thaliana*, we wondered whether a membrane-anchored PLCP inhibitor could also

have an effect on the colonization by other bacteria. When a small SynCom without PpCip1 was tested for its colonization of maize roots, it was observed that there were significant PpCip1-dependent changes in the community structure over the time course of the experiment (Figure 17B). After 3 hpi a significant reduction of *P. putida* Δ*cip1* was measured, which is in line with the observed early colonization difference on *A. thaliana* roots after 24 hours (Figure 17C). However, also three other bacteria showed a significantly difference in their early colonization, suggesting that PpCip1 also influences the colonization of other bacteria. It remains unclear whether the difference in colonization of the other bacteria is due to a lowered immune status of the root when PLCPs are inhibited or the inhibition of bacterial PLCPs, for example Cin_2970 (Suppl. Table 6). Unfortunately, the experiment lacked a proper input control, therefore it cannot be certainly determined, whether the early difference in abundance after three hours on the root is due to a technical error or is a real effect caused by PpCip1. Nevertheless, the results of this experiment indicate that PpCip1 might have an effect on the community structure and dynamics. Differences in the community structure were also visible at later timepoints (7 dpi and 14 dpi), suggesting that PpCip1 might also influence the community dynamics during the later colonization. Therefore, it would also be interesting to know what effect PpCip1 has *P. putida* colonization on a longer period of time, as some Pseudomonads were also described to colonize as endophytes (Niu *et al.*, 2017; Oukala *et al.*, 2021; Sheoran *et al.*, 2016; Weyens *et al.*, 2012) or to form biofilms requiring longer incubation times (Heredia-Ponce *et al.*, 2021; Mann & Wozniak, 2012).

3.1.3. Potential mode of actions of surface-localized PpCip1

In contrast to the report that PsCip1 is secreted by *P. syringae* and could be found in culture supernatants (Shindo *et al.*, 2016), in my analysis PpCip1 as well as all except two other Pseudomonads were predicted to be lipoproteins (Figure 10). Notably, a PpCip1 ortholog was also identified in the membrane fraction of the soil bacterium *P. putida* KT2440 via MS (Choi *et al.*, 2014), supporting our results that PpCip1 is membrane-anchored and surface localized (Figures 12-14). Unfortunately, our findings stand in contrast to data on surface-localized proteins of *P. aeruginosa*, as the conserved PaCip1 was not reported in their data (Reigada *et al.*, 2021; Vecchietti *et al.*, 2012), however PaCip1 could be downregulated under the tested conditions. Moreover, even though chagasin was shown to regulate the endogenous

cruzipain in *Trypanosoma cruzi* (Monteiro *et al.*, 2001; Santos *et al.*, 2005; Uehara *et al.*, 2012; Wang *et al.*, 2007), it was observed to be linked to the membrane with GPI-anchors and to be found on the parasites surface during some developmental states (Monteiro *et al.*, 2001), suggesting that it might also be a surface-localized lipoprotein in *T. cruzi*. Consequently, the convergent evidence of all experiments and predictions indicate a surface-localization of membrane-anchored PpCip1. This is an exciting discovery as all known PLCP inhibitors involved in plant-microbe interactions are secreted (Misas-Villamil *et al.*, 2016; Shindo & Van der Hoorn, 2008).

In the study reporting PsCip1, only a very weak signal for PsCip1 was detected in supernatants and also not in the apoplastic fluid of infected plants, leaving open the possibility that the PsCip1 found in the supernatant might have been released by cell damage or in another secreted manner such as by outer membrane vesicles (OMVs). OMVs contain proteins, lipids and small molecules involved in bacterial virulence (Orench-Rivera & Kuehn, 2016; Rybak & Robatzek, 2019; Schwechheimer & Kuehn, 2015). OMVs can integrate into plant plasma membranes by endocytosis resulting in strengthened plant defenses (Tran *et al.*, 2022). Interestingly, under apoplast mimicking conditions in a minimal medium with pH 5, OMVs of the pathogenic *P. syringae* pv. *tomato* (Pst) were shown to be enriched with virulence factors and also PstCip1 was present in these vesicles (McMillan & Kuehn, 2023). Similarly, a PpCip1 ortholog could be identified in OMV of the soil bacterium *P. putida KT2440* grown in minimal medium with succinate or benzoate, but not in full LB medium (Choi *et al.*, 2014), although in another study PpCip1 could not be observed in OMV after growth in M9 medium with glucose (Salvachúa *et al.*, 2020). Moreover, PaCip1 (PaICP) was found after 96h in OMVs of biofilm-forming *P. aeruginosa* PAO1 (Park *et al.*, 2015). In contrast, this enrichment in OMV was not observed for the beneficial bacterium *P. fluorescens* ATCC 13525 (McMillan & Kuehn, 2023) and *P. aeruginosa* UCBPP-PA14 (Ballok *et al.*, 2014). These findings of OMV-mediated transport might also be an alternative explanation why PsCip1 could have been found in bacterial supernatants. Moreover, OMVs have been reported to also serve as decoys, mimicking the bacterial cell to divert and neutralize threats by absorbing harmful molecules or degrading host proteins, thereby protecting the bacterial cell (Manning & Kuehn, 2011; Orench-Rivera & Kuehn, 2016; Urashima *et al.*, 2017). Could membrane-anchored PpCip1 also act as decoy for

PLCPs on OMVs? Membrane-anchored PpCip1 transported on OMVs could bind PLCPs in the distance from a bacterial cell, similarly to secreted inhibitors, thereby acting as a decoy and preventing contact to the bacterial cell surface. Moreover, OMVs have been shown to serve as public goods for bacterial communities that benefit also other microbial cells (Schwechheimer & Kuehn, 2015). Possibly, distribution of PpCip1 via OMVs could therefore also benefit other root-colonizing bacteria. However, it is unclear what might be the advantage of an OMV-mediated transport mechanism over a secreted inhibitor.

3.2. *De novo* discovery of putative protease inhibitors

3.2.1. Establishment of methods for inhibitor discovery

While PpCip1 was shown to be a potent PLCP inhibitor, it was discovered to not be the responsible protein for the PLCP suppression in *P. putida* supernatants, as the inhibition was still present when the supernatant of *P. putida* Δ*cip1* mutants was tested (Figure 18). This is not surprising since we could confirm that PpCip1 is membrane-anchored (Figure 12) and therefore not secreted. These findings also indicated that *P. putida* secretes other putative PLCP inhibitor(s). Substrate assays with *P. putida* supernatant inhibiting PLCP activity indicated that the putative inhibitor is proteinaceous, as the unknown molecule is heat-instable and larger than 10 kDa (Figure 6). I started the screening for PLCPs with a BLASTp search discovering only PpCip1, however no other inhibitors were found based on homology (Table 1), indicating that the putative inhibitor does not share sequence similarity to any already known inhibitor. Notably, time has passed since the BLASTp search for PLCP inhibitors was performed and many more PLCP inhibitors have been reported since then (Charova *et al.*, 2020; Li *et al.*, 2023; Liu *et al.*, 2024a; Pérez-López *et al.*, 2021; Yu *et al.*, 2024; Yuan *et al.*, 2024), suggesting that this search could be repeated in future. Another computational approach tested in this study was the prediction of protein-protein interactions using AlphaFold Multimer (Evans *et al.*, 2022; Jumper *et al.*, 2021), as a recent study could successfully identify novel protease inhibitors using this approach (Homma *et al.*, 2023, 2024). Different PLCPs (CP1A, RD19 and papain) were tested in the screening to identify possible false-positives, as all tested PLCPs were inhibited by *P. putida* supernatant *in vitro* (Figure 5). Complexes with interface scores above 0.75 (based on the reported threshold in previous publications) were selected and manually evaluated to determine whether the active

site is blocked (Figure 19). The manual evaluation of the active site is a crucial step, as AF-Multimer also provided many complex structures where the ligand does not block the active site (Figure 19) (Homma *et al.*, 2023). Unfortunately, all tested candidates from this approach did not show an inhibition of PLCPs (Figure 27, Table 3), similar to what was found in the AF-Multimer screening performed for *P. syringae* for PLCP inhibitors (Homma *et al.*, 2023). It remains unclear whether the putative inhibitor could also act as dimer, as observed for example for cystatins (Jurczak *et al.*, 2016; Schulze Hüynck, 2019). Under these circumstances the prediction might have failed to detect the inhibitor. Therefore, the predictions should also be repeated considering dimeric inhibitors, if computationally feasible. Furthermore, a strong disadvantage of the approach is its limitation to its predictive strength based on only the crystal structures deposited in the used database as well as in sequences in databases used for multiple sequence alignments within AlphaFold (Homma *et al.*, 2024).

To continue with the identification of the putative inhibitor, size-exclusion chromatography was tested as an approach to separate secreted *P. putid*a proteins by their size. A fraction with 20% inhibition contained one PLCP inhibitor candidate, Ppu_4449, which could strongly reduce PLCP activity using micromolar concentrations of the candidate (Figure 28). Besides, two other biochemical approaches were performed making use of the observed inhibition of papain by the *P. putida* culture supernatant. First, a pulldown of inhibitors using immobilized papain was established, which has been shown to be functional as maize cystatin CC1 could be enriched on the papain beads (Figure 23). Similar approaches using immobilized proteases have been successfully used to identify other protease inhibitors (Brillard-Bourdet *et al.*, 1998; Cotabarren *et al.*, 2021; Delfín *et al.*, 1996; dos Santos *et al.*, 2012; Guo & Ruckenstein, 2002; Kędzior *et al.*, 2018; Pernas *et al.*, 1998; Yadav *et al.*, 2013). When the pulldown was performed with bacterial supernatant, hundreds of proteins could be identified after MS analysis (Figure 24), indicating a strong unspecific binding to the papain beads and poor stringent washing steps. This is in line with other reports showing unspecific binding to immobilized papain (Brillard-Bourdet *et al.*, 1998; Yadav *et al.*, 2013). Nevertheless, one unknown protein, Ppu_1665, was identified to be enriched after strong filtering: predicted to be secreted and inhibited PLCP activity (Figure 25). Secondly, an affinity chromatography protocol

using immobilized papain as a stationary phase was implemented. After loading of the bacterial supernatant onto the column and washing, all bound proteins were eluted using an unspecific NaCl elution (Figure 26), as elution based on ionic strength was used for the identification of another PLCP inhibitor (Delfín *et al.*, 1996). Similar to the pulldown with papain, many proteins were eluted from the papain beads, however only six of these proteins were predicted to be secreted and with unknown function (Figure 26). Of the tested candidates only one candidate, Ppu_4757, was observed to strongly reduce PLCP activity (Figure 29). The MS analysis indicated that many non-secreted proteins got released during incubation prior to the collection of the bacterial supernatant (Figure 26), likely due to cell lysis. The identification of non-secreted proteins in bacterial supernatants lets the question arise whether the observed inhibition is indeed caused by a secreted protein. For future approaches it is recommended to perform shorter incubation times. Overall, I speculate that these approaches should still be able to identify a putative inhibitor. In line with this, we were able to identify three putative PLCP inhibitor candidates, of which at least two candidates might also be potential substrates (Figure 27).

3.2.2. Potential substrate-like inhibitors

Of all tested candidates, only purified His-Ppu_4449 and His-Ppu_4757 could reduce recombinant CP1A activity with an IC_{50} at the micromolar range (33 µM and approx. 5 µM, respectively) (Figure 28+29), while an IC_{50} could not be determined for His-Ppu_1665. There is not much known about Ppu_4757, which contains a domain of unknown function 1090 (DUF1090), Ppu_1665, which contains a DUF1329 domain, nor about Ppu_4449. DUF1090 proteins were identified only in bacteria and their function is not known according to the InterPro database (Hunter *et al.*, 2009). DUF1329 proteins were mostly found in *Pseudomonads* and contain a LolA-like domain, which has a low similarity to periplasmic molecular chaperone LolA, according to the database entry in the InterPro database (Hunter *et al.*, 2009). Additionally, LolA-like proteins were predicted to play a role in the outer membrane biogenesis (Price *et al.*, 2018) by interfering with the Lol system (Wang *et al.*, 2021a). Recently, DUF1329 family proteins were also hypothesized to function as esterases (Thompson *et al.*, 2020). Preliminary BLASTp search (Altschul *et al.*, 1990) with the Ppu_4449 sequence revealed that it is only encoded in the genomes of Pseudomonads as well as a few other proteobacteria (Suppl. Fig. 19). Besides this,

InterPro database searches (Hunter *et al.*, 2009) with these proteins did not reveal any other known domains or motifs in these proteins nor functions associated with them. A literature search using the tool paperBLAST, which uses text-mining in publications searching for orthologs identified by a BLAST search (Price & Arkin, 2017), did not return any other meaningful reports about sequence homologs identified in other organisms.

The most common mechanism of protease inhibition is the binding of an inhibitor to the active site in a substrate-like manner, thereby blocking the active site and preventing the protease's access to substrates (Farady & Craik, 2010). These inhibitors either are not cleaved (e.g. as observed for cystatins) (Balbinott & Margis, 2022; Benchabane *et al.*, 2010) or are cleaved but no product is released as this process can be reversed due to very slow hydrolysis of the acyl-enzyme formed as an intermediate during cleavage (e.g. as seen for Kazal, Kunitz and Bowman-Birk family inhibitors) (Laskowski & Kato, 1980; Luthy *et al.*, 1973; Radisky & Koshland, 2002; Zakharova *et al.*, 2009). Some inhibitors also act irreversible, as they stay covalently attached to the enzyme upon cleavage (e.g. serpins) (Cohen *et al.*, 2019). In contrast to the beforementioned mechanisms, inhibitors can also act as substrate-like mimicry molecules as it was shown for UmPit2 (Misas Villamil *et al.*, 2019). UmPit2 is an essential core effector of the biotrophic fungus *U. maydis* (Doehlemann *et al.*, 2011). Its function depends on the cleavage in the conserved PID14 domain of UmPit2, but PID14 alone, an inhibitor embedded in the UmPit2 protein, inhibits PLCP activity also on its own (Misas Villamil *et al.*, 2019; Mueller *et al.*, 2013). Moreover, the cMIP motif, which was based on PID14 and was found in several plant associated fungi and bacteria could also inhibit PLCP activity (Misas Villamil *et al.*, 2019). It has been shown for other enzymatic reactions that alternative substrates can reduce an enzymatic activity towards another substrate due to substrate competition, if their concentration is in a similar or higher concentration range to the tested substrate and in excess compared to the enzyme (Liacouras & Anderson, 1977; Pocklington & Jeffery, 1969; Thorn, 1949). In line with this mechanism of competing substrates, it was hypothesized that highly produced substrates like UmPit2 could keep apoplastic PLCPs "busy" and thereby reduce cleavage of substrates releasing immune signals or could reduce auto-catalytic

self-activation of PLCPs leading to suppression of immunity (Misas Villamil *et al.*, 2019).

Interestingly, in a co-incubation with recombinant CP1A, both candidates, Ppu_4757 and Ppu_4449, were observed to be cleaved (Figure 28+29). It is unclear, where and how often they can be cleaved, therefore an High-efficiency Undecanal-based N-Termini EnRichment (HUNTER) analysis can be performed to identify CP1A-processed proteoforms with unique N-termini via MS (Demir *et al.*, 2022). As Ppu_4449 and Ppu_4757 were shown to be cleaved by recombinant CP1A and simultaneously suppress CP1A activity on the synthetic substrate (Figure 28+29), they might also act as substrate-like mimicry molecules like UmPit2. Micromolar concentrations of the inhibitors (33 µM His-Ppu_4449 and 5 µM His-Ppu_4757 for 50% inhibition of recombinant CP1A) were necessary for strong PLCP inhibition, similar to the concentrations necessary of UmPit2 for inhibition of maize leave PLCPs (IC_{50} of 3 µM). These inhibitor concentrations are in a similar range as the concentration of the synthetic substrate used in the assays (10 µM Z-LR-AM), which suggests an protease inhibition via substrate competition, as observed for other enzymes (Liacouras & Anderson, 1977; Pocklington & Jeffery, 1969; Thorn, 1949). The difference in the required concentrations of Ppu_4449 and Ppu_4757 could be explained by different binding affinities to CP1A or by a different number of accessible cleavage sites within the proteins. Additionally, the protease concentration in apoplastic fluids cannot be quantified and can vary between experiments, therefore the calculated IC_{50} can only be seen as a rough estimate, as IC_{50} dependents on the enzyme concentration (Neubig *et al.*, 2003).

While both candidates were shown to inhibit CP1A *in vitro*, it remains unclear whether they can also act as inhibitors *in planta*. To test whether these inhibitors are biologically relevant, *P. putida* mutants lacking these inhibitors should be tested for their ability to inhibit maize PLCPs during root colonization and for their effect on root colonization. Notably, substrate-like inhibitors need to be present in a similar or higher concentration than proteases' substrates to have an inhibitory effect on the enzymes activity via a substrate-competition mechanism (Liacouras & Anderson, 1977; Pocklington & Jeffery, 1969; Thorn, 1949). Another important question still remains unanswered: what makes these substrates good inhibitors, while other proteins, potentially having also cleavage sites, are not inhibitors. A possible explanation could

be that the cleavage sites must be accessible or that some protein structures are more likely to slow down the activity of the proteases, similar to what was observed for Kazal, Kunitz and Bowman-Birk family inhibitors (Laskowski & Kato, 1980; Luthy *et al.*, 1973; Radisky & Koshland, 2002; Zakharova *et al.*, 2009).

3.3. Future perspectives

In this thesis I investigated whether also non-pathogenic bacteria use the modulation of PLCP activity to successfully colonize the plant. Furthermore, I aimed to identify potential inhibitors and studied their effect also on a community level.

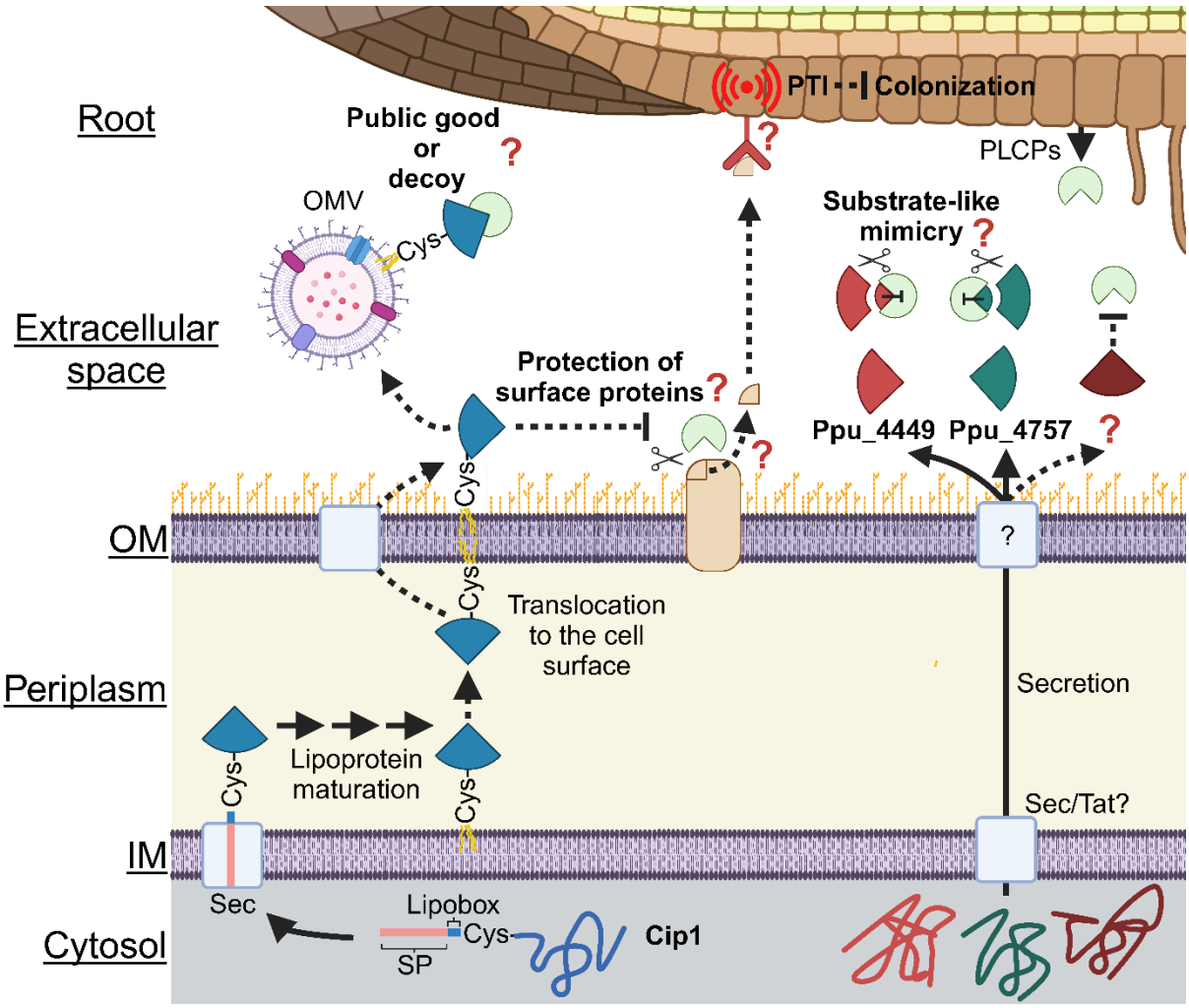

Figure 30: Model of how *Pseudomonas putida* might modulate plant immunity via inhibition of PLCPs.

The root commensal *P. putida* produces PLCP inhibitors, at least two secreted putative PLCP inhibitors and the chagasin-like inhibitor PpCip1. The inhibitor PpCip1 showed a novel mode of action for inhibitor delivery: PpCip1 is a predicted lipoprotein containing a signal peptide (SP) for the Sec pathway to be secreted and a lipobox motif to be attached to the membrane via lipid anchors. Our results indicate that

PpCip1 is translocated and localized to the cell surface. We hypothesize that PpCip1 can protect surface-localized proteins from cleavage by inhibiting plant apoplastic PLCPs. Fragments released from the surface-localized proteins could be recognized from plant PRR receptors as MAMPs and trigger PTI responses and therefore reducing colonization. Alternatively, PpCip1 could be released from the cell surface via outer membrane vesicles (OMV) acting as a decoy for PLCPs**,** mimicking the bacterial cell to divert and neutralize threats by absorbing PLCPs (Manning & Kuehn, 2011; Orench-Rivera & Kuehn, 2016; Urashima *et al.*, 2017), or as a public good, that benefits also microbial colonizers (Schwechheimer & Kuehn, 2015). Moreover, the two secreted putative PLCP inhibitors Ppu_4449 and Ppu_4757 could act as substrate-like mimicry molecules, similar to UmPit2 (Misas Villamil *et al.*, 2019), thereby modulating PLCP activity. It is possible that more unknown inhibitors are secreted. Dashes lines indicate unknown / not confirmed pathways. Red question marks indicate the most important questions for future research.

I could show that chagasin-like PLCP inhibitors in Pseudomonads are predicted to be membrane-anchored lipoproteins (Figure 10), like PpCip1, which are most likely surface localized to get into contact with host PLCPs. This delivery mechanism of a PLCP inhibitor was yet unknown in plant-microbe interactions (Suppl. Fig. 18). Notably, also the membrane-anchored protease inhibitor Omp19 was shown to protect an outer membrane protein from pancreatic elastase digestion (Pasquevich *et al.*, 2019), showing a similar mechanism as we hypothesize for PpCip1. The crucial open question is now: Why is PpCip1 localized at the cell surface? This localization could be resource-saving as PpCip1 cannot diffuse away and stays where it is needed. Our hypothesis is that PpCip1's role is to protect membrane proteins in its proximity from cleavage (Figure 30). Therefore, the next step would be to identify whether surface proteins are protected by PpCip1 from cleavage. Our ongoing MS analysis of surface-proteins of *P. putida* WT and *P. putida* Δ*cip1* preincubated with or without papain might give an answer to this question. Once protected substrates and the cleavage sites used by the PLCPs are identified, these sites could be mutagenized to prevent cleavage. It could be tested whether the mutagenized substrate cleavage sites would abolish the advantage of the WT colonizing the root over the mutant lacking PpCip1. To answer whether a membrane-anchored PpCip1 is resource-saving, the costs of a secreted PpCip1 for growth could be tested during infection of a plant or in contact with a PLCP by observing *in vitro* how a mutant lacking the lipobox motif can grow compared to the WT. By using this PpCip1 mutant lacking the lipobox, a pure cost effect (fixed membrane-anchored protein vs. diffusing and therefore continuously secreted protein) might be distinguishable from a cost effect plus a potential benefit from the delivery

system (diffusing secreted inhibitor can likely protect more (unnatural) targets than an anchored inhibitor most likely only able to protect surface proteins).

Besides being surface-localized, it is also conceivable that PpCip1 might be released from the surface during infection. For example, PpCip1 could be released on induced OMVs (Figure 30), as Cip1 orthologs have been identified on OMVs released upon apoplast mimicking conditions (McMillan & Kuehn, 2023). When released on OMVs, PpCip1 could act as a decoy neutralizing PLCPs before they come into contact with the bacterial cell surface or as a public good benefiting also other bacteria. A function of OMV cargo as decoy or as public good has also been shown for other proteins identified on OMVs (Manning & Kuehn, 2011; Orench-Rivera & Kuehn, 2016; Schwechheimer & Kuehn, 2015; Urashima *et al.*, 2017). To address how PpCip1 is delivered, monitoring labeled PpCip1 via immunogold-labeling on the cell surface and potentially also on OMVs could give an answer. Moreover, it could be investigated whether PpCip1 can be identified as cargo on isolated *P. putida* OMVs via MS and under which conditions these OMVs are released. Another explanation would be a targeted release from the cell surface via removal of the lipidated N-terminus by a bacterial protease, as the proteolytic release of lipoproteins from membranes has been observed for example in the gram-positive bacterium *Bacillus subtilis* (Antelmann *et al.*, 2001; Tjalsma & van Dijl, 2005) or gram-negative *Bacteroides fragilis* (Pierce *et al.*, 2021). To test for a possible release of PpCip1 from the cell surface via cleavage by proteases, the release of PpCip1 from the cell surface incubated with different proteases could be investigated by testing for the presence of PpCip1 in the supernatants or for the removal of PpCip1 from the cell surface, e.g. by biotin labeling.

Moreover, PpCip1 has been shown to promote early root colonization of *P. putida* on *A. thaliana* roots (Figure 16), similar to the role of PsCip1 in the infection of tomato by *P. syringae* (Shindo *et al.*, 2016). *P. putida* strains have been shown to be plant growth-promoting rhizobacteria commonly found on roots of a broad range of plants and in many different soils (Costa-Gutierrez *et al.*, 2022). Since the *P. putida* strain used in this study was isolated from maize roots, it would be advised to test also the effect of PpCip1 on root colonization of maize. Particularly maize as a monocot has a different root structure than *A. thaliana* and some components of the immune system might differ too (De Vleesschauwer *et al.*, 2014; Hochholdinger & Zimmermann, 2008),

therefore testing the role of PpCip1 on maize root colonization would give new insights onto bacterial colonization of crops and non-model plants. As PpCip1 was shown to promote colonization specifically in the meristematic and elongation zone of *A. thaliana* roots (Figure 16), the colonization of *P. putida* can be investigated in these zones of the maize roots, instead of whole roots. It would therefore be essential to also genetically modify the strains to harbor another fluorescent marker differing from the maize autofluorescence, which would allow an easier microscopic detection of those bacteria on maize roots. In addition, it needs to be shown that the colonization effect is indeed due to the inhibition of PLCPs. Therefore, we propose to complement the *P. putida* Δ*cip1* strain with a vector constitutively expressing either PpCip1 or PpCip1 lacking the chagasin motif NPTTG to observe whether the difference in colonization is indeed due to a suppression of PLCP activity, as the PpCip1 lacking the NPTTG motif, which is required for PLCP inhibition (dos Reis *et al.*, 2008; Shindo *et al.*, 2016), should not be able to suppress PLCP activity.

It is not yet clear how a surface-localized PpCip1, which can probably only protect substrates in its vicinity, might affect the colonization of other bacteria. If *P. putida* comes into close contact with other bacteria during colonization, e.g. in biofilms, PpCip1 might also protect substrates on their cell surface. We suggest that an indirect effect is also, as a PpCip1-mediated reduction of immune responses in the colonized root might also benefit other bacteria, as it indirectly increases the threshold for detection by the plant. Notably, the presence of PTI suppressor strains in bacterial communities has been shown to enhance the colonization of other commensal bacteria (Teixeira *et al.*, 2021). The effect of protease inhibitors, especially of a surface-localized inhibitor, on co-colonizing microbes is yet understudied. Our preliminary data suggests that PpCip1 has an effect on the structure and dynamics of the bacterial community. Nevertheless, as our SynCom experiment was inconclusive, a repetition using immune markers, ideally by RNAseq or fluorophore-inducing immune markers, could be performed in *A. thaliana* to determine whether the observed shifts in community structure are due to PpCip1-mediated reduction of the immune responses.

Furthermore, I suggest that also other Pseudomonads use the conserved chagasin-like inhibitors to inhibit their host's PLCPs, also from non-plant host. The transfer of knowledge from plant science to human/animal sciences would be beneficial for the

scientific community, therefore, if feasible, it would be advisable to test the effect of a PaCip1 knockdown also for infection by *P. aeruginosa*, which is a resilient human pathogen causing pneumonia and other lung diseases (Mulcahy *et al.*, 2014).

Finally, the bioinformatic and biochemical approaches led to the discovery of three additional inhibitor candidates. To investigate how two of these candidates, Ppu_4449 and Ppu_4757, can act as substrate-mimicking inhibitors, the cleavage sites in the substrates need to be identified. Mutagenesis of these cleavage sites would reveal the importance of the proteolytic cleavage for the inhibition. Furthermore, knock-out mutants lacking these proteins should be generated testing whether these proteins are responsible for the observed suppression of apoplastic root PLCPs by *P. putida* supernatant. Finally, it needs to be determined whether the inhibitory effect of the identified substrate-mimicking inhibitors is biologically relevant, i.e. by providing advantages in root colonization or microbe-microbe interactions, similar to what could be shown for the substrate-mimicking inhibitor UmPit2 (Mueller *et al.*, 2013).

In the future, the here established approaches using bioinformatics (AF-Multimer) and biochemistry (Pulldown and affinity chromatography) could be used for the large-scale identification of protease inhibitors in diverse plant-microbe interactions. By systematically uncovering the role of protease inhibitors, not only in pathogenic but also in beneficial interactions, this knowledge could pave the way for the development of innovative strategies to support sustainable agriculture. Such advances could lead to the breeding or engineering of crops with enhanced resistance to pathogens while promoting beneficial microbial associations, thereby reducing the need for chemical pesticides and synthetic fertilizers.

4. Material and Methods

4.1. Materials

4.1.1. Chemicals

The chemicals used in this study are listed in Table 4.

Table 4: Chemicals used in this study.

Chemical	Supplier / Reference
5-bromo-4-chloro-3-indolyl-β-D-galactopyranoside (X-Gal)	VWR
4-(2-Hydroxyethyl)piperazine-1-ethanesulfonic acid	Sigma Aldrich
5XROTI Quant	Roth
Acetic acid	Roth
Acetosyringone	Sigma Aldrich
Acetonitrile	Roth
Acrylamid/Bisacrylamid, 30% solution	Sigma Aldrich
Agarose	Bio-Budget
Ammonium bicarbonate	Merck
Ammonium chloride	Roth
Ammoniumperoxodisulfat (APS)	VWR
Bacto Agar	BD
Bacto Tryptone	BD
Bacto Yeast Extract	Gibco
Blauer Jonas	BIOZOL
Bovine serum albumin fraction V (BSA)	Roth
Bromophenol blue	Roth
Calcium chloride	VWR
Carbenicillin	Roth
Chloroform	Roth
Chloramphenicol	Roth
Chloroacetamide	Sigma Aldrich
Glycerol	Roth
Glycine	Roth
Goat serum	Sigma Aldrich
Iodoacetamid	Sigma Aldrich
Isopropanol	Roth
L-Cysteine Hydrochloride	Roth
Magnesium chloride	Roth
Magnesium sulfate	Roth
Manganese chloride	Roth
Methanol	VWR
3-(N-morpholino)propanesulfonic acid (MOPS)	Roth
Murashige and Skoog basal salts	Sigma Aldrich
MV201	(Richau *et al.*, 2012), Prof. Dr. Hermen S. Overkleeft
Paraformaldehyde	Sigma Aldrich
Plant agar	Duchefa Biochemie
Potassium acetate	Roth
Potassium dihydrogenphosphate	Roth
Rifampicin	Alfa Aesar
Rubidium chloride	Sigma Aldrich
Salicylic acid	Sigma Aldrich
Sucrose	Roth
Sodium acetate	Roth

cOmplete protease inhibitor cocktail	Roche
Coomassie brillant blue R250	Roth
DCG-04-Biotin	(Greenbaum *et al.*, 2000), Prof. Dr. Hermen S. Overkleeft
DCG-04-Cy5	(Stolze *et al.*, 2012), Prof. Dr. Hermen S. Overkleeft
Dimethyl sulfoxide (DMSO)	Roth
Disodium hydrogen phosphate	Roth
Dithiothreitol (DTT)	Applichem
E64	Sigma Aldrich
Ethanol	Roth
Ethidium bromide	Roth
Ethylenediaminetetraacetic acid (EDTA)	Roth
EZ-Link Sulfo-NHS-Biotin	Thermo Fisher Scientific
Formic acid	Roth
Gelatin from cold water fish skin	Sigma Aldrich
Gentamycin	Roth
Glutaraldehyde	Sigma Aldrich

Sodium cacodylate	Sigma Aldrich
Sodium chloride	Roth
Sodium dodecyl sulfate (SDS)	Roth
Sodium hypochlorite	Roth
Sodium phosphate	Roth
Spectinomycin	Sigma Aldrich
SYPRO Ruby Protein Gel Stain	Invitrogen
Tetramethylethylenediamine (TEMED)	Roth
Trizma base	Sigma Aldrich
Tris(2-carboxyethyl)phosphine hydrochloride (TCEP)	Sigma Aldrich
Trizol	Ambion
Tween-20	Roth
UVette cuvettes	Eppendorf
Uranylacetat-Dihydrat	Sigma Aldrich
Z-LR-AMC	Sigma Aldrich

4.1.2. Solutions and buffers

All solutions were prepared with deionized water unless stated differently and autoclaved for at least 20 min at 121°C. Solutions sensitive to heat were filter sterilized (0.2 µm pore size). The compositions of all solutions are indicated in Table 5.

Table 5: Solutions and buffers used in this study.

Name	Composition	Usage
1X M9 minimal medium (without glucose)	20% (v/v) 5X M9 salts 2 mM $MgSO_4$*$7H_2O$ 0.1 mM $CaCl_2$*$2H_2O$	Cultivation of bacterial synthetic community with nutrient starvation
5X M9 salt solution	256 mM Na_2HPO_4*$2H_2O$ 110 mM KH_2PO_4 43 mM NaCl 93.5 mM NH_4Cl	Cultivation of bacterial synthetic community with nutrient starvation
6X SDS protein loading dye	4 M Tris-HCl pH 6.8 6% (w/v) Sodium dodecyl sulfate (SDS) 0.15 % (w/v) Bromophenol blue 60% (v/v) Glycerol 100 mM DTT	Loading samples to a SDS-polyacrylamide gel
Biotin reagent solution	1 mg EZ-Link Sulfo-NHS Biotin (Thermo Scientific) + 224 µl MilliQ water	Biotinylation of surface proteins
Blocking solution	3% skim milk powder in TBS-T	Blocking of membranes
Coomassie brilliant blue destaining solution	45% (v/v) Methanol 10% (v/v) Acetic acid	Destaining of membranes
Coomassie brilliant blue staining solution	45% (v/v) Methanol 10% (v/v) Acetic acid 0.1% (w/v) Coomassie brillant blue R250	Staining of membranes
dYT liquid medium	1.6 % (w/v) Bacto Tryptone 1.0 % (w/v) Bacto Yeast Extract 0.5 % (w/v) NaCl	Cultivation of *E. coli*, *A. tumefaciens* and bacterial synthetic community
dYT solid medium	0.8 % (w/v) Bacto Tryptone 0.5 % (w/v) Bacto Yeast Extract 0.5 % (w/v) NaCl 1.4 % (w/v) Bacto Agar	Cultivation of *E. coli*, *A. tumefaciens* and bacterial synthetic community
Hoaglands medium	Hoaglands medium (ThermoFisher)	Cultivation of *P. putida* for root-on-a-chip experiment
LB medium	5 g/l Yeast extract 10 g/l Tryptone 0.5 g/l Sodium chloride	Growth medium for bacteria
Membrane protein buffer	50 mM Tris-HCl pH 8 150 mM NaCl 1% (v/v) Triton X 1X cOmplete protease inhibitor cocktail 0.5 % (w/v) Sodium deoxycholate	Solubilization of membrane proteins and lipoproteins
Ni-NTA binding buffer	20 mM $NaPO_4$ pH 7.4 500 mM NaCl 25 mM Imidazol	Equilibration buffer for Ni-NTA
Ni-NTA elution buffer	20 mM $NaPO_4$ pH 7.4 500 mM NaCl 500 mM Imidazol	Elution buffer for Ni-NTA

Ni-NTA lysis buffer	50 mM $NaPO_4$ pH 8 300 mM NaCl 10 mM Imidazol 0.01% (v/v) Benzoase 1X cOmplete protease inhibitor cocktail	Lysis buffer for Ni-NTA
PAB buffer	10 mM Na_2HPO_4, pH 6 150 mM NaCl 1 mM EDTA, pH 8 0.5 mM DTT	Reaction buffer for PLCP activity assay
PBS pH 7.2	137 mM NaCl 2.7 mM KCl 10 mM Na_2HPO_4 1.8 mM KH_2PO_4	Cell fractionation
PBS pH 8	137 mM NaCl 2.7 mM KCl 10 mM Na_2HPO_4 1.8 mM KH_2PO_4	Biotinylation of surface proteins
Prescission protease cleavage buffer	50 mM Tris-HCl pH 7.5 100 mM NaCl 1 mM EDTA 1 mM DTT	Removal of GST-tag using Prescission protease
RF1 solution pH 5.8	100mM RbCl 50 mM $MnCl_2$ 30 mM Potassium acetate pH 7.5 10 mM $CaCl_2$ 15 % (w/v) Glycerin	Preparation of chemocompetent cells
RF2 solution pH 5.8	10 mM MOPS pH 6.8 10 mM RbCl 75 mM $CaCl_2$ 15% (w/v) Glycerin	Preparation of chemocompetent cells
SDS gel running buffer	25 mM Tris-HCl pH 8.3 192 mM Glycine 4 mM Sodium dodecyl sulfate (SDS)	SDS gel running buffer
Sodium cacodylate buffer pH 6.9	Sodium cacodylate buffer pH 6.9	Preparations for immunogold labeling
SyproRuby fix solution	50% (v/v) Methanol 7% (v/v) Acetic acid	Fixation of proteins in a SDS-polyacrylamide gel
SyproRuby wash solution	10% (v/v) Methanol 7% (v/v) Acetic acid	Washing of a SDS-polyacrylamide gel
TBS-T buffer pH 7.5	0.5 M Tris-base 1.5 M Sodium chloride 0.1% (v/v) Tween-20	Blocking and Antibody binding on membranes
1M Tris-HCl buffer	121.14 g/L Trizma base, pH was set with HCl	Various applications

Tris-sucrose-EDTA (TSE) buffer pH 8	25 mM Tris pH 8 1mM EDTA 20% w/w Sucrose	Isolation of periplasmic proteins
Western blot transfer buffer	39 mM Glycine 48 mM Tris-base 0.0375% (m/v) Sodium dodecyl sulfate 20% (v/v) Methanol	Transfer buffer for transfer of proteins from an SDS-polyacrylamide gel onto a blot

4.1.3. Enzymes and Master mixes

Enzymes used in this study are listed in Table 6.

Table 6: Enzymes, buffers and master mixes used in this study.

Enzymes / Buffers / Master mixes	Supplier
DFS-Taq DNA polymerase	BIORON
10X Fast Digest Buffer	Thermo Fisher Scientific
10X NEB Cutsmart buffer	New England Biolabs (NEB)
2X GoTaq Green Master Mix	Promega
2X Xtreme buffer	Sigma Aldrich
Antarctic phosphatase	New England Biolabs (NEB)
ATP	Biomol
BsaI-HF	New England Biolabs (NEB)
DNAse	Thermo Fisher Scientific
dNTP Mix	New England Biolabs (NEB)
DpnI	Agilent
Exonuclease I	New England Biolabs (NEB)
FastDigest BpiI	Thermo Fisher Scientific
GoTaq qPCR Master Mix	Promega

Enzymes / Buffers / Master mixes	Supplier
KOD Xtreme Hot Start DNA Polymerase	Merck
KpnI	New England Biolabs (NEB)
NdeI	New England Biolabs (NEB)
Papain from papaya latex	Sigma Aldrich
PreScission protease	Sigma Aldrich
Proteinase K	Thermo Fisher Scientific
RNAse	Thermo Fisher Scientific
SacI	New England Biolabs (NEB)
T4 DNA Ligase	New England Biolabs (NEB)
Trypsin	Promega
XbaI	New England Biolabs (NEB)
XcmI	New England Biolabs (NEB)
XhoI	New England Biolabs (NEB)

4.1.4. Antibodies

Antibodies used in this study are listed in Table 7.

Table 7: Antibodies used in this study.

Antibodies	Clonality	Working dilution	Origin	Supplier
anti-Flag	Monoclonal	1:250	Mouse	Sigma (F1804)
anti-Flag	Monoclonal	1:250	Mouse	Sigma (F3165)
anti-FLAG-HRP (used for Wester Blots)	Monoclonal	1:1000	Mouse	Sigma Aldrich (A8592)
anti-GFP	Monoclonal	1:1000	Mouse	Roche (47859600)
anti-RFP	Polyclonal	1:50	Rabbit	Rockland (600-401-379)
anti-His	Monoclonal	1:10000	Mouse	Sigma (H-1029)
anti-ICDH	Polyclonal	1:10000	Rabbit	Millipore (ABS2090)
anti-Rabbit IgG Gold	Not described	1:20	Goat	bbisolutions (EM.GAR10/2)
anti-mouse-HRP	Polyclonal	1:2000	Horse	Cell Signaling (7076)
anti-OprF (*P. aeruginosa*)	Polyclonal	1:5000	Rabbit	Invitrogen (PA5-117553)
anti-rabbit-HRP	Monoclonal	1:3000	Goat	Cell Signaling (7074)
anti-Streptavidin-HRP	Monoclonal	1:1000	Unclear	Sigma Aldrich (S2438)

4.1.5. Commercial kits

All commercial kits used in this study are listed in Table 8.

Table 8: Commercial kits used in this study.

Kits	Supplier	Usage
AMPure XP	Beckman Coulter	DNA purification
PCR Cloning Kit	NEB	Blunt-end cloning into pMiniT backbone
FastDNA Spin Kit for Soil	MP Biomedicals	DNA isolation from soil/root samples
GeneJET genomic DNA purification kit	Thermo Fisher Scientific	Genomic DNA isolation from bacteria
Golden Gate Modular Cloning (MoClo) Plant Parts Kit (Engler *et al.*, 2014)	AddGene	Modules used for MoClo
MasterPure Complete DNA & RNA Purification kit	Epicentre	RNA isolation
NucleoSpin Gel and PCR Clean-up	Macherey-Nagel	PCR product clean-up
NucleoSpin Plasmid, Mini kit for plasmid DNA	Macherey-Nagel	Plasmid DNA extraction
Quant-iT™ PicoGreen™ dsDNA Assay-Kit and dsDNA reagents	Invitrogen	Quantification of DNA
QuikChange Multi Site-Directed Mutagenesis Kit	Agilent	Site-directed plasmid mutagenesis
RevertAid First Strand cDNA Synthesis Kit	Thermo Fisher Scientific	First strand cDNA synthesis
Super Signal West Femto	Thermo Fisher Scientific	Detection of Strep-HRP antibody
SuperSignal™ West Femto Maximum Sensitivity Substrate	Thermo Fisher Scientific	Western Blot detection
SuperSignal™ West Pico PLUS Chemiluminescent Substrate	Thermo Fisher Scientific	Western Blot detection
TURBO DNA-free Kit	Thermo Fisher Scientific	DNAse digest in RNA samples

4.1.6. DNA/Protein ladders and loading dyes

All used ladders and dyes used are listed in Table 9. Molecular weights of the bands were determined based on the manual of the manufacturer (Figure 31).

Table 9: Protein ladders and loading dye, DNA ladders and loading dye used in this study.

Ladders / Loading dyes	Supplier
GeneRuler 1 kb Plus DNA Ladder	Thermo Fisher Scientific
PageRuler Plus Prestained Protein Ladder	Thermo Fisher Scientific
PageRuler Prestained Protein Ladder	Thermo Fisher Scientific
Gel Loading Dye Purple (6X)	New England Biolabs (NEB)

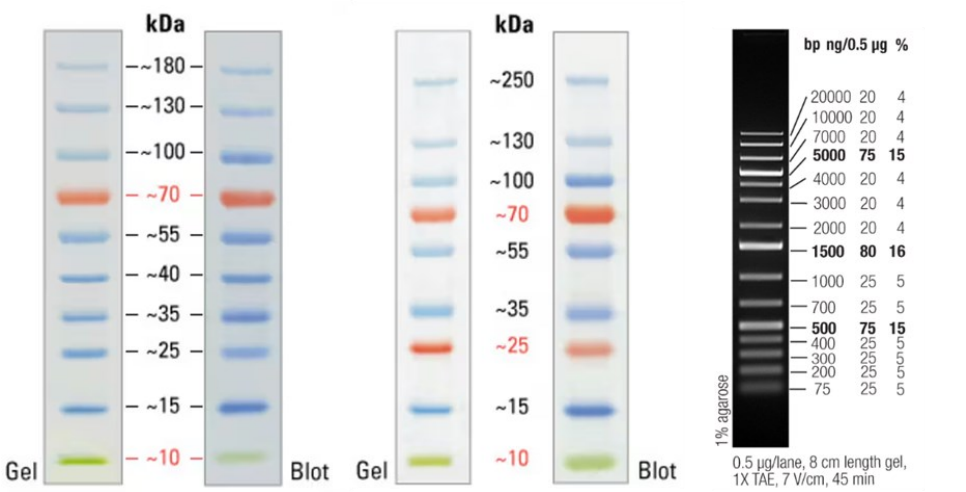

PageRuler Prestained Protein Ladder
26619
ThermoFisher Scientific

PageRuler Plus Prestained Protein Ladder
26616
ThermoFisher Scientific

GeneRuler 1 kb Plus DNA Ladder
SM1331
ThermoFisher Scientific

Figure 31: Protein and DNA ladders used in this study.

Images of these ladders were obtained from the manufacturer's manual.

4.1.7. Oligonucleotides

The used oligonucleotides/primer are listed in Table 10. The primers were synthesized by Eurofins Genomics or Sigma Aldrich.

Table 10: Oligonucleotides used in this thesis.

Primer ID	Sequence (5' -> 3')	Description
243	GAACAACTACAGCAGCCAGGTG	qPCR primer *pr3*
244	GAGACAATAGCTGACATGCGTC	qPCR primer *pr3*
251	GCGTTCAAGCCCATCGACA	qPCR primer *pr4*
252	CGTGTGGGATCACATCCATATAAC	qPCR primer *pr4*
253	TATCGGCCGGAATAGGCTCTG	qPCR primer *pr5*
254	CGCGTACATACAAATGCGTGC	qPCR primer *pr5*
749	TATGGGTCCTTGACGTTCTC	qPCR primer *cc9*
750	GGATCATCCGTAGCCATCTG	qPCR primer *cc9*
837	CATCTTCGCCATGTTCAACG	qPCR primer *pr6mb*
838	ATTTGTCCGGGTTGAAGAGG	qPCR primer *pr6mb*
2000	CTTCGGCATTGTTGAGGGTTTG	qPCR primer *gapdh*
2001	TCCTTGGCTGAGGGTCCGTC	qPCR primer *gapdh*
2554	GTTCATTTCATTTGGAGAGGACACG	Sequencing primer Molecular Cloning Level 1
2992	CGTTATCCCCTGATTCTGTGGATAAC	Sequencing primer Molecular Cloning Level 0 and pJT'Tmcs vectors
2993	GTCTCATGAGCGGATACATATTTGAATG	Sequencing primer Molecular Cloning Level 0
2995	CTGGTGGCAGGATATATTGTGGTG	Sequencing primer Molecular Cloning Level 1
2996	GTGGTGTAAACAAATTGACGC	Sequencing primer Molecular Cloning Level 1
2997	GGATAAACCTTTTCACGCCC	Sequencing primer Molecular Cloning Level 1
4738	AAGATACCCGAGCTGTAGAG	Sequencing primer Molecular Cloning Level 1
4921	GGCGGCATCACCACGGAAACCGACTACC	Site directed mutagenesis THI1-like (B4FS65), removal of internal BsaI site
5261	GATCCGGAGGTCAACATGG	Sequencing primer Molecular Cloning Level 1
5926	GGTCTCAAATGCCCTCCGTCCAC	L0 cloning XBCP3-like B4FYA3
5927	GGTCTCAAAGCTCATTGGTCCATCAACTCC	L0 cloning XBCP3-like B4FYA3
5928	GGTCTCAAATGGCTGCCTCCACCAC	L0 cloning CP1A
5929	GGTCTCAAAGCTCATGCGCTGCTCTTCATGC	L0 cloning CP1A
5932	TAATACGACTCACTATAGGG	pOPIN sequencing primer

5934	CAAGGGGCTTCATGATGTCC	pOPIN sequencing primer
5936	GGTGAAATCATGCCGAACATC	pOPIN sequencing primer
5992	TTGAAGACAAAGGTGTCGACGCGGAGGACCCGCTGA	L0 cloning RD19A-like
5993	TTGAAGACAAAAGCCTACTCCTTCGAGGCGTGGACTGCGGACAC	L0 cloning RD19A-like
5994	TTGAAGACAAAGGTGCGAGGGCCCACAGACGTGCCG	L0 cloning THI1-like B4FS65
5995	TTGAAGACAAAAGCTCACATTAGTGGATAGGACGGGCGGATGGCGA	L0 cloning THI1-like B4FS65
7032	ACAGCTATGACATGATTACGCCAAAGGATGGCCCAAGTGC	Amplification of upstream region of *cip1*
7033	TGACCAGCGCTGTGCGTTCAGGTGGCTCCAGAGGCTGACG	Amplification of upstream region of *cip1*
7034	CGTCAGCCTCTGGAGCCACCTGAACGCACAGCGCTGGTCA	Amplification of downstream region of *cip1*
7035	CCGGGTACCGAGCTCGAATTGTTCATCGCCACCACCGAGG	Amplification of downstream region of *cip1*
7036	TTGGTCTCAAATGTGCGCCCAGCAGCCG	pOPIN cloning of PpCip1
7037	TTGGTCTCAAAGCTCAGTCGACGCGGATCGC	pOPIN cloning of PpCip1
7038	GGCTCGTATGTTGTGTGGAATTGTG	pK19-mob-sacB sequencing primer
7039	GGATGTGCTGCAAGGCGATTAAG	pK19-mob-sacB sequencing primer
7190	TTCCCTTGTCCAGATAGCC	pK19-mob-sacB sequencing primer
7191	TTGTGCGTAACTAACTTGC	pK19-mob-sacB sequencing primer
7192	TGGTCGGTCATTTCGCTCGG	pK19-mob-sacB sequencing primer
7204	CGGATGCCAAGATCAAGATCG	Colony PCR primer for 300 bp downstream region
7205	GAGGCGAAGTTAAGGCATTGG	Colony PCR primer for 300 bp downstream region
7206	GAACCCAACCGTGGTGATTTC	Colony PCR primer for upstream region
7207	GAAGGGCAGGGTAAGGATGTC	Colony PCR primer for upstream region
7208	GGCATCCAACGTGCTACAAAG	Colony PCR primer for *cip1*
7514	AAGCGCAACAGCAGTCTCGTATC	qPCR primer for *ropD*
7515	CATCCGGAGCACTCTCGAATACG	qPCR primer for *ropD*
7516	GATCTAGGTACCATGGGTAAAGGAGAAGAAC	Amplification of *sfgfp* with KpnI overhang
7517	GGAGCTCTCGAGTCTAGAATC	Amplification of *sfgfp* with Xba overhang
7518	GATCTAGGTACCATGACTGCCCCTCGTCTGC	Amplification of *cip1* with KpnI overhang
7519	GATCTACTCGAGGTCGACGCGGATCGCGCAG	Amplification of *cip1* with XhoI overhang
7520	GATCTACTCGAGATGGGTAAAGGAGAAGAAC	Amplification of *sfgfp* with XhoI overhang

8133	TTGGTCTCAAATGGCGGAGGAAAACTTCGCC	pOPIN cloning of Ppu_0898
8134	TTGGTCTCAAAGCTCAGAACTTGTAAGTTGCTGCC	pOPIN cloning of Ppu_0898
8135	TTGGTCTCAAATGCAGACTACCGTGAGCGATGCC	pOPIN cloning of Ppu_1728
8136	TTGGTCTCAAAGCTCAGTGGTTCATGTGCATGTG	pOPIN cloning of Ppu_1728
8137	TTGGTCTCAAATGGCCAGCCTCAAGGACGTAGC	pOPIN cloning of Ppu_2532
8138	TTGGTCTCAAAGCTTATTCCACTTTAGCCGTTTGC	pOPIN cloning of Ppu_2532
8139	TTGGTCTCAAATGGCCGAGATTCCGATTGGC	pOPIN cloning of Ppu_2677
8140	TTGGTCTCAAAGCTCAGCGCCAGGTATCGAC	pOPIN cloning of Ppu_2677
8141	TTGGTCTCAAATGGCCTCCAAGCAGGAGTTCG	pOPIN cloning of Ppu_3965
8142	TTGGTCTCAAAGCTTACTTCTTCTTGTTGCCGG CG	pOPIN cloning of Ppu_3965
8143	TTGGTCTCAAATGGCACCGCTGCACAGCCAGTTC	pOPIN cloning of Ppu_4449
8144	TTGGTCTCAAAGCTCAACGCGAACGTACGGTAC	pOPIN cloning of Ppu_4449
8145	TTGGTCTCAAATGCATGAATACACTGTGGGCG	pOPIN cloning of Ppu_4631
8146	TTGGTCTCAAAGCTCAGTGCGCGTGTTCGTGGG	pOPIN cloning of Ppu_4631
8147	TTGGTCTCAAATGGCGGATGCCCTGAAGAGCC	pOPIN cloning of Ppu_4944
8148	TTGGTCTCAAAGCCTATTTCACAGTGACCGTAATC	pOPIN cloning of Ppu_4944
8677	ATGATGGAGCTCGGGCGGTTTTATGGACAG	Amplification of pNm_RBS
8678	ATGATGGGTACCTCCTCCTAAGCTTGGATCC	Amplification of pNm_RBS
8805	ATAGGTACCATGGTGAGCAAGGGCGAGGAG	Amplification of *mcherry* with KpnI overhang
8807	TGTTCTAGATCACTTGTACAGCTCGTCCATGCC	Amplification of *mcherry* with XbaI overhang
8810	CACTCTGTGGTCTCTCGAGGATTATAAGG	Amplification of 3xFlag-tag with XhoI overhang
8811	TGGTCTCTAGATCACTTATCGTC	Amplification of 3xFlag-tag with XbaI overhang
8887	GATGCCGCTGGATCTGGC	Sequencing primer pJT'Tmcs vectors
9000	CTATGACCATGATTACGCCAACAGCACCGTGGAGAAAACC	Amplication of sequence upstream from attTn7 site
9001	GCTGTCCATAAAACCGCCCGCTTGTGTTTTACCGGATGG	Amplication of sequence upstream from attTn7 site
9002	GGATGAGCTCTACAAATAATCCCTGGCCCAAAGCCGGGGC	Amplication of sequence downstream from attTn7 site
9004	CGGGCGGTTTTATGGACAGC	Amplication of *sfgfp* for integration into attTn7 site

9005	ATTATTTGTAGAGCTCATCCATG	Amplication of sf*gfp* for integration into attTn7 site
9006	CTTGCGGCAGCGTGAAGCTAGGATCTCGGCGGCAGACAGCC	Amplication of sequence downstream from attTn7 site
9076	CCTGCAAGTTACGACGCAGC	Colony PCR *sfgfp* genomic integration
9204	GTTGACCCTGGCTCTGGGC	Colony PCR sf*gfp* genomic integration
9353	TTGGTCTCAAATGGCCGACGAGCCGCGCTAC	pOPIN cloning of Ppu_4298
9354	TTGGTCTCAAAGCTTAGGGCATCTGCACTTCG	pOPIN cloning of Ppu_4298
9546	TTGGTCTCAAATGCAGGAAGCATTCCCGACGCC	pOPIN cloning of Ppu_1972
9547	TTGGTCTCAAAGCTCATTCGCTGGCGTTGACGTC	pOPIN cloning of Ppu_1972
9548	TTGGTCTCAAATGGCCCCCATGCCCCCGGCCAG	pOPIN cloning of Ppu_0571
9549	TTGGTCTCAAAGCCTATTCGCGATAAGCGTAATC	pOPIN cloning of Ppu_0571
9550	TTGGTCTCAAATGCTGGACACCCGCCAGACACC	pOPIN cloning of Ppu_2089
9551	TTGGTCTCAAAGCTTATTTGCATGGATAACTGTTC	pOPIN cloning of Ppu_2089
9552	TTGGTCTCAAATGGCGCAACTGACGGTAATGAC	pOPIN cloning of Ppu_5184
9553	TTGGTCTCAAAGCTTACCGGGCGACTGAATCCAG	pOPIN cloning of Ppu_5184
9554	TTGGTCTCAAATGGCAGACTACCGTGAGCGATG	pOPIN cloning of Ppu_1728
9555	TTGGTCTCAAAGCTCAGTGGTTCATGTGCATG	pOPIN cloning of Ppu_1728
9556	GGATCAGGTCGAAACCGTGAACAGTAC	pOPIN cloning of Ppu_2089, BsaI domestication
9557	GTACTGTTCACGGTTTCGACCTGATCC	pOPIN cloning of Ppu_2089, BsaI domestication
A296	TTGGTCTCAAATGGCTGTCTCAGCTGAAGAAGC	pOPIN cloning of Ppu_1665
A297	TTGGTCTCAAAGCTCAGCGAATGCCATCACCAG	pOPIN cloning of Ppu_1665
A298	CAAAACGCTCTTCGGCCTCCCTACAGTCATG	pOPIN cloning of Ppu_1665, BsaI domestication
A299	CATGACTGTAGGGAGGCCGAAGAGCGTTTTG	pOPIN cloning of Ppu_1665, BsaI domestication

4.1.8. Bacterial Strains

E. coli K-12 DH5α (in this study referred to as *E. coli* DH5α) had the following genotype: [*F-Φ80d lacZ ΔM15 Δ (lacZYA-argF) U169 deoR recA1 endA1 hsdR17 (rK-, mK+) phoA supE44 λ- thi-lgyr A96 relA1*] (Gibco BRL Life Technologies). *E. coli* K-12 Top10 (in this study referred to as *E. coli* Top10) had the following genotype: [*F- mcrA Δ(mrr-hsd RMS-mcrBC) Φ80lacZΔM15 ΔlacX74 nupG recA1 araDΔ139 Δ(ara98leu)7697 galK16 galE15(GalS) rpsL(StrR) endA1 λ*-] (NEB). Both strains were used for plasmid amplification and cloning. *E. coli* BL21(DE3) (in this study referred to as *E. coli* BL21) was used for heterologous protein production and has the following genotype: [*fhuA2 [lon] ompT gal λ sBamHIo ΔEcoRI-B int::(lacI::PlacUV5::T7 gene1 i21 Δnin5) [dcm] ΔhsdS*] (NEB).

Agrobacterium tumefaciens GV3101 contained a C58 background with a chromosomal rifampicin resistance, Ti-helper plasmid bearing a tetracycline resistance and the Ti-plasmid pMP90 (pTiC58DT-DNA) with virulence and gentamycin resistance genes (Intactgenomics). *A. tumefaciens* GV3101 #382 pL1M-F1-CP1Amut-nogran-mCherry-2x35S (Schulze Hüynck, 2019) was kindly provided by Dr. Jan Schulze Hüynck. *A. tumefaciens* GV3101 #155 pL1M-F3_2x35S-p19_pterm (Matei, 2016) was kindly provided by Dr. Alexandra Matei.

The commensal root bacteria (*Stenotrophomonas maltophilia* AA1, *Ochrobactrum pituitosum* AA2, *Curtobacterium pusillum* AA3, *Enterobacter cloacae* AA4, *Chryseobacterium indologenes* AA5, *Herbaspirillum frisingense* AA6, and *Pseudomonas putida* AA7) were isolated from *Zea mays* roots (Niu *et al.*, 2017) and were kindly provided by Prof. Dr. Roberto Kolter.

All used genetically modified bacterial strains are listed in Table 11-13.

Table 11: Genetically modified *E. coli* strains used and generated in this study.

Rif: Rifampicin, Gent: Gentamycin, Carb: Carbenicillin, Spec: Spectinomycin, Kana: Kanamycin.

Internal ID	Organism	Plasmid	Resistance	Reference
2086	*E. coli* Top10	pL1M-F1-Q10716-mCherry-2x35S	Carb	(Moser, 2021)
2531	*E. coli* DH5α	pL0M-SC1-cZmCP1A_no_SP_2	Spec	(Moser, 2021), provided by Laura Redzich
2532	*E. coli* DH5α	pL0M-SC1-cZmQ10716_no_SP_N1	Spec	(Moser, 2021)
2533	*E. coli* DH5α	pL0M-SC1-cZmB4FS65_no_SP_SDM1	Spec	(Moser, 2021)
2534	*E. coli* DH5α	pL0M-SC1-cZmB4FYA3_no_SP_4	Spec	(Moser, 2021), provided by Laura Redzich
2535	*E. coli* DH5α	pL1B-F1-p2x35S-sAG9-cZmCP1A-t35S_1	Carb	(Moser, 2021)
2537	*E. coli* DH5α	pL1B-F1-p2x35S-sAG9-cZmQ10716-t35S_1	Carb	(Moser, 2021)
2539	*E. coli* DH5α	pL1B-F1-p2x35S-sAG9-cZmB4FS65-t35S_1	Carb	(Moser, 2021)
2541	*E. coli* DH5α	pL1B-F1-p2x35S-sAG9-cZmB4FYA3-t35S_1	Carb	(Moser, 2021)
2717	*E. coli* DH5α	pK19-mob-sacB	Kan	this work, (Huang & Wilks, 2017; Schäfer *et al.*, 1994)
2731	*E. coli* TOP10	pOPIN-CarbR_6XHis-SUMO-PpCIP1like1	Carb	this work
2915	*E. coli* Top10	pFK78-sfGFP	Gent	(Misas-Villamil *et al.*, 2013)
2992	*E. coli* DH5α	pJT'Tmcs	Gent, Carb	this work, (Verhoef *et al.*, 2010)
3070	*E. coli* DH5α	pJT'Tmcs_sfGFP	Gent	this work
3071	*E. coli* DH5α	pJT'Tmcs_PpCIP1-sfGFP	Gent	this work
3278	*E. coli* TOP10	pOPIN-C_His-Ppu0898ΔSP	Carb	this work
3279	*E. coli* TOP10	pOPIN-C_His-Ppu1728ΔSP	Carb	this work
3280	*E. coli* TOP10	pOPIN-C_His-Ppu2532ΔSP	Carb	this work
3281	*E. coli* TOP10	pOPIN-C_His-Ppu2677ΔSP	Carb	this work
3282	*E. coli* TOP10	pOPIN-C_His-Ppu3965ΔSP	Carb	this work
3283	*E. coli* TOP10	pOPIN-C_His-Ppu4449ΔSP	Carb	this work
3284	*E. coli* TOP10	pOPIN-C_His-Ppu4631ΔSP	Carb	this work
3285	*E. coli* TOP10	pOPIN-C_His-Ppu4944ΔSP	Carb	this work
3288	*E. coli* Bl21	pOPIN-C_His-Ppu0898ΔSP	Carb	this work
3289	*E. coli* Bl21	pOPIN-C_His-Ppu1728ΔSP	Carb	this work
3290	*E. coli* Bl21	pOPIN-C_His-Ppu2532ΔSP	Carb	this work
3291	*E. coli* Bl21	pOPIN-C_His-Ppu2677ΔSP	Carb	this work

3292	*E. coli* Bl21	pOPIN-C_His-Ppu3965ΔSP	Carb	this work
3293	*E. coli* Bl21	pOPIN-C_His-Ppu4449ΔSP	Carb	this work
3294	*E. coli* Bl21	pOPIN-C_His-Ppu4631ΔSP	Carb	this work
3295	*E. coli* Bl21	pOPIN-C_His-Ppu4944ΔSP	Carb	this work
3444	*E. coli* TOP10	pJT'Tmcs_pNm_sfRBS	Gent	this work, lab internship Nina Solia
3445	*E. coli* TOP10	pJT'Tmcs_pNm_RBS_sfGFP	Gent	this work, lab internship Nina Solia
3446	*E. coli* TOP10	pJT'Tmcs_pNm_RBS_PpCip1-sfGFP	Gent	this work, lab internship Nina Solia
3511	*E. coli* TOP10	pJT'Tmcs_pNm_RBS_mCherry	Gent	(Solia, 2023)
3512	*E. coli* TOP10	pJT'Tmcs_pNm_RBS_PpCip1-mCherry	Gent	(Solia, 2023)
3514	*E. coli* TOP10	pJT'Tmcs_pNm_RBS_PpCip1-3xFlag	Gent	(Solia, 2023)
3564	*E. coli* TOP10	pK19-mob-sacB_sfGFP	Kana	(Solia, 2023)
3619	*E. coli* Bl21	pJT'Tmcs_pNm_RBS	Gent	(Solia, 2023)
3620	*E. coli* Bl21	pJT'Tmcs_pNm_RBS_PpCip1-3xFlag	Gent	(Solia, 2023)
3728	*E. coli* TOP10	pOPIN-C_His-Ppu4298ΔSP	Carb	this work
3729	*E. coli* Bl21	pOPIN-C_His-Ppu4298ΔSP	Carb	this work
3761	*E. coli* TOP10	pOPIN-C_His-Ppu1972ΔSP	Carb	this work
3762	*E. coli* TOP10	pOPIN-C_His-Ppu0571ΔSP	Carb	this work
3763	*E. coli* TOP10	pOPIN-C_His-Ppu2089ΔSP	Carb	this work
3764	*E. coli* TOP10	pOPIN-C_His-Ppu5184ΔSP	Carb	this work
3765	*E. coli* Bl21	pOPIN-C_His-Ppu1972ΔSP	Carb	this work
3766	*E. coli* Bl21	pOPIN-C_His-Ppu0571ΔSP	Carb	this work
3767	*E. coli* Bl21	pOPIN-C_His-Ppu2089ΔSP	Carb	this work
3768	*E. coli* Bl21	pOPIN-C_His-Ppu5184ΔSP	Carb	this work
3832	*E. coli* DH5α	pOPIN-C_His-Ppu4757ΔSP	Carb	this work, cloning by Melina Laporta
3833	*E. coli* BL21	pOPIN-C_His-Ppu4757ΔSP	Carb	this work, cloning by Melina Laporta
3834	*E. coli* DH5α	pOPIN-C_His-Ppu2699ΔSP	Carb	this work, cloning by Melina Laporta
3835	*E. coli* BL21	pOPIN-C_His-Ppu2699ΔSP	Carb	this work, cloning by Melina Laporta
4081	*E. coli* Top10	pOPIN-C_His-Ppu3051ΔSP	Carb	Master thesis Eva Slavic, in prep.

4082	*E. coli* BL21	pOPIN-C_His-Ppu3051ΔSP	Carb	Master thesis Eva Slavic, in prep.
4117	*E. coli* Top10	pOPIN-C_His-Ppu1665ΔSP	Carb	Master thesis Eva Slavic, in prep.
4118	*E. coli* BL21	pOPIN-C_His-Ppu1665ΔSP	Carb	Master thesis Eva Slavic, in prep.
-	*E. coli* DH5α	none	none	NEB
-	*E. coli* Top10	none	none	NEB

Table 12: Genetically modified *P. putida* strains used and generated in this study.

Gent: Gentamycin

Internal ID	Organism	Plasmid	Resistance	Reference
30	*P. putida* Δ*cip1* #3	-	-	this work
31	*P. putida* Δ*cip1* #2	-	-	this work
75	*P. putida* Δ*cip1* #2	pFK78-sfGFP	Gen	this work
90	*P. putida*	pJT'Tmcs_sfGFP	Gent	(Solia, 2023)
91	*P. putida*	pJT'Tmcs_PpCip1-sfGFP	Gent	(Solia, 2023)
92	*P. putida* Δ*cip1*	pJT'Tmcs_sfGFP	Gent	(Solia, 2023)
93	*P. putida* Δ*cip1*	pJT'Tmcs_PpCip1-sfGFP	Gent	(Solia, 2023)
97	*P. putida*	pJT'Tmcs_pNm_RBS	Gent	(Solia, 2023)
98	*P. putida*	pJT'Tmcs_pNm_RBS_sfGFP	Gent	(Solia, 2023)
99	*P. putida* Δ*cip1*	pJT'Tmcs_pNm_RBS	Gent	(Solia, 2023)
100	*P. putida* Δ*cip1*	pJT'Tmcs_pNm_RBS_sfGFP	Gent	(Solia, 2023)
101	*P. putida*	pJT'Tmcs_pNm_RBS_PpCip1-sfGFP	Gent	(Solia, 2023)
102	*P. putida* Δ*cip1*	pJT'Tmcs_pNm_RBS_PpCip1-sfGFP	Gent	(Solia, 2023)
103	*P. putida*	pJT'Tmcs_pNm_RBS_mCherry	Gent	(Solia, 2023)
104	*P. putida*	pJT'Tmcs_pNm_RBS_PpCip1-mCherry	Gent	(Solia, 2023)
106	*P. putida*	pJT'Tmcs_pNm_RBS_PpCip1-3xFlag	Gent	(Solia, 2023)
107	*P. putida* Δ*cip1*	pJT'Tmcs_pNm_RBS_mCherry	Gent	(Solia, 2023)
108	*P. putida* Δ*cip1*	pJT'Tmcs_pNm_RBS_PpCip1-mCherry	Gent	(Solia, 2023)
110	*P. putida* Δ*cip1*	pJT'Tmcs_pNm_RBS_PpCip1-3xFlag	Gent	(Solia, 2023)
130	*P. putida* pNm:sfGFP c10.16	-	-	(Solia, 2023)
131	*P. putida* Δ*cip1*#2 pNm:sfGFP c5.3	-	-	(Solia, 2023)

132	*P. putida* Δ*cip1*#2 pNm:sfGFP c5.4	-	-	(Solia, 2023)
133	*P. putida* Δ*cip1*#2 pNm:sfGFP c6.12	-	-	(Solia, 2023)
134	*P. putida* pNm:sfGFP c10.16	pJT'Tmcs-pNm::mCherry	Gent	(Solia, 2023)
135	*P. putida* pNm:sfGFP c10.16	pJT'Tmcs-pNm::PpCip1-mCherry	Gent	(Solia, 2023)
138	*P. putida* Δ*cip1*#2 pNm:sfGFP c5.3	pJT'Tmcs-pNm::mCherry	Gent	(Solia, 2023)
139	*P. putida* Δ*cip1*#2 pNm:sfGFP c5.3	pJT'Tmcs-pNm::PpCip1-mCherry	Gent	(Solia, 2023)
145	*P. putida* pNm:sfGFP c10.16	pJT'Tmcs_pNm_RBS (EVC)	Gent	(Solia, 2023)
146	*P. putida* pNm:sfGFP c10.16	pJT'Tmcs_pNm_RBS_PpCip1-3xFlag	Gent	(Solia, 2023)
147	*P. putida* Δ*cip1*#2 pNm:sfGFP c5.3	pJT'Tmcs_pNm_RBS (EVC)	Gent	(Solia, 2023)
148	*P. putida* Δ*cip1*#2 pNm:sfGFP c5.3	pJT'Tmcs_pNm_RBS_PpCip1-3xFlag	Gent	(Solia, 2023)

Table 13: Genetically modified *A. tumefaciens* strains used and generated in this study.

Rif: Rifampicin, Gent: Gentamycin, Carb: Carbenicillin.

Internal ID	Organism	Plasmid	Resistance	Reference
17	*Agrobacterium tumefaciens* GV3101	Ti-plasmid pMP90 (pTiC58DT-DNA)	Rif, Gent	Intact Genomics
155	*Agrobacterium tumefaciens* GV3101	pL1M-F3-2x35S-p19-pterm	Rif, Gent, Carb	(Matei, 2016)
382	*Agrobacterium tumefaciens* GV3101	pL1M-F1-CP1Amutnogran-mCherry-2x35S	Rif, Gent, Carb	(Schulze Hüynck, 2019)
548	*Agrobacterium tumefaciens* GV3101	pL1B-F1-p2x35S-sAG9-cZmCP1A-t35S_1	Rif, Gent, Carb	(Moser, 2021)
549	*Agrobacterium tumefaciens* GV3101	pL1B-F1-p2x35S-sAG9-cZmQ10716-t35S_1	Rif, Gent, Carb	(Moser, 2021)
576	*Agrobacterium tumefaciens* GV3101	pL1B-F1-p2x35S-sAG9-cZmB4FS65-t35S_1	Rif, Gent, Carb	(Moser, 2021)
577	*Agrobacterium tumefaciens* GV3101	pL1B-F1-p2x35S-sAG9-cZmB4FYA3-t35S_1	Rif, Gent, Carb	(Moser, 2021)

4.1.9. Plants

Zea mays cultivar Golden Bantham (Bingenheimer Saatgut AG) seeds were used for maize root colonization assays. *Arabidopsis thaliana* Col-0 seeds were used for root-on-a-chip experiments. *Nicotiana benthamiana* plants were used for *Agrobacterium*-mediated transformation and heterologous expression of PLCP in leaves.

4.1.10. Plasmids

The vectors pJT'Tmcs (Verhoef *et al.*, 2010) and pK19-moB-sacB (Huang & Wilks, 2017; Schäfer *et al.*, 1994) were kindly provided by Dr. Anita Loeschke. L0 vectors with the genes for CP1A or XBCP3-like (B4FYA3) were kindly provided by Laura Redzich. pFK78-GFP (Misas-Villamil *et al.*, 2013) was kindly provided by PD Dr. Johana Misas-Villamil. All used plasmids are listed in Table 14.

Table 14: Plasmids used in this study.

Internal ID	Vector name	Module content / Purpose	Reference
#2531	pL0M-SC1-cZmCP1A_noSP #2	L0 MoClo module ZmCP1A without signal peptide	(Moser, 2021), provided by Laura Redzich
#2532	pL0M-SC1-cZmQ10716_noSP #1	L0 MoClo module ZmRD19A-like without signal peptide	(Moser, 2021)
#2533	pL0M-SC1-cZmB4FS65_noSP #SDM1	L0 MoClo module ZmTHI1-like without signal peptide	(Moser, 2021)
#2534	pL0M-SC1-cZmB4FYA3_noSP #4	L0 MoClo module ZmXBCP3-like without signal peptide	(Moser, 2021), provided by Laura Redzich
#2535	pL1B-F1-p2x35S-sAG9-cZmCP1A-t35S_#1	L1 MoClo module ZmCP1AΔSP for het. expression in *N. benthamiana* via *A. tumefaciens* mediated transformation	(Moser, 2021)
#2537	pL1B-F1-p2x35S-sAG9-cZmQ10716-t35S_#1	L1 MoClo module ZmRD19ΔSP for het. expression in *N. benthamiana* via *A. tumefaciens* mediated transformation	(Moser, 2021)
#2539	pL1B-F1-p2x35S-sAG9-cZmB4FS65-t35S_#1	L1 MoClo module ZmTHI1ΔSP for het. expression in *N. benthamiana* via *A. tumefaciens* mediated transformation	(Moser, 2021)
#2541	pL1B-F1-p2x35S-sAG9-cZmB4FYA3-t35S_#1	L1 MoClo module ZmXBCP3ΔSP for het. expression in *N. benthamiana* via *A. tumefaciens* mediated transformation	(Moser, 2021)
#2631	pL0-pOPIN-F5_RFP_C	Backbone for *E. coli* expression vector (MoClo system) with N-term. tags	(Bentham *et al.*, 2021)
#2632	pL0-pICSL30019	L0 MoClo module with N-term. 6x-His-tag	(Bentham *et al.*, 2021)

#2634	pL0-pICSL30018	L0 MoClo module with N-term. His-SUMO-tag	(Bentham *et al.*, 2021)
#2717	pK19-mob-sacB	Plasmid used for generation of knock-outs or knock-ins in *P. putida*	(Huang & Wilks, 2017; Schäfer *et al.*, 1994)
#2731	pOPIN-CarbR_6XHis-SUMO-PpCip1like#1	Heterologous expression of 6xHis-SUMO-PpCip1ΔSP in *E. coli*	this work
#2766	pOPIN-CarbR_6XHis-PpCip1like#5	Heterologous expression of 6xHis-PpCip1ΔSP in *E. coli*	this work
#2915	pFK78-GFP	Heterologous expression of GFP in Pseudomonads	(Misas-Villamil *et al.*, 2013)
#2992	pJT'Tmcs	Backbone vector for heterologous expression of GOI in *P. putida*	(Verhoef *et al.*, 2010)
#3070	pJT'Tmcs_sfGFP	Heterologous expression of pTac-driven cyt. sfGFP in *P. putida*	this work
#3071	pJT'Tmcs_PpCip1-sfGFP	Heterologous expression of pTac-driven PpCip1-sfGFP in *P. putida*	this work
#3278	pOPIN-C_His-Ppu0898ΔSP	Heterologous expression of 6xHis-Ppu0898ΔSP (without SP) in *E. coli*	this work
#3279	pOPIN-C_His-Ppu1728ΔSP	Heterologous expression of 6xHis-Ppu1728ΔSP (without SP) in *E. coli*	this work
#3280	pOPIN-C_His-Ppu2532ΔSP	Heterologous expression of 6xHis-Ppu2532ΔSP (without SP) in *E. coli*	this work
#3281	pOPIN-C_His-Ppu2677ΔSP	Heterologous expression of 6xHis-Ppu2677ΔSP (without SP) in *E. coli*	this work
#3282	pOPIN-C_His-Ppu3965ΔSP	Heterologous expression of 6xHis-Ppu3965ΔSP (without SP) in *E. coli*	this work
#3283	pOPIN-C_His-Ppu4449ΔSP	Heterologous expression of 6xHis-Ppu4449ΔSP (without SP) in *E. coli*	this work
#3284	pOPIN-C_His-Ppu4631ΔSP	Heterologous expression of 6xHis-Ppu4631ΔSP (without SP) in *E. coli*	this work
#3285	pOPIN-C_His-Ppu4944ΔSP	Heterologous expression of 6xHis-Ppu4944ΔSP (without SP) in *E. coli*	this work
#3444	pJT'Tmcs_pNm_RBS	Backbone for het. expression of pNm-driven GOI in *P. putida* (EVC)	this work, lab internship Nina Solia
#3445	pJT'Tmcs_pNm_RBS_sfGFP	Heterologous expression of pNm-driven cyt. sfGFP in *P. putida*	this work, lab internship Nina Solia
#3446	pJT'Tmcs_pNm_RBS_PpCip1-sfGFP	Heterologous expression of pNm-driven PpCip1-sfGFP in *P. putida*	this work, lab internship Nina Solia
#3511	pJT'Tmcs_pNm_RBS_mCherry	Heterologous expression of pNm-driven cyt. mCherry in *P. putida*	(Solia, 2023)

#3512	pJT'Tmcs_pNm_RBS_PpCip1-mCherry	Heterologous expression of pNm-driven PpCip1-mCherry in *P. putida*	(Solia, 2023)
#3514	pJT'Tmcs_pNm_RBS_PpCip1-3xFlag	Heterologous expression of pNm-driven PpCip1-3xFlag in *P. putida*	(Solia, 2023)
#3564	pK19-mob-sacB_sfGFP	Knock-in of sfGFP into *P. putida* genome at attTn7 site downstream of the *glmS*	(Solia, 2023)
#3728	pOPIN-C_His-Ppu4298ΔSP	Heterologous expression of 6xHis-Ppu4298ΔSP (without SP) in *E. coli*	this work
#3761	pOPIN-C_His-Ppu1972ΔSP	Heterologous expression of 6xHis-Ppu1972ΔSP (without SP) in *E. coli*	this work
#3762	pOPIN-C_His-Ppu0571ΔSP	Heterologous expression of 6xHis-Ppu0571ΔSP (without SP) in *E. coli*	this work
#3763	pOPIN-C_His-Ppu2089ΔSP	Heterologous expression of 6xHis-Ppu2089ΔSP (without SP) in *E. coli*	this work
#3764	pOPIN-C_His-Ppu5184ΔSP	Heterologous expression of 6xHis-Ppu5184ΔSP (without SP) in *E. coli*	this work
#3832	pOPIN-C_His-Ppu4757ΔSP	Heterologous expression of 6xHis-Ppu4757ΔSP (without SP) in *E. coli*	this work, cloning by Melina Laporta
#3834	pOPIN-C_His-Ppu2699ΔSP	Heterologous expression of 6xHis-Ppu2699ΔSP (without SP) in *E. coli*	this work, cloning by Melina Laporta
#4081	pOPIN-C_His-Ppu3051ΔSP	Heterologous expression of 6xHis-Ppu3051ΔSP (without SP) in *E. coli*	Master thesis Eva Slavic, in prep.
#4117	pOPIN-C_His-Ppu1665ΔSP	Heterologous expression of 6xHis-Ppu1665ΔSP (without SP) in *E. coli*	Master thesis Eva Slavic, in prep.
/	pK19-moB-sacB_PpCip1-KO	Plasmid used for generation of *cip1* knock-out in *P. putida*	this work
AG9	pICH41258	NtPR1a signal peptide	(Grosse-Holz *et al.*, 2018)
PK15	pICH51288	Promoter (double), 35s (Cauliflower Mosaic Virus) + 5'UTR, omega (Tobacco Mosaic Virus)	(Engler *et al.*, 2014)
PK70	pICH41414	3'UTR, polyadenylation signal/terminator, 35s (Cauliflower Mosaic Virus)	(Engler *et al.*, 2014)
PK8	pICSL50007	C-terminal FLAG tag (3xFLAG octapeptide)	(Engler *et al.*, 2014)
PK9	pICSL50004	CDS, mCherry variant of RFP (*Discosoma* sp.)	(Engler *et al.*, 2014)
TK15	pICH47732	L1 cloning vector, binary vector for *Agrobacterium* T-DNA delivery to plant cells	(Engler *et al.*, 2014)
TK26	pICH41264	L0 cloning vector	(Engler *et al.*, 2014)

4.1.11. General Material and Machines

General material and machines used in this study are listed in Table 15.

Table 15: General material and machines used in this study.

Material / Machines	Manufacturer
1.0 mm cassettes	Novex
1.5 ml DNA LoBind tubes	Eppendorf
1.5 ml protein LoBind tubes	Eppendorf
5 kDa MWCO Vivaflow 200 protein concentrator	Sartorius
ÄKTA pure	Cytiva
ÄKTA start	Cytiva
Allegra X-15R Centrifuge	Beckman Coulter
Amersham Hybond P 0.45 PVDF	Cytiva
Centrifuge column, 0.8 ml	Pierce
CFX Connect Real-Time System	Bio-Rad
ChemiDoc MP Imaging System	Bio-Rad
Cryo pins	RMC Boeckeler
CVC 3000 vacuubrand (vacuum pump)	VWR
Electrophoresis power supply	Bio-Rad
Eporator	Eppendorf
EV202 Electrophoresis Power Supply	Consort
GENESYS 10S UV/VIS-Spectral-photometer	Thermo Fisher Scientific
HiLoad 16/600 Superdex 75 pg column	Cytiva
HisTrap FF Crude	Cytiva
Hitachi HT7800 transmission electron microscope (operating at 100 kV) equipped with an EMSIS Xarosa digital camera	Hitachi
Imaging System	PEQlab
Immobilized papain beads	Thermo Fisher Scientific
Leica EM HPM 100 high-pressure freezer	Leica Microsystems
Leica EM AFS2 freeze substitution device	Leica Microsystems
Microplate 96 well, PP, F-Bottom (Chimney well), black	Greiner Bio-One
Multipette M4	Eppendorf
Multiplate PCR Plates 96-well, clear	Bio-Rad
Nanodrop 2000c	Thermo Fisher Scientific
PureCube Compact Cartridge	Cube Biotech
Rotilabo sealing film, microtest plates	Roth
SelfPack Column	CoAnn Technologies ICT36007515F-50-5
Sepharose CL-4B agarose beads	Sigma Aldrich
Sep-Pak C18 Plus Short Cartridge, 360 mg Sorbent per Cartridge, 55 - 105 µm	Thermo Fisher Scientific
Seramis plant clay granulate	Seramis
Sera-Mag SpeedBead – hydrophylic (#45152105050250)	Cytiva

Sera-Mag SpeedBead – hydrophobic (#65152105050250)	Cytiva
Sonoplus sonification device	Bandelin
Sonoplus KE76 sonotrode	Bandelin
Sonoplus MS72 sonotrode	Bandelin
Steritop 45 mm Neck Size Millipore Express PLUS 0.22 µm PES, 150 ml	Millipore
Streptavidin beads	Thermo Fisher Scientific
Syringe filter (0.2 µm PES, sterile)	VWR
T100 Thermal cycler	Bio-Rad
Tecan Infinite 200 Pro plate reader	Tecan
Thermomixer comfort	Eppendorf
Trans-Blot Turbo Transfer System	Bio-Rad
Ultramicrotome PowerTome PTPC fitted with the cryosectioning system LN Ultra	RMC Boeckeler
Vivaspin 15R protein concentrator	Sartorius
Vivaspin 20 protein concentrator	Sartorius
Vivaspin 500 protein concentrator	Sartorius
Vivaspin Turbo 15 RC protein concentrator	Sartorius
VMV800 soil	Einheitserde®, Sinntal, Germany

4.1.12. Software

The software used in this thesis is listed in Table 16.

Table 16: Software used in this study.

Software
(Fiji Is Just) ImageJ 1.54j
AlphaFold 2.3.2 (Evans *et al.*, 2022; Jumper *et al.*, 2021)
Bio-Rad CFX Manager 3.1
BioRender 2021
Clone Manager 9
Clustal Omega 1.2.4 (Sievers *et al.*, 2011)
ColabFold 1.5.5. (Mirdita *et al.*, 2022)
dFast 1.2.10 (Tanizawa *et al.*, 2016, 2018)
Image Lab 6.0.1 (Bio-Rad)
InterPro 85.0 (Hunter *et al.*, 2009)
Origin 2023
Microsoft Excel (Microsoft 365 MSO v.16.0)
Miniconda 4.10.0
MView 1.68 (Brown *et al.*, 1998)
paperBLAST (Price & Arkin, 2017)
Protein-Protein BLAST 2.10.1 (Altschul *et al.*, 1990; Camacho *et al.*, 2009)
ProtParam (Gasteiger *et al.*, 2005)
PyMOL 3.1 (Schrödinger, 2015)

Python 3.8.5 with the following packages: numpy (Harris *et al.*, 2020a), pandas (McKinney, 2010), bio (Cock *et al.*, 2009), matplotlib (Hunter, 2007), pymol and their dependencies.
R 4.3.2 with the following packages: Tidyverse (Wickham *et al.*, 2019), rjson (Couture-Beil, 2024), ggrepel (Slowikowski, 2024), writexl (Ooms, 2024), Peptides (Osorio *et al.*, 2015), Biostrings (Pagès *et al.*, 2024), ampir (Fingerhut *et al.*, 2021), vegan (Oksanen *et al.*, 2018), ggVennDiagram (Gao *et al.*, 2021, 2024), ggseqlogo (Wagih, 2017), seqinr (Charif & Lobry, 2007), outliers (Komsta, 2006), multcompView (Graves *et al.*, 2024), svglite (Wickham *et al.*, 2024), ggpubr (Kassambara, 2023), patchwork (Lin Pedersen, 2024), readxl (Wickham & Bryan, 2023), scales (Wickham *et al.*, 2023) and their dependencies.
Rstudio 2023.12.1
Sypder 5
Tecan i-control 3.7
UNICORN 6.4 (Cytiva)

4.1.13. Data sources

The scan and full library of MEROPS (Rawlings *et al.*, 2014) was downloaded via https://ftp.ebi.ac.uk/pub/databases/merops/current_release/. Other inhibitor sequences (Suppl. Table 2) as well as proteins involved in the lipoprotein processing and delivery to the cell surface (Suppl. Table 4) were obtained via uniprot.org using their uniprot id (Bateman *et al.*, 2021). *Pseudomonas* protein sequences were obtained from the *Pseudomonas* Genome database (Winsor *et al.*, 2016) (version 22.1, 2023-10-06) via: https://pseudomonas.com/downloads/pseudomonas/pgd_r_22_1/Pseudomonas/complete/faa-complete.tar.gz

Sequences of maize PLCPs were obtained from the maize genome database (MaizeGDB) (Lawrence, 2004; Woodhouse *et al.*, 2021). Sequences of *Zea mays* B73 genome assemblies v4 (Jiao *et al.*, 2017) and v5 (Hufford *et al.*, 2021) were used.

AlphaFold version 2.3.2 (Evans *et al.*, 2022; Jumper *et al.*, 2021) was installed on the CHEOPS cluster. The UniRef30 database was updated to version 2023_02. Furthermore, ColabFold v1.5.5 (Mirdita *et al.*, 2022) was used for running some AlphaFold2 predictions using MMseqs2 (Steinegger & Söding, 2017) on Google Colab.

The crystal structure of chagasin in complex with papain (https://doi.org/10.2210/pdb3e1z/pdb) (Redzynia *et al.*, 2009) was obtained via rcsb.org. Information about the localization of the C-terminally tagged chagasin was obtained from the TrypTag project (http://tryptag.org/?id=Tb927.8.6450) (Billington *et al.*, 2023). Expression of PLCPs in the root was investigated using single cell transcriptome data deposited under https://bioit3.irc.ugent.be/plant-sc-atlas/root (Wendrich *et al.*, 2020).

4.2. Methods

4.2.1. Plant methods

4.2.1.1. Seed sterilization and Growth of plants

Nicotiana benthamiana plants were grown for six weeks for 16h with light at 23°C and for eight hours in darkness at 20°C with 30 % to 40 % humidity.

Maize seeds were washed for 5 min in 70 % Ethanol and afterward sterilized for 15 min with 1.2% sodium hypochlorite. Finally, the seeds were washed three times with sterile Milli-Q water. Seeds were placed in wells of a sterile 24-well plate filled with 500 µl sterile Milli-Q water and germinated in dark at RT for three days. Sterile maize seeds were either transferred into pots with sterile soil and/or sterile Seramis clay granulate or were grown on ½ MS 0.2% agar (2.2 g/l Murashige and Skoog basal salts, 10 g/l sucrose, 2 g/l plant agar) in tubes with wad pads on top of the agar. Maize plants (cultivar B73 or Golden Bantham) were grown for 16 h with light at 28°C and for 8 h in darkness at 22°C with 40 % humidity.

A. thaliana seeds were sterilized for four hours using chlorine gas (50 ml sodium hypochlorite and 1.5 ml HCl were mixed in desiccator).

4.2.1.2. SA treatment of maize roots

Maize plants were grown in sterile Seramis clay granulate for 7 to 10 days and then the roots were poured with 2 mM SA dissolved in 0.1% Ethanol every 12 hours for two days. As a control, mock treatment consisted of 0.1% Ethanol. Roots were collected 12h after the last treatment by cutting them off the shoot. Parts of the roots were used for RNA isolation, while the rest was used for apoplastic fluid isolation. Samples for RNA isolation were frozen with liquid nitrogen and stored at -80°C.

4.2.1.3. Heterologous expression of PLCPs in *N. benthamiana* leaves

A. tumefaciens containing the desired plasmids were grown overnight in 20 ml dYT media with the respective antibiotics (Table 18). Next day, the optical density of the culture was measured and the volume of each strain equal to a final OD_{600} of 1 in 10 ml was transferred to a 50 ml falcon tube. To each strain, the strain harboring the P19 plasmid was added with the same amount. The cells were pelleted with 10 min centrifugation at 4000 g and afterwards resuspended with 2ml sterile 10 mM $MgCl_2$ buffer. 2 µl of 200 µM Acetosyringone was added to the cells, the culture was mixed and left in the dark for 1 to 2 hours. After the incubation, the bacteria were infiltrated into 4-6 weeks old *N. benthamiana* leaves using a syringe without needle.

4.2.1.4. Isolation of apoplastic fluid

For root apoplastic fluid of maize, the granulate was removed carefully with forceps and Milli-Q water. Next, the roots were cut off and placed in a beaker filled with Milli-Q water. To ensure separation from the air, the roots were kept under water with a metal sieve. Afterwards, the roots were vacuum infiltrated in 3 cycles of each 15 min at 60 mbar separated by 2 min at atmospheric pressure. Finally, the roots were carefully surface-dried with paper towels, transferred to syringes without pistol hanging in 50 min falcon tubes and were centrifuged for 20 min at 3000 g and 4°C to collect apoplastic fluid. Apoplastic fluid from *N. benthamiana* leaves was collected as described above. Before storage at -20°C or usage in experiments, all apoplastic fluids were centrifuged maximal speed at 4°C to clear the samples from debris.

4.2.1.5. Amplicon Sequencing

Z. mays cultivar B73 seeds were sterilized and germinated. Sterilized 50 ml syringes without pistil were filled with sterilized soil:seramis granulate mixture (2:1). One germinated seed was placed into each syringe. Plants were grown under standard conditions and watered every two to three days with sterile MilliQ water. 8 replicates per SynCom (SynCom with *P. putida* WT or *P. putida* Δ*cip1*) and timepoint (0, 7 and 14 dpi) were prepared. One day after germinated seeds were added to the soil mixture the SynCom was added. SynCom and *P. putida* strains were grown individually overnight in dYT at 28°C with shaking. Syringes with germinated seedlings were selected. Two synthetic communities were assembled containing six of the seven members of the maize root SynCom and either with *P. putida* WT or *P. putida* Δ*cip1*. Each strain was diluted together with the other strains to OD_{600} = 0.0001 in 1L 10 mM $MgCl_2$. Each syringe was watered with 10 ml of the respective bacteria solution. After three hours seedlings for the 0 dpi timepoint were removed from the soil. Major soil particles were removed by hand and afterwards seedlings were washed by two times vortexing for 10 s in approx. 10 ml sterile MilliQ water. Roots were cut off below the seed and frozen with liquid nitrogen. Samples were stored at -80°C. This procedure was repeated for the seven and 14 dpi timepoints.

Equipment (e.g. mortar, pestle, tubes) was cooled with liquid nitrogen. Root samples were grinded with mortars and pestles until the material was a fine powder. Approx. 500 mg of grinded material were filled into sterile 2 ml tubes and stored at -80°C. DNA was isolated using the Fast DNA spin kit for soil according to the manufacturer's instructions. In short: Frozen samples were crushed for 2x 30 sec with 6200 rpm in tissue homogenizer. 978 µl of the supplied sodium phosphate buffer and supplied MT buffer was added. The samples were crushed again. Samples were centrifuged for 15 min at 14000 g and the supernatant was transferred into 2 ml tubes filled with supplied 250 µl PPS buffer. Tubes were inverted 10-times

and centrifuged for 5 min at 14000 g. 900 µl of the supernatant was mixed with 900 µl supplied binding matrix solution and incubated for 3 min on rotator. After the binding matrix was settled, 1100 µl of supernatant were discarded and the remaining sample was mixed and applied to spin filter columns. After 1 min centrifugation at 14000 g, the flow through was discarded and 500 µl supplied SEWS-M solution was added and mixed with the matrix. The previous centrifugation was repeated for 3 min and afterwards the DNA was eluted using 40 µl supplied DES elution buffer incubated for 5 min at RT on the matrix followed by 2 min centrifugation at 14000g. DNA samples were stored at -80°C.

The amplification of 16S rRNA was performed using the NovoSeq pipeline and previously established protocols (Durán *et al.*, 2018; Harbort *et al.*, 2020). DNA concentrations were quantified with a standard curve using Quant-iT™ PicoGreen. Afterwards, the DNA was diluted to 8.7 ng/µl. The 16S DNA (v5-v7 fragments of the 16S rRNA gene) was amplified by PCR (Table 20+21) using primer 799F and 1192R (Table 17) and the DFS-Taq polymerase according to the manufacture's manual (annealing temperature: 55°C, 25 cycles, extension time: 60s). Primers and enzymes were removed using Antarctic phosphatase and Exonuclease I (incubation at 37°C for 30 min and deactivation of enzymes at 85°C for 15 min). Each sample was specifically barcoded using a defined combination of barcoding primers (Table 17) and DFS-Taq polymerase according to the manufacture's manual (annealing temperature: 55°C, 10 cycles, extension time: 60 s). 5 µl of each sample was used for agarose gel electrophoresis (1.5% agarose gel). Samples were pooled (5-10 µl of each sample depending on band strength from agarose gel electrophoresis). The pooled sample was used completely for agarose gel electrophoresis (1.5% agarose gel), bands at approx. 500 bp were excited and purified using NucleoSpin Gel and PCR Clean-up kit. Next, AMPure XP magnetic beads were used to purify the extracted PCR products. Finally, purified DNA was stored at -20°C and sent for sequencing to Novogene UK Ltd.

Table 17: Primers used for Amplicon Sequencing.

Internal Primer ID	Sequence (5'-3')	Description
799F	A ACM GGA TTA GAT ACC CKG	Forward primer PCR 1
1192R	A CGT CAT CCC CAC CTT CC	Reverse primer PCR 1
B5-novo-F01	ACG ATT TAG AGG CTA ACM GGA TTA GAT ACC CKG	Forward barcoding primer PCR 2
B5-novo-R01	ACT CCC TTG TCT CCA CGT CAT CCC CAC CTT CC	Reverse barcoding primer PCR 2 sample 1
B5-novo-R02	ACA CGA GAC TGA TTA CGT CAT CCC CAC CTT CC	Reverse barcoding primer PCR 2 sample 2
B5-novo-R03	ACA CCG GTA TGT ACA CGT CAT CCC CAC CTT CC	Reverse barcoding primer PCR 2 sample 3
B5-novo-R04	ACT GCA TAC ACT GGA CGT CAT CCC CAC CTT CC	Reverse barcoding primer PCR 2 sample 4

B5-novo-R05	ACT GGT CAA CGA TAA CGT CAT CCC CAC CTT CC	Reverse barcoding primer PCR 2 sample 5
B5-novo-R06	ACA TCG CAC AGT AAA CGT CAT CCC CAC CTT CC	Reverse barcoding primer PCR 2 sample 6
B5-novo-R07	ACG TCG TGT AGC CTA CGT CAT CCC CAC CTT CC	Reverse barcoding primer PCR 2 sample 7
B5-novo-R08	ACT ACA GCG CAT ACA CGT CAT CCC CAC CTT CC	Reverse barcoding primer PCR 2 sample 8
B5-novo-R09	ACA TCC TTT GGT TCA CGT CAT CCC CAC CTT CC	Reverse barcoding primer PCR 2 sample 9
B5-novo-R10	ACA GTC GAA CGA GGA CGT CAT CCC CAC CTT CC	Reverse barcoding primer PCR 2 sample 10
B5-novo-R11	ACA CCA GTG ACT CAA CGT CAT CCC CAC CTT CC	Reverse barcoding primer PCR 2 sample 11
B5-novo-R12	ACC CAA TAC GCC TGA CGT CAT CCC CAC CTT CC	Reverse barcoding primer PCR 2 sample 12
B5-novo-R13	ACG CAA CAC CAT CCA CGT CAT CCC CAC CTT CC	Reverse barcoding primer PCR 2 sample 13
B5-novo-R14	ACA GTC GTG CAC ATA CGT CAT CCC CAC CTT CC	Reverse barcoding primer PCR 2 sample 14
B5-novo-R15	ACA GTT ACG AGC TAA CGT CAT CCC CAC CTT CC	Reverse barcoding primer PCR 2 sample 15
B5-novo-R16	ACT TGC GTT AGC AGA CGT CAT CCC CAC CTT CC	Reverse barcoding primer PCR 2 sample 16
B5-novo-R17	ACT ACG AGC CCT AAA CGT CAT CCC CAC CTT CC	Reverse barcoding primer PCR 2 sample 17
B5-novo-R18	ACT GTC GCA AAT AGA CGT CAT CCC CAC CTT CC	Reverse barcoding primer PCR 2 sample 18
B5-novo-R19	ACA CAA TAG ACA CCA CGT CAT CCC CAC CTT CC	Reverse barcoding primer PCR 2 sample 19
B5-novo-R20	ACT CTC TAC CAC TCA CGT CAT CCC CAC CTT CC	Reverse barcoding primer PCR 2 sample 20
B5-novo-R21	ACC GAT CGA ACA CTA CGT CAT CCC CAC CTT CC	Reverse barcoding primer PCR 2 sample 21
B5-novo-R22	ACA TTG CAA GCA ACA CGT CAT CCC CAC CTT CC	Reverse barcoding primer PCR 2 sample 22
B5-novo-R23	ACA GCG CTC ACA TCA CGT CAT CCC CAC CTT CC	Reverse barcoding primer PCR 2 sample 23
B5-novo-R24	ACT CGA CCA AAC ACA CGT CAT CCC CAC CTT CC	Reverse barcoding primer PCR 2 sample 24
B5-novo-R25	ACT GTG TTA CTC CTA CGT CAT CCC CAC CTT CC	Reverse barcoding primer PCR 2 sample 25
B5-novo-R26	ACT GCA CAG TCG CTA CGT CAT CCC CAC CTT CC	Reverse barcoding primer PCR 2 sample 26
B5-novo-R27	ACT TCT AGA GTG CGA CGT CAT CCC CAC CTT CC	Reverse barcoding primer PCR 2 sample 27
B5-novo-R28	ACA CAC CTG CGA TCA CGT CAT CCC CAC CTT CC	Reverse barcoding primer PCR 2 sample 28
B5-novo-R29	ACA TTC CTC TCC ACA CGT CAT CCC CAC CTT CC	Reverse barcoding primer PCR 2 sample 29
B5-novo-R30	ACC ATC GAC GAG TTA CGT CAT CCC CAC CTT CC	Reverse barcoding primer PCR 2 sample 30
B5-novo-R31	ACC ACC ACA GAA TCA CGT CAT CCC CAC CTT CC	Reverse barcoding primer PCR 2 sample 31
B5-novo-R32	ACG GTC TTA GCA CCA CGT CAT CCC CAC CTT CC	Reverse barcoding primer PCR 2 sample 32
B5-novo-R33	ACT ATC GCG CGA TAA CGT CAT CCC CAC CTT CC	Reverse barcoding primer PCR 2 sample 33
B5-novo-R34	ACC TCT ACG AAC AGA CGT CAT CCC CAC CTT CC	Reverse barcoding primer PCR 2 sample 34

B5-novo-R35	ACC TCC TCC CTT ACA CGT CAT CCC CAC CTT CC	Reverse barcoding primer PCR 2 sample 35
B5-novo-R36	ACC GTG TTA TGT GGA CGT CAT CCC CAC CTT CC	Reverse barcoding primer PCR 2 sample 36
B5-novo-R37	ACA TTA GCA GCG TAA CGT CAT CCC CAC CTT CC	Reverse barcoding primer PCR 2 sample 37
B5-novo-R38	ACC AAG TTT CCG CGA CGT CAT CCC CAC CTT CC	Reverse barcoding primer PCR 2 sample 38
B5-novo-R39	ACC CTT GTT CAC CTA CGT CAT CCC CAC CTT CC	Reverse barcoding primer PCR 2 sample 39
B5-novo-R40	ACA ACC AGC AGA TTA CGT CAT CCC CAC CTT CC	Reverse barcoding primer PCR 2 sample 40
B5-novo-R41	ACC TAG AGC TCC CAA CGT CAT CCC CAC CTT CC	Reverse barcoding primer PCR 2 sample 41
B5-novo-R42	ACC ACG CAG TCT ACA CGT CAT CCC CAC CTT CC	Reverse barcoding primer PCR 2 sample 42
B5-novo-R43	ACA CAA ACA TGG TCA CGT CAT CCC CAC CTT CC	Reverse barcoding primer PCR 2 sample 43
B5-novo-R44	ACT CGA AAC ATG CAA CGT CAT CCC CAC CTT CC	Reverse barcoding primer PCR 2 sample 44
B5-novo-R45	ACT TCC CAC CCA TTA CGT CAT CCC CAC CTT CC	Reverse barcoding primer PCR 2 sample 45
B5-novo-R46	ACA GCA GAA CAT CTA CGT CAT CCC CAC CTT CC	Reverse barcoding primer PCR 2 sample 46
B5-novo-R47	ACG AAA CAT CCC ACA CGT CAT CCC CAC CTT CC	Reverse barcoding primer PCR 2 sample 47
B5-novo-R48	ACC TGT CAG TGA CCA CGT CAT CCC CAC CTT CC	Reverse barcoding primer PCR 2 sample 48

Sequencing reads were demultiplexed and PCR primers were removed from the sequences using cutadapt software implemented in qiime2 (Bolyen *et al.*, 2019; Martin, 2011) (maximal error rate of 0.25, overlap of 10 nt) using scripts amplicon_sequencing_analysis/activate.sh, config_sc.sh, and amplicon_seq_data_analysis.sh. Finally, the reads were aligned to the 16S rRNA sequences of the SynCom member using BWA-MEM (Li, 2013) with a minimum quality score of 55 and otherwise default settings. Reads were normalized according to differences in 16S rRNA copy number. The relative abundance of the bacteria was determined relative the total number of reads in a sample. A Bray distance matrix was used for the Principal Coordinate Analysis (PCoA) analysis. This analysis was performed using amplicon_sequencing_analysis/amplicon_seq_SynCom_analysis.R script.

4.2.1.6. Root-on-a-chip

RootChip8NF is a modified version of the RootChip8S (Guichard *et al.*, 2020) being cast from a 3D printed instead of photolithographic molds. The design has been adjusted for horizontal and vertical placement featuring a U-shaped inlet and outlet layout linking all root channels to a single inlet, while retaining 8 linear channels for microscopy. The modified RootChip8NF was created by Christian-Frederic Kaiser (unpublished).

A. thaliana Col-0 seeds were sterilized with 70% Ethanol. Afterwards they were placed onto cut tips sitting on MS agar and were germinated, so that their roots grew into the cut tip. After 3 days the tips were transferred into the desired holes of RootChip8NF and the root grew further into the chips. *P. putida* WT_sfGFP (strain #130) and *P. putida* Δ*cip1*_sfGFP (strain #131) were grown in lysogeny broth (LB) medium supplemented with chloramphenicol (Table 18) overnight at 28°C. Next day, the bacterial solution was diluted in Hoaglands medium to an OD_{600} of 0.02. 1ml of the diluted cell culture was flushed into the chambers of the chips. The plants were grown for 10 days before inoculation. The bacteria colonized the root for one day. 1 dpi the chips were imaged with a custom-built high-resolution inverted epifluorescence microscope (Cairn GmbH, Heidelberg), equipped with water-immersive 25X Nikon objective (NA 1.1), motorized stage (ITK Dr. Kassen GmbH), laser launch (LDI 89 North), dichroic mirror (Chroma triple band 395/488/561), and Teledyne Photometrics Kinetics camera. The used settings were dynamic range, GFP, exposure time 50 ms, and dual cam. The images were taken with an automated grid from the root tip to approx. 5mm towards the other end of the root. The z-stack positions were oriented at the root tip having the highest position where the structures were still sharp. The other edge was set at the approx. 5 mm position at the middle of the root where the vasculature was clearly visible. After imaging the images were processed per root with a macro in ImageJ (root_on_a_chip/2024-07-18_ImportFromRAWData_Z-Stacking_v4.ijm). In short, background correction was performed and the range for the z-stack was redefined per position, and the z-stack was performed. In the next step the images of the root from the different positions were stitched together. If possible, the macros sequential stitching (root_on_a_chip/2024-07-16_SequentialStitching.ijm) or consecutive stitching (root_on_a_chip/2024-07-10_ConsecutiveStitching.ijm) were used as help. If not possible the individual positions were stitched together using pairwise stitching. Sometimes patches from two positions were created to support the stitching.

The stitched roots of all three replicates were manually checked for good stitching. Then the scale was adjusted in ImageJ with an original image to a µm scale. Next, a line segment with 500 px width was laid over the root from root tip to the end of the imaged root. Finally, the function plot profile was used to measure the intensity of the length of the line segment. All measurements were imported and combined with an R script (root_on_a_chip/root_on_a_chip_GFP_on_x_axis_v5.R) and normalized by subtraction of the fluorescence signal at 3000 µm away from the root tip. The signal in the different developmental zones was summarized and divided by the length of the different zones (meristematic zone: 0-200 µm from root tip, transition zone: 200-520 µm from root tip,

elongation zone: 520 µm-850µm from root tip, and differentiation zone: 850-1500µm from root tip, according to Verbelen *et al.*, 2006).

4.2.2. Microbiological methods

4.2.2.1. Cultivation of bacterial strains

The strains *Escherichia coli* strain Top10 or strain DH5α were used for cloning, while *Escherichia coli* strain BL21 (DE3) was used for expression of target proteins. All used strains and their growth conditions are listed in Table 11. *E. coli* strains were cultivated at 37°C either with 200 rpm shaking in dYT liquid medium or on YT agar plates, supplemented with the indicated antibiotics. *Agrobacterium tumefaciens* GV3101 strains, all bacteria of the maize root SynCom and *P. putida* strains were cultivated at 28°C either with 200 rpm shaking in dYT liquid medium or on YT agar plates, supplemented with the indicated antibiotics. Antibiotics used for cultivation of strains and their concentrations are listed in Table 18.

Table 18: Antibiotics used in this study.

Antibiotics	Concentration
Carbenicillin	100 µg/ml
Gentamycin	50 µg/ml
Rifampicin	40 µg/ml
Spectinomycin	100 µg/ml
Chloramphenicol	34 µg/ml

4.2.2.2. Preparation of chemically competent *E. coli*

Chemically competent *E. coli* cells were prepared in the following way: *E. coli* culture was cultivated in dYT overnight. 100 ml of new culture was inoculated and grown for 2 hours at 37°C until an OD_{600} of 0.6 was reached. Cells were transferred into centrifugation tubes and cooled for 30 min at 4°C before they were centrifuged for 8 min at 3000 rpm and 4°C. Supernatant was decanted, cells were resuspended in 33 ml RF1 solution pH 5.8 (100mM RbCl, 50 mM $MnCl_2$, 30 mM potassium acetate pH 7.5, 10 mM $CaCl_2$, 15 % (w/v) glycerin) and cooled at 4°C before they were centrifuged for 8 min at 3000 rpm and 4°C. Supernatant was decanted, cells were resuspended in 8 ml cold RF2 solution pH 5.8 (10 mM 3-(N-morpholino)propanesulfonic acid (MOPS) pH 6.8, 10 mM RbCl, 75 mM $CaCl_2$, 15% (w/v) glycerin) and cooled in at 0°C. Cells were aliquoted in precooled tubes and shock-frozen with liquid nitrogen and stored at -80°C.

4.2.2.3. Preparation of electroporation-competent *A. tumefaciens*

Electroporation-competent *Agrobacterium tumefaciens* GV3101 cells were prepared in the following way based on (Weigel & Glazebrook, 2006): *Agrobacterium tumefaciens* GV3101 was inoculated into 500 ml LB from an overnight culture and the culture was incubated for approx. 12 hours at 28°C. Once the culture reached an OD_{600} of 0.5-0.8 and the culture was placed on ice. Next, cells were pelleted at 4000g for 10 min at 4°C, the supernatant was discarded and cells were resuspended in 500 ml ice-cold water. The washing was repeated twice in total, first with 250 ml and then with 50 ml resuspension volume, respectively. Cells were pelleted again, cells were resuspended in 5 ml 10% (v/v) ice-cold glycerol, aliquoted and stored at -80°C.

4.2.2.3. Transformation and selection

Chemically competent *E. coli* were transformed using heat-shock transformation: 50 µl of frozen cells were thawed on ice. 1-5 µl plasmid DNA or 10 µl of a ligation mix was added to the cells dependent on the DNA concentration and the cell suspension was gently mixed. The cells were incubated for 30 min on ice and afterward the heat shock was performed with a 42 s heat pulse of 42°C on a heat block. Cells were cooled down at RT, 700 dYT was added and afterwards incubated for 1h at 37°C with 200 rpm shaking. Finally, 10-200 µl of the cell mix was plated onto a YT agar plate supplemented with the appropriate antibiotic. The plate was incubated over night at 37°C and next day, single colonies were transferred to new plates. Transformed were verified either via colony PCR or restriction digest of purified plasmid. Validation of the plasmids was performed via sequencing.

A. tumefaciens and *P. putida* were transformed using electroporation: 50 µl of frozen electro competent *Agrobacterium* cells were thawed and filled into an electroporation cuvette with 1 mm gap width. Next, 2 ng of plasmid DNA was added and mixed by pipetting the suspension up and down. Electroporation was performed in the Eporator with 1440 V for 5 ms. 400 µl of dYT media was added and afterwards incubated for 1h at room temperature with 200 rpm shaking. Finally, 10-200 µl of the cell mix was plated onto a YT agar plate supplemented with the appropriate antibiotic. The plate was incubated for two days at 28°C. Finally, single colonies were transferred to new plates with appropriate antibiotics. For transformation of *P. putida*, 3 ml dYT with appropriate antibiotics were inoculated with *P. putida* cells grown on plate. The culture was grown at 28°C with 200 rpm overnight. Next day, the optical density of the culture was determined, and the culture was diluted in 1 mM $MgSO_4$, followed by two more washes using centrifugation for 5 min at 4000 g and resuspension of the pellet in 1 mM $MgSO_4$. For the last resuspension of the pellet, the pellet was resuspended in 100 µl 1 mM $MgSO_4$ and transferred to an electroporation cuvette (1 mm width). Electroporation was performed in the

Eporator with 1.8 kV, 25 µF and 200 ohm. 700 µl of dYT media was added and afterwards incubated for 1h at 28°C with 200 rpm shaking. Finally, 10-200 µl of the cell mix was plated onto a YT agar plate supplemented with the appropriate antibiotic. The plate was incubated overnight at 28°C. Finally, single colonies were transferred to new plates with appropriate antibiotics.

Additionally, a blue-white selection was used to efficiently screen for positive transformants when the Modular cloning (MoClo) system was used: The insertion of the gene-of-interest (GOI) into the cloning site harboring the lacZ gene caused the lack of β-galactosidase expression. When transformants still harboring the lacZ gene (re-transformants or negative clones) grow on media containing 5-bromo-4-chloro-3-indolyl-β-D-galactopyranoside (X-Gal), they will appear blue due to the enzymatic activity of the β-galactosidase, while successful transformants (positive clones) lacking the lacZ gene appear white (Cronan *et al.*, 1988). For this selection method, 50 µl of 2% (w/v) X-Gal dissolved in dimethylformamid (DMF) was spread on solid YT plates. The red-white selection was used for the cloning of pOPIN constructs (Bentham *et al.*, 2021). The L0 backbone vector contains mCherry in its cloning site, which is constitutively expressed and lets clones appear red after more than two days in the refrigerator. However, when cloning is successful and the mCherry gene is replaced with the GOI, the transformants are white and were selected.

4.2.2.4. Genomic knock-in or knock-out of genes into *P. putida* via two-step allelic exchange

The cloning mix was transformed into *P. putida* via electroporation and genomic integrations or knock-outs were performed using two-step allelic exchange (Elmore *et al.*, 2017; Huang & Wilks, 2017). Deviating from the standard protocol, the cells were plated onto YT agar plates containing 25% (w/v) sucrose for selection of mutants without double crossover events which would have the *sacB* gene. The levansucrase sacB transforms sucrose to levan, which slows the grows of the bacteria or is lethal (Gay *et al.*, 1985; Huang & Wilks, 2017; Schäfer *et al.*, 1994). Hundreds of larger colonies were selected, transferred to new YT agar plates containing 25% (w/v) sucrose, and the new plates were incubated overnight at 28°C. Next day, these clones were transferred to YT agar plates with Kanamycin and YT agar plates with Kanamycin and 25% (w/v) sucrose and incubated at 28°C overnight. Clones growing on sucrose but not on Kanamycin were considered positive. 20-50 clones were checked via colony PCR for the right knock-in or knock-out (Suppl. Fig. 6+9). Used primers are displayed in Table 10. gDNA of clones which passed colony PCR was isolated and PCR was performed. The PCR product was sent for sequencing to confirm the successful transformation without mutations.

4.2.2.5. Isolation of bacterial culture supernatant and fractionation

Bacteria were grown in 20 ml dYT media at 28°C with 200 rpm agitation overnight. The optical density was determined and volumes equal to a final OD of 5 in 10 ml M9 were centrifuged for 10 min with 4000 g at 4°C, pellets were resuspended in 10 ml M9 minimal medium without glucose. M9 without glucose was used ensure that the different utilization of glucose by the different bacteria (Krumbach, 2020; Krumbach *et al.*, 2021) does not influence the screening. M9 medium was used to simulate minimal nutrient conditions and we speculated that this would stress the bacteria causing them to produce possible effectors. The bacteria were incubated in the M9 medium for four hours or overnight at 28°C with 200 rpm agitation. Four hours of incubation were used for the experiments with papain with heterologously expressed root PLCPs and with bacterial supernatants alone, while 24 hours of incubation were used for the screening of all SynCom members with root apoplastic fluid. After the incubation, the cells were pelleted by centrifugation at 4000 g for 20 min at 4°C and the supernatant was carefully collected. The supernatant was filter-sterilized with a 0.2 µm PES sterile syringe filter. Supernatants were stored at 4°C. Culture supernatants were fractionated in higher molecular weight fractions (HMWFs) and lower molecular weight fractions (LMWFs) using protein concentrator columns (dependent on the volume and molecular weight Vivaspin 500, 15R, 20, or 15RC) with defined molecular weight cut-offs (MWCO: 3 kDa, 5kDa or 10 kDa). The HMWF was the concentrate and the LMWF was the flow-through. The supernatant was ten times concentrated at 4°C with 4000 g. The fractions were stored at 4°C. For heat inactivation, the HMWF was incubated for 15 min at 95°C and afterwards centrifuged at max speed for 10 min.

4.2.2.6. Growth curves of bacteria

Growth curve measurements were performed using the Tecan plate reader. The bacterial cultures were diluted to an OD_{600} of 0.01. 10 µl of the diluted cultures were then mixed with 90 µl of dYT medium in the well of a flat transparent 96 plate. The plate was incubated in the plate reader holding a constant temperature of 28°C with a constant shaking of 3.5 rpm. The optical density was measured every 10 minutes for 24 hours in replicates.

4.2.2.7. Determination of cell density

The optical density (OD_{600}) of a culture was measured as absorbance at 600 nm in spectrophotometer with the corresponding medium as reference and in the linear range using appropriate dilutions.

4.2.2.8. Fluorescence microscopy of bacteria

P. putida WT_sfGFP_mCherry and *P. putida* WT_sfGFP_PpCip1-mCherry cells from fresh plates stored at 4°C were diluted and washed twice in PBS to an appropriate cell density level,

so that individual cells were visible. 10 µl of each sample was fixed by short heat application to the microscope slides. The samples were observed with an 100x oil immersion objective (NA: 1.45) using a Nikon Eclipse Ti operating system and a Hamamatsu orca-flash4.OLT digital camera. For sfGFP and mCherry excitation 488 nm and 543 nm were used, respectively. The emission of sfGFP and mCherry were measured between 500 nm to 535 nm and 575 and 650 nm for mCherry, respectively. The focus of the microscope was always based on the strongest GFP signal which localized in the cytosol. After the images were taken, the fluorescence intensities of sfGFP and mCherry throughout the cells were measured: An identical line (white line in graphs) was drawn with ImageJ orthogonal to the longer side of the cell in the sfGFP and mCherry images. At this line the plot profile of the intensity was measured. All measured intensity profiles were analyzed with an R script. The following script was used: intensity_surface_plot_microscopy/ surface_plot_microscopy.R. Within each profile the intensities were normalized to the minimum (0%) and maximum intensity (100%) of each profile. Next, the center position of the cell was determined as the position with the maximum sfGFP signal for each pair of sfGFP-mCherry profiles. The histograms with grouping by fluorescence signal were created using the geom_line function of the ggplot2 package and display the mean of each fluorescence signal (darker line) with the standard error of the mean (SEM) (lighter color). A paired two-sided t-test was performed for the signals of mCherry and sfGFP at approx. -0.52 µm, 0 µm, and 0.52 µm distance from the center using the t.test function in R. The significance of the differences at these positions was indicated by asterisks ($p>0.05$: n.s., $p<0.05$: *, $p<0.01$: **, $p<0.001$: ***).

4.2.2.9. Fixation, embedding, freezing and immunogold-labeling for transmission electron microscopy

Fixation, gelatin embedding, freezing, cryo-sectioning and imaging steps were based on (Danne, 2022; Wilson & Bacic, 2012) and were performed by Dr. Ulla Neumann at MPIPZ Cologne: Bacterial cultures (*P. putida* Δ*cip1*_EVC, *P. putida* Δ*cip1*_mCherry and *P. putida* Δ*cip1*_PpCip1-mCherry) were grown overnight in dYT with standard conditions. Cultures were transported on ice to the imaging facility. For fixation, 1 ml of culture was pipetted to 1 ml of 8% paraformaldehyde (PFA) in 0.1M sodium cacodylate pH 6.9 or 4% PFA + 0.4% glutaraldehyde in 0.1M sodium cacodylate pH 6.8, respectively, and incubated for four hours with agitation at RT. Next, the cells were centrifuged for 5 min at 5000 rpm, afterwards resuspended in 1 ml 4% PFA in 0.1M sodium phosphate buffer pH7.4 or 2% PFA + 0.2 glutaraldehyde in 0.1M sodium phosphate buffer pH 7.4, respectively, followed by incubation overnight at 4°C. Afterwards, the fixed cells were centrifuged for 5 min with 5000 rpm and afterwards were washed by resuspension in 2 ml 0.1M sodium phosphate buffer. This washing step was repeated. Next, cells were centrifuged for 5 min with 5000 rpm

and resuspended in 2 ml 0.1 M sodium phosphate buffer supplemented with 0.1% glycine. Afterwards, cells were centrifuged for 5 min at 5000 rpm and embedded by resuspending them in 0.5ml prewarmed 10% gelatin in 0.1 M sodium phosphate buffer. The mixture was pipetted into pre-warmed tube, centrifuged again until a pellet formed and was then solidified on ice. After solidification, small gelatin cubes were cut and incubated in 2.3M sucrose at 4°C overnight. Samples were mounted on cryo pins. Mounted samples were stored in liquid nitrogen. The ultramicrotome PowerTome PTPC fitted with the cryosectioning system LN Ultra was used to cut thin frozen sections. For freezing a Leica EM HPM 100 high-pressure freezer and for substitution a Leica EM AFS2 freeze substitution device were used.

Grids were placed on molten gelatin plates, were incubated for 30 min at 37°C and washed three times on 0.1M Tris(hydroxymethyl)aminomethane (Tris)-HCl buffer pH 6.9 for 2 min. Quenching with 0.05 M glycine in the 0.1M Tris-HCl buffer pH 6.9 was performed for 15 min. Samples were blocked by incubation on 0.1M Tris-HCl buffer pH 6.9 with 1% bovine serum albumin fraction V (BSA) and 1:20 dilution of goat serum for 30 min. The wash was performed three-times with 0.1M Tris-HCl buffer with 1% BSA und 1% gelatin (TRIS-BSA-FG) for 2 min. Next, samples were incubated with the primary anti-RFP antibody for 90 min. Samples were washed five-times with TRIS-BSA-FG for 5 min. Samples were then incubated with the secondary antibody (10 nm Goat anti-Rabbit IgG Gold, EM.GAR10/2) for 30 min, followed by washing 5-times with TRIS-BSA-FG for 5 min to remove unbound antibodies. Next, it was washed 5-times for 3 min with MilliQ water. Contrast staining of the samples was performed by staining them with 0.4% uranyl acetate pH 7 for 5 min on ice. Samples were looped out using a filter paper. Samples were imaged using a Hitachi HT7800 transmission electron microscope (operating at 100 kV) equipped with an EMSIS Xarosa digital camera. Images were analyzed by counting visible gold particles in the compartments of completely visible non-overlapping cells (surface, periplasm/inner/outer membrane and cytosol).

4.2.3. Molecular biological methods

4.2.3.1. Isolation of genomic DNA from bacteria

Genomic DNA of *P. putida* was isolated using the GeneJET genomic DNA purification kit according to the manufacturer's instructions (Gram-Negative Bacteria Genomic DNA Purification Protocol). Genomic DNA was stored at -20°C.

4.2.3.2. Plasmid isolation

Plasmid DNA of *E. coli* was isolated from bacterial cultures grown overnight. To isolate the DNA, NucleoSpin Plasmid Mini kit was used according to the manufacturer's instructions.

4.2.3.3. Isolation of RNA from bacteria and maize plants

Equipment used for grinding and other materials were cooled with liquid nitrogen. Furthermore, steps were undertaken to reduce the risk of RNA contamination, e.g. by using fresh gloves, wearing a lab coat, and cleaning the workspace and equipment properly.

Root samples were ground in the precooled mortars until the samples were finely powdered. Approx. 100 mg of each sample were transferred into pre-cooled 2 ml tubes and frozen with liquid nitrogen again. For RNA extraction, 1 ml of the TRIzol reagent was added to each of the samples. Next, the samples were mixed for 5 min on a vortexer. After the vortexing, 200 µl chloroform was added to each sample followed by 5 min vortexing. Samples were centrifuged at 13.3 g for 15 min, the upper aqueous phase was carefully transferred to a new tube filled with 400 µl isopropanol. The tubes were inverted, incubated for 10 min on ice and centrifuged at 4°C for 15 min with 13.3 g. The supernatant was removed, and the pellet was washed two times with 75% Ethanol by centrifugation at 4°C for 10 min at 13.3 g. Next, the supernatant was removed and the pellet was air-dried under the fume hood. Finally, the RNA was resuspended with 30 µl nuclease free water and stored at -80°C.

RNA from bacterial cells grown in culture was isolated using the MasterPure Complete DNA & RNA Purification kit: 300 µl of the provided Tissue and Cell lysis Solution and 1 µl Proteinase K was added the pelleted cells, incubated for 15 min at 65°C, cooled down, centrifuged for 5 min at 13000 rpm, and 150 µl supernatant was transferred to a new tube. 75 ml of the provided MPC Protein Precipitation Reagent was added and the sample was vortexed for 10s. The debris was pelleted for 10 min at 10000g and at 4°C, the supernatant was transferred and 500 µl isopropanol was added to the supernatant. The sample was inverted 30-40 times and the nucleic acids was pelleted by centrifugation for 10 min at 4°C with 10000g. Residual isopropanol was discarded and 200 µl provided DNAse I solution was added to resuspend the pellet. The sample was incubated for 10 min at 37°C. 200 µl 2X T and C Lysis Solution was added, the sample was mixed, 200 µl of MPC Protein Precipitation Reagent was added, the sample was mixed again for 3 min and the debris was pelleted for 10 min at 10000g and at 4°C, the supernatant was transferred and 500 µl isopropanol was added to the supernatant. The sample was inverted 30-40 times and the nucleic acids was pelleted by centrifugation for 10 min at 4°C with 10000g. After removal of isopropanol, the pellet was washed twice with 70% ethanol and the RNA was solubilized with 30 µl H_2O by incubation at 55°C for 10 min.

4.2.3.4. DNA removal after RNA isolation

The TURBO DNA-free kit was used for the removal of DNA from RNA samples: 20 µl of the RNA samples were mixed with the DNAse and the corresponding buffer and incubated at 37°C for 30 min. Next, the DNA digestion was stopped by addition of the DNAse inactivation

reagent and the reagent was removed by centrifugation. The DNAse-free sample was transferred to a new RNAse-free tube, the stability of the RNA was confirmed by a 1% agarose gel using gel electrophoresis, and the sample was stored at -80°C.

4.2.3.5. cDNA synthesis from RNA

The RevertAid First Strand cDNA Synthesis Kit was used to generate cDNA via oligo-dT primer from DNA-free RNA samples: 2 ng of RNA were mixed with 20U RiboLock RNAse inhibitor, 1.2 µM oligo-dT primer, 1 mM dNTPs, 1X reaction buffer, and 200 U RevertAid H Minus Reverse Transcriptase and incubated for 5 min at 25°C followed by 60 min at 42°C. Finally, the cDNA was stored at -20°C.

4.2.3.6. Quantitative real-time PCR

Quantitative real-time PCR (qPCR) was performed using the GoTaq qPCR Master Mix: cDNA was diluted 1:100 in nuclease-free water. A master mix containing 1X GoTaq qPCR Master Mix and 0.3 µM of the forward and reverse primers was prepared. 8.5 µl of the prepared Master Mix and 6.5 µl of the diluted cDNA were transferred to wells of a 96 well PCR plate. The measurements were performed in technical duplicates. The plate was sealed with a Rotilabo protection film followed by a short centrifugation to remove possible drops from the sealing. The qPCR was performed in a CFX Connect Real-Time System with the thermocycler protocol listed in Table 19 using the SYBR scan mode. The cycle threshold (Ct) values were automatically calculated by the Bio-Rad CFX Manager software.

Table 19: qPCR thermocycler protocol.

Temperature [°C]	Time [min]	Cycles
95	02:00	1x
95	00:30	45x
61	00:30	
72	00:30	
65	00:05	Gradient
95	00:05	

For plant gene expression and bacterial gene expression, the fold-change of gene expression of the GOI between treatments was calculated relative the *gapdh* (plant) or *ropd* (bacteria) reference gene using the "$2^{-\Delta\Delta Ct}$"-method (Livak & Schmittgen, 2001). Ct values above 35 were considered as contamination. To display zero values in a plot with log scale y-axis, these values were set to 0.0001. qPCR data plots were created using qPCR_Cip_expression_pseudomonas/ qPCR_Cip_expression_pseudomonas.R.

4.2.3.7. Determination of DNA and RNA concentration

DNA and RNA were quantified using the NanoDrop with its custom settings for DNA or RNA.

4.2.3.8. Polymerase Chain Reaction (PCR)

GOIs were amplified using Polymerase Chain Reaction (PCR) without signal peptide sequence. PLCP genes were amplified using KOD polymerase (Tables 20+21). Inhibitor candidates and *cip1* were amplified using GoTaq Green Master Mix (Tables 22+23). Used primers are displayed in Table 10. For colony PCR, instead of template very few cells of a colony were added to the GoTaq Green Master mix.

Table 20: KOD-Xtreme polymerase and GoTaq Green Master Mix reaction mix.

Component	Volume [µl]
2X Xtreme buffer	25
dNTPs (2 mM)	10
Forward primer (10 µM)	1.5
Reverse primer (10 µM)	1.5
Template (20-100 ng/µl)	1
KOD-Xtreme polymerase	1
Water	10

Component	Volume [µl]
2X GoTaq Green Master Mix	25
Forward primer (10 µM)	1
Reverse primer (10 µM)	1
Template (<250 ng)	X
Water	up to 23 µl

Table 21: KOD-Xtreme polymerase cycler protocol.

Temperature	Time	Cycles
94°C	2 min	1
98°C	15 s	30
Annealing Temp.	30 s	
68°C	1:30 min	
68°C	5 min	1
16°C	10 min	1

Table 22: GoTaq Green Master Mix cycler protocol.

Temperature	Time	Cycles
95°C	2 min	1
95°C	1 min	30
Annealing Temp.	30 s	
72°C (1 min/1000 bp)	X	
72°C	5 min	1
16°C	10 min	1

After the PCR finished, 5 µl of the reaction mix was mixed with 1 µl of 6X DNA loading dye and the DNA was evaluated on a 1% agarose gel containing ethidium bromide via agarose gel electrophoresis performed at 120 V for 20-30 min. The length of the observed bands visualized with UV light was compared to the predicted length of the PCR products. If required, a band was excised. After confirmation, the PCR product or gel slice with PCR product was cleaned up using the NucleoSpin Gel and PCR Clean-up kit according to the manufacturer's manual, followed by DNA quantification with the Nanodrop.

4.2.3.9. Extraction and purification of DNA

For DNA in agarose gels, the DNA was extracted using the NucleoSpin Gel and PCR clean-up kit following the manufacturer's instructions. For general DNA clean-up, the DNA was purified using the NucleoSpin Gel and PCR clean-up kit following the manufacturer's instructions for PCR clean-up.

4.2.3.10. Restriction digest of DNA

Many different restriction enzymes (Table 6) were used to cleave DNA at targeted sites either for cloning or for verification of successful cloning. The digestion was always performed according to the manufacturer's instructions. Usually, 1 µg DNA, 1X CutSmart buffer and 20u of each used restriction enzyme were used for a 50 µl reaction. The reaction mix was incubated for 1h at 37°C and enzymes were inactivated for 20 min at 65°C or 80°C depending on the enzymes used.

4.2.3.11. Ligation of DNA fragments

For ligation of DNA fragments, 1 µl of T4 DNA Ligase, 50 ng vector DNA, insert DNA in a 3:1 ration to the vector DNA and 1X T4 DNA Ligase Buffer were used in a 20 µl reaction. The ligation mix was incubated for 10 min at RT followed by heat inactivation for 10 min at 65°C. Finally, 10 µl of the ligation mix was directly used for transformation.

4.2.3.12. Site-directed mutagenesis

To mutate single to few nucleotides within plasmid DNA, the Quick-change Multi Site-Directed Mutagenesis Kit was used: In short, the target plasmid (usually PCR product was cloned into pMiniT vector using NEB PCR Cloning Kit) was amplified by the Quick Change Multi enzyme blend with a primer designed to have the desired mutation to introduce the base change at the desired position during amplification. The parental and methylated plasmids without the base exchange were digested by DpnI in another step. Finally, the plasmid was transformed into *E. coli* cells.

4.2.3.13. Gibson Assembly

NEBuilder® HiFi DNA Assembly Master Mix was used to assemble DNA molecules according to the manufacture's instruction. The DNA molecules were designed with 20 nt overlap for assembly via homologous recombination. For 2-3 fragment assemblies, a vector:insert ratio of 1:3 was used with 50 ng vector. The reaction mix containing the vector, inserts and the NEBuilder HiFi DNA Assembly Master Mix was incubated for 15 min at 50°C and was afterwards used for transformation.

4.2.3.13. Golden Gate Modular Cloning (MoClo)

Vectors for heterologous expression of PLCPs in *N. benthamiana* leaves were cloned via Golden Gate Modular Cloning (MoClo) with the "Golden Gate Modular Cloning Plant Parts Kit" and the "Golden Gate MoClo Plant Tool Kit" (Engler *et al.*, 2014; Weber *et al.*, 2011). Vectors for heterologous expression of inhibitor candidates in *E. coli* were cloned via Golden Gate Modular Cloning with the pOPIN-GG system (Bentham *et al.*, 2021). All used modules are displayed in Table 23. Genes of interest (GOI) were amplified by PCR from *Zea mays* cultivar B73 cDNA (PLCP genes) or *P. putida* gDNA (inhibitor candidates) using primers (Table 10) adding the correct overhangs, and BpiI or BsaI restriction sites for the MoClo reaction into level 0 (L0) or level 1 (L1) vectors (for inhibitor candidates directly L1 was used), respectively. In the case of RD19A-like (also termed Q10716 by its uniport id), the plasmid pL1M-F1-Q10716-mCherry-2x35S (#2086), kindly provided by (Schulze Hüynck, 2019), was used as template. For THI1-like (B4FS65), internal BsaI sites were removed using site-directed mutagenesis with a specific primer (#4921) by substituting a base. L0 vectors with CP1A or XBCP3-like (B4FYA3) were prepared and kindly provided by Laura Redzich as described above.

Table 23: Modules used for Golden Gate Modular Cloning.

Internal ID	Name	Module content / Purpose	Reference
AG9	pICH41258	NtPR1a signal peptide	(Grosse-Holz *et al.*, 2018)
TK26	pICH41264	L0 cloning vector	(Engler *et al.*, 2014)
TK15	pICH47732	Level 1 cloning vector, binary vector for *Agrobacterium* T-DNA delivery to plant cells	(Engler *et al.*, 2014)
PK15	pICH51288	Promoter (double), 35s (*Cauliflower Mosaic Virus*) + 5'UTR, omega (*Tobacco Mosaic Virus*)	(Engler *et al.*, 2014)
PK70	pICH41414	3'UTR, polyadenylation signal/terminator, 35s (*Cauliflower Mosaic Virus*)	(Engler *et al.*, 2014)
#2631	pL0-pOPIN-F5_RFP_C	Backbone for *E. coli* expression vector using the MoClo system with N-term. tags	(Bentham *et al.*, 2021)
#2632	pL0-pICSL30019	L0 MoClo module with N-term. 6x-His-tag and precision cleavage site	(Bentham *et al.*, 2021)
#2634	pL0-pICSL30018	L0 MoClo module with N-term. His-SUMO-tag and precision cleavage site	(Bentham *et al.*, 2021)

MoClo L0 reactions (Table 24) were performed in a thermocycler with three cycles of 10 min at 37°C and 10 min at 16°C, followed by transformation into *E. coli* DH5α or Top10 and blue-white selection was performed. MoClo L1 reactions (Tables 25+26) were performed in a thermocycler with five cycles of 10 min at 40°C and 10 min at 16°C, followed by 10 min at 50°C and 20 min at 80°C. The reaction mix was transformation into *E. coli* DH5α or Top10 and blue-white (Agrobacterium vectors) or red-white (pOPIN) selection was performed. After confirmation by sequencing, these vectors were either transformed into *A. tumefaciens* (PLCPs) or *E. coli* BL21 (inhibitor candidates) cells. MoClo L0 and L1 reactions for vectors with PLCPs were performed as part of my Master thesis (Moser, 2021).

Table 24: MoClo L0 reaction mix for heterologous expression of PLCPs.

Component	Amount
TK26 (L1 vector)	0.05 pmol
PCR product	0.10 pmol
FastDigest BpiI	0.5 µl
FastDigest Buffer 10X	1 µl
400 U T4 DNA Ligase	1 µl
10 mM ATP	2 µl
Nuclease-free water	up to 5.5 µl
total volume	10 µl

Table 25: MoClo L1 reaction mix for heterologous expression of PLCPs.

Component	Amount
TK15	0.03 pmol
PK70	0.06 pmol
PK15	0.06 pmol
AG9 or AG10	0.06 pmol
L0 vector with gene of interest	0.06 pmol
20U/µl BsaI	0.5 µl
10X NEB Cutsmart buffer	1 µl
1 U/µL T4 DNA Ligase	0.5 µl
10 mM ATP	1µl
Nuclease-free water	up to 7 µl
total volume	10 µl

Table 26: MoClo L1 reaction mix for heterologous expression of inhibitor candidates.

Component	Amount
pL0-pOPIN-F5_RFP_C	0.03 pmol
pL0-pICSL30019 (His-tag) or pL0-pICSL30018 (His-SUMO-tag)	0.06 pmol
PCR product of GOI	0.06 pmol
20U/µl BsaI	0.5 µl
10X NEB Cutsmart buffer	1 µl
1 U/µL T4 DNA Ligase	0.5 µl
10 mM ATP	1µl
Nuclease-free water	up to 7 µl
total volume	10 µl

4.2.3.13. Cloning of GFP-, mCherry- and Flag-tagged PpCip1 constructs and controls

The pJT'Tmcs vector (Verhoef *et al.*, 2010) for constitutive expression in *Pseudomonas putida* was kindly provided by Dr. Antia Loeschke. The *sfgfp* gene was amplified from the pFK78-GFP vector (Misas-Villamil *et al.*, 2013) via PCR either with KpnI and XbaI restriction sites or with XhoI and XbaI restriction site. The *cip1* gene was amplified via PCR from *P. putida* gDNA with KpnI and XhoI restriction sites. After PCR cleanup, restriction digest of all PCR products with the desired restriction enzymes was performed. The pJT'Tmcs vector was digested with KpnI and XbaI. The linearized pJT'Tmcs vector was ligated with the KpnI and XbaI cleaved *sfgfp* PCR-product yielding pJT'Tmcs_sfGFP. Next, the linearized pJT'Tmcs vector was ligated with the KpnI and XhoI cleaved *cip1* PCR product and the XhoI and XbaI cleaved sf*gfp*

PCR-product yielding pJT'Tmcs_PpCip1-sfGFP. Ligation mixtures were transformed into *E. coli* DH5α and correct plasmids were confirmed by sequencing.

However, since the inducible pTac promoter (synthetically derived from the trp and lac operons of *E. coli* (Amann *et al.*, 1988)), in the pJT'Tmcs MCS, was not suitable for constitutive expression in *P. putida*, the promoter and the RBS were exchanged with the constitutively active pNm promoter (Labes *et al.*, 1990) and another RBS: The pNm promoter and a RBS were amplified from the pFK78-GFP vector additionally adding SacI and KpnI restriction sites and digested with SacI and KpnI. pJT'Tmcs, pJT'Tmcs_sfGFP and pJT'Tmcs_PpCip1-sfGFP were linearized with SacI and KpnI. The pNm-RBS fragment was ligated into all linearized vectors, yielding pJT'Tmcs_pNm_RBS (EVC), pJT'Tmcs_pNm_RBS_sfGFP, pJT'Tmcs_pNm_RBS_PpCip1-sfGFP (performed by Nina Solia during lab internship). The ligation mix was transformed into *E. coli* Top10 and successful cloning was confirmed by sequencing.

To add C-terminal Flag- and mCherry-tags to PpCip1, the flag and mCherry sequences were amplified by PCR from PK8 (Flag-tag) or PK9 (mCherry), respectively and XhoI and XbaI restriction sites were added by the used primers. To create a vector with cytosolic mCherry, the mCherry sequence was amplified from PPK9 adding KpnI and XbaI cleavage sites. All PCR products were digested with the desired restriction enzymes (XhoI and XbaI, or KpnI and XbaI). The pJT'Tmcs_pNm_RBS_PpCip1-sfGFP was linearized with both restriction enzyme combinations. The digested PCR products of the amplified tags were ligated into the pJT'Tmcs_pNm_RBS_PpCip1-sfGFP vector linearized by XhoI and XbaI, yielding pJT'Tmcs_pNm_RBS_PpCip1-Flag and pJT'Tmcs_pNm_RBS_PpCip1-mCherry, respectively. The digested PCR product of the amplified mCherry was ligated into the pJT'Tmcs_pNm_RBS_PpCip1-sfGFP vector linearized by KpnI and XbaI, yielding pJT'Tmcs_pNm_RBS_mCherry (Solia, 2023). The ligation mixes were transformed into *E. coli* Top10 and successful cloning was confirmed by sequencing.

All used primers are displayed in Table 10. All generated plasmids were transformed into *P. putida* WT, *P. putida* Δ*cip1*, *P. putida* WT_sfGFP and *P. putida* Δ*cip1*_sfGFP. This cloning was performed by Nina Solia as part of her Master thesis under my supervision (Solia, 2023).

4.2.3.14. Cloning of *Pseudomonas* knock-in and knock-out vectors

For genomic knockout of *cip1* in *P. putida* 500 bp sequence upstream and downstream of the *cip1* gene were amplified with 20 bp overhangs. Used primers are displayed in Table 10. The pK19-moB-sacB vector (Huang & Wilks, 2017; Schäfer *et al.*, 1994) was linearized using restriction with EcoRI at 37°C for one hour. The upstream and downstream region were inserted into the linearized pK19-moB-sacB vector using Gibson Assembly. The reaction mix

was transformed into *E. coli* Top10 yielding pK19-moB-sacB_PpCip1-KO. After confirmation by sequencing, the vector was transformed into *P. putida WT* cells for integration via two-step allelic exchange, yielding *P. putida* Δ*cip1*.

Genomic integration of *sfgfp* into the attTn7 site downstream of the *glmS* gene (Matsumoto *et al.*, 2022) was performed via two-step allelic exchange (Huang & Wilks, 2017). Therefore, 500 bp sequence upstream and 500 bp sequence downstream from the integration site were amplified with 20 bp overhangs via PCR on *P. putida* gDNA. The *sfgfp* sequence was amplified from the pJT'Tmcs_pNm_RBS_sfGFP vector. Used primers are displayed in Table 10. The pK19-moB-sacB vector (Huang & Wilks, 2017; Schäfer *et al.*, 1994) was linearized using restriction with NheI and HindIII at 37°C for 40 minutes. The upstream region, *sfgfp* and downstream region were inserted into the linearized pK19-moB-sacB vector using Gibson Assembly. The reaction mix was transformed into *E. coli* Top10. After confirmation by sequencing, the vector was transformed into *P. putida WT* and *P. putida* Δ*cip1* cells for integration via two-step allelic exchange, yielding *P. putida* WT sfGFP and *P. putida* Δ*cip1* sfGFP. This cloning was performed by Nina Solia as part of her Master thesis under my supervision (Solia, 2023).

4.2.3.15. Sequencing

Plasmid DNA (50 ng/µl) was mixed with 2.5 µM primer (final conc.) and water to a total volume of 10 µl. The mix was sent to Eurofins Genomics for sequencing. Sequencing results were compared with the expected sequences using CloneManager Professional 9.

4.2.3.16. Agarose gel electrophoresis

To analyze the size of DNA or RNA on agarose gels, agarose gel electrophoresis was performed using 1% (w/v) agarose-TAE gels containing 0.35 mg/ml ethidium bromide. As a reference, GeneRuler 1kb Plus or the 100 bp ladder were used. The electrophoreses were performed with a voltage of 90 V for 30-50 min. The DNA intercalated with ethidium bromide was visualized using UV light and measured using the UV/VIS-spectrophotometer.

4.2.4. Biochemical methods

4.2.4.1. Heterologous protein expression

CC1-His was expressed and purified (only with affinity chromatography) according to the protocol established by (Schulze Hüynck, 2019) and finally the buffer was exchanged for use in assays. The remaining His-tagged constructs were heterologously expressed using the pOPIN system (Bentham *et al.*, 2021): An overnight culture of *E. coli* Bl21 cells harboring a pOPIN plasmid for overexpression of a GOI was used to inoculate the expression culture.

200 ml or 1 L of dYT with the desired antibiotic were inoculated to an OD_{600} of 0.1 with the overnight culture. The culture grew at 37°C with 200 rpm orbital shaking until an OD_{600} of 0.6-0.8 was reached. At this point, a sample was taken to check the expression without induction of expression. Next, the expression of the GOI was induced by addition of Isopropyl-B-D-thiogalactopyranoside (IPTG) to a final concentration of 0.5 mM and the culture was grown overnight at 37°C. Next day, samples were taken for later SDS-PAGE and split into soluble and insoluble fraction using max. speed centrifugation. Afterwards, the culture was centrifuged for 20 min at 6000 rpm and 4°C, the supernatant was discarded and the pellet was either stored at -20°C or directly processed.

4.2.4.2. Purification of His-tagged proteins

Prior to purification, the cells were lysed via sonification: The cell pellet was resuspended in 30 ml Ni-NTA lysis buffer and sonification was applied to the cell suspension (three cycles of 5 min with 0.5s pulse and 40% amplitude) using the KE76 sonotrode. Finally, the cell debris was separated from the soluble fraction using 25 min centrifugation at 20000 rpm at 4°C. The supernatant was filter-sterilized using a syringe filter with 0.2 µm pore size. Samples were taken for later SDS-PAGE. His-tagged proteins were purified using a 1 ml HisTrap FF Crude column on a ÄKTA start system: The column was equilibrated with Ni-NTA binding buffer. Protein purification was performed using the affinity chromatography program with 5 column volume (CV) equilibration, 15 CV wash and 7 CV elution. Proteins were eluted in 1 ml fractions with the Ni-NTA elution buffer. Samples were taken for later SDS-PAGE. The HisTrap columns were stored in 20% ethanol at 4°C.

4.2.4.3. Precision protease digest for removal of His-tags and solubility tags

In the case of PpCip1, the expression using a SUMO solubility tag was necessary to reach sufficient expression. To remove the solubility tag, the purified His-SUMO-PpCip1 was incubated with 250 µl precision protease in cleavage buffer (50 mM Tris HCl, 100 mM NaCl, 1 mM EDTA, 1 mM DTT, pH 7.5) overnight at 4°C. In some cases, due to the similar molecular weight (MW) of His-SUMO and PpCip1, the mix was rerun over a HisTrap column and the flow-through containing PpCip1 was collected. Further purification was performed using size-exclusion chromatography.

4.2.4.4. Size-exclusion chromatography

As a last step, proteins were purified via size-exclusion chromatography on a HiLoad 16/600 Superdex 75 pg column with 120 ml column volume using an ÄKTA pure system. The column was equilibrated with degassed 50 mM Tris-HCl 150 mM NaCl pH7 buffer. The 5 ml injection loop was cleaned with 15 ml of the same buffer before each run. 5 ml sample was loaded into

the injection loop (if needed, the protein was beforehand concentrated to have max. 5 ml volume). The sample was loaded onto the column and the proteins were separated on the column by size using a 1 ml/min flow rate and 1.5 CV of the equilibration buffer. The peaks were collected using a fraction collector (5 ml fractions, collection when UV signal > 3 mAu). The column was stored in 20% ethanol at 4°C.

4.2.4.5. Determination of protein concentrations

Protein concentrations were either determined by the NanoDrop using UVette cuvettes with the protein-specific extinction coefficient calculated using ProtParam (Gasteiger *et al.*, 2005) or using a Bradford Assay: 2X ROTI Quant reagent was used for determination of protein concentration via the Bradford method: A standard curve was created with 0 µg/ml to 100 µg/ml BSA with 200 µl volume. All samples (200 ml) were mixed with 200 µl 2X ROTI Quant, incubated for 5 min and then the OD_{595} was measured and used for quantification.

4.2.4.6. Interactor pulldown using papain beads

Interactor pulldown was performed using papain beads. As a control agarose beads (Sepharose 4B, control) were used. 160 µl of the beads were washed twice with 1 ml equilibration buffer (50 mM $NaPO_4$ pH6, 200 mM NaCl) in 1.5 ml protein LoBind tubes and finally, the buffer was removed. Afterwards, the papain was inactivated using 1 ml inactivation buffer (50 mM $NaPO_4$ pH6, 200 mM NaCl, 10 mM sodium chloroacetate) by incubation for 3h at RT on a tube rotator. Next, the beads were washed four-times with 1 ml equilibration buffer and finally, the buffer was removed. *P. putida* Δ*cip1* was grown overnight in dYT at 28°C. The cells were diluted to an OD_{600} of 1 in 10 ml M9 media and was incubated for 4 hours at 28°C with orbital shaking. The cells were pelleted by centrifugation (20 min at 4000g and 4°C) and the supernatant was concentrated using a 5 kDa protein concentrator column to a final volume of 1 ml. The sample was loaded onto the beads and incubated on the beads overnight at 4°C on a tube rotator. One sample of the papain beads was not mixed with the sample and served as background control. Next day, the beads were centrifuged for 1 min at 10000 g, the supernatant was discarded and the beads were washed 6-times with equilibration buffer. The buffer was removed, beads were resuspended with 400 µl equilibration buffer and split into half to be used for SDS-PAGE and MS analysis.

4.2.4.7. Affinity chromatography with papain beads

Affinity chromatography was performed using papain beads. 1 ml of papain beads or agarose beads (Sepharose 4B, control) were filled into 1 ml PureCube Compact Cartridge according to the manufacture manual. The columns were equilibrated with 10 CV equilibration buffer (20 mM $NaPO_4$ pH6, 10 mM EDTA, 20 mM L-Cysteine-HCl). *P. putida* Δ*cip1* was grown

overnight in dYT at 28°C. The cells were diluted to an OD_{600} of 1 in 200 ml M9 media and was incubated for 4 hours at 28°C with orbital shaking. The cells were pelleted by centrifugation (20 min at 4000g and 4°C) and the supernatant was concentrated using a 5 kDa MWCO Vivaflow 200 concentrator column to a final volume of 1 ml. 9 ml of equilibration buffer was added to the sample and the sample was filter sterilized using a syringe filter with 0.2 µm pore size. The sample was split in half to be used for the affinity chromatography of the papain and agarose beads and runs were performed consecutively. Samples were loaded onto the columns with 0.5 ml/min via the 5 ml sample loop using the ÄKTA pure system. The columns were washed with 15 CV equilibration buffer (10 CV at 0.5 ml/min speed, 5 CV 1 ml/min). Interactors were eluted with 10 CV elution buffer (20 mM $NaPO_4$ pH6, 10 mM EDTA, 20 mM L-Cysteine-HCl, 3 M NaCl) and the elution was collected using a fraction collector (fixed 0.5 ml fractions). The ÄKTA image of the ÄKTA run was created using: proteomics_MS_data_analysis/ ÄKTA_image_ACE_0819_papain_beads_affinity_chrom.R.

4.2.4.8. Sodium dodecyl sulfate-polyacrylamide gel electrophoresis (SDS-PAGE)

Proteins were separated based on their molecular weight using Sodium dodecyl sulfate-polyacrylamide gel electrophoresis (SDS-PAGE). Protein samples were denatured using 1X SDS-loading dye and incubation at 98°C for at least 5 min. The polyacrylamide (PAA) gels contained an upper stacking and a lower resolving gel (Table 27-28).

Table 27: PAA stacking gel.

Components	Final concentration
Polyacrylamide	6% (v/v)
Tris-HCl pH 6.8	125 mM
Sodium dodecyl sulfate (SDS)	0.1% (w/v)
Ammoniumpersulfate (APS)	0.1% (w/v)
Tetramethylethylenediamine (TEMED)	0.1% (v/v)

Table 28: PAA resolving gel.

Components	Final concentration
Polyacrylamide	15% (v/v)
Tris-HCl pH 8.8	375 mM
Sodium dodecyl sulfate (SDS)	0.1% (w/v)
Ammoniumpersulfate (APS)	0.1% (w/v)
Tetramethylethylenediamine (TEMED)	0.04% (v/v)

10-15 µl of each sample were loaded into the wells of the PAA gels. 2.5 µl of PageRuler Prestained Protein Ladder was used as a reference. SDS-PAGE was performed with 200 V for 70 minutes (used mainly for ABPP with gels in Novex 1.0 mm cassettes) or with 90 V for 30 min followed by 120 V for 60-65 min (for standard 1.0- or 1.5-mm Bio-Rad gels).

4.2.4.9. Staining of polyacrylamide gels

SYPRO Ruby staining was used for staining of lower concentrations of proteins (e.g. in activity-based protein profiling): First, the proteins in the PAA gels were fixed for 20-30 min on a shaker in SYPRO Ruby fix solution. Secondly, the gels were stained overnight in reusable SYPRO Ruby staining solution on a shaker. Finally, the gels were washed for 20-30 min in SYPRO Ruby wash solution on a shaker, rinsed with water and imaged using the ChemiDoc imager (Excitation: 450 nm, Emission: 610 nm). Blauer Jonas staining was performed for staining of higher concentrations of proteins (e.g. in protein purifications): First, the gel stained with reusable Blauer Jonas staining solution for 20 min or overnight on a shaker. Finally, the staining was washed away for at least 20 min with water on a shaker and the stained gels were imaged using the ChemiDoc imager (white plate, no filter, white epi illumination).

4.2.4.10. Western Blot

After SDS-PAGE, proteins were transferred from the PAA gel onto a 0.2µm PVDF membrane via semi-dry transfer using the Trans-Blot Turbo Transfer System. The transfer was performed with 25V for 30 min in Western blot transfer buffer. PVDF membranes were briefly activated with methanol. After the blotting, the membrane was blocked either for 60 min at RT or overnight at 4°C with 3% low-fat milk powder dissolved in 1X TBS-T buffer. Blocking, washing and incubation of the membrane were performed either in 50 ml falcons on rolling devices or in trays on a shaker. Next, the membrane was incubated with the primary antibody applied to 3% low-fat milk powder dissolved in 1X TBS-T buffer in the desired concentration (Table 7) for 1-2 h at RT or overnight at 4°C. After the incubation, the membrane was washed 3 times with TBS-T buffer for 15 min. When required, the membrane was incubated with the secondary antibody applied to 3% low-fat milk powder dissolved in 1X TBS-T buffer in the desired concentration (Table 7) for 1-2 h at RT. After the incubation, the membrane was washed 3 times with TBS-T buffer for 15 min. Finally, the SuperSignal™ West Pico PLUS chemiluminescent signal kit was used according to manufacturer's instructions: SuperSignal West Pico PLUS Stable Peroxide and SuperSignal West Pico PLUS Luminol/Enhancer were missed in a ratio of 1:1 and were added to the membrane. When needed, SuperSignal West Femto Maximum Sensitivity Substrate was used for more sensitive detection. The chemiluminescence signal detected using a ChemiDoc (no filter, no illumination, signal accumulation mode).

4.2.4.11. Activity-based protein profiling (ABPP)

Activity-based protein profiling (ABPP) was performed to detect active PLCPs using probes covalently binding to the active site of PLCPs (Van der Hoorn *et al.*, 2011). The probes can either have a fluorescent tag for direct detection after SDS-PAGE or a Biotin-tag for detection

by Western blot or pulldown: Apoplastic fluid (usually 46 µl were used) was incubated in 50 mM sodium acetate buffer pH 6 with 10 mM DTT and either with 40 µM E64 dissolved in DMSO or with DMSO for 30 min. During this preincubation, the covalently binding PLCP-specific inhibitor E64 blocks active PLCPs (Hanada *et al.*, 1978) and hinders their labeling, serving as a control for correct labeling of PLCPs. After the preincubation the probe (MV201 (Richau *et al.*, 2012), DCG04-Cy5 (Stolze *et al.*, 2012), or DCG04-Biotin (Greenbaum *et al.*, 2000)) was added to a final concentration of 0.6 µM and the ABPP was performed in darkness for 2 hours (MV201, DCG04-Cy5) or 4 hours (DCG04-Biotin). MV201 and DCG04-Cy5 were kindly provided by Prof. Hermen Overkleeft (Leiden University). In later experiments confirming successful heterologous expression of PLCPs, DCG04-Cy5 was used instead of MV201 for ABPP. A non-probe control was performed by not adding probe to a replicate of the prepared sample allowing detection of unspecific background signals. After the ABPP, the reaction was stopped by addition of 15 µl 6X SDS-loading dye and incubation at 98°C for at least 5 min. Samples were used for SDS-PAGE and PLCPs were detect either directly when fluorescent probes were used or via Western Blot, when Biotin tagged probes were used. SDS-PAGE were performed using PAA gels in Novex 1.0 mm cassettes (200V for 70 min) and in darkness, when fluorescent probes were used.

4.2.4.12. Protein stability assay with CP1A

The protein of interest (conc indicated in Figure) and apoplastic fluid (usually 20 µl) containing overexpressed CP1A or inactive $CP1A_{mut}$-mCherry was incubated in 50 mM sodium acetate buffer pH 6 with 10 mM DTT and either with 40 µM E64 dissolved in DMSO or with DMSO for 30 min. SDS-PAGE was performed using PAA gels in Novex 1.0 mm cassettes (200V for 70 min) and proteins were visualized by Blauer Jonas staining or SYPRO Ruby staining.

4.2.4.13. Substrate cleavage assay

Substrate cleavage assays were used to determine the activity of proteases via cleavage of the synthetic substrate Z-LR-AMC, which was shown to be a major substrate of maize PLCPs (Schulze Hüynck *et al.*, 2019). 10 µl of the tested protease or apoplastic fluid was mixed with 10 µl PAB buffer pH 6 and 70 µl of the tested treatment (e.g. buffer control, E64 control, culture supernatants, candidate proteins or fractions) in a well of a 96 well plate. The samples were always tested at least in triplicates. 20 µM E64 was used as a control for PLCP activity. The mix was incubated for 15 min, so that PLCPs became activated or inactivated when in contact with inhibitors. After the incubation, the plate was placed in a Tecan plate reader and the prepared script was started. Within the script, 10 µl 100 µM Z-LR-AMC was added quickly to each filled well of the plate and after short mixing the measurement of AMC fluorescence (Top mode, excitation: 350 nm, Emission: 460 nm, number of flashes: 10, Z-position: 16000 µm,

gain: 90, integration time: 20 µs, settle time: 0 ms, and lag time: 0 µs) was started. After the measurement, protease activity in RFU/s was determined by the increase of fluorescence within 100 s (linear range) via the slope function of Excel. The results of replicates were averaged and the standard error was determined after the removal of outliers. To determine PLCP activity, the E64 control was set to 0% PLCP activity, while the buffer control was set to 100% activity. IC_{50} was calculated using the Hill-function (Neubig *et al.*, 2003) in Origin or R or were estimated based on 50% inhibition, if fitting was not possible. Tecan results were analyzed and visualized with different R scripts: Tecan_PLCP_Ppu_SN/HK+10kDafilter_v1.R, Tecan_PLCP_Ppu_SN/ SNs_alone_v1.R, Tecan_PLCP_Ppu_SN/Tecan_Combined_RAF-LAF-papain_v5.R, candidate_inhibition_tests/Ppu_4757_visualization.R and candidate_inhibition_tests/candidate_testing_visualization.R, candidate_inhibition_tests/Cip1_testing_visualization_v1.R.

4.2.4.14. Cell fractionation

To localize bacterial proteins within the bacterial cell, cell fractionation analysis (Paredes-Osses & Hardie, 2013) was performed by Nina Solia: Overnight cultures of *P. putida* were used to inoculate new cultures in dYT medium with an OD_{600} of 0.4 which were incubated for three to four hours until an OD_{600} of 1 was reached. At this point the cultures were centrifuged for 5 min at 3000 g at 4 °C and afterwards the supernatant was carefully discarded. The remaining pellet was gently resuspended in 10 ml 1X PBS pH 7.2 buffer. The resuspension and centrifugation steps were repeated in total three times to wash the cells. In the final step, the pellet was resuspended in 35 ml 1X PBS pH 7.2 buffer and the OD_{600} was determined. The cell suspension was diluted to an OD_{600} of 1, which was used for further fractionations as main suspension and was kept at 4°C.

To isolate the cytosolic and membrane fraction, 30 ml of the main solution were centrifuged for 10 min at 3000 g and at 4°C. After the supernatant was discarded, the pellet was resuspended in in 30 ml 20 mM Tris-HCl buffer pH 7.4 containing 0.1 mg/ml RNAse and 1.2 U/ml DNAse I. This suspension was homogenized twice using a multi-cycle cell disruptor at 1.5 to 2.5 kbar. 1 ml of the disrupted cells was used as whole cell fraction (WCF) sample. To remove non-lysed cells, the remaining solution was centrifuged for 20 min at 3000 g at 4°C. Next, the supernatant was centrifuged for 60 min at 183000 g at 4°C. A sample was taken from the supernatant which was labeled as “cytosol 1” (Cyt.1) and the pellet (membrane fraction) was resuspended in 400 µl PBS.

To isolate the periplasmic fraction and the 2nd cytoplasmic fraction, 2 ml of the main solution were centrifuged for 10 min at 3000 g at 4°C. After the supernatant was removed carefully using a pipette, the cell pellet was gently resuspended in 1 ml 25 mM Tris-sucrose-EDTA

(TSE) pH 8 buffer containing the 1X cOmplete protease inhibitor cocktail using a wire loop and incubated for 30 min on ice. Next, the suspension was centrifuged for 30 min at 16000 g at 4°C. 1 ml sample was taken from the supernatant containing the periplasmic fraction. The pellet was resuspended in 600 µl 10 mM Tris-HCl pH 7.4 buffer containing 1X cOmplete protease inhibitor cocktail and three freeze and thawing cycles with liquid nitrogen were used to lyse the cells. Next, 19.9 µl 1M $MgCl_2$ and 1 µl 1 U/ml DNAse I was mixed with the lysed cells using inversions and incubated for 15 min at 37°C. Afterwards the samples were centrifuged for 15 min at max. speed and samples were obtained from the supernatant which contained the 2nd cytosolic fraction. All samples were mixed with SDS-loading dye and were incubated for at least 5 min at 95°C.

4.2.4.15. Papain treatment on *P. putida* cells

P. putida WT and Δ*cip1* cells were diluted to an OD_{600} of 0.3 in 1 ml of 1XPBS buffer pH 8. The cells were washed twice in this buffer. Next, the cells were incubated in 1XPBS buffer pH 8 with or without 100 nM Papain for 30 min. Finally, the cells were washed twice with 1XPBS buffer pH 8 supplemented with 20 µM E64. Finally, the cells were resuspended in 1XPBS buffer pH 8 with 1 mg/ml EZ-Link Sulfo-NHS-Biotin and incubated for 30 min. Further processing was performed as described for biotin labeling. Beads are resuspended in 200 µl membrane protein buffer, 150 µl are used for MS and the rest for Western Blot analysis. Samples are stored at -80°C.

4.2.4.16. Biotin labeling

For specific labeling of cell surface proteins with biotin, the commercially available biotinylating reagent EZ-Link Sulfo-NHS-Biotin reagent was used. Its negatively charged Sulfo group prevents its passage through cell membranes allowing the labeling of surface proteins of intact cells (Daniels & Amara, 1998; Huh & Wenthold, 1999). The OD_{600} of a *P. putida* Δ*cip1*_sfGFP_PpCip1-Flag overnight culture was measured and an equivalent of OD_{600} = 0.3 in 1ml was collect. The cells were washed three times with cold 1X PBS using centrifugation (5 min at 4000 g) and resuspension steps. Finally, the cells were resuspended in 1 ml PBS. 200 µl of the freshly prepared Sulfo-NHS-Biotin reagent were added to the cells, briefly mixed by inversion and incubated for 30 min at RT. Next, the reagent was quenched using three washes with 1X PBS containing 100 mM glycine. Finally, the cells were resuspended in 500 µl membrane protein buffer. Cells were sonicated for 2 min with 40% amplitude on ice using the MS72 sonotrode. 150 µl Streptavidin beads were prepared by washing them three times with 500 µl 50 mM Tris-HCl pH 8 containing 1X Protein Inhibitor Mix (centrifugation at 1400 g, 3 min). After lysis, 250 µl beads were added to the lysed cells and were incubated for 1 h rotating (speed 4). Afterwards, the sample was transferred onto a 0.8 ml Pierce centrifuge

column and washed twice with 500 µl membrane protein buffer. Beads were resuspended in 100 µl MilliQ water. 20 µl SDS loading dye was added to the beads and the beads were incubated at 95°C for 10 min to release bound proteins. Samples from all steps were used SDS-PAGE followed by Wester-Blot analysis.

4.2.4.17. Liquid chromatography–mass spectrometry

Samples were prepared either with Tryptic in-gel digest or on-beads digest by the MS facility using only MS grade solutions: For in-gel digest, gel pieces were washed twice with 500 µl water and twice with 500 µl 100 mM Ammonium bicarbonate. 300 µl 10 mM Tris(2-chlorethyl)phosphate (TCEP) in 100 mM Ammonium bicarbonate was added to the sample, incubated at 62°C for 30 min. Supernatant was removed by short centrifugation. 300 µl 55 mM Iodoacetamid (IAM) in 100 mM Ammonium bicarbonate was added to the sample and was incubated at 37°C with 1000 rpm shaking at 37°C in the dark. Afterwards, supernatant was removed again via short centrifugation. The sample was washed three-times with 500 µl 50:50 100 mM Ammonium bicarbonate / 100% acetonitrile and was incubated for 15 min with 1000 rpm shaking, followed by short centrifugation steps to remove supernatants. 100 µl 100% acetonitrile was added to the sample and supernatant was removed via short centrifugation. Gel pieces were dried using a vacuum centrifuge for 10 min at 45°C. 200 ng trypsin in 25 mM Ammonium bicarbonate was added and incubated for 10 min at room temperature. Next, approx. 200 µl 25 mM Ammonium bicarbonate was added to the gel slices and the sample was incubated for 37°C with 1000 rpm shaking for 17 hours. Afterwards, the supernatant was transferred to Protein LoBind tubes. Remaining gel pieces were covered with 5% formic acid (approx. 100-150µ), incubated for 15 min at room temperature with 1000 rpm shaking. Afterwards, the supernatant was combined with the previous supernatant, 100 µl 100% acetonitrile was added, incubated for 15 min at room temperature with 1300 rpm shaking, and supernatant was combined with previous supernatant. This step was repeated with 70µl 100% acetonitrile and 50 µl 100% acetonitrile. Peptide samples were dried using a vacuum centrifuge for 2:40h at 45°C.

For on-bead digest, 2x Lysis Buffer (2% SDS, 20 mM TCEP, 80 mM Chloroacetamide, 100 mM 4-(2-Hydroxyethyl)piperazine-1-ethanesulfonic acid (HEPES)) was added to the samples, samples were incubated at 90°C for 7 min. The supernatant was filtered through glass fiber tips into 96 well plates. 150 µg of magnetic beads (1:1 mix of Sera-Mag SpeedBead – Hydrophylic and Sera-Mag SpeedBead – hydrophobic) was added and incubated for 2 min. Then 60 ml ethanol was added and incubated for 18 min at 24°C followed by a brief centrifugation. Samples were placed on a magnet for at least three min and the supernatant was discarded. The beads were washed four-times with 180 µl 80% ethanol using a magnet

as before. Finally, 100 µl 10 µg/ml trypsin in 25 mM Ammonium bicarbonate was added and incubated overnight. Next day, beads were collected on a magnet for five minutes and the supernatant and used for purification of peptides via C18-StageTips.

Samples where further processed using 200 µl C18-StageTips according to (Rappsilber *et al.*, 2007): 50 µl methanol was added to the StageTips and centrifuged for 2 min at 600 g. Afterwards, 50 µl of 0.5% (v/v) formic acid in 80% (v/v) acetonitrile/water was added and centrifuged for 2 min at 600 g. Next, 50 µl 0.5% (v/v) formic acid in water was added and centrifuged for 2 min at 600 g. Dried peptides were solved with 100 µL 0.5% (v/v) formic acid in water by shaking at 25°C for 30 min with 1300 rpm. The peptide solution was added to the equilibrated StageTips and centrifuged at 800 g for 3 min. Peptides were washed with 50 µl 0.5% (v/v) formic acid in water, followed by centrifuged at 800 g for 3 min and repeated with 20 µl 0.5% (v/v) formic acid in water. Peptides were eluted twice with 25 µl 0.5% (v/v) formic acid in 80% (v/v) acetonitrile/water followed by centrifugation at 800 g for 3 min. Eluted peptides were dried in a vacuum centrifuge until all acetonitrile was evaporated. 10-15 µl of 0.1% formic acid was added to 1 µl of the peptide concentrate. Liquid chromatography–mass spectrometry (LC-MS) was used to identify proteins in samples derived from size-exclusion chromatography, papain beads pulldown, and papain affinity chromatography using the settings and protocols listed in Table 29:

Table 29: Settings used for LC-MS and data analysis.

	Size-exclusion chromatography	**Papain beads pulldown**	**Papain affinity chromatography**
LC-MS	MS device: Orbitrap Fusion Lumos		
	LC device: Thermo Easy-nLC 1200		LC device: Thermo Vanquish Neo
	Ion source: Thermo Nanospray Flex		
Analytical	Self-packed fused silica capillary with an integrated sintered frit; CoAnn Technologies ICT36007515F-50-5		
	Length = 44 cm ID = 75µm OD = 360 µm Emitter 15 µm	Length = 41 cm ID = 75µm OD = 360 µm Emitter 15 µm	Length = 28 cm ID = 75µm OD = 360 µm Emitter 15 µm
Stationary	Reprosil-Pur 120 C18-AQ	Phenomenex Kinetex C18-XB core shell	
	Particle diameter: 1.9 µm	Particle diameter: 1.7 µm	
	Pore size: 120 Å	Pore size: 100 Å	Pore size: 120 Å
	Sonation column oven PRSO-V2, 50°C		
Solvents	A: 0.1% Formic acid in UPLC water	A: 0.2% Formic acid in UPLC water	A: 0.2% Formic acid, 2% Acetonitrile, 98% H_2O
	B: 0.1% Formic acid, 20% H_2O, 80% Acetonitrile	B: 0.2% Formic acid 20% H_2O 80% Acetonitrile	

	Gradient from 2-98% B		Gradient from 2-99% B
Sample preparation	In-gel digest. Purification with C18-StageTips	On-beads digest Purification with C18-StageTips	On-beads digest Purification with C18-StageTips
Setti	Tune v3.3.2782.28 Gradient: 70 min		Tune v3.5.3881.18 Xcalibur v4.5.445.18 Gradient: 30 min
Settings MS1	Analyzer: Fourier Transform max. Resolution: 240000 (120000 for papain beads pulldown) Scan range: 375 - 1500 (1600 for papain beads pulldown) Automatic gain control: Standard max. Ion acquisition time [ms]: 50 ms RF lens: 30 Data-dependent mode: CT/3sec		
Settings MS2	Analyzer: IT Res./ScR: -/rapid Scan Range: Auto Automatic gain control: 300% max. Ion acquisition time: 120 ms charge states used for fragmentation: +2 to +7 Isolation mode: Q Isolation window: 1.2 Fragmentation: stepped HCD Normalized collision energy: 20,30,40	Analyzer: IT Res./ScR: -/rapid Scan Range: Auto Automatic gain control: 200% max. Ion acquisition time: 120ms charge states used for fragmentation: +2 to +7 Isolation mode: Q Isolation window: 1.6 Fragmentation: stepped HCD Normalized collision energy: 27, 30, 33	Analyzer: IT Res./ScR: -/rapid Scan Range: Auto Automatic gain control: 300% max. Ion acquisition time: 35 ms charge states used for fragmentation: +2 to +7 Isolation mode: Q Isolation window: 1.6 Fragmentation: HCD Normalized collision energy: 32
Special settings	MS1 in Orbitrap at high resolution and data dependent MS2 in Iontrap at rapid scan rate. Dynamic exclusion enabled (exclude after n times=1; Exclusion duration (s)= 30; mass tolerance= ± 10ppm)	MS1 and data dependent MS2 in Iontrap. Dynamic exclusion enabled (exclude after n times=1; Exclusion duration (s)= 60; mass tolerance= ± 2ppm)	MS1 in Orbitrap at high resolution and data dependent MS2 in Iontrap at rapid scan range. Dynamic exclusion enabled (exclude after n times=1; Exclusion duration (s)= 20; mass tolerance= ± 10ppm) Intensity Threshold: 5000 Ion transfer Tube Temp: 230°C Ion Source Voltage: 2100 V

Data analysis	Program: Proteome Discoverer 2.4. Search engine: Sequest HT and MS Amanda 2.0 Static modification: Carbamidomethyl (C) Digestion mode: Trypsin/P (specific), 2 missed cleavages Dynamic modification: Acetyl (N-term); Oxidation (M) Modification included in quantification Oxidation (M)	Program: MaxQuant v2.0.2.0 Search engine: Andromeda Static modification: Carbamidomethyl (C) Digestion mode: Trypsin/P (semi-specific), 2 missed cleavages Parameter groups: Only one group Dynamic modification: Acetyl (N-term); Oxidation (M) Modification included in quantification: Oxidation (M)	Program: MaxQuant v 2.0.3.0 Search engine: Andromeda Static modification: Carbamidomethyl (C) Digestion mode: Trypsin/P (specific), 2 missed cleavages Dynamic modification: Acetyl (N-term); Oxidation (M) Modification included in quantification: Oxidation (M)
Database	*P. putida* AA7 predicted proteins	*P. putida* AA7 predicted proteins, Papain	*P. putida* AA7 predicted proteins, Papain
Analysis	/proteomics_MS_data_analysis/		
	ACE_0677_SEC_MS_data_analysis_part_1.py, ACE_0677_SEC_MS_data_analysis_part_2.py	ACE_0680_MS_Papain_Beads_pulldown_analysis_v14.R	ACE_0819_MS_Papain_Beads_Column_NaCl.R, ÄKTA_image_ACE_0819_papain_beads_affinity_chrom.R

All solvents were of UPLC grade.

4.2.5. Bioinformatical and statistical methods

4.2.5.1. Bacterial genome annotation

The genomes of all SynCom bacteria were annotated using the dFast software (Tanizawa *et al.*, 2016, 2018) with its standard settings. Unique identifiers were assigned to each protein consisting of the three-letter abbreviation of the taxa and an incrementing number (e. g. *P. putida* protein #1 is Ppu_0001).

4.2.5.2. BLASTp searches

Protein-protein Basic Local Alignment Search Tool (BLASTp) searches were performed with the standalone software BLAST+ (Camacho *et al.*, 2009) to allow multiple BLASTp searches to be run within a single run. A BLAST database containing all predicted bacterial proteins of the SynCom or individual strains was created with the BLAST+ application (default settings). In the BLAST searches, proteins required for maturation and transport of lipoproteins (Suppl. Table 4), cysteine proteases (Clan CA), PLCPs (family C1) or cysteine protease inhibitors deposited in the MEROPS database (Suppl. Table 1) (Rawlings *et al.*, 2014)) were used as search queries against all predicted proteins of the SynCom or an individual SynCom member with an expectation value (e-value) threshold of 0.001. Hits were filtered (Inhibitors: Identity > 20%, query coverage > 20%; clan CA: Identity > 30%, query coverage > 70%; C1

family & Lipoprotein machinery: no filters), and signal peptides for secretion via the Sec or Tat pathway were predicted via the SignalP5/6, except for the lipoprotein machinery (Almagro Armenteros *et al.*, 2019; Teufel *et al.*, 2022). The scripts "BLAST_merops_SynCom_inhibitor/Pipeline_BLAST_results_analysis_inhibitor_search_specific_classes.py", "lipoprotein_machinery/analysis_lipoprotein_machinery.R", "BLAST_merops_Ppu_CA/CA_proteases_in_Ppu.R" or "BLAST_merops_SynCom_C1A/C1_in_SynCom.R" were used for this task, respectively. Additionally, microbial inhibitor sequences known from literature (Suppl. Table 2) were searched in the same way with an expectation value threshold of 0.05. Hits were filtered (% Identity > 10%, % query coverage > 10%, e-value < 0.05) %), and signal peptides for secretion via the Sec or Tat pathway were predicted via the SignalP5 (Almagro Armenteros *et al.*, 2019). The python script "BLAST_merops_SynCom_inhibitor/inhibitor_analysis.py" was used for this task. The DIAMOND BLASTp search (Buchfink *et al.*, 2015) was performed on all complete proteomes deposited in the Pseudomonas Genome Database (Winsor *et al.*, 2016) with PpCip1 as query (E-value cutoff: $1x10^{-4}$, query coverage: 40%, identity cutoff: 40%). Signal peptide predictions were performed via SignalP6 (Teufel *et al.*, 2022).

4.2.5.3. Multiple Sequence Alignment

Multiple sequence alignment (MSA) was performed using CLUSTAL Omega (Sievers *et al.*, 2011) via the EMBL-EBI Job Dispatcher (Madeira *et al.*, 2024) with the standard setting. MSAs were visualized with MView (Brown *et al.*, 1998) with modified standard setting (in the case of the large MSA *Pseudomonas* chagasins: -in clustal -html full -label0 -sort cov:pid -ruler on -reference "P._putida_AA7_[BUQ73_RS03925]" -
conservation on -bold -css on -width 71 -consensus on -con_coloring any -con_ignore class -con_threshold 90 -
find "[LVI][ASTVI][GAS][C]:[DN]P[AST][ST]G:G[SANG][SAG]G:[RQ]P[W]", in the case of the small MSA of Pseudomonas chagasins-like inhibitors, chagasin and CbMER0090314: "-in clustal -html full -label0 -sort cov:pid -ruler on -reference "PpCip1" -conservation on -bold -width 50 -consensus on -con_coloring any -con_ignore class -con_threshold 90"). The output HTML was later modified removing some labels.

4.2.5.4. Chagasin motif identification

MSA was performed with all chagasin-like proteins identified via DIAMOND BLASTp. The chagasin motifs were identified using regular expression searches. Presence and absence of chagasin motifs were displayed with ggVennDiagram (Gao *et al.*, 2021, 2024). Identified original and alternative chagasin motifs were used to create motifs logos via ggseqlogo

(Wagih, 2017). The data analysis was performed with "chagasin_motif_and_lipobox_identification/Cip1_ortholog_BLAST_analysis.R".

4.2.5.5. Candidate selection for AlphaFold Multimer predictions

To select candidates for AlphaFold Multimer predictions, SignalP6 (Teufel *et al.*, 2022) was used to predict which proteins have Sec or Tat signal peptides. These proteins were filtered selecting proteins with less than 50 kDa and prepared for the following analysis using AlphaFold_Multimer_modelling/prepare_alphafold_queue.R, annotate_secreted_proteins.R and annotate_secreted_proteins_second_round.R. These candidates were used for AlphaFold Multimer predictions in complex with RD19A-like. Results were analyzed with AlphaFold_Multimer_modelling/alphafold_multimer_result_analysis.R. Candidates with interface score (ipTM+pTM) larger than 0.75 were selected. These candidates were also modeled with papain and CP1A and models were analyzed (AlphaFold_Multimer_modelling/alphafold_multimer_result_analysis_2nd round.R). Models were manually evaluated via PyMOL to validate whether the protease active site is blocked. Candidates with interface scores above 0.7 for all candidates were selected for biochemical testing.

4.2.5.6. Protein structure predictions via AlphaFold

AlphaFold version 2.3.2 (Evans *et al.*, 2022; Jumper *et al.*, 2021) was run on the CHEOPS HPC cluster for multimer predictions of inhibitor candidates and PLCPs (papain, CP1A, RD19A-like) using the shell script AlphaFold_Multimer_modelling /alphafold_sequence.sh. Furthermore, ColabFold v1.5.5 (Mirdita *et al.*, 2022) was used for AlphaFold2 predictions of papain with PpCip1 using standard settings.

4.2.5.7. Protein Structure Analysis

Protein structures were analyzed using PyMOL. For AlphaFold structures of inhibitor candidates with PLCPs the script AlphaFold_Multimer_modelling/pymol_prepare_complex_alphafold_screen3.py was used to standardize the procedure. The AlphaFold multimer model of chagasin with PpCip1 was aligned to the structure of TcChagasin in complex with papain (PDB: 3E1Z) (Redzynia *et al.*, 2009).

4.3. Data availability

All data created during this thesis as well as used scripts are deposited under https://github.com/dmoser1/Pseudomonas_PLCP_inhibitors. (Note: Repository will be made public upon publication of this thesis or upon request).

5. Supplementary data

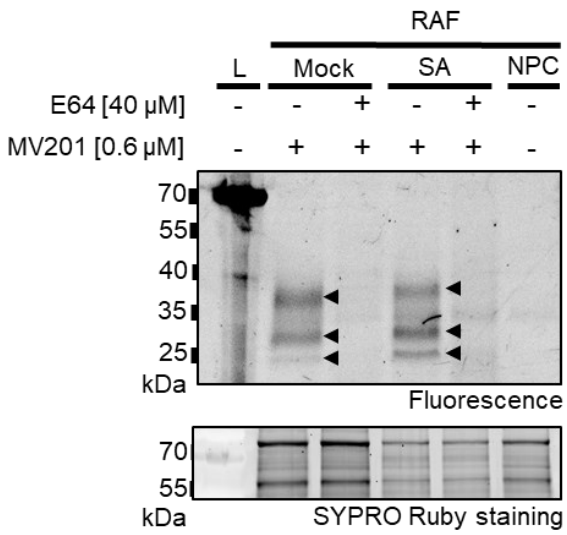

Suppl. Fig. 1: Activity-based protein profiling of PLCPs in maize root apoplastic fluid.

Root apoplastic fluids (RAF) was isolated from SA or mock-treated *Z. mays* seedlings. The RAF was pre-incubated with PLCP inhibitor E64 (Hanada *et al.*, 1978) or DMSO for 30 min. PLCPs were labeled with PLCP-specific fluorescent probe MV201 (Richau *et al.*, 2012). SA- and mock-treated RAFs were mixed 1:1, incubated without E64 nor the probe and served as a none-probe control (NPC). SYPRO Ruby staining was used as loading control as well as to estimate the bands of the ladder. This experiment was performed three times with similar results. These results were obtained and published during my Master thesis (Moser, 2021).

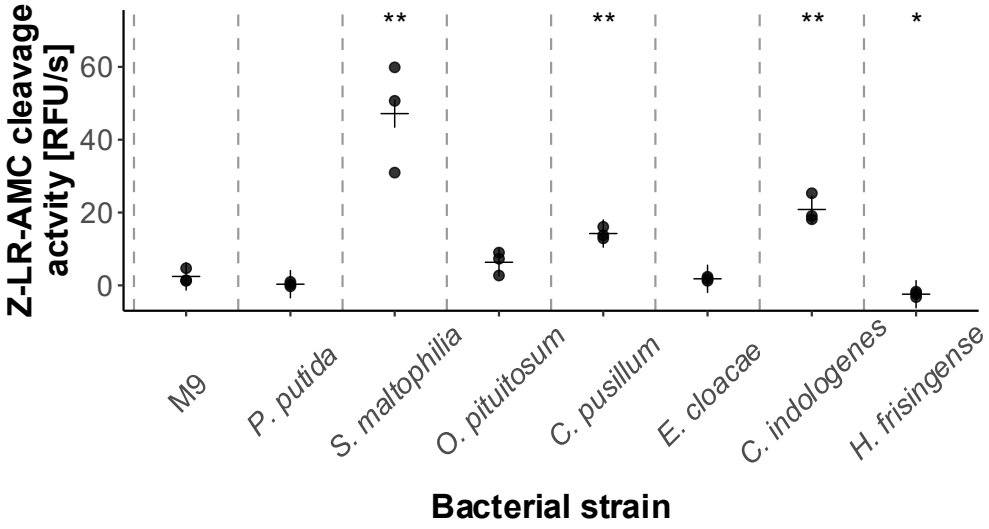

Suppl. Fig. 2: Bacterial proteases in supernatants of *S. maltophilia*, *C. pusillum* and *C. indologenes* show Z-LR-AMC cleavage.

Bacterial supernatants of SynCom bacteria (OD_{600} of 5) incubated in M9 minimal medium for four hours were tested for cleavage of the synthetic substrate Z-LR-AMC. Protease activity was measured by the release of fluorescent AMC. The experiment was performed with three independent biological replicates (dots), with each having three technical replicates. Means are represented as black crosses. A two-sided t-test was performed ($p<0.05$: *; $p<0.01$: **; $p<0.001$: ***). This data was obtained during my Master thesis (Moser, 2021).

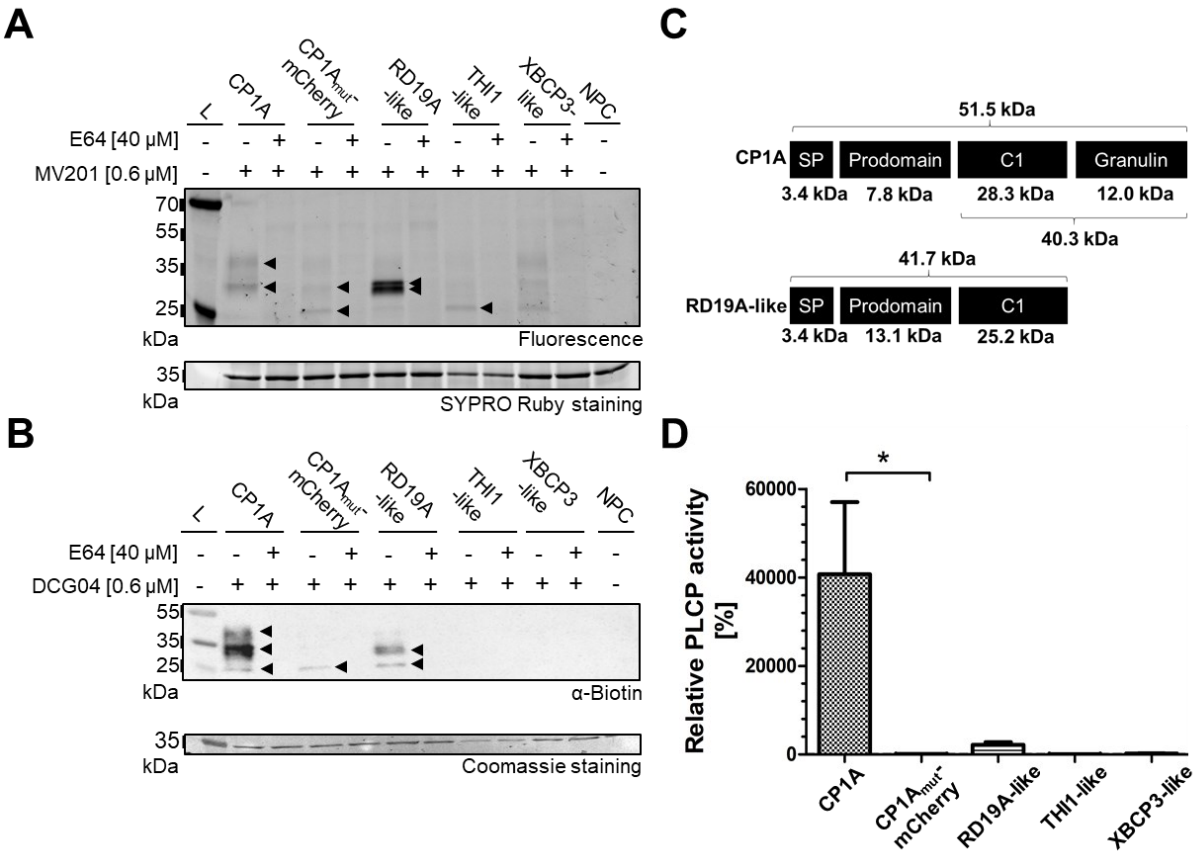

Suppl. Fig. 3: Heterologous expression of maize root PLCPs in apoplastic fluid of *Nicotiana benthamiana* via agrobacterium-mediated transformation.

(A) Maize SA-specific root PLCPs (RD19A-like, THI1-like, XBCP3-like) (Schulze Hüynck *et al.*, 2019) as well as immunity-related CP1A (Schulze Hüynck, 2019; van der Linde *et al.*, 2012a) and inactive CP1A$_{mut}$-mCherry (Schulze Hüynck, 2019) were heterologously expressed in *N. benthamiana* leaves via agrobacterium-mediated transformation and were secreted into the leaf apoplast due to an apoplast secretion signal. Leaf apoplastic fluid (LAF) was isolated and used for activity-based protein profiling using the PLCP-specific probe **MV201** (Richau *et al.*, 2012). PLCP inhibitor E64 (Hanada *et al.*, 1978) was used as a control for PLCP activity. LAFs were mixed and were incubated without E64 (-) nor MV201(-) and used as a none-probe control (NPC). The position of the bands of the ladder (L) in the MV201 fluorescence image was estimated based on the SYPRO Ruby staining. This experiment was performed once with all samples, however always for CP1A, CP1A$_{mut}$-mCherry and RD19A-like when new apoplastic fluid was isolated showing similar results. **(B)** Maize SA-specific root PLCPs (RD19A-like, THI1-like, XBCP3-like) (Schulze Hüynck *et al.*, 2019) as well as immunity-related CP1A (Schulze Hüynck, 2019; van der Linde *et al.*, 2012a) and inactive CP1A$_{mut}$-mCherry (Schulze Hüynck, 2019) were heterologously expressed in *N. benthamiana* leaves via agrobacterium-mediated transformation and were secreted into the leaf apoplast due to an apoplast secretion signal. Leaf apoplastic fluid (LAF) was isolated and used for activity-based protein profiling using the PLCP-specific probe **DCG-04-Biotin** (Greenbaum *et al.*, 2000). PLCP inhibitor E64 (Hanada *et al.*, 1978) was used as a control for PLCP activity. LAFs were mixed and were incubated without E64 (-) nor MV201(-) and used as a none-probe control (NPC). This experiment was performed once. **(C)** Domain structure of CP1A and RD19A-like protease. Both proteases contain a signal peptide, an inhibitory prodomain and the C1 domain with the active site. CP1A additionally has a granulin domain (van der Linde *et al.*, 2012a). **(D)** The activity of all LAFs containing the PLCPs was tested using the synthetic substrate Z-LR-AMC in a substrate cleavage assay. PLCP activity was measured by the increase of fluorescent 7-amino-4-methyl coumarin (AMC) release and was normalized to the background activity (E64 treated sample and LAF with CP1A$_{mut}$-mCherry). A two-sided t-test was performed ($p<0.05$: *; $p<0.01$: **; $p<0.001$: ***). These results (A-D) were obtained during my Master thesis (Moser, 2021).

Suppl. Table 1: Cysteine protease inhibitors deposited in the MEROPS database and used for BLASTp searches for putative inhibitors in *P. putida*.

These cysteine protease inhibitor of different inhibitor families were derived from the MEROPS database (Rawlings *et al.*, 2014) and were used as queries in BLASTp searches (status of 2021). This BLAST database was already created during my Master thesis (Moser, 2021).

Families	Type of inhibitor	Number of inhibitors
I04	alpha-1-peptidase inhibitor	795
I25	cystatin A	350
I31	equistatin inhibitor unit 1	480
I32	survivin	460
I39	alpha-2-macroglobulin	544
I42	chagasin	9
I48	clitocypin	1
I57	staphostatin B	1
I58	staphostatin A	1
I69	streptopain inhibitor	4
I79	AVR2 protein	2
I85	macrocypin 1	3

Suppl. Table 2: Known PLCP inhibitors involved in plant-microbe interactions.

These known PLCP inhibitors were identified using a literature search for inhibitors involved in plant-microbe interactions. Sequences of these inhibitors were used for BLASTp searches for PLCP inhibitors in *P. putida.* MEROPS classes (Rawlings *et al.*, 2014) were indicated, if the inhibitors were classified. This BLAST database (status of 2021) was already created during my Master thesis (Moser, 2021).

Name	UniProt ID	MEROPS class	Organism	References
AVR2	Q8NID8	I79	*Cladosporium fulvum*	(Shabab *et al.*, 2008; Van Esse *et al.*, 2008)
CC9	Q4FZ48	I25	*Zea mays*	(van der Linde *et al.*, 2012a)
PsCip1	Q87XG7	I42	*Pseudomonas syringae* pv. *tomato*	(Shindo *et al.*, 2016)
EPIC1	A1L015	I25	*Phytophthora infestans*	(Kaschani *et al.*, 2010; Song *et al.*, 2009; Tian *et al.*, 2007)
EPIC2B	A1L017	I25	*Phytophthora infestans*	(Kaschani *et al.*, 2010; Song *et al.*, 2009; Tian *et al.*, 2007)
Pit2	A0A0D1EAR7	Not classified	*Ustilago maydis*	(Misas Villamil *et al.*, 2019; Mueller *et al.*, 2013)
SDE1	C6XGX6	Not classified	*Candidatus Liberibacter asiaticus*	(Clark *et al.*, 2018, 2020)
VAP1	G1JUH0	Not classified	*Globodera rostochiensis*	(Lozano-Torres *et al.*, 2012)

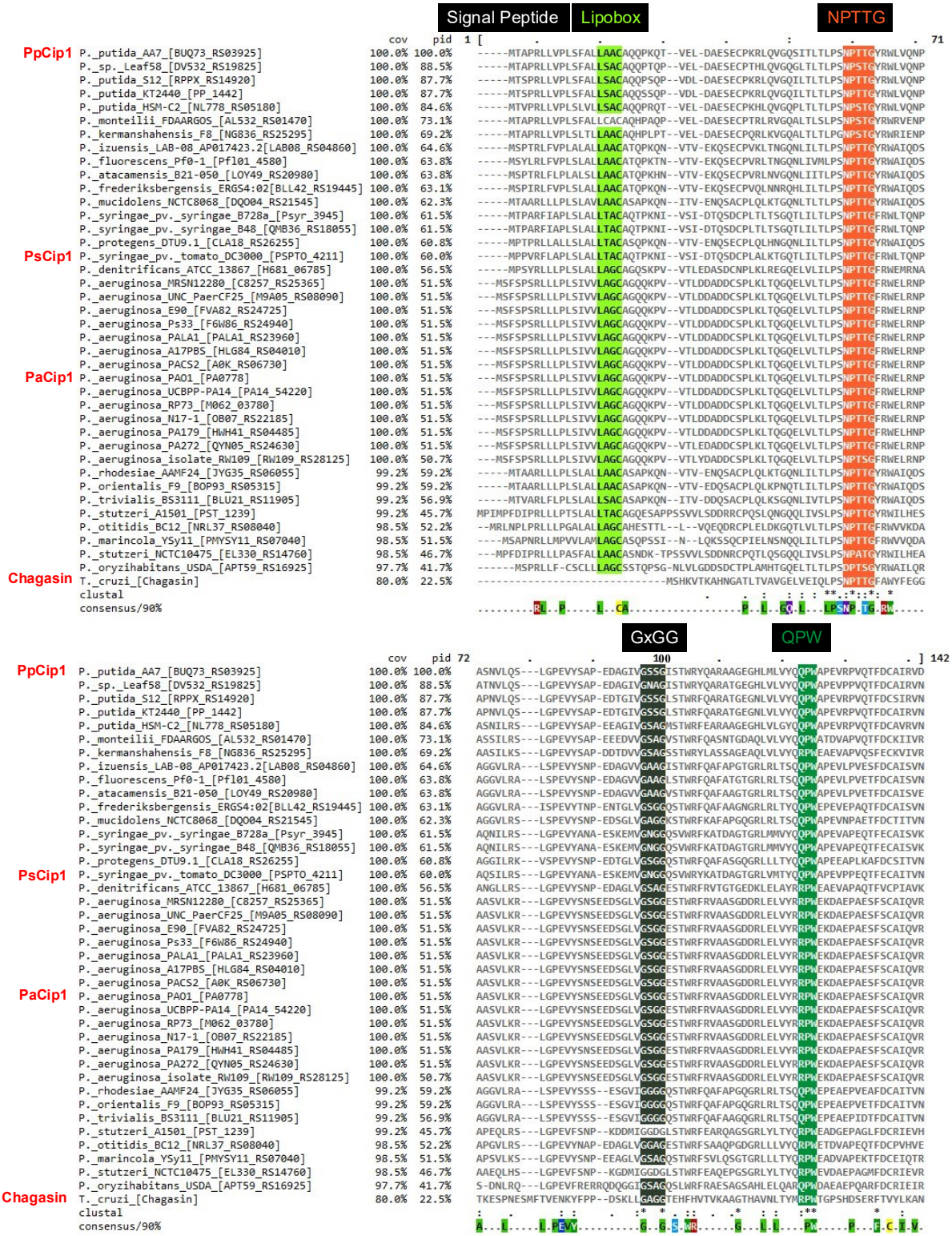

Suppl. Fig. 4: *Pseudomonas* chagasin-like inhibitors are predicted to be a membrane-anchored PLCP inhibitors.

CLUSTAL alignment (Sievers *et al.*, 2011) of chagasin-like proteins from *P. putida*, *P. syringae*, *P. aeruginosa, Trypanosoma cruzi* and a selection of other Pseudomonads showing conserved chagasin motifs NPTTG (red), GxGG (darkgrey) and (Q/R)PW (darkgreen) (dos Reis *et al.*, 2008; Shindo *et al.*, 2016), signal peptide for Sec/SPII pathway with a lipobox ([LVI][ASTVI][AGS]) followed by a cysteine residue which is predicted to be lipidated (light green) (LoVullo *et al.*, 2015). Stars indicate identical amino acids in all sequences. Double points indicate conserved substitutions. Points indicate semi conserved amino acids, i.e. amino acids having similar shape.

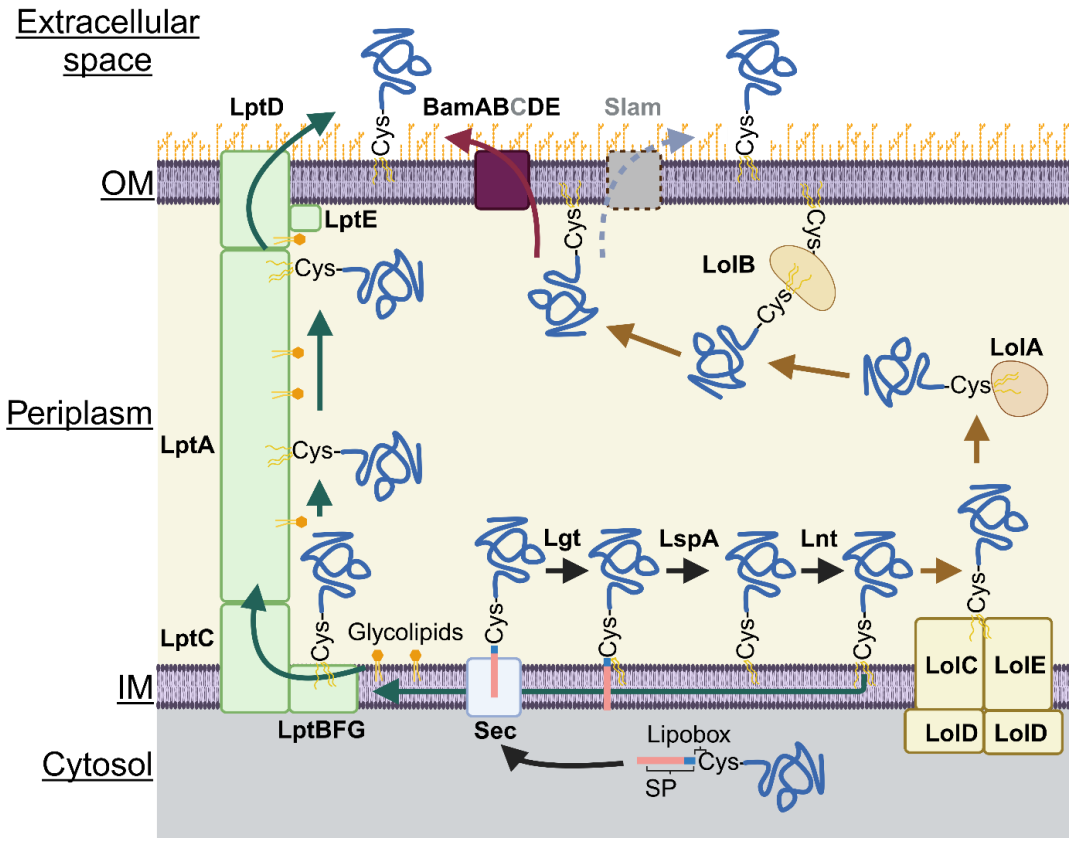

Suppl. Fig. 5: Schematic representation of the Sec-dependent transport of lipoproteins to the cell surface.

Proteins with a signal peptide for the Sec translocon pathway and a lipobox ([LVI][ASTVI][AGS]) are prolipoproteins, which will be secreted by the Sec translocon into the periplasm (LoVullo *et al.*, 2015; Natale *et al.*, 2008). The prolipoprotein will be lipidated on the cysteine sulfhydryl group following the lipobox via the preprolipoprotein diacyglyceryl transferase (Lgt) anchoring the protein to the membrane (Sankaran & Wu, 1994; Tokunaga *et al.*, 1982). Afterward, the signal peptide including the lipobox will be cleaved off from the diacylglyceryl-prolipoprotein by the Signal Peptidase II (LspA) (Tokunaga *et al.*, 1984). After the removal of the signal peptide and the lipobox, the N-terminal cysteine of the apolipoprotein will be N-terminal lipidated via the apolipoprotein N-acyltransferase (Lnt) (Gupta *et al.*, 1993). Finally, the mature lipoprotein can either stay in the inner membrane, if it contains a retention signal, or can be relocalized to the outer membrane via the localization of lipoproteins (Lol) system (LolA-E, brown) (LoVullo *et al.*, 2015; Narita & Tokuda, 2007; Remans *et al.*, 2010) or an unknown LolAB-independent system (Grabowicz & Silhavy, 2017). Lipoproteins can either stay on the periplasmic side of the outer membrane or can be translocated across the outer membrane. Several translocator complexes have been shown to be involved in this process in different organisms, as for example the β-barrel assembly machinery (Bam, in purple) complex exporting mainly β-barrel proteins (Leyton *et al.*, 2012), the surface lipoprotein assembly modulator (SLAM, in grey) (Hooda *et al.*, 2016, 2017; Huynh *et al.*, 2022) or the outer membrane LPS translocase LptDE (lipopolysaccharide transport D and E, in green), which also transports glycolipids (He *et al.*, 2023; Luo *et al.*, 2022). There are several examples of surface-exposed lipoproteins, however, the required signals and mechanisms are not well understood yet (Cole *et al.*, 2021; Huynh *et al.*, 2022; Konovalova & Silhavy, 2015). Proteins not identified in *P. putida* via BLASTp search have been marked in grey and with dotted lines.

Suppl. Table 3: Lipoproteins with retention signals remain at the inner membrane.

This table lists all known retention signals, which were reported to lead to the retention of lipoproteins at the inner membrane.

Retention signal	Organism	References
Asp at the +2 position after the $^{+1}$Cys	*E. coli*	(Gennity & Inouye, 1991; Lewenza *et al.*, 2006; Yamaguchi *et al.*, 1988)
Glu, Asp, Gln, or Asn at the +3 position after the $^{+1}$Cys	*E. coli*	(Terada *et al.*, 2001)
Trp, Phe, Pro, Gly, and Tyr at the +2 position after the $^{+1}$Cys (possibly due to nonfunctional interactions with the LolCDE complex, but these signals were not found in lipoproteins)	*E. coli*	(Grabowicz, 2019; Lewenza *et al.*, 2006; Seydel *et al.*, 1999)
Asp at the +2 position, a Lys at the +3 position and Ser at the +4 position after the $^{+1}$Cys	*Pseudomonas aeruginosa*	(Lewenza *et al.*, 2008; Lorenz *et al.*, 2019; Narita & Tokuda, 2007; Tanaka *et al.*, 2007)

Suppl. Table 4: Main components for modification and transport of lipoproteins are present in *P. putida*.

BLASTp search (Altschul *et al.*, 1990) for orthologs of proteins involved in the modification and transport of lipoproteins was performed in the *P. putida* genome.

Uniprot ID	Description	Subject ID	E-value	Cover-age	Ident-ity
C3SWJ2	Phosphatidylglycerol-prolipoprotein diacylglyceryl transferase (Lgt) [*E. coli*]	Ppu_4930	8.32×10^{-93}	98%	50%
P00804	Lipoprotein signal peptidase (LspA) [*E. coli*]	Ppu_4560	2.56×10^{-23}	75%	46%
J7R1Z2	Apolipoprotein N-acyltransferase (Lnt) [*E. coli*]	Ppu_0313	4.64×10^{-98}	94%	40%
P61316	Outer-membrane lipoprotein carrier protein (LolA) [*E. coli*]	Ppu_1507	2.43×10^{-26}	96%	33%
P61320	Outer-membrane lipoprotein (LolB) [*E. coli*]	Ppu_4470	9.41×10^{-16}	92%	29%
C3TDL7	Transporter (LolC) [*E. coli*]	Ppu_1327	1.21×10^{-82}	100%	39%

P75957	Lipoprotein-releasing system ATP-binding protein (LolD) [*E. coli*]	Ppu_1328	$5.53x10^{-87}$	96%	59%
P75958	Lipoprotein-releasing system transmembrane protein (LolE) [*E. coli*]	Ppu_1329	$2.11x10^{-90}$	99%	37%
P0A940	Outer membrane protein assembly factor (BamA) [*E. coli*]	Ppu_4075	0	99%	40%
P77774	Outer membrane protein assembly factor (BamB) [*E. coli*]	Ppu_4327	$2.61x10^{-54}$	96%	30%
P0A903	Outer membrane protein assembly factor (BamC) [*E. coli*]	/	/	/	/
P0AC02	Outer membrane protein assembly factor (BamD) [*E. coli*]	Ppu_4550	$2.94x10^{-57}$	98%	39%
P0A937	Outer membrane protein assembly factor (BamE) [*E. coli*]	Ppu_0386	$4.89x10^{-5}$	41%	36%
Q9K165	Surface lipoprotein assembly modifier 1 (Slam1) [*Neisseria meningitidis*]	/	/	/	/
Q9HVV7	Lipopolysaccharide transport periplasmic protein (LptA) [*P. aeruginosa]*	Ppu_4266	$6.89x10^{-61}$	100%	61%
Q9HVV6	LPS export ABC transporter ATP-binding protein (LptB) [*P. aeruginosa]*	Ppu_4267	$5.9x10^{-164}$	100%	92%
Q9HVV8	LPS export ABC transporter periplasmic protein (LptC) [*P. aeruginosa]*	Ppu_4265	$9.38x10^{-66}$	88%	60%
Q9I5U2	LPS-assembly protein (LptD) [*P. aeruginosa*]	Ppu_0141	0	98%	65%
Q9HX32	LPS assembly lipoprotein (LptE) [*P. aeruginosa*]	Ppu_0309	$2.36x10^{-76}$	95%	56%
Q9HXH4	LPS export ABC transporter permease (LptF) [*P. aeruginosa*]	Ppu_4240	0	100%	76%
Q9HXH5	LPS export ABC transporter permease (LptG) [*P. aeruginosa*]	Ppu_4239	0	100	74%

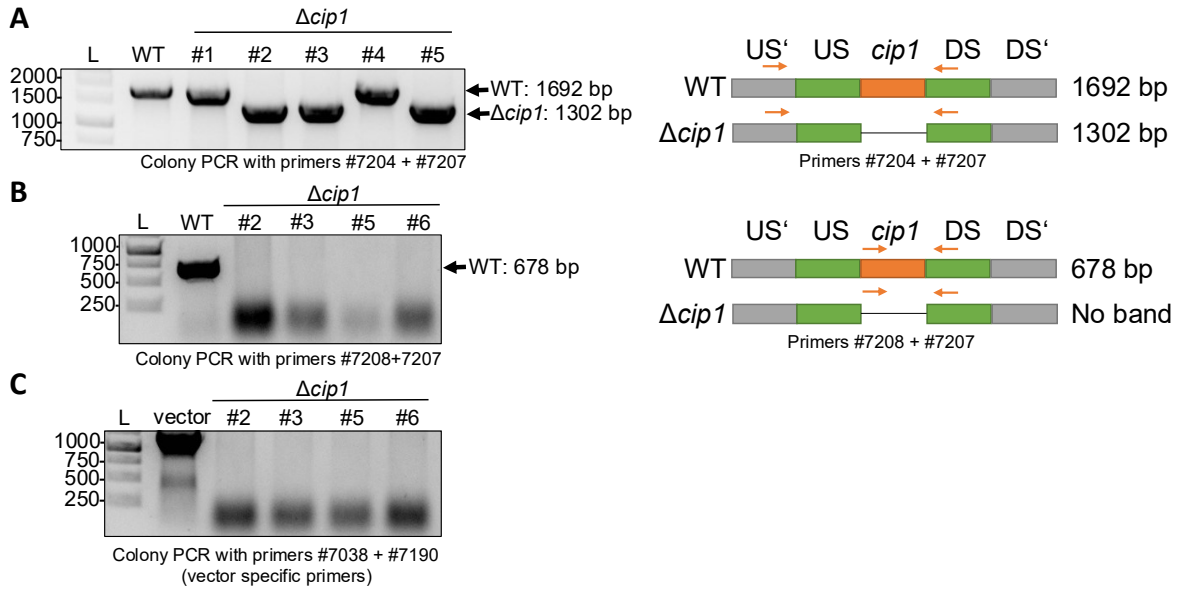

Suppl. Fig. 6: Confirmation of genomic knockout of PpCip1 in *P. putida*.

The genomic knockout of PpCip1 was tested using multiple rounds of colony PCR and finally confirmed *P. putida* Δ*cip1* clones #2 and #3 via sequencing of the US' to DS region (primers #7204 or #7207). **(A)** The removal of *cip1* between upstream sequence (US) and downstream (DS) sequence was tested via PCR with primers #7204 and #7207 binding in the US' and DS region. A 1302 bp band indicated absence of the *cip1* sequence. **(B)** The removal of *cip1* was furthermore tested via PCR with primers #7208 and #7207 binding in the *cip1* and DS sequence. The presence of a 678 bp indicates presence of PpCip1. **(C)** The absence of the vector was tested with vector specific primers #7038 and #7190.

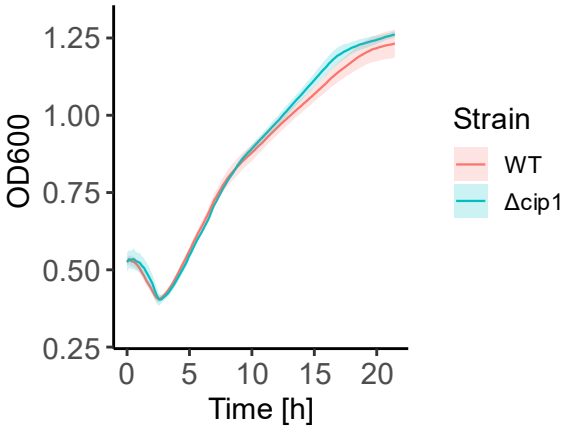

Suppl. Fig. 7: Growth curve of *P. putida* WT and *P. putida* Δ*cip1* #2 grown in dYT full medium.

Tecan plate reader was used to measure the optical density (OD_{600}) of strains grown in dYT medium at 28°C with constant shaking for 24 hours. Dark line represents the mean of three (Δ*cip1*) / five (WT) replicates. Light area displays standard deviation of the measurement.

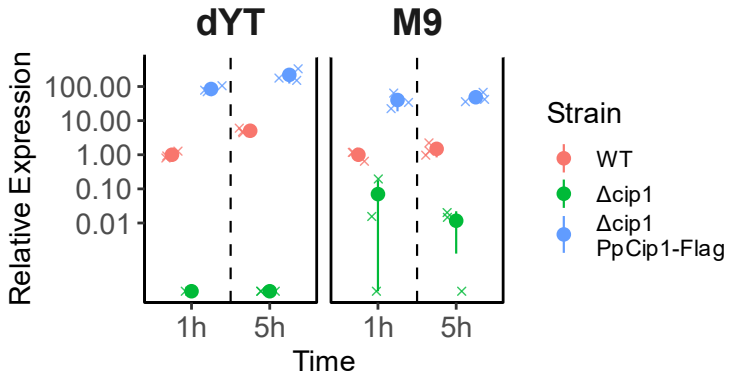

Suppl. Fig. 8: Expression of *cip1* in *P. putida*.

RNA was isolated from *P. putida* WT_EVC, *P. putida* Δ*cip1*_EVC and *P. putida* Δ*cip1*_PpCip1-Flag grown/incubated for one or five hours in dYT or M9 medium. Gene expression was determined by qPCR on cDNA using *cip1*- as well as reference gene *ropD*-specific primers (Ct > 35 were removed). Relative expression was calculated using $2^{-\Delta\Delta CT}$ method (Livak & Schmittgen, 2001) and finally normalized to the value of *P. putida* EVC set to 1. Amplicons of *cip1* in *P. putida* Δ*cip1*_EVC could be observed however with Ct values above 35, indicating either unspecific binding or contamination. Point range displays the average of three replicates (point) with the standard error (line). Crosses represent individual replicates. Not detected or values derived from Ct>35 values were set to 0.0001 for plotting with log-scale. This experiment was performed with three independent replicates.

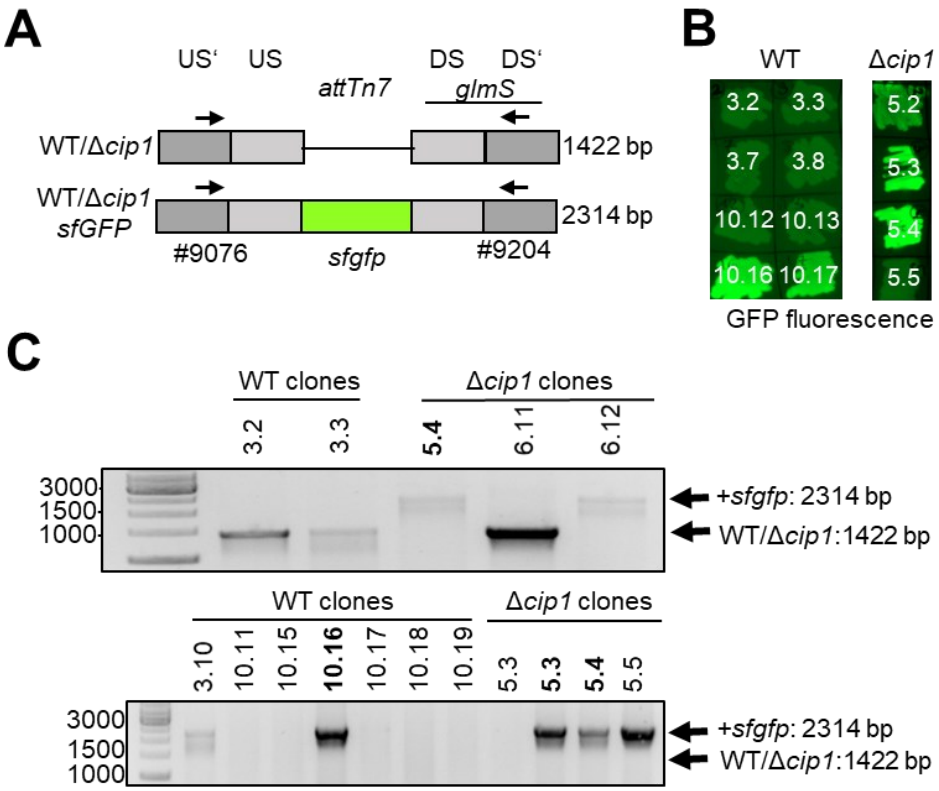

Suppl. Fig. 9: Confirmation of genomic integration of *sfgfp* the attTn7 locus in *P. putida*.

(A, C) The genomic integration of *sfgfp* was tested using colony PCR and finally confirmed *P. putida* WT_sfGFP clone #10.16. *P. putida* Δ*cip1*_sfGFP clones #5.3 and #5.4 via sequencing of the upstream (US') to downstream (DS') region (primers #9076 or #9204). A 2314 bp band indicated the presence of the *sfgfp* sequence in the attTn7 locus upstream of the *glmS* gene. **(B)** GFP fluorescence of clones was evaluated using ChemiDoc Imager. This experiment was performed by Nina Solia during her Master thesis project (Solia, 2023) under my supervision

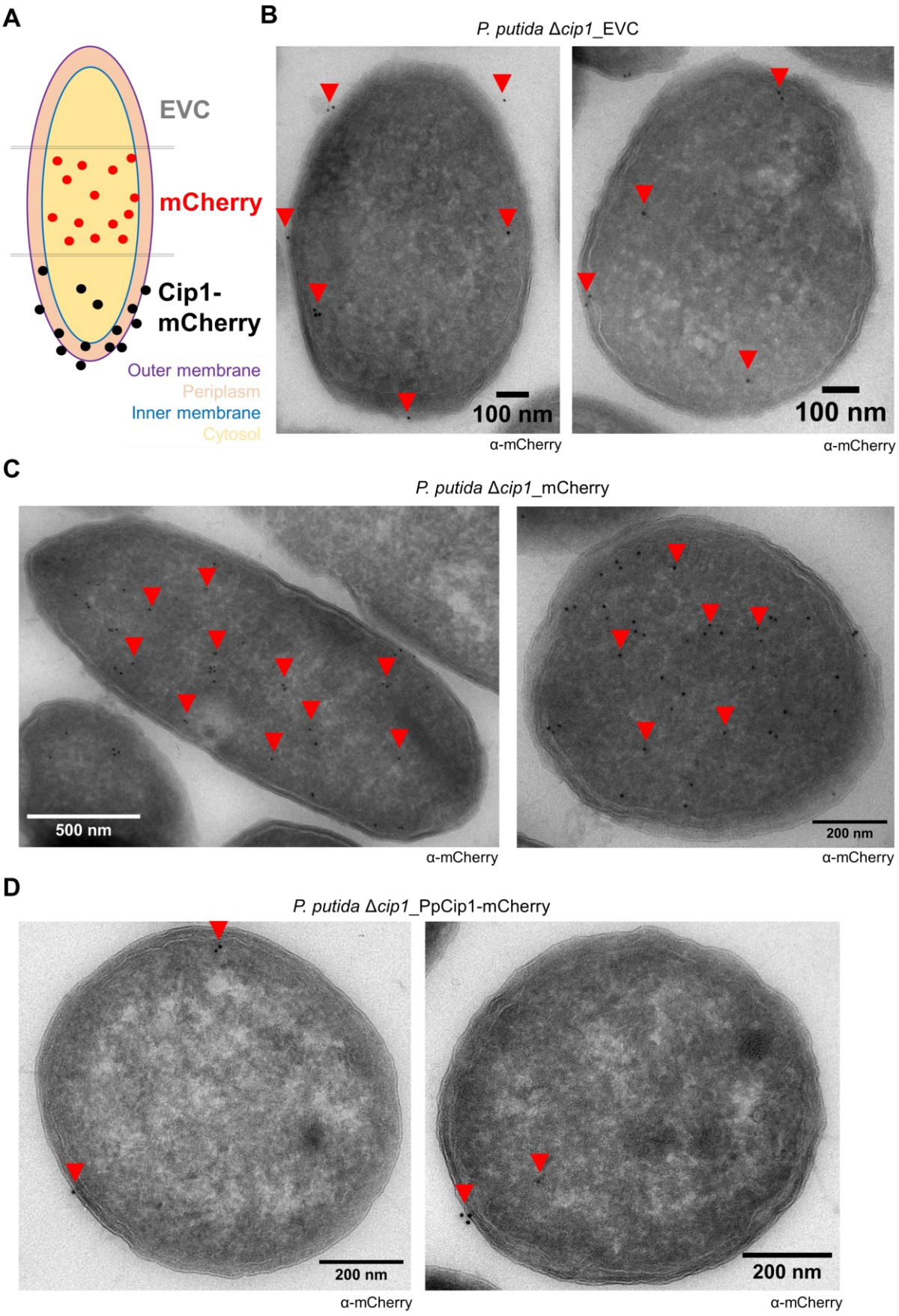

Suppl. Fig. 10: Immunogold-labeling of PpCip1-mCherry.

(A) Predicted localization of gold-particles labeling mCherry (red dots) or PpCip1-mCherry (black dots) in *P. putida* Δ*cip1*_EVC (grey), *P. putida* Δ*cip1*_mCherry (red) and *P. putida* Δ*cip1*_PpCip1-mCherry (black) in their cytosol (light orange), at the inner membrane (blue), periplasm (dark orange), outer membrane (violet), or cell surface. **(B)** *P. putida* Δ*cip1*_EVC, **(C)** *P. putida* Δ*cip1*_mCherry, and **(D)** *P. putida* Δ*cip1*_PpCip1-mCherry samples were fixed using the Tokuyasu technique (Tokuyasu, 1973), embedded, cryo sectioned, immunogold labeled with a polyclonal mCherry antibody and imaged with transmission electron microscopy. Some gold-particles are highlighted with red arrowheads. These experiments were performed by Dr. Ulla Neumann at the Max Planck Institute for Plant Breeding in Cologne. The experiment was performed once.

Suppl. Table 5: Immunogold-labeling of PpCip1-mCherry.

P. putida Δ*cip1*_EVC, *P. putida* Δ*cip1*_mCherry and *P. putida* Δ*cip1*_PpCip1-mCherry were fixed using the Tokuyasu technique (Tokuyasu, 1973), embedded, cryo sectioned, immunogold labeled with a polyclonal mCherry antibody and imaged with transmission electron microscopy. Gold particles in the cytosol, periplasm and on the surface of the cells were counted. These experiments were performed by Dr. Ulla Neumann at the Max Planck Institute for Plant Breeding in Cologne.

Sample	Cytosol	Periplasm	Surface	n (Cells)	Gold particles / cell
EVC	59%	36%	5%	36	5.9
mCherry	92%	6%	2%	19	29.2
PpCip1-mCherry	47%	42%	11%	97	4.9

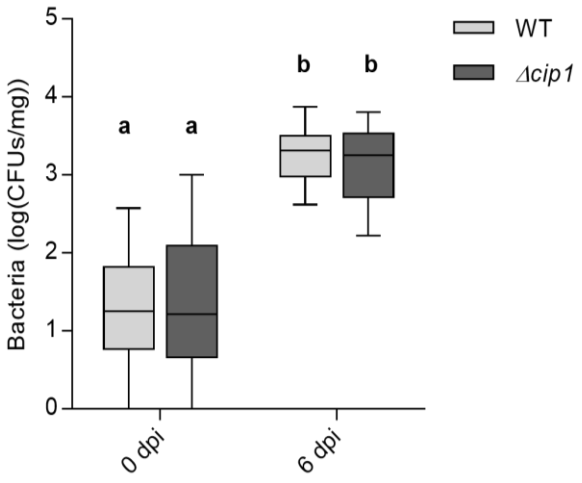

Suppl. Fig. 11: No difference in colonization of the whole maize root by *P. putida* WT and Δ*cip1* at 6 dpi.

Maize were grown for 3 hours (0 dpi) or 6 days in soil inoculated with *P. putida* WT or Δ*cip1* at OD_{600} of 0.001. Roots were removed from soil and washed in sterile water. Next, the whole root was grinded in sterile water and colony forming units were determined. This experiment and analysis was performed by Nina Solia with three independent experiments each having six tested plants during her Master thesis project (Solia, 2023) under my supervision. Error bars represented the standard error of the mean. Statistical testing was performed by two-way ANOVA followed by post-hoc Tukey test.

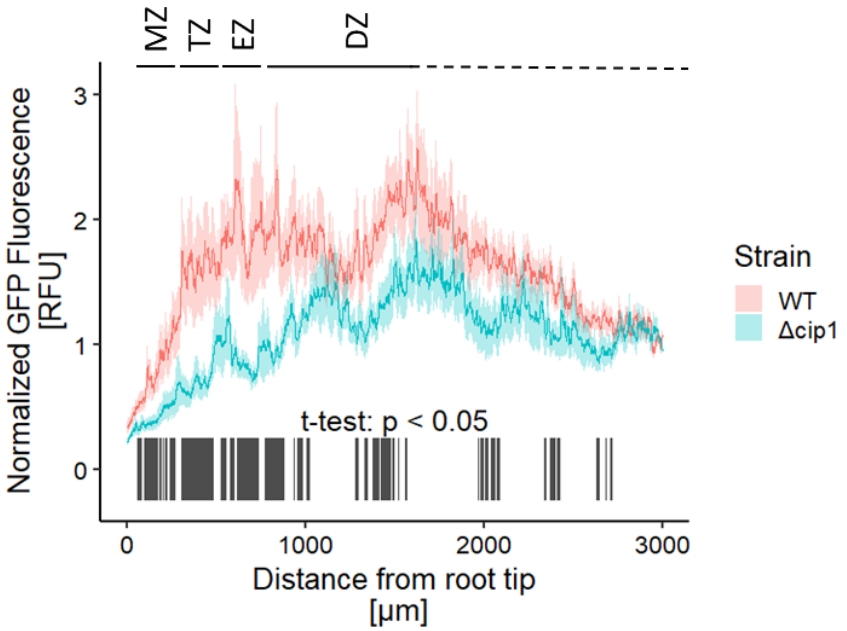

Suppl. Fig. 12: Zones of *P. puti*da WT sfGFP or *P. putida* Δ*cip* sfGFP root colonization on *A. thaliana* Col-0.

P. putida WT_sfGFP or *P. putida* Δ*cip1*_sfGFP were inoculated onto 10 days old *A. thaliana* Col-0 roots growing in a root-on-a-chip (modified version of chip reported by (Guichard *et al.*, 2020)). 1 dpi GFP fluorescence on the root was imaged. The Average normalized GFP fluorescence of *P. putida* WT_sfGFP (red) or *P. putida* Δ*cip1*_sfGFP (blue) is visualized with standard error of the mean (SEM). Meristematic zone (MZ): 0-200 µm from root tip, transition zone (TZ): 200-520 µm from root tip, elongation zone (EZ): 520-850 µm from root tip, and differentiation zone (DZ): 850-1500 µm from root tip, estimated according to Verbelen *et al.* (2006). A two-sided t-test was performed per measured position ($p<0.05$: grey bar).

Suppl. Table 6: C1A proteases in SynCom.

BLASTp search (Altschul *et al.*, 1990; Camacho *et al.*, 2009) was performed for C1A proteases in the SynCom using C1A proteases deposited in the MEROPS database (Rawlings *et al.*, 2014) as queries. The presence or absence of a signal peptide for secretion was predicted using SignalP6 (Teufel *et al.*, 2022).

Query	Subject	E-value	Query Coverage [%]	Identity [%]	Description	Probability for Signal Peptide (Sec/SPI)
C1A unassigned peptidase (*Bacteroides thetaiotaomicron*) MER0066230	Cin_2970	$1.09x10^{-96}$	97.0	43.1	C1 family peptidase	99.9 %

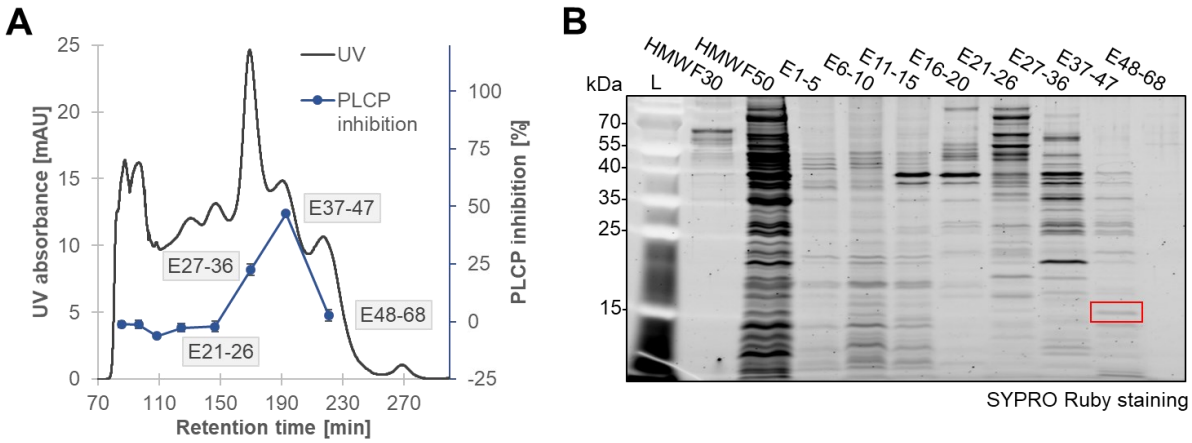

Suppl. Fig. 13: Identification of PLCP inhibitors via size-exclusion chromatography (SEC) of *P. putida* culture supernatant.

(A) SEC of 10X concentrated HMWF of *P. putida* Δ*cip1* culture supernatant was performed with Tris-HCl buffer pH7, 150 mM NaCl. Fractions of UV absorbance peaks (black) were pooled and tested for CP1A inhibition (blue) via the substrate cleavage assay with Z-LR-AMC. The peak of interest is marked with a red arrow. This experiment was only performed once. **(B)** Pooled fractions were loaded onto PAA gels and SDS-PAGE was performed to separate proteins in the samples by size. SYPRO Ruby staining of the proteins was performed. Red box indicates band of interest found also in the other SEC.

Suppl. Table 7: Secreted proteins identified in band of fraction E44-55 from size-exclusion chromatography.

Band of fraction E44-55 was excised from PAA-gel after size exclusion chromatography. Proteins in this band were identified via mass spectrometry and were filtered for secreted proteins (Sec or Tat signal peptide) via SignalP6 (Teufel *et al.*, 2022).

Accession	Description
Ppu_0686	DNA binding protein
Ppu_0843	glycine zipper 2TM domain-containing protein
Ppu_0898	outer membrane beta-barrel protein
Ppu_1728	copper chaperone PCu(A)C
Ppu_2532	serine protease inhibitor ecotin
Ppu_2677	hypothetical protein
Ppu_3965	quorum-sensing-regulated virulence factor family protein
Ppu_4121	hypothetical protein
Ppu_4230	DUF5064 domain-containing protein
Ppu_4445	YajG family lipoprotein
Ppu_4449	hypothetical protein
Ppu_4631	copper chaperone PCu(A)C
Ppu_4944	DUF4399 domain-containing protein

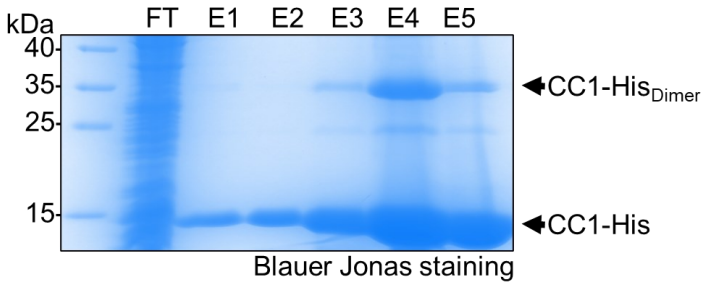

Suppl. Fig. 14: Purification of heterologously expressed CC1-His via affinity chromatography using Ni-NTA column.

CC1-His was heterologously expressed as described in (Schulze Hüynck, 2019) and purified using affinity chromatography on a Ni-NTA column. Flow-through (FT) and elution (E) fractions were collected, used for SDS-PAGE and successful purification was confirmed via Blauer Jonas staining.

Suppl. Table 8: Secreted proteins found eluted from papain beads during affinity chromatography.

Proteins marked in bold were selected as candidates as they had no (clear) functional annotation or were a protease inhibitor.

ID	Description
Ppu_0072	ATP-dependent zinc protease
Ppu_0466	gamma-glutamyltransferase
Ppu_0578	amino acid ABC transporter substrate-binding protein
Ppu_0754	DegQ family serine endoprotease
Ppu_0789	glutamate/aspartate ABC transporter substrate-binding protein
Ppu_0898	outer membrane beta-barrel protein
Ppu_0949	outer membrane protein transport protein
Ppu_0979	carboxy terminal-processing peptidase
Ppu_1257	OmpA family protein
Ppu_1411	ATP-dependent zinc protease
Ppu_2420	arylsulfatase
Ppu_2532	**serine protease inhibitor ecotin**
Ppu_2677	**hypothetical protein**
Ppu_2699	**YMGG-like glycine zipper-containing protein**
Ppu_3857	**hypothetical protein**
Ppu_3890	malate dehydrogenase (quinone)

Ppu_3927	Tol-Pal system beta propeller repeat protein TolB
Ppu_3965	quorum-sensing-regulated virulence factor family protein
Ppu_4266	lipopolysaccharide transport periplasmic protein LptA
Ppu_4298	**SIMPL domain-containing protein**
Ppu_4675	iron ABC transporter substrate-binding protein
Ppu_4757	**DUF1090 domain-containing protein**
Ppu_4848	S41 family peptidase
Ppu_4873	thermonuclease family protein
Ppu_5397	OprD family outer membrane porin
Ppu_5434	OprD family porin

>Ppu_1665 hypothetical protein

MNTAFRKVILSSAIGACALLSFNTYAAVSAEEAAKLKTELTPFGAERKGNADGSIPAWDGGLKDASSVTSAGKRGDPFS
SEKPLFTITSANMEQYKDKLSIGTQAMLKKYPDSYKLEVYKTHRTAAAPDSVYAASLANATSVSLVQGAAGPMPSGGAG
GIPFPVAKTGEEAIWNHLLRWRGSAWQSNITQYLTTADGKHVLTNNSRVLSQMPWFQQGNGADKGVYWELRILNDGP
PLRAGEAILGVQNIDAEKTSSWTYLPGQRRVRRLPNACCDTPTPATAGVMSFDEVTVFQGRIDRFDWKLVGKREMYIP
YNANGVFVADKPEDIMLPRHLNPGVVRWELHRVWVVEATLKSGARHVMPKSTYYLDEDTWSAVLGERYDGKGQLSKT
LFGLPTVMPDIPAVATTTTGFYDLVSGTWFVGDVFAGSRDQYKIVEPFNSSVFTADSLAGDGIR

>Ppu_4449 hypothetical protein

MRAILPLLLAVSLPLAAAPLHSQFLPPDDQSLRQEAPTGQQLLQVTDYSVVVGAQRQSDQQPIPITASLQMRLKGKPLS
KGATIGQVLLNFDGEAGKSLKKPVYDDKTRTLNLNYPVSDYRVIMDLLRNETVYVQFLTYANGHIWADLHTGTVRSR

>Ppu_4757 hypothetical protein

MKLISTLALLTTLGLAAGVAQAAQPDAGLTGCAAKRSAIENQLKIARDHGNSDQVAGLEEALRGVDNCTDASLRKEREQ
KVLDARHEVAQREKDLKKAEKKGDAEKINKRKDKLAESRKELQEAVDDLDR

Suppl. Fig. 15: Sequences of PLCP inhibitor candidates Ppu_1665, Ppu_4449 and Ppu_4757.

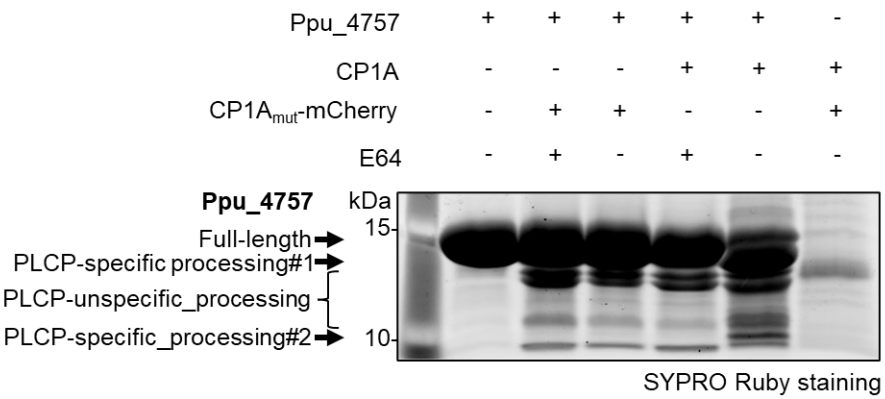

Suppl. Fig. 16: Ppu_4757 contains at least two cleavage sites for CP1A.

His-Ppu_4757 was heterologous expressed and purified. The stability of 5 µg His-Ppu_4757 in presence of CP1A was tested by incubating CP1A or inactive CP1A$_{mut}$-mCherry with His-Ppu_4757, and with or without the PLCP inhibitor E64 (Hanada *et al.*, 1978) for 30 min at room temperature. Afterwards the samples were visualized by SDS-PAGE followed by SYPRO Ruby staining. Arrows/brackets indicate His-Ppu_4757 and its PLCP-specific or PLCP-unspecific degradation products. The experiment was performed twice. This experiment was performed under my supervision by Eva Slavic during her Master thesis.

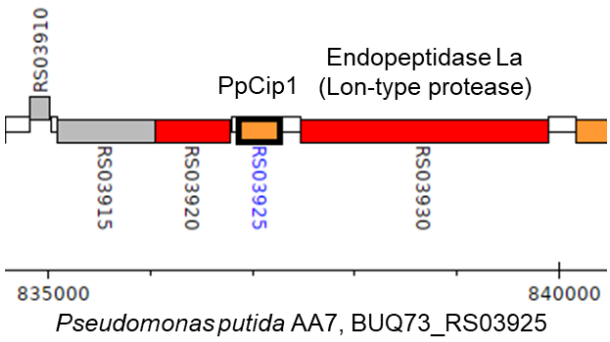

Suppl. Fig. 17: Lon-type protease encoded next to the *cip1* gene in the genome of *P. putida*.

Genome information and graphical display was obtained from pseudomonas.com (Winsor *et al.*, 2016) and modified. Colors indicated localization predicted by the database via PSORTb v3.0 (red: cytoplasmic, orange: **c**ytoplasmic membrane, grey, white: intergenic regions, notably PSORTb is not able to detect lipoproteins) (Yu *et al.*, 2010).

PubMed database search:
(„protease inhibitor"[Title/Abstract]) AND („lipoprotein"[Title/Abstract]) NOT ("low-density lipoprotein"[Title/Abstract]) NOT ("high-density lipoprotein"[Title/Abstract])

21.10.2024 – 7:00 pm (UTC+1)

Results:
70 article titles/abstracts matching the search query
From this **two articles mention a protease inhibitor predicted to be a lipoprotein**:

- Pasquevich KA, Carabajal MV, Guaimas FF, Bruno L, Roset MS, Coria LM, Rey Serrantes DA, Comerci DJ, Cassataro J. Omp19 Enables *Brucella abortus* to Evade the Antimicrobial Activity From Host's Proteolytic Defense System. Front Immunol. 2019 Jun 26;10:1436. doi: 10.3389/fimmu.2019.01436. PMID: 31297115; PMCID: PMC6607954.
  The bacterium ***Brucella* Omp19 lipoprotein** functions as a protease inhibitor, protecting the bacterium from gastrointestinal and lysosomal proteases. The loss of Omp19 results in **heightened susceptibility to host proteases**, cell division defects, and increased macrophage killing, which compromises infection establishment and persistence.
- Charova SN, Dölfors F, Holmquist L, Moschou PN, Dixelius C, Tzelepis G. The RsRlpA Effector Is a Protease Inhibitor Promoting *Rhizoctonia solani* Virulence through Suppression of the Hypersensitive Response. Int J Mol Sci. 2020 Oct 29;21(21):8070. doi: 10.3390/ijms21218070. PMID: 33138028; PMCID: PMC7662947.
  The fungus ***Rhizoctonia solani*** employs the **effector protein RsRlpA**, a **rare lipoprotein with protease inhibitor activity**, to **suppress host immune responses**, including the hypersensitive response and ROS burst. RsRlpA is induced during early infection and is essential for virulence, facilitating the pathogen's transition from a biotrophic to a necrotrophic lifestyle.

Suppl. Fig. 18: Literature search for other reports about protease inhibitors which are (predicted) lipoproteins.

The literature search identified 70 articles matching the used search criterium. Of these articles only two articles mention protease inhibitors, which are (predicted) lipoproteins: *Brucella abortus* Omp19 (Pasquevich *et al.*, 2019; Tibor *et al.*, 1999) and *Rhizoctonia solani* RsRlpA (Charova *et al.*, 2020). A short summary of these abstracts was added.

1862 sequences selected

Taxonomy	Number of hits	Number of Organisms	Description
⊟Bacteria	4847	1575	
. ⊟Pseudomonadota	4846	1574	
. . ⊟Gammaproteobacteria	1	1565	Gammaproteobacteria hits
. . . ⊞Pseudomonadales	4804	1551	
. . . ⊞Enterobacterales	11	8	
. . . Aeromonas caviae	1	1	Aeromonas caviae hits
. . . Gammaproteobacteria bacterium	6	1	Gammaproteobacteria bacterium hits
. . . Acinetobacter baumannii	1	1	Acinetobacter baumannii hits
. . . Xanthomonas sp. WHRI 1810A	2	1	Xanthomonas sp. WHRI 1810A hits
. . . Halomonas sp.	1	1	Halomonas sp. hits
. . ⊞Burkholderiales	5	4	
. . Pseudomonadota bacterium	7	1	Pseudomonadota bacterium hits
. . ⊟Alphaproteobacteria	7	4	
. . . ⊞Phyllobacteriaceae	5	2	
. . . ⊟Rhodobacterales	1	2	Rhodobacterales hits
. . . . Halocynthiibacter styelae	1	1	Halocynthiibacter styelae hits
. Listeria monocytogenes	1	1	Listeria monocytogenes hits

Suppl. Fig. 19: Ppu_4449 is mostly found in Pseudomonads.

BLASTp searches (Altschul *et al.*, 1990) with the Ppu_4449 sequence against the non-redundant (nr) GenBank CDS database revealed that most hits belong to Pseudomonads as well as a few other bacteria (E value <0.05, maximum hit limit: 5000, standard settings).

References

Alfano, J. R., Charkowski, A. O., Deng, W.-L., Badel, J. L., Petnicki-Ocwieja, T., van Dijk, K., & Collmer, A. (2000). The *Pseudomonas syringae* Hrp pathogenicity island has a tripartite mosaic structure composed of a cluster of type III secretion genes bounded by exchangeable effector and conserved effector loci that contribute to parasitic fitness and pathogenicity in pl. *Proceedings of the National Academy of Sciences*, *97*(9), 4856–4861. https://doi.org/10.1073/pnas.97.9.4856

Almagro Armenteros, J. J., Tsirigos, K. D., Sønderby, C. K., Petersen, T. N., Winther, O., Brunak, S., von Heijne, G., & Nielsen, H. (2019). SignalP 5.0 improves signal peptide predictions using deep neural networks. *Nature Biotechnology*, *37*(4), 420–423. https://doi.org/10.1038/s41587-019-0036-z

Altschul, S. F., Gish, W., Miller, W., Myers, E. W., & Lipman, D. J. (1990). Basic local alignment search tool. *Journal of Molecular Biology*, *215*(3), 403–410. https://doi.org/10.1016/S0022-2836(05)80360-2

Amann, E., Ochs, B., & Abel, K.-J. (1988). Tightly regulated tac promoter vectors useful for the expression of unfused and fused proteins in *Escherichia coli*. *Gene*, *69*(2), 301–315. https://doi.org/10.1016/0378-1119(88)90440-4

Anderson, J. P., Gleason, C. A., Foley, R. C., Thrall, P. H., Burdon, J. B., & Singh, K. B. (2010). Plants versus pathogens: an evolutionary arms race. *Functional Plant Biology*, *37*(6), 499. https://doi.org/10.1071/FP09304

Antelmann, H., Tjalsma, H., Voigt, B., Ohlmeier, S., Bron, S., van Dijl, J. M., & Hecker, M. (2001). A Proteomic View on Genome-Based Signal Peptide Predictions. *Genome Research*, *11*(9), 1484–1502. https://doi.org/10.1101/gr.182801

Aoyagi, T., Takeuchi, T., Matsuzaki, A., Kawamura, K., & Kondo, S. (1969). Leupeptins, new protease inhibitors from Actinomycetes. *The Journal of Antibiotics*, *22*(6), 283–286. https://doi.org/10.7164/antibiotics.22.283

Arslan, E., & Akkaya, Ö. (2020). Biotization of *Arabidopsis thaliana* with *Pseudomonas putida* and assessment of its positive effect on in vitro growth. *In Vitro Cellular & Developmental Biology - Plant*, *56*(2), 184–192. https://doi.org/10.1007/s11627-019-10045-z

Avrova, A. O., Stewart, H. E., De Jong, W., Heilbronn, J., Lyon, G. D., & Birch, P. R. J. (1999). A Cysteine Protease Gene Is Expressed Early in Resistant Potato Interactions with *Phytophthora infestans*. *Molecular Plant-Microbe Interactions®*, *12*(12), 1114–1119. https://doi.org/10.1094/MPMI.1999.12.12.1114

Azarkan, M., Dibiani, R., Baulard, C., & Baeyens-Volant, D. (2006). Effects of mechanical wounding on *Carica papaya* cysteine endopeptidases accumulation and activity. *International Journal of Biological Macromolecules*, *38*(3–5), 216–224. https://doi.org/10.1016/j.ijbiomac.2006.02.021

Bai, Y., Müller, D. B., Srinivas, G., Garrido-Oter, R., Potthoff, E., Rott, M., Dombrowski, N., Münch, P. C., Spaepen, S., Remus-Emsermann, M., Hüttel, B., McHardy, A. C., Vorholt, J. A., & Schulze-Lefert, P. (2015). Functional overlap of the *Arabidopsis* leaf and root microbiota. *Nature*, *528*(7582), 364–369. https://doi.org/10.1038/nature16192

Balbinott, N., & Margis, R. (2022). Review: Unraveling the origin of the structural and functional diversity of plant cystatins. *Plant Science*, *321*, 111342. https://doi.org/https://doi.org/10.1016/j.plantsci.2022.111342

Ballok, A. E., Filkins, L. M., Bomberger, J. M., Stanton, B. A., & O'Toole, G. A. (2014). Epoxide-mediated differential packaging of Cif and other virulence factors into outer membrane vesicles. *Journal of Bacteriology*, *196*(20), 3633–3642. https://doi.org/10.1128/JB.01760-14

Bar-Ziv, A., Levy, Y., Citovsky, V., & Gafni, Y. (2015). The Tomato yellow leaf curl virus (TYLCV) V2 protein inhibits enzymatic activity of the host papain-like cysteine protease CYP1. *Biochemical and Biophysical Research Communications*, *460*(3), 525–529. https://doi.org/10.1016/j.bbrc.2015.03.063

Bar-Ziv, A., Levy, Y., Hak, H., Mett, A., Belausov, E., Citovsky, V., & Gafni, Y. (2012). The tomato yellow leaf curl virus (TYLCV) V2 protein interacts with the host papain-like cysteine protease CYP1. *Plant Signaling & Behavior*, *7*(8), 983–989. https://doi.org/10.4161/psb.20935

Bardoel, B. W., van der Ent, S., Pel, M. J. C., Tommassen, J., Pieterse, C. M. J., van Kessel, K. P. M., & van Strijp, J. A. G. (2011). *Pseudomonas* Evades Immune Recognition of Flagellin in Both Mammals and Plants. *PLoS Pathogens*, *7*(8), e1002206. https://doi.org/10.1371/journal.ppat.1002206

Barghahn, S., Saridis, G., Mantz, M., Meyer, U., Mellüh, J. C., Misas Villamil, J. C., Huesgen, P. F., & Doehlemann, G. (2023). Combination of transcriptomic, proteomic, and degradomic profiling reveals common and distinct patterns of pathogen-induced cell death in maize. *The Plant Journal*, *116*(2), 574–596. https://doi.org/10.1111/tpj.16356

Barrett, A. J. (1985). The cystatins: small protein inhibitors of cysteine proteinases. *Progress in Clinical and Biological Research*, *180*, 105–116. http://www.ncbi.nlm.nih.gov/pubmed/3875863

Barrett, A. J., Kembhavi, A. A., Brown, M. A., Kirschke, H., Knight, C. G., Tamai, M., & Hanada, K. (1982). L-trans-Epoxysuccinyl-leucylamido(4-guanidino)butane (E-64) and its analogues as inhibitors of cysteine proteinases including cathepsins B, H and L. *The Biochemical Journal*, *201*(1), 189–198. https://doi.org/10.1042/bj2010189

Bastedo, D. P., Khan, M., Martel, A., Seto, D., Kireeva, I., Zhang, J., Masud, W., Millar, D., Lee, J. Y., Lee, A. H.-Y., Gong, Y., Santos-Severino, A., Guttman, D. S., & Desveaux, D. (2019). Perturbations of the ZED1 pseudokinase activate plant immunity. *PLOS Pathogens*, *15*(7), e1007900. https://doi.org/10.1371/journal.ppat.1007900

Bateman, A., & Bennett, H. P. (1998). Granulins: the structure and function of an emerging family of growth factors. *The Journal of Endocrinology*, *158*(2), 145–151. https://doi.org/10.1677/joe.0.1580145

Bateman, A., Martin, M.-J., Orchard, S., Magrane, M., Agivetova, R., Ahmad, S., Alpi, E., Bowler-Barnett, E. H., Britto, R., Bursteinas, B., Bye-A-Jee, H., Coetzee, R., Cukura, A., Da Silva, A., Denny, P., Dogan, T., Ebenezer, T., Fan, J., Castro, L. G., … Teodoro, D. (2021). UniProt: the universal protein knowledgebase in 2021. *Nucleic Acids Research*, *49*(D1), D480–D489. https://doi.org/10.1093/nar/gkaa1100

Benchabane, M., Schlüter, U., Vorster, J., Goulet, M.-C., & Michaud, D. (2010). Plant cystatins. *Biochimie*, *92*(11), 1657–1666. https://doi.org/10.1016/j.biochi.2010.06.006

Bentham, A. R., Youles, M., Mendel, M. N., Varden, F. A., & De, J. C. (2021). pOPIN-GG : A resource for modular assembly in protein expression vectors. *BioRxiv*, 0–3. https://doi.org/10.1101/2021.08.10.455798

Berendsen, R. L., van Verk, M. C., Stringlis, I. A., Zamioudis, C., Tommassen, J., Pieterse, C. M. J., & Bakker, P. A. H. M. (2015). Unearthing the genomes of plant-beneficial *Pseudomonas* model strains WCS358, WCS374 and WCS417. *BMC Genomics*, *16*(1), 539. https://doi.org/10.1186/s12864-015-1632-z

Bernal, P., Llamas, M. A., & Filloux, A. (2018). Type VI secretion systems in plant-associated bacteria. *Environmental Microbiology*, *20*(1), 1–15. https://doi.org/10.1111/1462-2920.13956

Bernoux, M., Timmers, T., Jauneau, A., Brière, C., De Wit, P. J. G. M., Marco, Y., & Deslandesa, L. (2008). RD19, an *Arabidopsis* cysteine protease required for RRS1-R-mediated resistance, is relocalized to the nucleus by the *Ralstonia solanacearum* PopP2 effector. *Plant Cell*, *20*(8), 2252–2264. https://doi.org/10.1105/tpc.108.058685

Besteiro, S., Coombs, G. H., & Mottram, J. C. (2004). A potential role for ICP, a leishmanial inhibitor of cysteine peptidases, in the interaction between host and parasite. *Molecular Microbiology*, *54*(5), 1224–1236. https://doi.org/10.1111/j.1365-2958.2004.04355.x

Bi, G., Su, M., Li, N., Liang, Y., Dang, S., Xu, J., Hu, M., Wang, J., Zou, M., Deng, Y., Li, Q., Huang, S., Li, J., Chai, J., He, K., Chen, Y., & Zhou, J.-M. (2021). The ZAR1 resistosome is a calcium-permeable channel triggering plant immune signaling. *Cell*, *184*(13), 3528-3541.e12. https://doi.org/10.1016/j.cell.2021.05.003

Biessy, A., & Filion, M. (2018). Phenazines in plant-beneficial *Pseudomonas* spp.: biosynthesis, regulation, function and genomics. *Environmental Microbiology*, *20*(11), 3905–3917. https://doi.org/10.1111/1462-2920.14395

Billington, K., Halliday, C., Madden, R., Dyer, P., Barker, A. R., Moreira-Leite, F. F., Carrington, M., Vaughan, S., Hertz-Fowler, C., Dean, S., Sunter, J. D., Wheeler, R. J., & Gull, K. (2023). Genome-wide subcellular protein map for the flagellate parasite *Trypanosoma brucei*. *Nature Microbiology*, *8*(3), 533–547. https://doi.org/10.1038/s41564-022-01295-6

Bode, W., & Huber, R. (2000). Structural basis of the endoproteinase–protein inhibitor interaction. *Biochimica et Biophysica Acta (BBA) - Protein Structure and Molecular Enzymology*, *1477*(1–2), 241–252. https://doi.org/10.1016/S0167-4838(99)00276-9

Bolyen, E., Rideout, J. R., Dillon, M. R., Bokulich, N. A., Abnet, C. C., Al-Ghalith, G. A., Alexander, H., Alm, E. J., Arumugam, M., Asnicar, F., Bai, Y., Bisanz, J. E., Bittinger, K., Brejnrod, A., Brislawn, C. J., Brown, C. T., Callahan, B. J., Caraballo-Rodríguez, A. M., Chase, J., … Caporaso, J. G. (2019). Reproducible, interactive, scalable and extensible microbiome data science using QIIME 2. *Nature Biotechnology*, *37*(8), 852–857. https://doi.org/10.1038/s41587-019-0209-9

Bozkurt, T. O., Schornack, S., Win, J., Shindo, T., Ilyas, M., Oliva, R., Cano, L. M., Jones, A. M. E., Huitema, E., Van Der Hoorn, R. A. L., & Kamoun, S. (2011). *Phytophthora infestans* effector AVRblb2 prevents secretion of a plant immune protease at the haustorial interface. *Proceedings of the National Academy of Sciences of the United States of America*, *108*(51), 20832–20837. https://doi.org/10.1073/pnas.1112708109

Bretz, J., Losada, L., Lisboa, K., & Hutcheson, S. W. (2002). Lon protease functions as a negative regulator of type III protein secretion in *Pseudomonas syringae*. *Molecular Microbiology*, *45*(2), 397–409. https://doi.org/https://doi.org/10.1046/j.1365-2958.2002.03008.x

Brillard-Bourdet, M., Nguyên, V., Ferrer-Di Martino, M., Gauthier, F., & Moreau, T. (1998). Purification and characterization of a new cystatin inhibitor from Taiwan cobra (*Naja naja atra*) venom. *Biochemical Journal*, *331*(1), 239–244. https://doi.org/10.1042/bj3310239

Brown, N. P., Leroy, C., & Sander, C. (1998). MView: a web-compatible database search or multiple alignment viewer. *Bioinformatics*, *14*(4), 380–381. https://doi.org/10.1093/bioinformatics/14.4.380

Brutus, A., Sicilia, F., Macone, A., Cervone, F., & De Lorenzo, G. (2010). A domain swap approach reveals a role of the plant wall-associated kinase 1 (WAK1) as a receptor of oligogalacturonides. *Proceedings of the National Academy of Sciences*, *107*(20), 9452–9457. https://doi.org/10.1073/pnas.1000675107

Buchfink, B., Xie, C., & Huson, D. H. (2015). Fast and sensitive protein alignment using DIAMOND. *Nature Methods*, *12*(1), 59–60. https://doi.org/10.1038/nmeth.3176

Bulgarelli, D., Schlaeppi, K., Spaepen, S., Van Themaat, E. V. L., & Schulze-Lefert, P. (2013). Structure and functions of the bacterial microbiota of plants. *Annual Review of Plant Biology*, *64*, 807–838. https://doi.org/10.1146/annurev-arplant-050312-120106

Buscaill, P., Chandrasekar, B., Sanguankiattichai, N., Kourelis, J., Kaschani, F., Thomas, E. L., Morimoto, K., Kaiser, M., Preston, G. M., Ichinose, Y., & van der Hoorn, R. A. L. (2019). Glycosidase and glycan polymorphism control hydrolytic release of immunogenic flagellin peptides. *Science*, *364*(6436). https://doi.org/10.1126/science.aav0748

Buscaill, P., Sanguankiattichai, N., Kaschani, F., Huang, J., Mooney, B. C., Li, Y., Lyu, J., Sueldo, D., Kaiser, M., & van der Hoorn, R. A. L. (2024). Subtilase SBT5.2 inactivates flagellin immunogenicity in the plant apoplast. *Nature Communications*, *15*(1), 10431. https://doi.org/10.1038/s41467-024-54790-1

Calabria, J., Rast-Somssich, M. I., Wang, L., Chen, H.-W., Watt, M., Idnurm, A., Persson, S., & Somssich, M. (2023). pGG-PIP: A GreenGate (GG) entry vector collection with Plant Immune system Promoters (PIP). *BioRxiv*, 2022.12.20.521163. https://doi.org/10.1101/2022.12.20.521163

Camacho, C., Coulouris, G., Avagyan, V., Ma, N., Papadopoulos, J., Bealer, K., & Madden, T. L. (2009). BLAST+: architecture and applications. *BMC Bioinformatics*, *10*, 421. https://doi.org/10.1186/1471-2105-10-421

Canarini, A., Kaiser, C., Merchant, A., Richter, A., & Wanek, W. (2019). Root exudation of primary metabolites: Mechanisms and their roles in plant responses to environmental stimuli. *Frontiers in Plant Science*, *10*(February). https://doi.org/10.3389/fpls.2019.00157

Cervone, F., Hahn, M. G., De Lorenzo, G., Darvill, A., & Albersheim, P. (1989). Host-Pathogen Interactions : XXXIII. A Plant Protein Converts a Fungal Pathogenesis Factor into an Elicitor of Plant Defense Responses. *Plant Physiology*, *90*(2), 542–548. https://doi.org/10.1104/pp.90.2.542

Chai, J., Song, W., & Parker, J. E. (2023). New Biochemical Principles for NLR Immunity in Plants. *Molecular Plant-Microbe Interactions®*, *36*(8), 468–475. https://doi.org/10.1094/MPMI-05-23-0073-HH

Charif, D., & Lobry, J. R. (2007). *SeqinR 1.0-2: A Contributed Package to the R Project for Statistical Computing Devoted to Biological Sequences Retrieval and Analysis* (U. Bastolla, M. Porto, H. E. Roman, & M. Vendruscolo (eds.); pp. 207–232). Springer Berlin Heidelberg. https://doi.org/10.1007/978-3-540-35306-5_10

Charova, S. N., Dölfors, F., Holmquist, L., Moschou, P. N., Dixelius, C., & Tzelepis, G. (2020). The RsRlpA Effector Is a Protease Inhibitor Promoting *Rhizoctonia solani* Virulence through Suppression of the Hypersensitive Response. *International Journal of Molecular Sciences*, *21*(21), 1–17. https://doi.org/10.3390/ijms21218070

Chen, C., Buscaill, P., Sanguankiattichai, N., Huang, J., Kaschani, F., Kaiser, M., & van der Hoorn, R. A. L. (2024a). Extracellular plant subtilases dampen cold-shock peptide elicitor levels. *Nature Plants*. https://doi.org/10.1038/s41477-024-01815-8

Chen, D., Cao, Y., Li, H., Kim, D., Ahsan, N., Thelen, J., & Stacey, G. (2017). Extracellular ATP elicits DORN1-mediated RBOHD phosphorylation to regulate stomatal aperture. *Nature Communications*, *8*(1), 2265. https://doi.org/10.1038/s41467-017-02340-3

Chen, J., Xu, F., Qiang, X., Liu, H., Wang, L., Jiang, L., Li, C., Wang, B., Luan, S., Wu, D., Zhou, F., & Yu, F. (2024b). Regulated cleavage and translocation of FERONIA control immunity in *Arabidopsis* roots. *Nature Plants*, 2023.10.16.562456. https://doi.org/10.1038/s41477-024-01823-8

Chen, Y.-L., Lin, F.-W., Cheng, K.-T., Chang, C.-H., Hung, S.-C., Efferth, T., & Chen, Y.-R. (2023). XCP1 cleaves Pathogenesis-related protein 1 into CAPE9 for systemic immunity in *Arabidopsis*. *Nature Communications*, *14*(1), 4697. https://doi.org/10.1038/s41467-023-40406-7

Chen, Y. L., Lee, C. Y., Cheng, K. T., Chang, W. H., Huang, R. N., Nam, H. G., & Chen, Y. R. (2014). Quantitative peptidomics study reveals that a wound-induced peptide from PR-1 regulates immune signaling in tomato. *Plant Cell*, *26*(10), 4135–4148. https://doi.org/10.1105/tpc.114.131185

Cheng, J. H. T., Bredow, M., Monaghan, J., & Di Cenzo, G. C. (2021). Proteobacteria contain diverse flg22 epitopes that elicit varying immune responses in *Arabidopsis thaliana*. *Molecular Plant-Microbe Interactions*, *34*(5), 504–510. https://doi.org/10.1094/MPMI-11-20-0314-SC

Chinchilla, D., Bauer, Z., Regenass, M., Boller, T., & Felix, G. (2006). The *Arabidopsis* receptor kinase FLS2 binds flg22 and determines the specificity of flagellin perception. *Plant Cell*, *18*(2), 465–476. https://doi.org/10.1105/tpc.105.036574

Choe, Y., Leonetti, F., Greenbaum, D. C., Lecaille, F., Bogyo, M., Brömme, D., Ellman, J. A., & Craik, C. S. (2006). Substrate profiling of cysteine proteases using a combinatorial peptide library identifies functionally unique specificities. *Journal of Biological Chemistry*, *281*(18), 12824–12832. https://doi.org/10.1074/jbc.M513331200

Choi, C.-W., Park, E. C., Yun, S. H., Lee, S.-Y., Lee, Y. G., Hong, Y., Park, K. R., Kim, S.-H., Kim, G.-H., & Kim, S. Il. (2014). Proteomic Characterization of the Outer Membrane Vesicle of *Pseudomonas putida* KT2440. *Journal of Proteome Research*, *13*(10), 4298–4309. https://doi.org/10.1021/pr500411d

Clark, K., Franco, J. Y., Schwizer, S., Pang, Z., Hawara, E., Liebrand, T. W. H., Pagliaccia, D., Zeng, L., Gurung, F. B., Wang, P., Shi, J., Wang, Y., Ancona, V., Van Der Hoorn, R. A. L., Wang, N., Coaker, G., & Ma, W. (2018). An effector from the Huanglongbing-associated pathogen targets citrus proteases. *Nature Communications*, *9*(1), 1–11. https://doi.org/10.1038/s41467-018-04140-9

Clark, K. J., Pang, Z., Trinh, J., Wang, N., & Ma, W. (2020). Sec-Delivered Effector 1 (SDE1) of "*Candidatus Liberibacter asiaticus*" Promotes Citrus Huanglongbing. *Molecular Plant-Microbe Interactions : MPMI*, *33*(12), 1394–1404. https://doi.org/10.1094/MPMI-05-20-0123-R

Cock, P. J. A., Antao, T., Chang, J. T., Chapman, B. A., Cox, C. J., Dalke, A., Friedberg, I., Hamelryck, T., Kauff, F., Wilczynski, B., & de Hoon, M. J. L. (2009). Biopython: freely available Python tools for computational molecular biology and bioinformatics. *Bioinformatics*, *25*(11), 1422–1423. https://doi.org/10.1093/bioinformatics/btp163

Cohen, M., Davydov, O., & Fluhr, R. (2019). Plant serpin protease inhibitors: specificity and duality of function. *Journal of Experimental Botany*, *70*(7), 2077–2085. https://doi.org/10.1093/jxb/ery460

Cole, G. B., Bateman, T. J., & Moraes, T. F. (2021). The surface lipoproteins of gram-negative bacteria: Protectors and foragers in harsh environments. *Journal of Biological Chemistry*, *296*(1679), 100147. https://doi.org/10.1074/jbc.REV120.008745

Collins, A. J., Pastora, A. B., Smith, T. J., & O'Toole, G. A. (2020). MapA, a Second Large RTX Adhesin Conserved across the Pseudomonads, Contributes to Biofilm Formation by *Pseudomonas fluorescens*. *Journal of Bacteriology*, *202*(18), 10.1128/jb.00277-20. https://doi.org/10.1128/JB.00277-20

Conrath, U., Beckers, G. J. M., Langenbach, C. J. G., & Jaskiewicz, M. R. (2015). Priming for Enhanced Defense. *Annual Review of Phytopathology*, *53*, 97–119. https://doi.org/10.1146/annurev-phyto-080614-120132

Coria, L. M., Ibañez, A. E., Tkach, M., Sabbione, F., Bruno, L., Carabajal, M. V, Berguer, P. M., Barrionuevo, P., Schillaci, R., Trevani, A. S., Giambartolomei, G. H., Pasquevich, K. A., & Cassataro, J. (2016). A *Brucella* spp. Protease Inhibitor Limits Antigen Lysosomal Proteolysis, Increases Cross-Presentation, and Enhances CD8+ T Cell Responses. *Journal of Immunology (Baltimore, Md. : 1950)*, *196*(10), 4014–4029. https://doi.org/10.4049/jimmunol.1501188

Costa-Gutierrez, S. B., Adler, C., Espinosa-Urgel, M., & de Cristóbal, R. E. (2022). *Pseudomonas putida* and its close relatives: mixing and mastering the perfect tune for plants. *Applied Microbiology and Biotechnology*, *106*(9–10), 3351–3367. https://doi.org/10.1007/s00253-022-11881-7

Costa, T. F. R., Goundry, A., Morrot, A., Grab, D. J., Mottram, J. C., & Lima, A. P. C. A. (2022). *Trypanosoma brucei rhodesiense* Inhibitor of Cysteine Peptidase (ICP) Is Required for Virulence in Mice and to Attenuate the Inflammatory Response. *International Journal of Molecular Sciences*, *24*(1), 656. https://doi.org/10.3390/ijms24010656

Costa, T. F. R., & Lima, A. P. C. A. (2016). Natural cysteine protease inhibitors in protozoa: Fifteen years of the chagasin family. *Biochimie*, *122*, 197–207. https://doi.org/10.1016/j.biochi.2015.11.002

Cotabarren, J., Claver, S., Payrol, J. A., Garcia-Pardo, J., & Obregón, W. D. (2021). Purification and Characterization of a Novel Thermostable Papain Inhibitor from *Moringa oleifera* with Antimicrobial and Anticoagulant Properties. *Pharmaceutics*, *13*(4), 512. https://doi.org/10.3390/pharmaceutics13040512

Couto, D., & Zipfel, C. (2016). Regulation of pattern recognition receptor signalling in plants. *Nature Reviews Immunology*, *16*(9), 537–552. https://doi.org/10.1038/nri.2016.77

Couture-Beil, A. (2024). *rjson* (0.2.23). https://cran.r-project.org/web/packages/rjson/rjson.pdf

Cronan, J. E., Narasimhan, M. L., & Rawlings, M. (1988). Insertional restoration of β-galactosidase α-complementation (white-to-blue colony screening) facilitates assembly of synthetic genes. *Gene*, *70*(1), 161–170. https://doi.org/10.1016/0378-1119(88)90114-X

Danhorn, T., & Fuqua, C. (2007). Biofilm formation by plant-associated bacteria. *Annual Review of Microbiology*, *61*, 401–422. https://doi.org/10.1146/annurev.micro.61.080706.093316

Daniels, G. M., & Amara, S. G. (1998). Selective labeling of neurotransmitter transporters at the cell surface. *Methods in Enzymology*, *296*, 307–318. https://doi.org/10.1016/s0076-6879(98)96023-2

Danne, J. C. (2022). Tokuyasu processing and immuno-electron microscopy of tissue v1. protocols.io. https://doi.org/10.17504/protocols.io.5jyl8jj9dg2w/v1

De Meyer, F., & Carlier, A. (2023). Ecotin: A versatile protease inhibitor of bacteria and eukaryotes. *Frontiers in Microbiology*, *14*(January), 1–8. https://doi.org/10.3389/fmicb.2023.1114690

De Vleesschauwer, D., Xu, J., & Höfte, M. (2014). Making sense of hormone-mediated defense networking: from rice to *Arabidopsis*. *Frontiers in Plant Science*, *5*, 611. https://doi.org/10.3389/fpls.2014.00611

de Wit, P. J. G. M. (2007). How plants recognize pathogens and defend themselves. *Cellular and Molecular Life Sciences : CMLS*, *64*(21), 2726–2732. https://doi.org/10.1007/s00018-007-7284-7

Delfín, J., Martínez, I., Antuch, W., Morera, V., González, Y., Rodríguez, R., Márquez, M., Saroyán, A., Larionova, N., Díaz, J., Padrón, G., & Chávez, M. (1996). Purification, characterization and immobilization of proteinase inhibitors from *Stichodactyla helianthus*. *Toxicon : Official Journal of the International Society on Toxinology*, *34*(11–12), 1367–1376. https://doi.org/10.1016/s0041-0101(96)00114-6

Demidchik, V., Shang, Z., Shin, R., Thompson, E., Rubio, L., Laohavisit, A., Mortimer, J. C., Chivasa, S., Slabas, A. R., Glover, B. J., Schachtman, D. P., Shabala, S. N., & Davies, J. M. (2009). Plant extracellular ATP signalling by plasma membrane NADPH oxidase and Ca 2+ channels. *The Plant Journal*, *58*(6), 903–913. https://doi.org/10.1111/j.1365-313X.2009.03830.x

Demir, F., Perrar, A., Mantz, M., & Huesgen, P. F. (2022). Sensitive Plant N-Terminome Profiling with HUNTER (Vol. 1905, Issue page 114, pp. 139–158). https://doi.org/10.1007/978-1-0716-2079-3_12

Doehlemann, G., Reissmann, S., Assmann, D., Fleckenstein, M., & Kahmann, R. (2011). Two linked genes encoding a secreted effector and a membrane protein are essential for *Ustilago maydis*-induced tumour formation. *Molecular Microbiology*, *81*(3), 751–766. https://doi.org/10.1111/j.1365-2958.2011.07728.x

Dong, S., Stam, R., Cano, L. M., Song, J., Sklenar, J., Yoshida, K., Bozkurt, T. O., Oliva, R., Liu, Z., Tian, M., Win, J., Banfield, M. J., Jones, A. M. E., van der Hoorn, R. A. L., & Kamoun, S. (2014). Effector specialization in a lineage of the Irish potato famine pathogen. *Science (New York, N.Y.)*, *343*(6170), 552–555. https://doi.org/10.1126/science.1246300

Dongus, J. A., & Parker, J. E. (2021). EDS1 signalling: At the nexus of intracellular and surface receptor immunity. *Current Opinion in Plant Biology*, *62*, 102039. https://doi.org/10.1016/j.pbi.2021.102039

dos Reis, F. C. G., Smith, B. O., Santos, C. C., Costa, T. F. R., Scharfstein, J., Coombs, G. H., Mottram, J. C., & Lima, A. P. C. A. (2008). The role of conserved residues of chagasin in the inhibition of cysteine peptidases. *FEBS Letters*, *582*(4), 485–490. https://doi.org/10.1016/j.febslet.2008.01.008

dos Santos, E. A., de Oliveira, A. S., Arajo Rablo, L. M., Ferreira, A., & Arajo Morais, A. H. (2012). Affinity Chromatography as a Key Tool to Purify Protein Protease Inhibitors from Plants. In *Affinity Chromatography*. InTech. https://doi.org/10.5772/34982

Durán, P., Thiergart, T., Garrido-Oter, R., Agler, M., Kemen, E., Schulze-Lefert, P., & Hacquard, S. (2018). Microbial Interkingdom Interactions in Roots Promote *Arabidopsis* Survival. *Cell*, *175*(4), 973-983.e14. https://doi.org/10.1016/j.cell.2018.10.020

El Moussaoui, A., Nijs, M., Paul, C., Wintjens, R., Vincentelli, J., Azarkan, M., & Looze, Y. (2001). Revisiting the enzymes stored in the laticifers of *Carica papaya* in the context of their possible participation in the plant defence mechanism. *Cellular and Molecular Life Sciences : CMLS*, *58*(4), 556–570. https://doi.org/10.1007/PL00000881

Elmore, J. R., Furches, A., Wolff, G. N., Gorday, K., & Guss, A. M. (2017). Development of a high efficiency integration system and promoter library for rapid modification of *Pseudomonas putida* KT2440. *Metabolic Engineering Communications*, *5*(November 2016), 1–8. https://doi.org/10.1016/j.meteno.2017.04.001

Emonet, A., Zhou, F., Vacheron, J., Heiman, C. M., Dénervaud Tendon, V., Ma, K.-W., Schulze-Lefert, P., Keel, C., & Geldner, N. (2021). Spatially Restricted Immune Responses Are Required for Maintaining Root Meristematic Activity upon Detection of Bacteria. *Current Biology*, *31*(5), 1012-1028.e7. https://doi.org/10.1016/j.cub.2020.12.048

Engler, C., Youles, M., Gruetzner, R., Ehnert, T.-M., Werner, S., Jones, J. D. G., Patron, N. J., & Marillonnet, S. (2014). A Golden Gate Modular Cloning Toolbox for Plants. *ACS Synthetic Biology*, *3*(11), 839–843. https://doi.org/10.1021/sb4001504

Esparza-Reynoso, S., Ayala-Rodríguez, J. Á., & López-Bucio, J. (2024). *Pseudomonas putida* configures *Arabidopsis* root architecture through modulating the sensing systems for phosphate and iron acquisition. *Plant Science : An International Journal of Experimental Plant Biology*, *342*, 112028. https://doi.org/10.1016/j.plantsci.2024.112028

Espinosa-Urgel, M., & Ramos-González, M. I. (2023). Becoming settlers: Elements and mechanisms for surface colonization by *Pseudomonas putida*. *Environmental Microbiology*, *25*(9), 1575–1593. https://doi.org/10.1111/1462-2920.16385

Evans, R., O'Neill, M., Pritzel, A., Antropova, N., Senior, A., Green, T., Žídek, A., Bates, R., Blackwell, S., Yim, J., Ronneberger, O., Bodenstein, S., Zielinski, M., Bridgland, A., Potapenko, A., Cowie, A., Tunyasuvunakool, K., Jain, R., Clancy, E., … Hassabis, D. (2022). Protein complex prediction with AlphaFold-Multimer. *BioRxiv*, 2021.10.04.463034. https://doi.org/10.1101/2021.10.04.463034

Farady, C. J., & Craik, C. S. (2010). Mechanisms of Macromolecular Protease Inhibitors. *ChemBioChem*, *11*(17), 2341–2346. https://doi.org/10.1002/cbic.201000442

Feehan, J. M., Wang, J., Sun, X., Choi, J., Ahn, H.-K., Ngou, B. P. M., Parker, J. E., & Jones, J. D. G. (2023). Oligomerization of a plant helper NLR requires cell-surface and intracellular immune receptor activation. *Proceedings of the National Academy of Sciences*, *120*(11), 2017. https://doi.org/10.1073/pnas.2210406120

Felix, G., Duran, J. D., Volko, S., & Boller, T. (1999). Plants have a sensitive perception system for the most conserved domain of bacterial flagellin. *The Plant Journal*, *18*(3), 265–276. https://doi.org/10.1046/j.1365-313X.1999.00265.x

Fernández-Fernández, Á. D., Stael, S., & Van Breusegem, F. (2023). Mechanisms controlling plant proteases and their substrates. *Cell Death & Differentiation*, *May 2022*, 1–12. https://doi.org/10.1038/s41418-023-01120-5

Fingerhut, L. C. H. W., Miller, D. J., Strugnell, J. M., Daly, N. L., & Cooke, I. R. (2021). ampir: an R package for fast genome-wide prediction of antimicrobial peptides. *Bioinformatics*, *36*(21), 5262–5263. https://doi.org/10.1093/bioinformatics/btaa653

Flemming, H.-C., & Wingender, J. (2010). The biofilm matrix. *Nature Reviews. Microbiology*, *8*(9), 623–633. https://doi.org/10.1038/nrmicro2415

Fu, Y. (2009). Structure and dynamics of *Pseudomonas aeruginosa* ICP. University of Glasgow.

Gao, C.-H., Yu, G., & Cai, P. (2021). ggVennDiagram: An Intuitive, Easy-to-Use, and Highly Customizable R Package to Generate Venn Diagram. *Frontiers in Genetics*, *12*(September). https://doi.org/10.3389/fgene.2021.706907

Gao, C., Chen, C., Akyol, T., Dusa, A., Yu, G., Cao, B., & Cai, P. (2024). ggVennDiagram: Intuitive Venn diagram software extended. *IMeta*, *3*(1), 2–5. https://doi.org/10.1002/imt2.177

Gasteiger, E., Hoogland, C., Gattiker, A., Duvaud, S., Wilkins, M. R., Appel, R. D., & Bairoch, A. (2005). The Proteomics Protocols Handbook. *The Proteomics Protocols Handbook*, 571–608. https://doi.org/10.1385/1592598900

Gay, P., Le Coq, D., Steinmetz, M., Berkelman, T., & Kado, C. I. (1985). Positive selection procedure for entrapment of insertion sequence elements in gram-negative bacteria. *Journal of Bacteriology*, *164*(2), 918–921. https://doi.org/10.1128/jb.164.2.918-921.1985

Gennity, J. M., & Inouye, M. (1991). The protein sequence responsible for lipoprotein membrane localization in *Escherichia coli* exhibits remarkable specificity. *Journal of Biological Chemistry*, *266*(25), 16458–16464. https://doi.org/10.1016/S0021-9258(18)55322-9

Geudens, N., & Martins, J. C. (2018). Cyclic Lipodepsipeptides From *Pseudomonas* spp. - Biological Swiss-Army Knives. *Frontiers in Microbiology*, *9*, 1867. https://doi.org/10.3389/fmicb.2018.01867

Gfeller, A., Liechti, R., & Farmer, E. E. (2010). *Arabidopsis* Jasmonate Signaling Pathway. *Science Signaling*, *3*(109), cm4–cm4. https://doi.org/10.1126/scisignal.3109cm4

Ghequire, M. G. K., & De Mot, R. (2014). Ribosomally encoded antibacterial proteins and peptides from *Pseudomonas*. *FEMS Microbiology Reviews*, *38*(4), 523–568. https://doi.org/10.1111/1574-6976.12079

Ghosh, D., Sen, S., & Mohapatra, S. (2017). Modulation of proline metabolic gene expression in *Arabidopsis thaliana* under water-stressed conditions by a drought-mitigating *Pseudomonas putida* strain. *Annals of Microbiology*, *67*(10), 655–668. https://doi.org/10.1007/s13213-017-1294-y

Glazebrook, J. (2005). Contrasting mechanisms of defense against biotrophic and necrotrophic pathogens. *Annual Review of Phytopathology*, *43*, 205–227. https://doi.org/10.1146/annurev.phyto.43.040204.135923

Gómez-Gómez, L., & Boller, T. (2000). FLS2: an LRR receptor-like kinase involved in the perception of the bacterial elicitor flagellin in *Arabidopsis*. *Molecular Cell*, *5*(6), 1003–1011. https://doi.org/10.1016/s1097-2765(00)80265-8

Gómez-Gómez, L., Felix, G., & Boller, T. (1999). A single locus determines sensitivity to bacterial flagellin in *Arabidopsis thaliana*. *The Plant Journal*, *18*(3), 277–284. https://doi.org/10.1046/j.1365-313X.1999.00451.x

Gómez Expósito, R., de Bruijn, I., Postma, J., & Raaijmakers, J. M. (2017). Current Insights into the Role of Rhizosphere Bacteria in Disease Suppressive Soils. *Frontiers in Microbiology*, *8*(DEC), 1–12. https://doi.org/10.3389/fmicb.2017.02529

Goodwin, R. H., & Kavanagh, F. (1948). Fluorescing Substances in Roots. *Bulletin of the Torrey Botanical Club*, *75*(1), 1. https://doi.org/10.2307/2482135

Gottesman, S. (1996). Proteases and their targets in *Escherichia coli*. *Annual Review of Genetics*, *30*, 465–506. https://doi.org/10.1146/annurev.genet.30.1.465

Goulas, T., Garcia-Ferrer, I., Marrero, A., Marino-Puertas, L., Duquerroy, S., & Gomis-Rüth, F. X. (2017). Structural and functional insight into pan-endopeptidase inhibition by α2-macroglobulins. *Biological Chemistry*, *398*(9), 975–994. https://doi.org/10.1515/hsz-2016-0329

Grabowicz, M. (2019). Lipoproteins and Their Trafficking to the Outer Membrane. *EcoSal Plus*, *8*(2). https://doi.org/10.1128/ecosalplus.esp-0038-2018

Grabowicz, M., & Silhavy, T. J. (2017). Redefining the essential trafficking pathway for outer membrane lipoproteins. *Proceedings of the National Academy of Sciences*, *114*(18), 4769–4774. https://doi.org/10.1073/pnas.1702248114

Graves, S., Piepho, H.-P., & Selzer, L. (2024). *multcompView* (0.1-10). https://cran.r-project.org/web/packages/multcompView/multcompView.pdf

Greenbaum, D., Medzihradszky, K. F., Burlingame, A., & Bogyo, M. (2000). Epoxide electrophiles as activity-dependent cysteine protease profiling and discovery tools. *Chemistry and Biology*, *7*(8), 569–581. https://doi.org/10.1016/S1074-5521(00)00014-4

Gross, H., & Loper, J. E. (2009). Genomics of secondary metabolite production by *Pseudomonas* spp. *Natural Product Reports*, *26*(11), 1408–1446. https://doi.org/10.1039/b817075b

Grosse-Holz, F. M., & van der Hoorn, R. A. L. (2016). Juggling jobs: roles and mechanisms of multifunctional protease inhibitors in plants. *The New Phytologist*, *210*(3), 794–807. https://doi.org/10.1111/nph.13839

Grosse-Holz, F., Madeira, L., Zahid, M. A., Songer, M., Kourelis, J., Fesenko, M., Ninck, S., Kaschani, F., Kaiser, M., & van der Hoorn, R. A. L. (2018). Three unrelated protease inhibitors enhance accumulation of pharmaceutical recombinant proteins in *Nicotiana benthamiana*. *Plant Biotechnology Journal*, *16*(10), 1797–1810. https://doi.org/10.1111/pbi.12916

Gu, C., Shabab, M., Strasser, R., Wolters, P. J., Shindo, T., Niemer, M., Kaschani, F., Mach, L., & van der Hoorn, R. A. L. (2012). Post-translational regulation and trafficking of the granulin-containing protease RD21 of *Arabidopsis thaliana*. *PloS One*, *7*(3), e32422. https://doi.org/10.1371/journal.pone.0032422

Guichard, M., Bertran Garcia de Olalla, E., Stanley, C. E., & Grossmann, G. (2020). Microfluidic systems for plant root imaging. In *Methods in Cell Biology* (1st ed., Vol. 160, pp. 381–404). Elsevier Inc. https://doi.org/10.1016/bs.mcb.2020.03.012

Gumtow, R., Wu, D., Uchida, J., & Tian, M. (2018). A *Phytophthora palmivora* extracellular cystatin-like protease inhibitor targets papain to contribute to virulence on papaya. *Molecular Plant-Microbe Interactions*, *31*(3), 363–373. https://doi.org/10.1094/MPMI-06-17-0131-FI

Guo, F., & Huang, B. Q. (2015). Immunogold Labeling for Electron Microscopy: Strategy and Problem Solving. In E. C. T. Yeung, C. Stasolla, M. J. Sumner, & B. Q. Huang (Eds.), *Plant Microtechniques and Protocols* (pp. 225–249). Springer International Publishing. https://doi.org/10.1007/978-3-319-19944-3_14

Guo, W., & Ruckenstein, E. (2002). Crosslinked mercerized cellulose membranes for the affinity chromatography of papain inhibitors. *Journal of Membrane Science*, *197*(1–2), 53–62. https://doi.org/10.1016/S0376-7388(01)00619-6

Gupta, S. D., Gan, K., Schmid, M. B., & Wu, H. C. (1993). Characterization of a temperature-sensitive mutant of *Salmonella typhimurium* defective in apolipoprotein N-acyltransferase. *Journal of Biological Chemistry*, *268*(22), 16551–16556. https://doi.org/10.1016/S0021-9258(19)85454-6

Haichar, F. el Z., Santaella, C., Heulin, T., & Achouak, W. (2014). Root exudates mediated interactions belowground. *Soil Biology and Biochemistry*, *77*, 69–80. https://doi.org/10.1016/j.soilbio.2014.06.017

Hale, M. G., & Moore, L. D. (1980). Factors Affecting Root Exudation Ii: 1970–1978. In N. C. Brady (Ed.), *Advances in Agronomy* (Vol. 31, pp. 93–124). Academic Press. https://doi.org/10.1016/S0065-2113(08)60137-6

Hanada, K., Tamai, M., Yamagishi, M., Ohmura, S., Sawada, J., & Tanaka, I. (1978). Isolation and Characterization of E–64, a New Thiol Protease Inhibitor. *Agricultural and Biological Chemistry*, *42*(3), 523–528. https://doi.org/10.1080/00021369.1978.10863014

Hander, T., Fernández-Fernández, Á. D., Kumpf, R. P., Willems, P., Schatowitz, H., Rombaut, D., Staes, A., Nolf, J., Pottie, R., Yao, P., Gonçalves, A., Pavie, B., Boller, T., Gevaert, K., Van Breusegem, F., Bartels, S., & Stael, S. (2019). Damage on plants activates Ca 2+ -dependent metacaspases for release of immunomodulatory peptides. *Science*, *363*(6433). https://doi.org/10.1126/science.aar7486

Harbort, C. J., Hashimoto, M., Inoue, H., Niu, Y., Guan, R., Rombolà, A. D., Kopriva, S., Voges, M. J. E. E. E. E. E. E., Sattely, E. S., Garrido-Oter, R., & Schulze-Lefert, P. (2020). Root-Secreted Coumarins and the Microbiota Interact to Improve Iron Nutrition in *Arabidopsis*. *Cell Host & Microbe*, *28*(6), 825-837.e6. https://doi.org/10.1016/j.chom.2020.09.006

Harris, C. R., Millman, K. J., van der Walt, S. J., Gommers, R., Virtanen, P., Cournapeau, D., Wieser, E., Taylor, J., Berg, S., Smith, N. J., Kern, R., Picus, M., Hoyer, S., van Kerkwijk, M. H., Brett, M., Haldane, A., del Río, J. F., Wiebe, M., Peterson, P., … Oliphant, T. E. (2020a). Array programming with NumPy. *Nature*, *585*(7825), 357–362. https://doi.org/10.1038/s41586-020-2649-2

Harris, J. M., Balint-Kurti, P., Bede, J. C., Day, B., Gold, S., Goss, E. M., Grenville-Briggs, L. J., Jones, K. M., Wang, A., Wang, Y., Mitra, R. M., Sohn, K. H., & Alvarez, M. E. (2020b). What are the Top 10 Unanswered Questions in Molecular Plant-Microbe Interactions? *Molecular Plant-Microbe Interactions®*, *X*(X), MPMI-08-20-0229. https://doi.org/10.1094/mpmi-08-20-0229-cr

Harris, P. J., & Hartley, R. D. (1980). Phenolic constituents of the cell walls of monocotyledons. *Biochemical Systematics and Ecology*, *8*(2), 153–160. https://doi.org/10.1016/0305-1978(80)90008-3

He, H., Pramanik, A. S., Swanson, S. K., Johnson, D. K., Florens, L., & Zückert, W. R. (2023). A *Borrelia burgdorferi* LptD homolog is required for flipping of surface lipoproteins through the spirochetal outer membrane. *Molecular Microbiology*, *119*(6), 752–767. https://doi.org/10.1111/mmi.15072

Heese, A., Hann, D. R., Gimenez-Ibanez, S., Jones, A. M. E., He, K., Li, J., Schroeder, J. I., Peck, S. C., & Rathjen, J. P. (2007). The receptor-like kinase SERK3/BAK1 is a central regulator of innate immunity in plants. *Proceedings of the National Academy of Sciences*, *104*(29), 12217–12222. https://doi.org/10.1073/pnas.0705306104

Heredia-Ponce, Z., de Vicente, A., Cazorla, F. M., & Gutiérrez-Barranquero, J. A. (2021). Beyond the Wall: Exopolysaccharides in the Biofilm Lifestyle of Pathogenic and Beneficial Plant-Associated *Pseudomonas*. *Microorganisms*, *9*(2), 445. https://doi.org/10.3390/microorganisms9020445

Hiltner, L. (1904). Über neuere Erfahrungen und Probleme auf dem Gebiet der Bodenbakteriologie und unter besonderer Berücksichtigung der Gründüngung und Brache. *Arbeiten Der Deutschen Landwirtschaftlichen Gesellschaft*, *98*, 59.

Hinsa, S. M., Espinosa-Urgel, M., Ramos, J. L., & O'Toole, G. A. (2003). Transition from reversible to irreversible attachment during biofilm formation by *Pseudomonas fluorescens* WCS365 requires an ABC transporter and a large secreted protein. *Molecular Microbiology*, *49*(4), 905–918. https://doi.org/10.1046/j.1365-2958.2003.03615.x

Hochholdinger, F., & Zimmermann, R. (2008). Conserved and diverse mechanisms in root development. *Current Opinion in Plant Biology*, *11*(1), 70–74. https://doi.org/10.1016/j.pbi.2007.10.002

Homma, F., Huang, J., & van der Hoorn, R. A. L. (2023). AlphaFold-Multimer predicts cross-kingdom interactions at the plant-pathogen interface. *Nature Communications*, *14*(1), 6040. https://doi.org/10.1038/s41467-023-41721-9

Homma, F., Lyu, J., & van der Hoorn, R. A. L. (2024). Using AlphaFold Multimer to discover interkingdom protein–protein interactions. *The Plant Journal*, 2024.06.14.599045. https://doi.org/10.1111/tpj.16969

Hooda, Y., Lai, C. C.-L., Judd, A., Buckwalter, C. M., Shin, H. E., Gray-Owen, S. D., & Moraes, T. F. (2016). Slam is an outer membrane protein that is required for the surface display of lipidated virulence factors in *Neisseria*. *Nature Microbiology*, *1*(4), 16009. https://doi.org/10.1038/nmicrobiol.2016.9

Hooda, Y., Lai, C. C. L., & Moraes, T. F. (2017). Identification of a large family of slam-dependent surface lipoproteins in gram-negative bacteria. *Frontiers in Cellular and Infection Microbiology*, *7*(MAY), 1–12. https://doi.org/10.3389/fcimb.2017.00207

Huang, W., & Wilks, A. (2017). A rapid seamless method for gene knockout in *Pseudomonas aeruginosa*. *BMC Microbiology*, *17*(1), 199. https://doi.org/10.1186/s12866-017-1112-5

Huffaker, A., Pearce, G., & Ryan, C. A. (2006). An endogenous peptide signal in *Arabidopsis* activates components of the innate immune response. *Proceedings of the National Academy of Sciences of the United States of America*, *103*(26), 10098–10103. https://doi.org/10.1073/pnas.0603727103

Hufford, M. B., Seetharam, A. S., Woodhouse, M. R., Chougule, K. M., Ou, S., Liu, J., Ricci, W. A., Guo, T., Olson, A., Qiu, Y., Della Coletta, R., Tittes, S., Hudson, A. I., Marand, A. P., Wei, S., Lu, Z., Wang, B., Tello-Ruiz, M. K., Piri, R. D., … Dawe, R. K. (2021). De novo assembly, annotation, and comparative analysis of 26 diverse maize genomes. *Science*, *373*(6555), 655–662. https://doi.org/10.1126/science.abg5289

Huh, K.-H., & Wenthold, R. J. (1999). Turnover Analysis of Glutamate Receptors Identifies a Rapidly Degraded Pool of the N-Methyl-d-aspartate Receptor Subunit, NR1, in Cultured Cerebellar Granule Cells. *Journal of Biological Chemistry*, *274*(1), 151–157. https://doi.org/10.1074/jbc.274.1.151

Hunter, J. D. (2007). Matplotlib: A 2D Graphics Environment. *Computing in Science & Engineering*, *9*(3), 90–95. https://doi.org/10.1109/MCSE.2007.55

Hunter, S., Apweiler, R., Attwood, T. K., Bairoch, A., Bateman, A., Binns, D., Bork, P., Das, U., Daugherty, L., Duquenne, L., Finn, R. D., Gough, J., Haft, D., Hulo, N., Kahn, D., Kelly, E., Laugraud, A., Letunic, I., Lonsdale, D., … Yeats, C. (2009). InterPro: the integrative protein signature database. *Nucleic Acids Research*, *37*(Database issue), D211–D215. https://doi.org/10.1093/nar/gkn785

Huynh, M. S., Hooda, Y., Li, Y. R., Jagielnicki, M., Lai, C. C. L., & Moraes, T. F. (2022). Reconstitution of Surface Lipoprotein Translocation Through the Slam Translocon. *ELife*, *11*, 1–24. https://doi.org/10.7554/eLife.72822

Ibañez, A. E., Coria, L. M., Carabajal, M. V., Delpino, M. V., Risso, G. S., Cobiello, P. G., Rinaldi, J., Barrionuevo, P., Bruno, L., Frank, F., Klinke, S., Goldbaum, F. A., Briones, G., Giambartolomei, G. H., Pasquevich, K. A., & Cassataro, J. (2015). A bacterial protease inhibitor protects antigens delivered in oral vaccines from digestion while triggering specific mucosal immune responses. *Journal of Controlled Release*, *220*, 18–28. https://doi.org/10.1016/j.jconrel.2015.10.011

Ilyas, M., Hörger, A. C., Bozkurt, T. O., van den Burg, H. A., Kaschani, F., Kaiser, M., Belhaj, K., Smoker, M., Joosten, M. H. A. J., Kamoun, S., & van der Hoorn, R. A. L. (2015). Functional Divergence of Two Secreted Immune Proteases of Tomato. *Current Biology : CB*, *25*(17), 2300–2306. https://doi.org/10.1016/j.cub.2015.07.030

Jiao, Y., Peluso, P., Shi, J., Liang, T., Stitzer, M. C., Wang, B., Campbell, M. S., Stein, J. C., Wei, X., Chin, C.-S., Guill, K., Regulski, M., Kumari, S., Olson, A., Gent, J., Schneider, K. L., Wolfgruber, T. K., May, M. R., Springer, N. M., … Ware, D. (2017). Improved maize reference genome with single-molecule technologies. *Nature*, *546*(7659), 524–527. https://doi.org/10.1038/nature22971

Jones, D. L., Nguyen, C., & Finlay, R. D. (2009). Carbon flow in the rhizosphere: carbon trading at the soil–root interface. *Plant and Soil*, *321*(1–2), 5–33. https://doi.org/10.1007/s11104-009-9925-0

Jones, J. D. G., & Dangl, J. L. (2006). The plant immune system. *Nature*, *444*(7117), 323–329. https://doi.org/10.1038/nature05286

Jones, J. D. G., Vance, R. E., & Dangl, J. L. (2016). Intracellular innate immune surveillance devices in plants and animals. *Science*, *354*(6316). https://doi.org/10.1126/science.aaf6395

Jumper, J., Evans, R., Pritzel, A., Green, T., Figurnov, M., Ronneberger, O., Tunyasuvunakool, K., Bates, R., Žídek, A., Potapenko, A., Bridgland, A., Meyer, C., Kohl, S. A. A., Ballard, A. J., Cowie, A., Romera-Paredes, B., Nikolov, S., Jain, R., Adler, J., … Hassabis, D. (2021). Highly accurate protein structure prediction with AlphaFold. *Nature*, *596*(7873), 583–589. https://doi.org/10.1038/s41586-021-03819-2

Jurczak, P., Groves, P., Szymanska, A., & Rodziewicz-Motowidlo, S. (2016). Human cystatin C monomer, dimer, oligomer, and amyloid structures are related to health and disease. *FEBS Letters*, *590*(23), 4192–4201. https://doi.org/10.1002/1873-3468.12463

Kaku, H., Nishizawa, Y., Ishii-Minami, N., Akimoto-Tomiyama, C., Dohmae, N., Takio, K., Minami, E., & Shibuya, N. (2006). Plant cells recognize chitin fragments for defense signaling through a plasma membrane receptor. *Proceedings of the National Academy of Sciences of the United States of America*, *103*(29), 11086–11091. https://doi.org/10.1073/pnas.0508882103

Kanaoka, Y., Takahashi, T., Nakayama, H., Ueno, T., & Sekine, T. (1982). Synthesis of a new fluorogenic substrate for cystine aminopeptidase. *Chemical & Pharmaceutical Bulletin*, *30*(4), 1485–1487. https://doi.org/10.1248/cpb.30.1485

Kantyka, T., Rawlings, N. D., & Potempa, J. (2010). Prokaryote-derived protein inhibitors of peptidases: A sketchy occurrence and mostly unknown function. *Biochimie*, *92*(11), 1644–1656. https://doi.org/10.1016/j.biochi.2010.06.004

Kaschani, F., Shabab, M., Bozkurt, T., Shindo, T., Schornack, S., Gu, C., Ilyas, M., Win, J., Kamoun, S., & van der Hoorn, R. A. L. (2010). An effector-targeted protease contributes to defense against *Phytophthora infestans* and is under diversifying selection in natural hosts. *Plant Physiology*, *154*(4), 1794–1804. https://doi.org/10.1104/pp.110.158030

Kaschani, F., & van der Hoorn, R. A. L. (2011). A model of the C14-EPIC complex indicates hotspots for a protease-inhibitor arms race in the oomycete-potato interaction. *Plant Signaling and Behavior*, *6*(1), 109–112. https://doi.org/10.4161/psb.6.1.14190

Kassambara, A. (2023). *ggpubr: "ggplot2" Based Publication Ready Plots* (0.6.0). https://github.com/kassambara/ggpubr

Katzy, P. (2025). *Identification of signaling peptides involved in immune responses in Zea mays*. University of Cologne.

Kędzior, M., Pawlak, A., Seredyński, R., Bania, J., Platt-Samoraj, A., Czemplik, M., Klausa, E., Bugla-Płoskońska, G., & Gutowicz, J. (2018). Revealing the inhibitory potential of *Yersinia enterocolitica* on cysteine proteases of the papain family. *Microbiological Research*, *207*(December 2017), 211–225. https://doi.org/10.1016/j.micres.2017.12.005

Klessig, D. F., Choi, H. W., & Dempsey, D. A. (2018). Systemic Acquired Resistance and Salicylic Acid: Past, Present, and Future. *Molecular Plant-Microbe Interactions : MPMI*, *31*(9), 871–888. https://doi.org/10.1094/MPMI-03-18-0067-CR

Koenig, M., Moser, D., Leusner, J., Depotter, J. R. L., Doehlemann, G., & Misas Villamil, J. (2023). Maize Phytocytokines Modulate Pro-Survival Host Responses and Pathogen Resistance. *Molecular Plant-Microbe Interactions®*, *36*(9), 592–604. https://doi.org/10.1094/MPMI-01-23-0005-R

Komsta, L. (2006). Processing data for outliers. *R News*, *6*(2), 10–13. https://cran.r-project.org/doc/Rnews/Rnews_2006-2.pdf

Kondo, S. I., Kawamura, K., Iwanaga, J., Hamada, M., & Aoyagi, T. (1969). Isolation and characterization of leupeptins produced by Actinomycetes. *Chemical & Pharmaceutical Bulletin*, *17*(9), 1896–1901. https://doi.org/10.1248/cpb.17.1896

König, M. F. (2024). *Role of signalling peptides in protease- mediated defence responses of maize*. Universität zu Köln.

Konovalova, A., & Silhavy, T. J. (2015). Outer membrane lipoprotein biogenesis: Lol is not the end. *Philosophical Transactions of the Royal Society B: Biological Sciences*, *370*(1679), 20150030. https://doi.org/10.1098/rstb.2015.0030

Krüger, J., Thomas, C. M., Golstein, C., Dixon, M. S., Smoker, M., Tang, S., Mulder, L., & Jones, J. D. G. (2002). A tomato cysteine protease required for Cf-2-dependent disease resistance and suppression of autonecrosis. *Science (New York, N.Y.)*, *296*(5568), 744–747. https://doi.org/10.1126/science.1069288

Krumbach, J. (2020). *Metabolic interactions facilitating stability in a model bacterial synthetic community from maize roots.* University of Cologne.

Krumbach, J., Kroll, P., Wewer, V., Metzger, S., Ischebeck, T., & Jacoby, R. P. (2021). Metabolic analysis of a bacterial synthetic community from maize roots provides new mechanistic insights into microbiome stability. *BioRxiv*, 2021.11.28.470254. https://doi.org/10.1101/2021.11.28.470254

Labes, M., Pühler, A., & Simon, R. (1990). A new family of RSF1010-derived expression and lac-fusion broad-host-range vectors for Gram-negative bacteria. *Gene*, *89*(1), 37–46. https://doi.org/10.1016/0378-1119(90)90203-4

Laflamme, B., Dillon, M. M., Martel, A., Almeida, R. N. D., Desveaux, D., & Guttman, D. S. (2020). The pan-genome effector-triggered immunity landscape of a host-pathogen interaction. *Science*, *367*(6479), 763–768. https://doi.org/10.1126/science.aax4079

Lampl, N., Alkan, N., Davydov, O., & Fluhr, R. (2013). Set-point control of RD21 protease activity by AtSerpin1 controls cell death in *Arabidopsis*. *The Plant Journal : For Cell and Molecular Biology*, *74*(3), 498–510. https://doi.org/10.1111/tpj.12141

Lan, L., Deng, X., Xiao, Y., Zhou, J.-M., & Tang, X. (2007). Mutation of Lon protease differentially affects the expression of *Pseudomonas syringae* type III secretion system genes in rich and minimal media and reduces pathogenicity. *Molecular Plant-Microbe Interactions : MPMI*, *20*(6), 682–696. https://doi.org/10.1094/MPMI-20-6-0682

Laskowski, M., & Kato, I. (1980). Protein Inhibitors of Proteinases. *Annual Review of Biochemistry*, *49*(1), 593–626. https://doi.org/10.1146/annurev.bi.49.070180.003113

Laura Darriba, M., Castro, C. P., Coria, L. M., Bruno, L., Laura Cerutti, M., Otero, L. H., Chemes, L. B., Rasia, R. M., Klinke, S., Cassataro, J., & Pasquevich, K. A. (2022). A disordered region retains the full protease inhibitor activity and the capacity to induce CD8+ T cells in vivo of the oral vaccine adjuvant U-Omp19. *Computational and Structural Biotechnology Journal*, *20*, 5098–5114. https://doi.org/10.1016/j.csbj.2022.08.054

Lawrence, C. J. (2004). MaizeGDB, the community database for maize genetics and genomics. *Nucleic Acids Research*, *32*(90001), 393D – 397. https://doi.org/10.1093/nar/gkh011

Lewenza, S., Mhlanga, M. M., & Pugsley, A. P. (2008). Novel Inner Membrane Retention Signals in *Pseudomonas aeruginosa* Lipoproteins. *Journal of Bacteriology*, *190*(18), 6119–6125. https://doi.org/10.1128/JB.00603-08

Lewenza, S., Vidal-Ingigliardi, D., & Pugsley, A. P. (2006). Direct Visualization of Red Fluorescent Lipoproteins Indicates Conservation of the Membrane Sorting Rules in the Family Enterobacteriaceae. *Journal of Bacteriology*, *188*(10), 3516–3524. https://doi.org/10.1128/JB.188.10.3516-3524.2006

Lewis, J. D., Lee, A. H.-Y., Hassan, J. A., Wan, J., Hurley, B., Jhingree, J. R., Wang, P. W., Lo, T., Youn, J.-Y., Guttman, D. S., & Desveaux, D. (2013). The *Arabidopsis* ZED1 pseudokinase is required for ZAR1-mediated immunity induced by the *Pseudomonas syringae* type III effector HopZ1a. *Proceedings of the National Academy of Sciences*, *110*(46), 18722–18727. https://doi.org/10.1073/pnas.1315520110

Lewis, J. D., Wu, R., Guttman, D. S., & Desveaux, D. (2010). Allele-Specific Virulence Attenuation of the *Pseudomonas syringae* HopZ1a Type III Effector via the *Arabidopsis* ZAR1 Resistance Protein. *PLoS Genetics*, *6*(4), e1000894. https://doi.org/10.1371/journal.pgen.1000894

Leyton, D. L., Rossiter, A. E., & Henderson, I. R. (2012). From self sufficiency to dependence: mechanisms and factors important for autotransporter biogenesis. *Nature Reviews Microbiology*, *10*(3), 213–225. https://doi.org/10.1038/nrmicro2733

Li, C., Luo, S., Feng, L., Wang, Q., Cheng, J., Xie, J., Lin, Y., Fu, Y., Jiang, D., & Chen, T. (2023). Protist ubiquitin ligase effector PbE3-2 targets cysteine protease RD21A to impede plant immunity. *Plant Physiology*, 2022.10.26.513834. https://doi.org/10.1093/plphys/kiad603

Li, H. (2013). *Aligning sequence reads, clone sequences and assembly contigs with BWA-MEM*. *00*(00), 1–3. http://arxiv.org/abs/1303.3997

Li, Q., Shao, J., Luo, M., Chen, D., Tang, D., & Shi, H. (2024a). BRASSINOSTEROID-SIGNALING KINASE1 associates with and is required for cysteine protease RESPONSE TO DEHYDRATION 19-mediated disease resistance in *Arabidopsis*. *Plant Science : An International Journal of Experimental Plant Biology*, *342*, 112033. https://doi.org/10.1016/j.plantsci.2024.112033

Li, T., Moreno-Pérez, A., & Coaker, G. (2024b). Plant Pattern recognition receptors: Exploring their evolution, diversification, and spatiotemporal regulation. *Current Opinion in Plant Biology*, *82*, 102631. https://doi.org/10.1016/j.pbi.2024.102631

Liacouras, A. S., & Anderson, E. P. (1977). Uridine-cytidine kinase III. Competition between uridine and cytidine for a single enzyme. *Molecular and Cellular Biochemistry*, *17*(3), 141–146. https://doi.org/10.1007/BF01730833

Lin Pedersen, T. (2024). *patchwork: The Composer of Plots* (1.3.0.9000). https://github.com/thomasp85/patchwork

Ling, C., Zhang, J., Lin, D., & Tao, A. (2015). Approaches for the generation of active papain-like cysteine proteases from inclusion bodies of *Escherichia coli*. *World Journal of Microbiology and Biotechnology*, *31*(5), 681–690. https://doi.org/10.1007/s11274-015-1804-7

Liu, H., Hu, M., Wang, Q., Cheng, L., & Zhang, Z. (2018a). Role of papain-like cysteine proteases in plant development. *Frontiers in Plant Science*, *871*(December), 1–10. https://doi.org/10.3389/fpls.2018.01717

Liu, M., Wang, F., He, B., Hu, J., Dai, Y., Chen, W., Yi, M., Zhang, H., Ye, Y., Cui, Z., Zheng, X., Wang, P., Xing, W., & Zhang, Z. (2024a). Targeting *Magnaporthe oryzae* effector MoErs1 and host papain-like protease OsRD21 interaction to combat rice blast. *Nature Plants*, *10*(4), 618–632. https://doi.org/10.1038/s41477-024-01642-x

Liu, P., Shi, C., Liu, S., Lei, J., Lu, Q., Hu, H., Ren, Y., Zhang, N., Sun, C., Chen, L., Jiang, Y., Feng, L., Zhang, T., Zhong, K., Liu, J., Zhang, J., Zhang, Z., Sun, B., Chen, J., … Yang, J. (2023). A papain-like cysteine protease-released small signal peptide confers wheat resistance to wheat yellow mosaic virus. *Nature Communications*, *14*(1), 7773. https://doi.org/10.1038/s41467-023-43643-y

Liu, Y., Gong, T., Kong, X., Sun, J., & Liu, L. (2024b). XYLEM CYSTEINE PEPTIDASE 1 and its inhibitor CYSTATIN 6 regulate pattern-triggered immunity by modulating the stability of the NADPH oxidase RESPIRATORY BURST OXIDASE HOMOLOG D. *The Plant Cell*, *36*(2), 471–488. https://doi.org/10.1093/plcell/koad262

Liu, Y., Jackson, E., Liu, X., Huang, X., van der Hoorn, R. A. L., Zhang, Y., & Li, X. (2024c). Proteolysis in plant immunity. *The Plant Cell*, *36*(9), 3099–3115. https://doi.org/10.1093/plcell/koae142

Liu, Y., Wang, K., Cheng, Q., Kong, D., Zhang, X., Wang, Z., Wang, Q., Xie, Q., Yan, J., Chu, J., Ling, H.-Q., Li, Q., Miao, J., & Zhao, B. (2020). Cysteine protease RD21A regulated by E3 ligase SINAT4 is required for drought-induced resistance to *Pseudomonas syringae* in *Arabidopsis*. *Journal of Experimental Botany*, *71*(18), 5562–5576. https://doi.org/10.1093/jxb/eraa255

Liu, Z., Beskrovnaya, P., Melnyk, R. A., Hossain, S. S., Khorasani, S., O'Sullivan, L. R., Wiesmann, C. L., Bush, J., Richard, J. D., & Haney, C. H. (2018b). A Genome-Wide Screen Identifies Genes in Rhizosphere-Associated *Pseudomonas* Required to Evade Plant Defenses. *MBio*, *9*(6). https://doi.org/10.1128/mBio.00433-18

Livak, K. J., & Schmittgen, T. D. (2001). Analysis of relative gene expression data using real-time quantitative PCR and the 2-ΔΔCT method. *Methods*, *25*(4), 402–408. https://doi.org/10.1006/meth.2001.1262

Loper, J. E., Hassan, K. A., Mavrodi, D. V, Davis, E. W. 2nd, Lim, C. K., Shaffer, B. T., Elbourne, L. D. H., Stockwell, V. O., Hartney, S. L., Breakwell, K., Henkels, M. D., Tetu, S. G., Rangel, L. I., Kidarsa, T. A., Wilson, N. L., van de Mortel, J. E., Song, C., Blumhagen, R., Radune, D., … Paulsen, I. T. (2012). Comparative genomics of plant-associated *Pseudomonas* spp.: insights into diversity and inheritance of traits involved in multitrophic interactions. *PLoS Genetics*, *8*(7), e1002784. https://doi.org/10.1371/journal.pgen.1002784

Lorenz, C., Dougherty, T. J., & Lory, S. (2019). Correct sorting of lipoproteins into the inner and outer membranes of *Pseudomonas aeruginosa* by the *Escherichia coli* LolCDE transport system. *MBio*, *10*(2), 1–13. https://doi.org/10.1128/MBIO.00194-19

Losada, L. C., & Hutcheson, S. W. (2005). Type III secretion chaperones of *Pseudomonas syringae* protect effectors from Lon-associated degradation. *Molecular Microbiology*, *55*(3), 941–953. https://doi.org/10.1111/j.1365-2958.2004.04438.x

LoVullo, E. D., Wright, L. F., Isabella, V., Huntley, J. F., & Pavelka, M. S. (2015). Revisiting the gram-negative lipoprotein paradigm. *Journal of Bacteriology*, *197*(10), 1705–1715. https://doi.org/10.1128/JB.02414-14

Lozano-Torres, J. L., Wilbers, R. H. P., Gawronski, P., Boshoven, J. C., Finkers-Tomczak, A., Cordewener, J. H. G., America, A. H. P., Overmars, H. A., Van 't Klooster, J. W., Baranowski, L., Sobczak, M., Ilyas, M., Van Der Hoorn, R. A. L., Schots, A., De Wit, P. J. G. M., Bakker, J., Goverse, A., & Smant, G. (2012). Dual disease resistance mediated by the immune receptor Cf-2 in tomato requires a common virulence target of a fungus and a nematode. *Proceedings of the National Academy of Sciences of the United States of America*, *109*(25), 10119–10124. https://doi.org/10.1073/pnas.1202867109

Lozano-Torres, J. L., Wilbers, R. H. P., Warmerdam, S., Finkers-Tomczak, A., Diaz-Granados, A., van Schaik, C. C., Helder, J., Bakker, J., Goverse, A., Schots, A., & Smant, G. (2014). Apoplastic Venom Allergen-like Proteins of Cyst Nematodes Modulate the Activation of Basal Plant Innate Immunity by Cell Surface Receptors. *PLoS Pathogens*, *10*(12), e1004569. https://doi.org/10.1371/journal.ppat.1004569

Lü, P., Liu, Y., Yu, X., Shi, C.-L., & Liu, X. (2022). The right microbe-associated molecular patterns for effective recognition by plants. *Frontiers in Microbiology*, *13*(September), 1–10. https://doi.org/10.3389/fmicb.2022.1019069

Luo, Q., Wang, C., Qiao, S., Yu, S., Chen, L., Kim, S., Wang, K., Zheng, J., Zhang, Y., Wu, F., Lei, X., Lou, J., Hennig, M., Im, W., Miao, L., Zhou, M., & Huang, Y. (2022). Lipoprotein sorting to the cell surface via a crosstalk between the Lpt and Lol pathways during outer membrane biogenesis. In *bioRxiv* (p. 2022.12.25.521893). https://doi.org/10.1101/2022.12.25.521893

Luthy, J. A., Praissman, M., Finkenstadt, W. R., & Laskowski, M. (1973). Detailed mechanism of interaction of bovine-trypsin with soybean trypsin inhibitor (Kunitz). I. Stopped flow measurements. *The Journal of Biological Chemistry*, *248*(5), 1760–1771. http://www.ncbi.nlm.nih.gov/pubmed/4735140

Ma, W., Dong, F. F. T., Stavrinides, J., & Guttman, D. S. (2006). Type III Effector Diversification via Both Pathoadaptation and Horizontal Transfer in Response to a Coevolutionary Arms Race. *PLoS Genetics*, *2*(12), e209. https://doi.org/10.1371/journal.pgen.0020209

Madeira, F., Madhusoodanan, N., Lee, J., Eusebi, A., Niewielska, A., Tivey, A. R. N., Lopez, R., & Butcher, S. (2024). The EMBL-EBI Job Dispatcher sequence analysis tools framework in 2024. *Nucleic Acids Research*, *52*(W1), W521–W525. https://doi.org/10.1093/nar/gkae241

Mann, E. E., & Wozniak, D. J. (2012). *Pseudomonas* biofilm matrix composition and niche biology. *FEMS Microbiology Reviews*, *36*(4), 893–916. https://doi.org/10.1111/j.1574-6976.2011.00322.x

Manning, A. J., & Kuehn, M. J. (2011). Contribution of bacterial outer membrane vesicles to innate bacterial defense. *BMC Microbiology*, *11*(1), 258. https://doi.org/10.1186/1471-2180-11-258

Martin, M. (2011). Cutadapt removes adapter sequences from high-throughput sequencing reads. *EMBnet.Journal*, *17*(1), 10. https://doi.org/10.14806/ej.17.1.200

Martínez-Gil, M., Yousef-Coronado, F., & Espinosa-Urgel, M. (2010). LapF, the second largest *Pseudomonas putida* protein, contributes to plant root colonization and determines biofilm architecture. *Molecular Microbiology*, *77*(3), 549–561. https://doi.org/10.1111/j.1365-2958.2010.07249.x

Martínez, M., Cambra, I., González-Melendi, P., Santamaría, M. E., & Díaz, I. (2012). C1A cysteine-proteases and their inhibitors in plants. *Physiologia Plantarum*, *145*(1), 85–94. https://doi.org/10.1111/j.1399-3054.2012.01569.x

Martinez, M., & Diaz, I. (2008). The origin and evolution of plant cystatins and their target cysteine proteinases indicate a complex functional relationship. *BMC Evolutionary Biology*, *8*, 198. https://doi.org/10.1186/1471-2148-8-198

Matei, A. (2016). *Identification of seedling-specific effectors in the Ustilago maydis – maize interaction : From organ to cell type specificity* (Prof. Dr. Döhlemann (ed.)). Philipps-Universität Marburg. https://doi.org/10.17192/z2017.0074 CN - diss/z2017/0074

Matilla, M. A., Espinosa-Urgel, M., Rodríguez-Herva, J. J., Ramos, J. L., & Ramos-González, M. I. (2007). Genomic analysis reveals the major driving forces of bacterial life in the rhizosphere. *Genome Biology*, *8*(9), R179. https://doi.org/10.1186/gb-2007-8-9-r179

Matsui, S., Noda, S., Kuwata, K., Nomoto, M., Tada, Y., Shinohara, H., & Matsubayashi, Y. (2024). *Arabidopsis* SBT5.2 and SBT1.7 subtilases mediate C-terminal cleavage of flg22 epitope from bacterial flagellin. *Nature Communications*, *15*(1), 3762. https://doi.org/10.1038/s41467-024-48108-4

Matsumoto, A., Schlüter, T., Melkonian, K., Takeda, A., Nakagami, H., & Mine, A. (2022). A versatile Tn7 transposon-based bioluminescence tagging tool for quantitative and spatial detection of bacteria in plants. *Plant Communications*, *3*(1), 100227. https://doi.org/10.1016/j.xplc.2021.100227

Matsumoto, K., Yamamoto, D., Ohishi, H., Tomoo, K., Ishida, T., Inoue, M., Sadatome, T., Kitamura, K., & Mizuno, H. (1989). Mode of binding of E-64-c, a potent thiol protease inhibitor, to papain as determined by X-ray crystal analysis of the complex. *FEBS Letters*, *245*(1–2), 177–180. https://doi.org/10.1016/0014-5793(89)80216-9

Mavrodi, D. V., Joe, A., Mavrodi, O. V., Hassan, K. A., Weller, D. M., Paulsen, I. T., Loper, J. E., Alfano, J. R., & Thomashow, L. S. (2011). Structural and Functional Analysis of the Type III Secretion System from *Pseudomonas fluorescens* Q8r1-96. *Journal of Bacteriology*, *193*(1), 177–189. https://doi.org/10.1128/JB.00895-10

McConnell, R. M., York, J. L., Frizzell, D., & Ezell, C. (1993). Inhibition studies of some serine and thiol proteinases by new leupeptin analogs. *Journal of Medicinal Chemistry*, *36*(8), 1084–1089. https://doi.org/10.1021/jm00060a016

McKinney, W. (2010). Data Structures for Statistical Computing in Python. *Proceedings of the 9th Python in Science Conference*, *1*(Scipy), 56–61. https://doi.org/10.25080/majora-92bf1922-00a

McMillan, H. M., & Kuehn, M. J. (2023). Proteomic Profiling Reveals Distinct Bacterial Extracellular Vesicle Subpopulations with Possibly Unique Functionality. *Applied and Environmental Microbiology*, *89*(1), e0168622. https://doi.org/10.1128/aem.01686-22

Meyer, J. M. (2000). Pyoverdines: pigments, siderophores and potential taxonomic markers of fluorescent *Pseudomonas* species. *Archives of Microbiology*, *174*(3), 135–142. https://doi.org/10.1007/s002030000188

Miller, G., Schlauch, K., Tam, R., Cortes, D., Torres, M. A., Shulaev, V., Dangl, J. L., & Mittler, R. (2009). The plant NADPH oxidase RBOHD mediates rapid systemic signaling in response to diverse stimuli. *Science Signaling*, *2*(84), 1–10. https://doi.org/10.1126/scisignal.2000448

Millet, Y. A., Danna, C. H., Clay, N. K., Songnuan, W., Simon, M. D., Werck-Reichhart, D., & Ausubel, F. M. (2010). Innate Immune Responses Activated in *Arabidopsis* Roots by Microbe-Associated Molecular Patterns. *The Plant Cell*, *22*(3), 973–990. https://doi.org/10.1105/tpc.109.069658

Mirdita, M., Schütze, K., Moriwaki, Y., Heo, L., Ovchinnikov, S., & Steinegger, M. (2022). ColabFold: making protein folding accessible to all. *Nature Methods*, *19*(6), 679–682. https://doi.org/10.1038/s41592-022-01488-1

Misas-Villamil, J. C., Kolodziejek, I., Crabill, E., Kaschani, F., Niessen, S., Shindo, T., Kaiser, M., Alfano, J. R., & van der Hoorn, R. A. L. (2013). *Pseudomonas syringae* pv. *syringae* Uses Proteasome Inhibitor Syringolin A to Colonize from Wound Infection Sites. *PLoS Pathogens*, *9*(3), e1003281. https://doi.org/10.1371/journal.ppat.1003281

Misas-Villamil, J. C., van der Hoorn, R. A. L., & Doehlemann, G. (2016). Papain-like cysteine proteases as hubs in plant immunity. *New Phytologist*, *212*(4), 902–907. https://doi.org/10.1111/nph.14117

Misas Villamil, J. C., Mueller, A. N., Demir, F., Meyer, U., Ökmen, B., Schulze Hüynck, J., Breuer, M., Dauben, H., Win, J., Huesgen, P. F., & Doehlemann, G. (2019). A fungal substrate mimicking molecule suppresses plant immunity via an inter-kingdom conserved motif. *Nature Communications*, *10*(1). https://doi.org/10.1038/s41467-019-09472-8

Miya, A., Albert, P., Shinya, T., Desaki, Y., Ichimura, K., Shirasu, K., Narusaka, Y., Kawakami, N., Kaku, H., & Shibuya, N. (2007). CERK1, a LysM receptor kinase, is essential for chitin elicitor signaling in *Arabidopsis*. *Proceedings of the National Academy of Sciences of the United States of America*, *104*(49), 19613–19618. https://doi.org/10.1073/pnas.0705147104

Monteiro, A. C. S., Abrahamson, M., Lima, A. P. C. A., Vannier-Santos, M. A., & Scharfstein, J. (2001). Identification, characterization and localization of chagasin, a tight-binding cysteine protease inhibitor in *Trypanosoma cruzi*. *Journal of Cell Science*, *114*(21), 3933–3942. https://doi.org/10.1242/jcs.114.21.3933

Moser, D. (2021). *Root immune signaling: proteases, their inhibitors and signaling peptides*. Heinrich-Heine-Universität Düsseldorf.

Mueller, A. N., Ziemann, S., Treitschke, S., Aßmann, D., & Doehlemann, G. (2013). Compatibility in the *Ustilago maydis*-Maize Interaction Requires Inhibition of Host Cysteine Proteases by the Fungal Effector Pit2. *PLoS Pathogens*, *9*(2). https://doi.org/10.1371/journal.ppat.1003177

Mulcahy, L. R., Isabella, V. M., & Lewis, K. (2014). *Pseudomonas aeruginosa* Biofilms in Disease. *Microbial Ecology*, *68*(1), 1–12. https://doi.org/10.1007/s00248-013-0297-x

Muriel, C., Jalvo, B., Redondo-Nieto, M., Rivilla, R., & Martín, M. (2015). Chemotactic Motility of *Pseudomonas fluorescens* F113 under Aerobic and Denitrification Conditions. *PLOS ONE*, *10*(7), e0132242. https://doi.org/10.1371/journal.pone.0132242

Narita, S.-I., & Tokuda, H. (2007). Amino Acids at Positions 3 and 4 Determine the Membrane Specificity of *Pseudomonas aeruginosa* Lipoproteins. *Journal of Biological Chemistry*, *282*(18), 13372–13378. https://doi.org/10.1074/jbc.M611839200

Natale, P., Brüser, T., & Driessen, A. J. M. (2008). Sec- and Tat-mediated protein secretion across the bacterial cytoplasmic membrane-Distinct translocases and mechanisms. *Biochimica et Biophysica Acta - Biomembranes*, *1778*(9), 1735–1756. https://doi.org/10.1016/j.bbamem.2007.07.015

Neubig, R. R., Spedding, M., Kenakin, T., & Christopoulos, A. (2003). International Union of Pharmacology Committee on Receptor Nomenclature and Drug Classification. XXXVIII. Update on Terms and Symbols in Quantitative Pharmacology. *Pharmacological Reviews*, *55*(4), 597–606. https://doi.org/10.1124/pr.55.4.4

Ngou, B. P. M., Ding, P., & Jones, J. D. G. (2022). Thirty years of resistance: Zig-zag through the plant immune system. *The Plant Cell*, *34*(5), 1447–1478. https://doi.org/10.1093/plcell/koac041

Niño, M. C., Kang, K. K., & Cho, Y.-G. (2020). Genome-wide transcriptional response of papain-like cysteine protease-mediated resistance against *Xanthomonas oryzae* pv. *oryzae* in rice. *Plant Cell Reports*, *39*(4), 457–472. https://doi.org/10.1007/s00299-019-02502-1

Nishad, R., Ahmed, T., Rahman, V. J., & Kareem, A. (2020). Modulation of Plant Defense System in Response to Microbial Interactions. *Frontiers in Microbiology*, *11*(July), 1–13. https://doi.org/10.3389/fmicb.2020.01298

Niu, B., Paulson, J. N., Zheng, X., & Kolter, R. (2017). Simplified and representative bacterial community of maize roots. *Proceedings of the National Academy of Sciences of the United States of America*, *114*(12), E2450–E2459. https://doi.org/10.1073/pnas.1616148114

Oksanen, J., Blanchet, F. G., Kindt, R., Legendre, P., Minchin, P., O'Hara, B., Simpson, G., Solymos, P., Stevens, H., & Wagner, H. (2018). *Vegan: Community Ecology Package*. https://github.com/vegandevs/vegan

Ooms, J. (2024). *writexl: Export Data Frames to Excel "xlsx" Format.* (1.5.1). https://ropensci.r-universe.dev/writexl

Orench-Rivera, N., & Kuehn, M. J. (2016). Environmentally controlled bacterial vesicle-mediated export. *Cellular Microbiology*, *18*(11), 1525–1536. https://doi.org/10.1111/cmi.12676

Orozco-Cardenas, M., & Ryan, C. A. (1999). Hydrogen peroxide is generated systemically in plant leaves by wounding and systemin via the octadecanoid pathway. *Proceedings of the National Academy of Sciences of the United States of America*, *96*(11), 6553–6557. https://doi.org/10.1073/pnas.96.11.6553

Osorio, D., Rondon-Villarreal, P., & Torres, R. (2015). Peptides: A package for data mining of antimicrobial peptides. *The R Journal*, *7*(1), 4–14. https://journal.r-project.org/archive/2015/RJ-2015-001/RJ-2015-001.pdf

Oukala, N., Aissat, K., & Pastor, V. (2021). Bacterial Endophytes: The Hidden Actor in Plant Immune Responses against Biotic Stress. *Plants*, *10*(5), 1012. https://doi.org/10.3390/plants10051012

Pagès, H., Aboyoun, P., Gentleman, R., & DebRoy, S. (2024). *Biostrings: Efficient manipulation of biological strings.* (2.74). https://doi.org/10.18129/B9.bioc.Biostrings

Paireder, M., Mehofer, U., Tholen, S., Porodko, A., Schähs, P., Maresch, D., Biniossek, M. L., Van Der Hoorn, R. A. L., Lenarcic, B., Novinec, M., Schilling, O., & Mach, L. (2016). The death enzyme CP14 is a unique papain-like cysteine proteinase with a pronounced S2 subsite selectivity. *Archives of Biochemistry and Biophysics*, *603*, 110–117. https://doi.org/10.1016/j.abb.2016.05.017

Parales, R. E., Luu, R. A., Chen, G. Y., Liu, X., Wu, V., Lin, P., Hughes, J. G., Nesteryuk, V., Parales, J. V, & Ditty, J. L. (2013). *Pseudomonas putida* F1 has multiple chemoreceptors with overlapping specificity for organic acids. *Microbiology*, *159*(Pt_6), 1086–1096. https://doi.org/10.1099/mic.0.065698-0

Paredes-Osses, E., & Hardie, K. (2013). Cell Fractionation of *Pseudomonas aeruginosa*. *BIO-PROTOCOL*, *3*(19), 2–6. https://doi.org/10.21769/BioProtoc.922

Park, A. J., Murphy, K., Surette, M. D., Bandoro, C., Krieger, J. R., Taylor, P., & Khursigara, C. M. (2015). Tracking the Dynamic Relationship between Cellular Systems and Extracellular Subproteomes in *Pseudomonas aeruginosa* Biofilms. *Journal of Proteome Research*, *14*(11), 4524–4537. https://doi.org/10.1021/acs.jproteome.5b00262

Pasquevich, K. A., Carabajal, M. V., Guaimas, F. F., Bruno, L., Roset, M. S., Coria, L. M., Rey Serrantes, D. A., Comerci, D. J., & Cassataro, J. (2019). Omp19 Enables *Brucella abortus* to Evade the Antimicrobial Activity From Host's Proteolytic Defense System. *Frontiers in Immunology*, *10*(JUN), 1436. https://doi.org/10.3389/fimmu.2019.01436

Passarge, A., Demir, F., Green, K., Depotter, J. R. L., Scott, B., Huesgen, P. F., Doehlemann, G., & Misas Villamil, J. C. (2021). Host apoplastic cysteine protease activity is suppressed during the mutualistic association of *Lolium perenne* and *Epichloë festucae*. *Journal of Experimental Botany*, *72*(9), 3410–3426. https://doi.org/10.1093/jxb/erab088

Paulus, J. K., Kourelis, J., Ramasubramanian, S., Homma, F., Godson, A., Hörger, A. C., Hong, T. N., Krahn, D., Carballo, L. O., Wang, S., Win, J., Smoker, M., Kamoun, S., Dong, S., & Van Der Hoorn, R. A. L. (2020). Extracellular proteolytic cascade in tomato activates immune protease Rcr3. *Proceedings of the National Academy of Sciences of the United States of America*, *117*(29), 17409–17417. https://doi.org/10.1073/pnas.1921101117

Pechan, T., Ye, L., Chang, Y., Mitra, A., Lin, L., Davis, F. M., Williams, W. P., & Luthe, D. S. (2000). A unique 33-kD cysteine proteinase accumulates in response to larval feeding in maize genotypes resistant to fall armyworm and other Lepidoptera. *The Plant Cell*, *12*(7), 1031–1040. https://doi.org/10.1105/tpc.12.7.1031

Peix, A., Ramírez-Bahena, M.-H., & Velázquez, E. (2018). The current status on the taxonomy of *Pseudomonas* revisited: An update. *Infection, Genetics and Evolution*, *57*(October 2017), 106–116. https://doi.org/10.1016/j.meegid.2017.10.026

Pérez-López, E., Hossain, M. M., Wei, Y., Todd, C. D., & Bonham-Smith, P. C. (2021). A clubroot pathogen effector targets cruciferous cysteine proteases to suppress plant immunity. *Virulence*, *12*(1), 2327–2340. https://doi.org/10.1080/21505594.2021.1968684

Pernas, M., Sánchez-Monge, R., Gómez, L., & Salcedo, G. (1998). A chestnut seed cystatin differentially effective against cysteine proteinases from closely related pests. *Plant Molecular Biology*, *38*(6), 1235–1242. https://doi.org/10.1023/a:1006154829118

Petricka, J. J., Winter, C. M., & Benfey, P. N. (2012). Control of *Arabidopsis* root development. *Annual Review of Plant Biology*, *63*, 563–590. https://doi.org/10.1146/annurev-arplant-042811-105501

Pierce, J. V., Fellows, J. D., Anderson, D. E., & Bernstein, H. D. (2021). A clostripain-like protease plays a major role in generating the secretome of enterotoxigenic *Bacteroides fragilis*. *Molecular Microbiology*, *115*(2), 290–304. https://doi.org/10.1111/mmi.14616

Pieterse, C. M. J., Van der Does, D., Zamioudis, C., Leon-Reyes, A., & Van Wees, S. C. M. (2012). Hormonal modulation of plant immunity. *Annual Review of Cell and Developmental Biology*, *28*, 489–521. https://doi.org/10.1146/annurev-cellbio-092910-154055

Pocklington, T., & Jeffery, J. (1969). Competition of two substrates for a single enzyme. A simple kinetic theorem exemplified by a hydroxy steroid dehydrogenase reaction. *The Biochemical Journal*, *112*(3), 331–334. https://doi.org/10.1042/bj1120331

Pogorelko, G. V, Juvale, P. S., Rutter, W. B., Hütten, M., Maier, T. R., Hewezi, T., Paulus, J., van der Hoorn, R. AL, Grundler, F. M., Siddique, S., Lionetti, V., Zabotina, O. A., & Baum, T. J. (2019). Re-targeting of a plant defense protease by a cyst nematode effector. *The Plant Journal*, *98*(6), 1000–1014. https://doi.org/10.1111/tpj.14295

Poncini, L., Wyrsch, I., Dénervaud Tendon, V., Vorley, T., Boller, T., Geldner, N., Métraux, J.-P., & Lehmann, S. (2017). In roots of *Arabidopsis thaliana*, the damage-associated molecular pattern AtPep1 is a stronger elicitor of immune signalling than flg22 or the chitin heptamer. *PLOS ONE*, *12*(10), e0185808. https://doi.org/10.1371/journal.pone.0185808

Price, M. N., & Arkin, A. P. (2017). PaperBLAST: Text Mining Papers for Information about Homologs. *MSystems*, *2*(4), 10.1128/msystems.00039-17. https://doi.org/10.1128/mSystems.00039-17

Price, M. N., Wetmore, K. M., Waters, R. J., Callaghan, M., Ray, J., Liu, H., Kuehl, J. V., Melnyk, R. A., Lamson, J. S., Suh, Y., Carlson, H. K., Esquivel, Z., Sadeeshkumar, H., Chakraborty, R., Zane, G. M., Rubin, B. E., Wall, J. D., Visel, A., Bristow, J., … Deutschbauer, A. M. (2018). Mutant phenotypes for thousands of bacterial genes of unknown function. *Nature*, *557*(7706), 503–509. https://doi.org/10.1038/s41586-018-0124-0

Radisky, E. S., & Koshland, D. E. (2002). A clogged gutter mechanism for protease inhibitors. *Proceedings of the National Academy of Sciences*, *99*(16), 10316–10321. https://doi.org/10.1073/pnas.112332899

Rappsilber, J., Mann, M., & Ishihama, Y. (2007). Protocol for micro-purification, enrichment, pre-fractionation and storage of peptides for proteomics using StageTips. *Nature Protocols*, *2*(8), 1896–1906. https://doi.org/10.1038/nprot.2007.261

Rascovan, N., Carbonetto, B., Perrig, D., Díaz, M., Canciani, W., Abalo, M., Alloati, J., González-Anta, G., & Vazquez, M. P. (2016). Integrated analysis of root microbiomes of soybean and wheat from agricultural fields. *Scientific Reports*, *6*(1), 28084. https://doi.org/10.1038/srep28084

Rawlings, N. D., Waller, M., Barrett, A. J., & Bateman, A. (2014). MEROPS: the database of proteolytic enzymes, their substrates and inhibitors. *Nucleic Acids Research*, *42*(Database issue), D503-9. https://doi.org/10.1093/nar/gkt953

Reavy, B., Bagirova, S., Chichkova, N. V., Fedoseeva, S. V., Kim, S. H., Vartapetian, A. B., & Taliansky, M. E. (2007). Caspase-resistant VirD2 protein provides enhanced gene delivery and expression in plants. *Plant Cell Reports*, *26*(8), 1215–1219. https://doi.org/10.1007/s00299-007-0335-6

Redondo-Nieto, M., Barret, M., Morrissey, J., Germaine, K., Martínez-Granero, F., Barahona, E., Navazo, A., Sánchez-Contreras, M., Moynihan, J. A., Muriel, C., Dowling, D., O'Gara, F., Martín, M., & Rivilla, R. (2013). Genome sequence reveals that *Pseudomonas fluorescens* F113 possesses a large and diverse array of systems for rhizosphere function and host interaction. *BMC Genomics*, *14*(1), 54. https://doi.org/10.1186/1471-2164-14-54

Redzynia, I., Ljunggren, A., Abrahamson, M., Mort, J. S., Krupa, J. C., Jaskolski, M., & Bujacz, G. (2008). Displacement of the Occluding Loop by the Parasite Protein, Chagasin, Results in Efficient Inhibition of Human Cathepsin B. *Journal of Biological Chemistry*, *283*(33), 22815–22825. https://doi.org/10.1074/jbc.M802064200

Redzynia, I., Ljunggren, A., Bujacz, A., Abrahamson, M., Jaskolski, M., & Bujacz, G. (2009). Crystal structure of the parasite inhibitor chagasin in complex with papain allows identification of structural requirements for broad reactivity and specificity determinants for target proteases. *FEBS Journal*, *276*(3), 793–806. https://doi.org/10.1111/j.1742-4658.2008.06824.x

Rehman, A. A., Ahsan, H., & Khan, F. H. (2013). Alpha-2-macroglobulin: A physiological guardian. *Journal of Cellular Physiology*, *228*(8), 1665–1675. https://doi.org/10.1002/jcp.24266

Reigada, I., San-Martin-Galindo, P., Gilbert-Girard, S., Chiaro, J., Cerullo, V., Savijoki, K., Nyman, T. A., Fallarero, A., & Miettinen, I. (2021). Surfaceome and Exoproteome Dynamics in Dual-Species *Pseudomonas aeruginosa* and *Staphylococcus aureus* Biofilms. *Frontiers in Microbiology*, *12*. https://doi.org/10.3389/fmicb.2021.672975

Remans, K., Vercammen, K., Bodilis, J., & Cornelis, P. (2010). Genome-wide analysis and literature-based survey of lipoproteins in *Pseudomonas aeruginosa*. *Microbiology (Reading, England)*, *156*(Pt 9), 2597–2607. https://doi.org/10.1099/mic.0.040659-0

Remick, B. C., Gaidt, M. M., & Vance, R. E. (2023). Effector-Triggered Immunity. *Annual Review of Immunology*, *41*(1), 453–481. https://doi.org/10.1146/annurev-immunol-101721-031732

Richau, K. H., Kaschani, F., Verdoes, M., Pansuriya, T. C., Niessen, S., Stüber, K., Colby, T., Overkleeft, H. S., Bogyo, M., & van der Hoorn, R. A. L. (2012). Subclassification and biochemical analysis of plant papain-like cysteine proteases displays subfamily-specific characteristics. *Plant Physiology*, *158*(4), 1583–1599. https://doi.org/10.1104/pp.112.194001

Rigden, D. J., Mosolov, V. V., & Galperin, M. Y. (2002). Sequence conservation in the chagasin family suggests a common trend in cysteine proteinase binding by unrelated protein inhibitors. *Protein Science*, *11*(8), 1971–1977. https://doi.org/10.1110/ps.0207202

Rivilla, R., & Malone, J. G. (2023). Plant-Associated Pseudomonads. *Microorganisms*, *11*(5), 1216. https://doi.org/10.3390/microorganisms11051216

Rizaludin, M. S., Stopnisek, N., Raaijmakers, J. M., & Garbeva, P. (2021). The chemistry of stress: Understanding the 'cry for help' of plant roots. *Metabolites*, *11*(6). https://doi.org/10.3390/metabo11060357

Robatzek, S., Chinchilla, D., & Boller, T. (2006). Ligand-induced endocytosis of the pattern recognition receptor FLS2 in *Arabidopsis*. *Genes & Development*, *20*(5), 537–542. https://doi.org/10.1101/gad.366506

Robert-Genthon, M., Casabona, M. G., Neves, D., Couté, Y., Cicéron, F., Elsen, S., Dessen, A., & Attrée, I. (2013). Unique Features of a *Pseudomonas aeruginosa* α2-Macroglobulin Homolog. *MBio*, *4*(4), 1–10. https://doi.org/10.1128/mBio.00309-13

Rooney, H. C. E., Van't Klooster, J. W., van der Hoorn, R. A. L., Joosten, M. H. A. J., Jones, J. D. G., & de Wit, P. J. G. M. (2005). *Cladosporium* Avr2 inhibits tomato Rcr3 protease required for Cf-2-dependent disease resistance. *Science (New York, N.Y.)*, *308*(5729), 1783–1786. https://doi.org/10.1126/science.1111404

Rufián, J. S., Rueda-Blanco, J., López-Márquez, D., Macho, A. P., Beuzón, C. R., & Ruiz-Albert, J. (2021). The bacterial effector HopZ1a acetylates MKK7 to suppress plant immunity. *New Phytologist*, *231*(3), 1138–1156. https://doi.org/10.1111/nph.17442

Ryan, S. N., Laing, W. A., & McManus, M. T. (1998). A cysteine proteinase inhibitor purified from apple fruit. *Phytochemistry*, *49*(4), 957–963. https://doi.org/10.1016/S0031-9422(98)00206-4

Rybak, K., & Robatzek, S. (2019). Functions of Extracellular Vesicles in Immunity and Virulence. *Plant Physiology*, *179*(4), 1236–1247. https://doi.org/10.1104/pp.18.01557

Ryu, C.-M., Hu, C.-H., Locy, R. D., & Kloepper, J. W. (2005). Study of mechanisms for plant growth promotion elicited by rhizobacteria in *Arabidopsis thaliana*. *Plant and Soil*, *268*(1), 285–292. https://doi.org/10.1007/s11104-004-0301-9

Rzemieniewski, J., & Stegmann, M. (2022). Regulation of pattern-triggered immunity and growth by phytocytokines. *Current Opinion in Plant Biology*, *68*, 102230. https://doi.org/10.1016/j.pbi.2022.102230

Saijo, Y., Loo, E. P.-I., & Yasuda, S. (2018). Pattern recognition receptors and signaling in plant-microbe interactions. *The Plant Journal : For Cell and Molecular Biology*, *93*(4), 592–613. https://doi.org/10.1111/tpj.13808

Salmon, D., do Aido-Machado, R., Diehl, A., Leidert, M., Schmetzer, O., de A Lima, A. P. C., Scharfstein, J., Oschkinat, H., & Pires, J. R. (2006). Solution structure and backbone dynamics of the *Trypanosoma cruzi* cysteine protease inhibitor chagasin. *Journal of Molecular Biology*, *357*(5), 1511–1521. https://doi.org/10.1016/j.jmb.2006.01.064

Salvachúa, D., Werner, A. Z., Pardo, I., Michalska, M., Black, B. A., Donohoe, B. S., Haugen, S. J., Katahira, R., Notonier, S., Ramirez, K. J., Amore, A., Purvine, S. O., Zink, E. M., Abraham, P. E., Giannone, R. J., Poudel, S., Laible, P. D., Hettich, R. L., & Beckham, G. T. (2020). Outer membrane vesicles catabolize lignin-derived aromatic compounds in *Pseudomonas putida* KT2440. *Proceedings of the National Academy of Sciences*, *117*(17), 9302–9310. https://doi.org/10.1073/pnas.1921073117

Sampedro, I., Parales, R. E., Krell, T., & Hill, J. E. (2014). *Pseudomonas* chemotaxis. *FEMS Microbiology Reviews*, *39*(1), n/a-n/a. https://doi.org/10.1111/1574-6976.12081

Sanderson, S. J. J., Westrop, G. D. D., Scharfstein, J., Mottram, J. C. C., & Coombs, G. H. H. (2003). Functional conservation of a natural cysteine peptidase inhibitor in protozoan and bacterial pathogens. *FEBS Letters*, *542*(1–3), 12–16. https://doi.org/10.1016/S0014-5793(03)00327-2

Sankaran, K., & Wu, H. C. (1994). Lipid modification of bacterial prolipoprotein. Transfer of diacylglyceryl moiety from phosphatidylglycerol. *Journal of Biological Chemistry*, *269*(31), 19701–19706. https://doi.org/10.1016/S0021-9258(17)32077-X

Santos, C. C., Sant'Anna, C., Terres, A., Cunha-e-Silva, N. L., Scharfstein, J., & Lima, A. P. C. d. A. (2005). Chagasin, the endogenous cysteine-protease inhibitor of *Trypanosoma cruzi*, modulates parasite differentiation and invasion of mammalian cells. *Journal of Cell Science*, *118*(5), 901–915. https://doi.org/10.1242/jcs.01677

Santos, C. C., Scharfstein, J., & Ana Paula, A. P. C. (2006). Role of chagasin-like inhibitors as endogenous regulators of cysteine proteases in parasitic protozoa. In *Parasitology Research* (Vol. 99, Issue 4, pp. 323–324). https://doi.org/10.1007/s00436-006-0195-y

Schäfer, A., Tauch, A., Jäger, W., Kalinowski, J., Thierbach, G., & Pühler, A. (1994). Small mobilizable multi-purpose cloning vectors derived from the *Escherichia coli* plasmids pK18 and pK19: selection of defined deletions in the chromosome of *Corynebacterium glutamicum*. *Gene*, *145*(1), 69–73. https://doi.org/10.1016/0378-1119(94)90324-7

Schilling, O., Huesgen, P. F., Barré, O., Auf Dem Keller, U., & Overall, C. M. (2011). Characterization of the prime and non-prime active site specificities of proteases by proteome-derived peptide libraries and tandem mass spectrometry. *Nature Protocols*, *6*(1), 111–120. https://doi.org/10.1038/nprot.2010.178

Schmidt, H., Nunan, N., Höck, A., Eickhorst, T., Kaiser, C., Woebken, D., & Raynaud, X. (2018). Recognizing Patterns: Spatial Analysis of Observed Microbial Colonization on Root Surfaces. *Frontiers in Environmental Science*, *6*. https://doi.org/10.3389/fenvs.2018.00061

Schrödinger, L. (2015). *The PyMOL Molecular Graphics System, Version 1.8*.

Schroth, M. N., Hildebrand, D. C., & Panopoulos, N. (2006). Phytopathogenic Pseudomonads and Related Plant-Associated Pseudomonads. In *The Prokaryotes* (pp. 714–740). Springer New York. https://doi.org/10.1007/0-387-30746-X_23

Schulze Hüynck, J. (2019). *Cysteine proteases and their inhibitors in microbe - maize root interactions* [Universität zu Köln]. https://kups.ub.uni-koeln.de/10436/

Schulze Hüynck, J., Kaschani, F., van der Linde, K., Ziemann, S., Müller, A. N., Colby, T., Kaiser, M., Misas Villamil, J. C., & Doehlemann, G. (2019). Proteases underground: Analysis of the maize root apoplast identifies organ specific papain-like cysteine protease activity. *Frontiers in Plant Science*, *10*(April), 1–16. https://doi.org/10.3389/fpls.2019.00473

Schuster, M., Paulus, J. K., Kourelis, J., & van der Hoorn, R. A. L. (2022). Purification of His-Tagged Proteases from the Apoplast of Agroinfiltrated *N. benthamiana*. In *Methods in Molecular Biology* (Vol. 2447, pp. 53–66). https://doi.org/10.1007/978-1-0716-2079-3_5

Schwechheimer, C., & Kuehn, M. J. (2015). Outer-membrane vesicles from Gram-negative bacteria: biogenesis and functions. *Nature Reviews Microbiology*, *13*(10), 605–619. https://doi.org/10.1038/nrmicro3525

Seto, D., Koulena, N., Lo, T., Menna, A., Guttman, D. S., & Desveaux, D. (2017). Expanded type III effector recognition by the ZAR1 NLR protein using ZED1-related kinases. *Nature Plants*, *3*(4), 17027. https://doi.org/10.1038/nplants.2017.27

Seydel, A., Gounon, P., & Pugsley, A. P. (1999). Testing the '+2 rule' for lipoprotein sorting in the *Escherichia coli* cell envelope with a new genetic selection. *Molecular Microbiology*, *34*(4), 810–821. https://doi.org/10.1046/j.1365-2958.1999.01647.x

Shabab, M., Shindo, T., Gu, C., Kaschani, F., Pansuriya, T., Chintha, R., Harzen, A., Colby, T., Kamoun, S., & Van Der Hoorn, R. A. L. (2008). Fungal effector protein AVR2 targets diversifying defense-related cys proteases of tomato. *Plant Cell*, *20*(4), 1169–1183. https://doi.org/10.1105/tpc.107.056325

Shan, L., He, P., Li, J., Heese, A., Peck, S. C., Nürnberger, T., Martin, G. B., & Sheen, J. (2008). Bacterial Effectors Target the Common Signaling Partner BAK1 to Disrupt Multiple MAMP Receptor-Signaling Complexes and Impede Plant Immunity. *Cell Host and Microbe*, *4*(1), 17–27. https://doi.org/10.1016/j.chom.2008.05.017

Shen, W., Liu, J., & Li, J.-F. (2019). Type-II Metacaspases Mediate the Processing of Plant Elicitor Peptides in *Arabidopsis*. *Molecular Plant*, *12*(11), 1524–1533. https://doi.org/10.1016/j.molp.2019.08.003

Sheoran, N., Kumar, A., Munjal, V., Nadakkakath, A. V., & Eapen, S. J. (2016). *Pseudomonas putida* BP25 alters root phenotype and triggers salicylic acid signaling as a feedback loop in regulating endophytic colonization in *Arabidopsis thaliana*. *Physiological and Molecular Plant Pathology*, *93*, 99–111. https://doi.org/10.1016/j.pmpp.2016.01.008

Shepherd, S., Yuen, E. L. H., Carella, P., & Bozkurt, T. O. (2023). The wheels of destruction: Plant NLR immune receptors are mobile and structurally dynamic disease resistance proteins. *Current Opinion in Plant Biology*, *74*, 102372. https://doi.org/10.1016/j.pbi.2023.102372

Shindo, T., Kaschani, F., Yang, F., Kovács, J., Tian, F., Kourelis, J., Hong, T. N., Colby, T., Shabab, M., Chawla, R., Kumari, S., Ilyas, M., Hörger, A. C., Alfano, J. R., & van der Hoorn, R. A. L. (2016). Screen of Non-annotated Small Secreted Proteins of *Pseudomonas syringae* Reveals a Virulence Factor That Inhibits Tomato Immune Proteases. *PLOS Pathogens*, *12*(9), e1005874. https://doi.org/10.1371/journal.ppat.1005874

Shindo, T., Misas-Villamil, J. C., Hörger, A. C., Song, J., & van der Hoorn, R. A. L. (2012). A role in immunity for *Arabidopsis* cysteine protease RD21, the ortholog of the tomato immune protease C14. *PLoS ONE*, *7*(1), 1–9. https://doi.org/10.1371/journal.pone.0029317

Shindo, T., & Van der Hoorn, R. A. L. (2008). Papain-like cysteine proteases: key players at molecular battlefields employed by both plants and their invaders. *Molecular Plant Pathology*, *9*(1), 119–125. https://doi.org/10.1111/j.1364-3703.2007.00439.x

Sievers, F., Wilm, A., Dineen, D., Gibson, T. J., Karplus, K., Li, W., Lopez, R., McWilliam, H., Remmert, M., Söding, J., Thompson, J. D., & Higgins, D. G. (2011). Fast, scalable generation of high-quality protein multiple sequence alignments using Clustal Omega. *Molecular Systems Biology*, *7*(1). https://doi.org/10.1038/msb.2011.75

Slowikowski, K. (2024). *ggrepel: Automatically Position Non-Overlapping Text Labels with "ggplot2."* https://ggrepel.slowkow.com/

Solia, N. (2023). *The Role of Pseudomonas putida Cip1 in Plant-Microbe Interaction*. University of Cologne.

Somssich, M., Khan, G. A., & Staffan, S. P. (2016). Cell wall heterogeneity in root development of *Arabidopsis*. *Frontiers in Plant Science*, *7*(AUG2016), 1–11. https://doi.org/10.3389/fpls.2016.01242

Song, C. J., Steinebrunner, I., Wang, X., Stout, S. C., & Roux, S. J. (2006). Extracellular ATP Induces the Accumulation of Superoxide via NADPH Oxidases in *Arabidopsis*. *Plant Physiology*, *140*(4), 1222–1232. https://doi.org/10.1104/pp.105.073072

Song, J., Win, J., Tian, M., Schornack, S., Kaschani, F., Ilyas, M., van der Hoorn, R. A. L., & Kamoun, S. (2009). Apoplastic effectors secreted by two unrelated eukaryotic plant pathogens target the tomato defense protease Rcr3. *Proceedings of the National Academy of Sciences*, *106*(5), 1654–1659. https://doi.org/10.1073/pnas.0809201106

Srivastava, S., Chaudhry, V., Mishra, A., Chauhan, P. S., Rehman, A., Yadav, A., Tuteja, N., & Nautiyal, C. S. (2012). Gene expression profiling through microarray analysis in *Arabidopsis thaliana* colonized by *Pseudomonas putida* MTCC5279, a plant growth promoting rhizobacterium. *Plant Signaling & Behavior*, *7*(2), 235–245. https://doi.org/10.4161/psb.18957

Srivastava, S., & Srivastava, S. (2020). Prescience of endogenous regulation in *Arabidopsis thaliana* by *Pseudomonas putida* MTCC 5279 under phosphate starved salinity stress condition. *Scientific Reports*, *10*(1), 5855. https://doi.org/10.1038/s41598-020-62725-1

Stavrinides, J., McCann, H. C., & Guttman, D. S. (2008). Host-pathogen interplay and the evolution of bacterial effectors. *Cellular Microbiology*, *10*(2), 285–292. https://doi.org/10.1111/j.1462-5822.2007.01078.x

Steinegger, M., & Söding, J. (2017). MMseqs2 enables sensitive protein sequence searching for the analysis of massive data sets. *Nature Biotechnology*, *35*(11), 1026–1028. https://doi.org/10.1038/nbt.3988

Stolze, S. C., Deu, E., Kaschani, F., Li, N., Florea, B. I., Richau, K. H., Colby, T., van der Hoorn, R. A. L., Overkleeft, H. S., Bogyo, M., & Kaiser, M. (2012). The Antimalarial Natural Product Symplostatin 4 Is a Nanomolar Inhibitor of the Food Vacuole Falcipains. *Chemistry & Biology*, *19*(12), 1546–1555. https://doi.org/10.1016/j.chembiol.2012.09.020

Tanaka, S., Narita, S., & Tokuda, H. (2007). Characterization of the *Pseudomonas aeruginosa* Lol System as a Lipoprotein Sorting Mechanism. *Journal of Biological Chemistry*, *282*(18), 13379–13384. https://doi.org/10.1074/jbc.M611840200

Tanizawa, Y., Fujisawa, T., Kaminuma, E., Nakamura, Y., & Arita, M. (2016). DFAST and DAGA: web-based integrated genome annotation tools and resources. *Bioscience of Microbiota, Food and Health*, *35*(4), 173–184. https://doi.org/10.12938/bmfh.16-003

Tanizawa, Y., Fujisawa, T., & Nakamura, Y. (2018). DFAST: a flexible prokaryotic genome annotation pipeline for faster genome publication. *Bioinformatics*, *34*(6), 1037–1039. https://doi.org/10.1093/bioinformatics/btx713

Teixeira, P. J. P. L., Colaianni, N. R., Law, T. F., Conway, J. M., Gilbert, S., Li, H., Salas-González, I., Panda, D., Del Risco, N. M., Finkel, O. M., Castrillo, G., Mieczkowski, P., Jones, C. D., & Dangl, J. L. (2021). Specific modulation of the root immune system by a community of commensal bacteria. *Proceedings of the National Academy of Sciences*, *118*(16), e2100678118. https://doi.org/10.1073/pnas.2100678118

Terada, M., Kuroda, T., Matsuyama, S., & Tokuda, H. (2001). Lipoprotein Sorting Signals Evaluated as the LolA-dependent Release of Lipoproteins from the Cytoplasmic Membrane of *Escherichia coli*. *Journal of Biological Chemistry*, *276*(50), 47690–47694. https://doi.org/10.1074/jbc.M109307200

Teufel, F., Almagro Armenteros, J. J., Johansen, A. R., Gíslason, M. H., Pihl, S. I., Tsirigos, K. D., Winther, O., Brunak, S., von Heijne, G., & Nielsen, H. (2022). SignalP 6.0 predicts all five types of signal peptides using protein language models. *Nature Biotechnology*, *40*(7), 1023–1025. https://doi.org/10.1038/s41587-021-01156-3

Thompson, M. G., Incha, M. R., Pearson, A. N., Schmidt, M., Sharpless, W. A., Eiben, C. B., Cruz-Morales, P., Blake-Hedges, J. M., Liu, Y., Adams, C. A., Haushalter, R. W., Krishna, R. N., Lichtner, P., Blank, L. M., Mukhopadhyay, A., Deutschbauer, A. M., Shih, P. M., & Keasling, J. D. (2020). Fatty Acid and Alcohol Metabolism in *Pseudomonas putida*: Functional Analysis Using Random Barcode Transposon Sequencing. *Applied and Environmental Microbiology*, *86*(21), 1–23. https://doi.org/10.1128/AEM.01665-20

Thorn, M. B. (1949). A method for determining the ratio of the Michaelis constants of an enzyme with respect to two substrates. *Nature*, *164*(4157), 27–29. https://doi.org/10.1038/164027a0

Tian, M., Win, J., Song, J., van der Hoorn, R., van der Knaap, E., & Kamoun, S. (2007). A *Phytophthora infestans* Cystatin-Like Protein Targets a Novel Tomato Papain-Like Apoplastic Protease. *Plant Physiology*, *143*(1), 364–377. https://doi.org/10.1104/pp.106.090050

Tibor, A., Decelle, B., & Letesson, J. J. (1999). Outer membrane proteins Omp10, Omp16, and Omp19 of *Brucella* spp. are lipoproteins. *Infection and Immunity*, *67*(9), 4960–4962. https://doi.org/10.1128/IAI.67.9.4960-4962.1999

Tjalsma, H., & van Dijl, J. M. (2005). Proteomics-based consensus prediction of protein retention in a bacterial membrane. *Proteomics*, *5*(17), 4472–4482. https://doi.org/10.1002/pmic.200402080

Tokunaga, M., Loranger, J. M., & Wu, H. C. (1984). Prolipoprotein modification and processing enzymes in *Escherichia coli*. *Journal of Biological Chemistry*, *259*(6), 3825–3830. https://doi.org/10.1016/S0021-9258(17)43170-X

Tokunaga, M., Tokunaga, H., & Wu, H. C. (1982). Post-translational modification and processing of *Escherichia coli* prolipoprotein in vitro. *Proceedings of the National Academy of Sciences*, *79*(7), 2255–2259. https://doi.org/10.1073/pnas.79.7.2255

Tokuyasu, K. T. (1973). A technique for ultracryotomy of cell suspensions and tissues. *The Journal of Cell Biology*, *57*(2), 551–565. https://doi.org/10.1083/jcb.57.2.551

Tran, T. M., Chng, C.-P., Pu, X., Ma, Z., Han, X., Liu, X., Yang, L., Huang, C., & Miao, Y. (2022). Potentiation of plant defense by bacterial outer membrane vesicles is mediated by membrane nanodomains. *The Plant Cell*, *34*(1), 395–417. https://doi.org/10.1093/plcell/koab276

Trivedi, P., Delgado-Baquerizo, M., Trivedi, C., Hamonts, K., Anderson, I. C., & Singh, B. K. (2017). Keystone microbial taxa regulate the invasion of a fungal pathogen in agro-ecosystems. *Soil Biology and Biochemistry*, *111*, 10–14. https://doi.org/10.1016/j.soilbio.2017.03.013

Tsai, H.-H., Wang, J., Geldner, N., & Zhou, F. (2023). Spatiotemporal control of root immune responses during microbial colonization. *Current Opinion in Plant Biology*, *74*(May), 102369. https://doi.org/10.1016/j.pbi.2023.102369

Turk, B., Turk, V., & Turk, D. (1997). Structural and functional aspects of papain-like cysteine proteinases and their protein inhibitors. *Biological Chemistry*, *378*(3–4), 141–150. http://www.ncbi.nlm.nih.gov/pubmed/9165064

Tušar, L., Usenik, A., Turk, B., & Turk, D. (2021). Mechanisms Applied by Protein Inhibitors to Inhibit Cysteine Proteases. *International Journal of Molecular Sciences*, *22*(3), 1–32. https://doi.org/10.3390/ijms22030997

Uehara, L. A., Moreira, O. C., Oliveira, A. C., Azambuja, P., Lima, A. P. C. A., Britto, C., dos Santos, A. L. S., Branquinha, M. H., & D'Avila-Levy, C. M. (2012). Cruzipain Promotes *Trypanosoma cruzi* Adhesion to Rhodnius prolixus Midgut. *PLoS Neglected Tropical Diseases*, *6*(12), e1958. https://doi.org/10.1371/journal.pntd.0001958

Urashima, A., Sanou, A., Yen, H., & Tobe, T. (2017). Enterohaemorrhagic *Escherichia coli* produces outer membrane vesicles as an active defence system against antimicrobial peptide LL-37. *Cellular Microbiology*, *19*(11), e12758. https://doi.org/10.1111/cmi.12758

Van Der Hoorn, R. A. L. (2008). Plant proteases: From phenotypes to molecular mechanisms. *Annual Review of Plant Biology*, *59*, 191–223. https://doi.org/10.1146/annurev.arplant.59.032607.092835

Van der Hoorn, R. A. L., Colby, T., Nickel, S., Richau, K. H., Schmidt, J., & Kaiser, M. (2011). Mining the active proteome of *Arabidopsis thaliana*. *Frontiers in Plant Science*, *2*(NOV), 1–11. https://doi.org/10.3389/fpls.2011.00089

van der Hoorn, R. A. L., Leeuwenburgh, M. A., Bogyo, M., Joosten, M. H. A. J., & Peck, S. C. (2004). Activity profiling of papain-like cysteine proteases in plants. *Plant Physiology*, *135*(3), 1170–1178. https://doi.org/10.1104/pp.104.041467

van der Linde, K., Hemetsberger, C., Kastner, C., Kaschani, F., van der Hoorn, R. A. L., Kumlehn, J., & Doehlemann, G. (2012a). A maize cystatin suppresses host immunity by inhibiting apoplastic cysteine proteases. *Plant Cell*, *24*(3), 1285–1300. https://doi.org/10.1105/tpc.111.093732

van der Linde, K., Mueller, A. N., Hemetsberger, C., Kashani, F., van der Hoorn, R. A. L., & Doehlemann, G. (2012b). The maize cystatin CC9 interacts with apoplastic cysteine proteases. *Plant Signaling & Behavior*, *7*(11), 1397–1401. https://doi.org/10.4161/psb.21902

Van Esse, H. P., Van't Klooster, J. W., Bolton, M. D., Yadeta, K. A., Van Baarlen, P., Boeren, S., Vervoort, J., Dewit, P. J. G. M., & Thomma, B. P. H. J. (2008). The *Cladosporium fulvum* virulence protein Avr2 inhibits host proteases required for basal defense. *Plant Cell*, *20*(7), 1948–1963. https://doi.org/10.1105/tpc.108.059394

Van Loon, L. C., Rep, M., & Pieterse, C. M. J. (2006). Significance of inducible defense-related proteins in infected plants. *Annual Review of Phytopathology*, *44*, 135–162. https://doi.org/10.1146/annurev.phyto.44.070505.143425

Van Melderen, L., & Aertsen, A. (2009). Regulation and quality control by Lon-dependent proteolysis. *Research in Microbiology*, *160*(9), 645–651. https://doi.org/https://doi.org/10.1016/j.resmic.2009.08.021

van Midden, K. P., Mantz, M., Fonovič, M., Gazvoda, M., Svete, J., Huesgen, P. F., van der Hoorn, R. A. L., & Klemenčič, M. (2024). Mechanistic insights into CrCEP1: A dual-function cysteine protease with endo- and transpeptidase activity. *International Journal of Biological Macromolecules*, 132505. https://doi.org/10.1016/j.ijbiomac.2024.132505

Varughese, K. I., Ahmed, F. R., Carey, P. R., Hasnain, S., Huber, C. P., & Storer, A. C. (1989). Crystal structure of a papain-E-64 complex. *Biochemistry*, *28*(3), 1330–1332. https://doi.org/10.1021/bi00429a058

Vecchietti, D., Di Silvestre, D., Miriani, M., Bonomi, F., Marengo, M., Bragonzi, A., Cova, L., Franceschi, E., Mauri, P., & Bertoni, G. (2012). Analysis of *Pseudomonas aeruginosa* Cell Envelope Proteome by Capture of Surface-Exposed Proteins on Activated Magnetic Nanoparticles. *PLoS ONE*, *7*(11), e51062. https://doi.org/10.1371/journal.pone.0051062

Vega-Muñoz, I., Duran-Flores, D., Fernández-Fernández, Á. D., Heyman, J., Ritter, A., & Stael, S. (2020). Breaking Bad News: Dynamic Molecular Mechanisms of Wound Response in Plants. *Frontiers in Plant Science*, *11*(December). https://doi.org/10.3389/fpls.2020.610445

Verbelen, J.-P., Cnodder, T. De, Le, J., Vissenberg, K., & Baluška, F. (2006). The Root Apex of *Arabidopsis thaliana* Consists of Four Distinct Zones of Growth Activities. *Plant Signaling & Behavior*, *1*(6), 296–304. https://doi.org/10.4161/psb.1.6.3511

Verhoef, S., Ballerstedt, H., Volkers, R. J. M., de Winde, J. H., & Ruijssenaars, H. J. (2010). Comparative transcriptomics and proteomics of p-hydroxybenzoate producing *Pseudomonas putida* S12: novel responses and implications for strain improvement. *Applied Microbiology and Biotechnology*, *87*(2), 679–690. https://doi.org/10.1007/s00253-010-2626-z

Verma, S., Dixit, R., & Pandey, K. C. (2016). Cysteine proteases: Modes of activation and future prospects as pharmacological targets. *Frontiers in Pharmacology*, *7*(APR), 1–12. https://doi.org/10.3389/fphar.2016.00107

Vernet, T., Khouri, H. E., Laflamme, P., Tessier, D. C., Musil, R., Gour-Salin, B. J., Storer, A. C., & Thomas, D. Y. (1991). Processing of the papain precursor. Purification of the zymogen and characterization of its mechanism of processing. *Journal of Biological Chemistry*, *266*(32), 21451–21457. https://doi.org/10.1016/S0021-9258(18)54660-3

Wadhwa, N., & Berg, H. C. (2022). Bacterial motility: machinery and mechanisms. *Nature Reviews Microbiology*, *20*(3), 161–173. https://doi.org/10.1038/s41579-021-00626-4

Wagih, O. (2017). ggseqlogo: a versatile R package for drawing sequence logos. *Bioinformatics*, *33*(22), 3645–3647. https://doi.org/10.1093/bioinformatics/btx469

Wang, G., Roux, B., Feng, F., Guy, E., Li, L., Li, N., Zhang, X., Lautier, M., Jardinaud, M.-F., Chabannes, M., Arlat, M., Chen, S., He, C., Noël, L. D., & Zhou, J.-M. (2015). The Decoy Substrate of a Pathogen Effector and a Pseudokinase Specify Pathogen-Induced Modified-Self Recognition and Immunity in Plants. *Cell Host & Microbe*, *18*(3), 285–295. https://doi.org/10.1016/j.chom.2015.08.004

Wang, J., Hao, C., Cao, L., Yao, Y., Ding, Y., Yang, Y., Tang, X.-F., & Tang, B. (2021a). Enhancing extracellular production of recombinant proteins in *Escherichia coli* by co-expressing with a haloarchaeal protein containing a putative LolA-like domain. *Applied Microbiology and Biotechnology*, *105*(11), 4609–4620. https://doi.org/10.1007/s00253-021-11352-5

Wang, J. J., Hu, M., Wang, J. J., Qi, J., Han, Z., Wang, G., Qi, Y., Wang, H.-W., Zhou, J.-M., & Chai, J. (2019a). Reconstitution and structure of a plant NLR resistosome conferring immunity. *Science*, *364*(6435), eaav5870. https://doi.org/10.1126/science.aav5870

Wang, S. X., Pandey, K. C., Scharfstein, J., Whisstock, J., Huang, R. K., Jacobelli, J., Fletterick, R. J., Rosenthal, P. J., Abrahamson, M., Brinen, L. S., Rossi, A., Sali, A., & McKerrow, J. H. (2007). The Structure of Chagasin in Complex with a Cysteine Protease Clarifies the Binding Mode and Evolution of an Inhibitor Family. *Structure*, *15*(5), 535–543. https://doi.org/10.1016/j.str.2007.03.012

Wang, S., Xing, R., Wang, Y., Shu, H., Fu, S., Huang, J., Paulus, J. K., Schuster, M., Saunders, D. G. O., Win, J., Vleeshouwers, V., Wang, Y., Zheng, X., van der Hoorn, R. A. L., & Dong, S. (2021b). Cleavage of a pathogen apoplastic protein by plant subtilases activates host immunity. *New Phytologist*, *229*(6), 3424–3439. https://doi.org/10.1111/nph.17120

Wang, Y., Garrido-Oter, R., Wu, J., Winkelmüller, T. M., Agler, M., Colby, T., Nobori, T., Kemen, E., & Tsuda, K. (2019b). Site-specific cleavage of bacterial MucD by secreted proteases mediates antibacterial resistance in *Arabidopsis*. *Nature Communications*, *10*(1), 2853. https://doi.org/10.1038/s41467-019-10793-x

Weber, E., Engler, C., Gruetzner, R., Werner, S., & Marillonnet, S. (2011). A modular cloning system for standardized assembly of multigene constructs. *PLoS ONE*, *6*(2). https://doi.org/10.1371/journal.pone.0016765

Weigel, D., & Glazebrook, J. (2006). Transformation of *Agrobacterium* Using Electroporation. *Cold Spring Harbor Protocols*, *2006*(7), pdb.prot4665. https://doi.org/10.1101/pdb.prot4665

Wendrich, J. R., Yang, B., Vandamme, N., Verstaen, K., Smet, W., Van de Velde, C., Minne, M., Wybouw, B., Mor, E., Arents, H. E., Nolf, J., Van Duyse, J., Van Isterdael, G., Maere, S., Saeys, Y., & De Rybel, B. (2020). Vascular transcription factors guide plant epidermal responses to limiting phosphate conditions. *Science*, *370*(6518), eaay4970. https://doi.org/10.1126/science.aay4970

Weyens, N., Boulet, J., Adriaensen, D., Timmermans, J. P., Prinsen, E., van Oevelen, S., D'Haen, J., Smeets, K., van der Lelie, D., Taghavi, S., & Vangronsveld, J. (2012). Contrasting colonization and plant growth promoting capacity between wild type and a gfp-derative of the endophyte *Pseudomonas putida* W619 in hybrid poplar. *Plant and Soil*, *356*(1–2), 217–230. https://doi.org/10.1007/s11104-011-0831-x

Wickham, H., Averick, M., Bryan, J., Chang, W., McGowan, L., François, R., Grolemund, G., Hayes, A., Henry, L., Hester, J., Kuhn, M., Pedersen, T., Miller, E., Bache, S., Müller, K., Ooms, J., Robinson, D., Seidel, D., Spinu, V., … Yutani, H. (2019). Welcome to the Tidyverse. *Journal of Open Source Software*, *4*(43), 1686. https://doi.org/10.21105/joss.01686

Wickham, H., & Bryan, J. (2023). *readxl: Read Excel Files* (1.4.3.). https://readxl.tidyverse.org

Wickham, H., Henry, L., Pedersen, T. L., Luciani, T. J., Decorde, M., & Lise, V. (2024). *svglite: An "SVG" Graphics Device* (2.1.3.9000). https://svglite.r-lib.org/

Wickham, H., Pedersen, T. L., & Seidel, D. (2023). *scales: Scale Functions for Visualization.* (1.3.0). https://github.com/r-lib/scales

Wilson, S. M., & Bacic, A. (2012). Preparation of plant cells for transmission electron microscopy to optimize immunogold labeling of carbohydrate and protein epitopes. *Nature Protocols*, *7*(9), 1716–1727. https://doi.org/10.1038/nprot.2012.096

Winsor, G. L., Griffiths, E. J., Lo, R., Dhillon, B. K., Shay, J. A., & Brinkman, F. S. L. (2016). Enhanced annotations and features for comparing thousands of *Pseudomonas* genomes in the *Pseudomonas* genome database. *Nucleic Acids Research*, *44*(D1), D646–D653. https://doi.org/10.1093/nar/gkv1227

Woodhouse, M. R., Cannon, E. K., Portwood, J. L., Harper, L. C., Gardiner, J. M., Schaeffer, M. L., & Andorf, C. M. (2021). A pan-genomic approach to genome databases using maize as a model system. *BMC Plant Biology*, *21*(1), 385. https://doi.org/10.1126/science.abg5

Wurtz, A., & Bouchut, E. (1879). Digestive Ferment of *Carica papaya*. *Scientific American*, *8*(203supp), 3231–3231. https://doi.org/10.1038/scientificamerican11221879-3231esupp

Xin, X.-F., Kvitko, B., & He, S. Y. (2018). *Pseudomonas syringae*: what it takes to be a pathogen. *Nature Reviews Microbiology*, *16*(5), 316–328. https://doi.org/10.1038/nrmicro.2018.17

Yadav, V. K., Chhikara, N., Gill, K., Dey, S., Singh, S., & Yadav, S. (2013). Three low molecular weight cysteine proteinase inhibitors of human seminal fluid: purification and enzyme kinetic properties. *Biochimie*, *95*(8), 1552–1559. https://doi.org/10.1016/j.biochi.2013.04.007

Yamada, K., Matsushima, R., Nishimura, M., & Hara-Nishimura, I. (2001). A slow maturation of a cysteine protease with a granulin domain in the vacuoles of senescing *Arabidopsis* leaves. *Plant Physiology*, *127*(4), 1626–1634. https://doi.org/10.1104/pp.010551

Yamaguchi, K., Yu, F., & Inouye, M. (1988). A single amino acid determinant of the membrane localization of lipoproteins in *E. coli. Cell*, *53*(3), 423–432. https://doi.org/10.1016/0092-8674(88)90162-6

Yamaguchi, Y., Huffaker, A., Bryan, A. C., Tax, F. E., & Ryan, C. A. (2010). PEPR2 is a second receptor for the Pep1 and Pep2 peptides and contributes to defense responses in *Arabidopsis*. *Plant Cell*, *22*(2), 508–522. https://doi.org/10.1105/tpc.109.068874

Yang, Y., Dong, C., Yu, J., Shi, L., Tong, C., Li, Z., Huang, J., & Liu, S. (2014). Cysteine Protease 51 (CP51), an anther-specific cysteine protease gene, is essential for pollen exine formation in *Arabidopsis*. *Plant Cell, Tissue and Organ Culture*, *119*(2), 383–397. https://doi.org/10.1007/s11240-014-0542-0

Yousef-Coronado, F., Travieso, M. L., & Espinosa-Urgel, M. (2008). Different, overlapping mechanisms for colonization of abiotic and plant surfaces by *Pseudomonas putida*. *FEMS Microbiology Letters*, *288*(1), 118–124. https://doi.org/10.1111/j.1574-6968.2008.01339.x

Yu, J., Yuan, Q., Chen, C., Xu, T., Jiang, Y., Hu, W., Liao, A., Zhang, J., Le, X., Li, H., & Wang, X. (2024). A root-knot nematode effector targets the *Arabidopsis* cysteine protease RD21A for degradation to suppress plant defense and promote parasitism. *Plant Journal*, *118*(5), 1500–1515. https://doi.org/10.1111/tpj.16692

Yu, K., Pieterse, C. M. J., Bakker, P. A. H. M., & Berendsen, R. L. (2019). Beneficial microbes going underground of root immunity. *Plant, Cell & Environment*, *42*(10), 2860–2870. https://doi.org/10.1111/pce.13632

Yu, N. Y., Wagner, J. R., Laird, M. R., Melli, G., Rey, S., Lo, R., Dao, P., Sahinalp, S. C., Ester, M., Foster, L. J., & Brinkman, F. S. L. (2010). PSORTb 3.0: improved protein subcellular localization prediction with refined localization subcategories and predictive capabilities for all prokaryotes. *Bioinformatics (Oxford, England)*, *26*(13), 1608–1615. https://doi.org/10.1093/bioinformatics/btq249

Yuan, M., Ngou, B. P. M., Ding, P., & Xin, X. F. (2021). PTI-ETI crosstalk: an integrative view of plant immunity. *Current Opinion in Plant Biology*, *62*, 102030. https://doi.org/10.1016/j.pbi.2021.102030

Yuan, W., Chen, X., Du, K., Jiang, T., Li, M., Cao, Y., Li, X., Doehlemann, G., Fan, Z., & Zhou, T. (2024). NIa-Pro of sugarcane mosaic virus targets Corn Cysteine Protease 1 (CCP1) to undermine salicylic acid-mediated defense in maize. *PLoS Pathogens*, *20*(3), 1–30. https://doi.org/10.1371/journal.ppat.1012086

Zakharova, E., Horvath, M. P., & Goldenberg, D. P. (2009). Structure of a serine protease poised to resynthesize a peptide bond. *Proceedings of the National Academy of Sciences*, *106*(27), 11034–11039. https://doi.org/10.1073/pnas.0902463106

Zamioudis, C., & Pieterse, C. M. J. (2012). Modulation of host immunity by beneficial microbes. *Molecular Plant-Microbe Interactions : MPMI*, *25*(2), 139–150. https://doi.org/10.1094/MPMI-06-11-0179

Zboralski, A., & Filion, M. (2020). Genetic factors involved in rhizosphere colonization by phytobeneficial *Pseudomonas* spp. *Computational and Structural Biotechnology Journal*, *18*, 3539–3554. https://doi.org/10.1016/j.csbj.2020.11.025

Zeng, Y., Zheng, Z., Hessler, G., Zou, K., Leng, J., Bautor, J., Stuttmann, J., Xue, L., Parker, J. E., & Cui, H. (2023). *Arabidopsis* PHYTOALEXIN DEFICIENT 4 promotes the maturation and nuclear accumulation of immune-related cysteine protease RD19. *Journal of Experimental Botany*, *November*, 1–17. https://doi.org/10.1093/jxb/erad454

Zhang, B., Tremousaygue, D., Denancé, N., Van Esse, H. P., Hörger, A. C., Dabos, P., Goffner, D., Thomma, B. P. H. J., Van Der Hoorn, R. A. L., & Tuominen, H. (2014). PIRIN2 stabilizes cysteine protease XCP2 and increases susceptibility to the vascular pathogen *Ralstonia solanacearum* in *Arabidopsis*. *Plant Journal*, *79*(6), 1009–1019. https://doi.org/10.1111/tpj.12602

Zhou, F., Emonet, A., Dénervaud Tendon, V., Marhavy, P., Wu, D., Lahaye, T., & Geldner, N. (2020). Co-incidence of Damage and Microbial Patterns Controls Localized Immune Responses in Roots. *Cell*, *180*(3), 440-453.e18. https://doi.org/10.1016/j.cell.2020.01.013

Zhou, J.-M., & Zhang, Y. (2020). Plant Immunity: Danger Perception and Signaling. *Cell*, *181*(5), 978–989. https://doi.org/10.1016/j.cell.2020.04.028

Zhou, J., Wang, P., Claus, L. A. N., Savatin, D. V., Xu, G., Wu, S., Meng, X., Russinova, E., He, P., & Shan, L. (2019). Proteolytic Processing of SERK3/BAK1 Regulates Plant Immunity, Development, and Cell Death. *Plant Physiology*, *180*(1), 543–558. https://doi.org/10.1104/pp.18.01503

Ziemann, S., Van Der Linde, K., Lahrmann, U., Acar, B., Kaschani, F., Colby, T., Kaiser, M., Ding, Y., Schmelz, E., Huffaker, A., Holton, N., Zipfel, C., & Doehlemann, G. (2018). An apoplastic peptide activates salicylic acid signalling in maize. *Nature Plants*, *4*(3), 172–180. https://doi.org/10.1038/s41477-018-0116-y

List of Figures

List of Tables

Publication Licenses

- Moser, D. & Doehlemann, G. (2025). Plants rely on a two-branched immune system to recognize microbes. Created in BioRender. https://BioRender.com/k51j278
- Moser, D. & Doehlemann, G. (2025). Functions of proteases in plant immunity. Created in BioRender. https://BioRender.com/k29h484
- Moser, D. & Doehlemann, G. (2025). Suppression of papain-like cysteine proteases (PLCPs). Created in BioRender. https://BioRender.com/m24e150
- Moser, D. & Doehlemann, G. (2025). Working hypothesis: Non-pathogenic bacteria also secrete inhibitors to modulate PLCP activity. Created in BioRender. https://BioRender.com/o67i385
- Moser, D. & Doehlemann, G. (2025). Model of the putative transport of membrane-anchored PpCip1 to the cell surface. Created in BioRender. https://BioRender.com/g02m571
- Moser, D. & Doehlemann, G. (2025). Model how Pseudomonas putida might modulate plant immunity via inhibition of PLCPs. Created in BioRender. https://BioRender.com/m78q124
- Moser, D. & Doehlemann, G. (2025). Schematic representation of the Sec-dependent transport of lipoproteins to the cell surface. Created in BioRender. https://BioRender.com/c60j023
- Moser, D. & Doehlemann, G. (2025). Presence of PpCip1 modulates the structure of the synthetic community (SynCom). Created in BioRender. https://BioRender.com/t26p187

Delimitation of own contribution

Collaborations

Christian Frederick Kaiser and Sabrina Egli (Heinrich-Heine-University Düsseldorf) prepared plants, cultures and chips, inoculated chips and supported during the microscopy of the roots and data analysis (Figure 16). Christian Frederick Kaiser provided ImageJ makro scripts for the analysis of the microscopy images and measured intensity profiles of one of the replicates. Prof. Dr. Guido Grossmann provided valuable feedback during the collaboration.

Dr. Ulla Neumann and her team (Max Planck Institute for Plant Breeding Research in Cologne) performed the sample processing for the immunogold labeling, transmission electron microscopy and image acquisition (Suppl. Fig. 10).

Dr. Lioba Rüger, Dr. Noah Kürtös, Dr. Ryohei Thomas Nakano (Max Planck Institute for Plant Breeding Research in Cologne) supported during the preparation of samples for amplicon sequencing and in the data analysis (Figure 17). Dr. Tonni Grube Andersen provided valuable feedback during the collaboration and as a TAC member.

Melissa Mantz (University of Freiburg) performed the processing and analysis of PICS samples. Prof. Dr. Pitter Huesgen provided valuable feedback during the collaboration.

Supervision

During the course of this PhD thesis, I supervised the following students and their work contributed to this thesis:

Master thesis

Nina Solia (2023): The Role of *Pseudomonas putida* Cip1 in Plant-Microbe Interaction

Nina Solia helped with the literature search about lipoproteins. She generated several strains during her Master thesis and research internship (Table 11+12). She performed the cell fractionation to identify the localization of PpCip1 (Figure 12). We performed the fluorescence

microscopy of fluorescently tagged PpCip1 together (Figure 13). She established and performed maize root colonization assays (Suppl. Fig. 11).

> Eva Slavič (expected 2025): *Modulation of maize proteases in bacterial interactions and immunity* (provisional title), University of Ljubljana, Slovenia

Eva Slavic cloned, expressed, purified and tested many PLCP inhibitor candidate proteins (Ppu3051, Ppu_0571, Ppu_1665, Ppu_1728, Ppu_1972, Ppu_2089, Ppu_2532, Ppu_2677, Ppu_2699, Ppu_4298, Ppu_4757, Ppu_5184) (Table 3+11, Figure 27+29, Suppl. Fig. 16).

Internship students

> Dorrie Wamser: The inhibitive abilities of *P. putida* and *cip1* knockout mutants against maize PLCPs (2021), University of Cologne

Dorrie Wamser conducted some replications of the PLCP inhibition experiments with HMWFs of the *P. putida* Δ*cip1* mutants (Figure 18).

> Melina Laporta: Cloning, Expression, Purification and Testing of Protease Inhibitor Candidates of Pseudomonas putida (2023), University of Cologne

Melina Laporta cloned, expressed, purified and tested some PLCP inhibitor candidate proteins (Ppu_1972, Ppu_2089, Ppu_4298, Ppu_4757, Ppu_2699) (Figure 27, Table 11).

> Lucie Hansen: Determination of the orientation of the bacterial PLCP inhibitor Cip1 at the outer membrane (2024), University of Cologne

Lucie Hansen supported the establishment of assays to determine the orientation/localization of PpCip1 at the inner or outer membrane using the Protease K protection assay and biotin labeling followed by pulldown.

Own work

Some of the experiments or material used in this PhD thesis were performed or generated during my Master thesis and my prior research internship:

> Root immune signaling: proteases, their inhibitors and signaling peptides (2021), Heinrich-Heine-Universität Düsseldorf

and contributed to this thesis or were precursors for further experiments of this PhD thesis: The isolation and evaluation experiments of SA-activated root apoplastic fluid (Suppl. Fig. 1), cloning of constructs for heterologous expression in *N. benthamiana* (Table 11+13), isolation and evaluation experiments of *N. benthamiana* leaf apoplastic fluids used for the following experiments (Suppl. Fig. 3), first version of bacterial genome annotations, substrate cleavage assays using SynCom member's supernatants and their fractions as well as with papain, CP1A and other SA-activated maize root PLCPs (Figure 5, Suppl. Fig. 2) and BLAST searches using inhibitors for homologs in the *P. putida* proteome (Table 1).

Technical assistance during this study

Dr. Farnusch Kaschani and his technical team (University of Duisburg-Essen) performed the processing of MS samples and provided pre-processed data. Ute Meyer (University of Cologne) gave technical assistance in some parts of this thesis (Grinding of maize roots, qPCR, RNA extraction, Western Blotting, SYPRO Ruby staining).